



National Library
of Canada

Acquisitions and
Bibliographic Services Branch

395 Wellington Street
Ottawa, Ontario
K1A 0N4

Bibliothèque nationale
du Canada

Direction des acquisitions et
des services bibliographiques

395, rue Wellington
Ottawa (Ontario)
K1A 0N4

pour les microformes

pour les microformes

NOTICE

The quality of this microform is heavily dependent upon the quality of the original thesis submitted for microfilming. Every effort has been made to ensure the highest quality of reproduction possible.

If pages are missing, contact the university which granted the degree.

Some pages may have indistinct print especially if the original pages were typed with a poor typewriter ribbon or if the university sent us an inferior photocopy.

Reproduction in full or in part of this microform is governed by the Canadian Copyright Act, R.S.C. 1970, c. C-30, and subsequent amendments.

AVIS

La qualité de cette microforme dépend grandement de la qualité de la thèse soumise au microfilmage. Nous avons tout fait pour assurer une qualité supérieure de reproduction.

S'il manque des pages, veuillez communiquer avec l'université qui a conféré le grade.

La qualité d'impression de certaines pages peut laisser à désirer, surtout si les pages originales ont été dactylographiées à l'aide d'un ruban usé ou si l'université nous a fait parvenir une photocopie de qualité inférieure.

La reproduction, même partielle, de cette microforme est soumise à la Loi canadienne sur le droit d'auteur, SRC 1970, c. C-30, et ses amendements subséquents.

University of Alberta

Effect of Air Leakage on Moisture Deposition in Walls

by

Paul Wan Pui Lam



**A thesis submitted to the Faculty of Graduate Studies and Research in partial fulfilment
of**

the requirements for the degree of Master of Science

Department of Mechanical Engineering

Edmonton, Alberta

Spring 1996



National Library
of Canada

Acquisitions and
Bibliographic Services Branch

395 Wellington Street
Ottawa, Ontario
K1A 0N4

Bibliothèque nationale
du Canada

Direction des acquisitions et
des services bibliographiques

395, rue Wellington
Ottawa (Ontario)
K1A 0N4

Your file - Votre référence

Our file - Notre référence

The author has granted an irrevocable non-exclusive licence allowing the National Library of Canada to reproduce, loan, distribute or sell copies of his/her thesis by any means and in any form or format, making this thesis available to interested persons.

L'auteur a accordé une licence irrévocable et non exclusive permettant à la Bibliothèque nationale du Canada de reproduire, prêter, distribuer ou vendre des copies de sa thèse de quelque manière et sous quelque forme que ce soit pour mettre des exemplaires de cette thèse à la disposition des personnes intéressées.

The author retains ownership of the copyright in his/her thesis. Neither the thesis nor substantial extracts from it may be printed or otherwise reproduced without his/her permission.

L'auteur conserve la propriété du droit d'auteur qui protège sa thèse. Ni la thèse ni des extraits substantiels de celle-ci ne doivent être imprimés ou autrement reproduits sans son autorisation.

ISBN 0-612-10726-4

Canada

University of Alberta

Library Release Form

Name of Author: Paul Wan Pui Lam

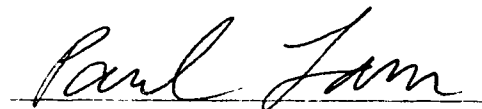
Title of Thesis: Effect of Air Leakage on Moisture Deposition in Walls

Degree: Master of Science

Year this Degree Granted: 1996

Permission is hereby granted to the University of Alberta Library to reproduce single copies of this thesis and to lend or sell such copies for private, scholarly, or scientific research purposes only.

The author reserves all other publications and other rights in association with the copyright in the thesis, and except as hereinbefore provided, neither the thesis nor any substantial portion thereof may be printed or otherwise reproduced in any material form whatever the author's prior written permission.

A handwritten signature in cursive script, reading "Paul Wan Pui Lam", written over a horizontal line.

3303-112B St.
Edmonton, Alberta
T6J 3W6

April 15, 1996

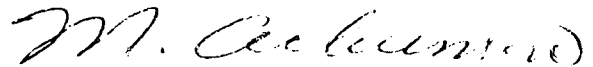
University of Alberta

Faculty of Graduate Studies and Research

The undersigned certify that they have read, and recommend to the Faculty of Graduate Studies and Research for acceptance, a thesis entitled, Effect of Air Leakage on Moisture Deposition in Walls submitted by Paul Wan Pui Lam in partial fulfilment of the requirements for the degree of Master of Science.



Dr. T.W. Forest



Mr. M.Y. Ackerman



Dr. J.D. Dale



Dr. P. Dozzi

April 10, 1996

ABSTRACT

Condensation inside wall cavities of a house can be a major threat to the integrity of the building envelope. Moisture damage to a house may range from nuisances such as peeling paint and mildew to structural damage due to wood decay. In developing a model which can predict condensation inside a wall cavity, it is necessary to address air leakage flow through wall cavities because the amount of moisture deposition is strongly dependent on the air leakage flow rate. Hence, a ventilation model, Local Leaks (Walker 1993), and a cavity moisture deposition model, Wetwall (Nikel 1991) were validated individually to provide the basis for coupling the two to produce a complete model.

A field experiment was carried out at the Alberta Home Heating Research Facility (AHHRF) of the University of Alberta from February 7, 1994 to April 28, 1995 to produce data to validate Local Leaks and Wetwall. A total of approximately 10700 hours of data on the air leakage flow through the cavity and moisture deposition on the exterior cavity sheathing were collected. In addition, Local Leaks was modified to predict air leakage flow rates across the cavity and Wetwall was coupled to a model for moisture diffusion across the exterior sheathing.

Local Leaks correctly predicted the trends of the air leakage flow rate across the cavity except for low leakage rates under $0.1 \text{ m}^3/\text{hr}$ and flow rates under east and west winds due to the difference in the pressure coefficient correlation used in the model and that in the experiment. The model correlation was developed for a house in the middle of a row of houses, while the experiment was conducted in a house at the end of the row which has asymmetric wind shelter. Local Leaks also consistently under predicted the magnitude of the air leakage flow for both infiltration and exfiltration. The under prediction was mainly due to the variation of the wind pressure coefficient along the height of the wall. The magnitude of the wall average pressure coefficient in the model is smaller than the actual one for the exterior leakage site at the top of the wall.

Wetwall responded well to the wetting phase, but not to the drying phase. The slow response to drying was due to the influence of the exponential term in the analytical solution for moisture deposition in the model. The moisture content at the internal nodes of the model was observed to be highly sensitive to the mass diffusivity for water diffusion across wood.

ACKNOWLEDGEMENT

I would like to acknowledge the guidance and assistance of Dr. Forest and Prof. Ackerman throughout my research. I would also like to thank the help provided by John Foy, Terry Nord, the technicians and machinists of the Department of Mechanical Engineering.

TABLE OF CONTENTS

	Page
1 INTRODUCTION	1
1.1 HISTORICAL DEVELOPMENT AND LITERATURE REVIEW . . .	4
1.2 VALIDATION OF THE VENTILATION AND MOISTURE DEPOSITION MODELS	6
2 MODEL DEVELOPMENT	9
2.1 SUMMARY OF Local Leaks MODEL	9
2.1.1 Pressure Difference For Leakage Flow Across The House	11
2.1.2 Calculation Of The Ventilation Rate	15
2.1.3 Use Of The Ventilation Model In Present Study	16
2.2 SUMMARY OF Wetwall MOISTURE DEPOSITION MODEL . . .	20
2.2.1 Moisture Deposition In The Cavity	22
2.2.2 Region Of Validity For Wetwall	25
2.3 DEVELOPMENT OF THE WALL MOISTURE DEPOSITION MODEL	25
2.3.1 Moisture Content\ Vapour Pressure\ Temperature Relationship For Wood	26
2.3.2 Moisture Transport Model For Exterior Sheathing	27
2.3.3 Calculation Of The Amount Of Condensation	35
3 EXPERIMENTAL METHODS	50
3.1 DESCRIPTION OF THE TEST SITE	50
3.2 DESCRIPTION OF THE TEST CAVITY AND INSTRUMENTATION	51
3.3 MEASUREMENTS AND OTHER INSTRUMENTATION	54
3.3.1 Moisture Content	54
3.3.2 Relative Humidity	57
3.3.3 Temperature	57
3.3.4 Wind Speed And Direction	58
3.3.5 Fan Performance Test	58
3.3.6 Leakage Air Flow Measurements	59
3.3.7 Data Acquisition and Storage	61
3.4 LEAKAGE FLOW CHARACTERISTICS	62
3.4.1 Background Leakage Of The Test House	62
3.4.2 Leakage Characteristics Of The Cavity	64
3.5 TEST PROCEDURE	65

4	EXPERIMENTAL RESULTS	83
4.1	AIR LEAKAGE FLOW MEASUREMENTS	83
4.1.1	Variation Of Air Leakage Flow With Wind Speed	86
4.1.2	Variation Of Air Leakage Flow With Wind Direction	87
4.1.3	Variation Of Indoor/outdoor Temperature Difference On Air Leakage Flow	89
4.2	MOISTURE DISTRIBUTION	90
4.3	AIR LEAKAGE AND CONDENSATION	92
4.4	RELATIVE HUMIDITY DISTRIBUTION	93
4.5	TEMPERATURE DISTRIBUTION	94
5	MODEL VALIDATION	116
5.1	COMPARISON OF MEASURED AND PREDICTED AIR LEAKAGE FLOW RATES	116
5.2	EFFECT OF WIND DIRECTION ON AIR LEAKAGE FLOW PREDICTIONS	119
5.3	EFFECT OF INDOOR/OUTDOOR TEMPERATURE DIFFERENCE ON AIR LEAKAGE FLOW PREDICTIONS	122
5.4	Wetwall PREDICTIONS FOR EXTERIOR SHEATHING SURFACE DEPOSITION AND WOOD MOISTURE CONTENT	123
5.5	COMPARISON OF MEASURED AND PREDICTED SHEATHING SURFACE DEPOSITION AND MOISTURE CONTENT	126
5.6	MODEL SENSITIVITY TO MASS DIFFUSIVITY	133
6	CONCLUSIONS AND RECOMMENDATIONS	199
6.1	CONCLUSIONS	200
6.2	RECOMMENDATIONS	203
	REFERENCES	204
APPENDIX A	CALIBRATION AND TEST RESULTS FOR WOOD MOISTURE CONTENT, SURFACE SENSORS, RELATIVE HUMIDITY, FAN PERFORMANCE, AIR LEAKAGE FLOW, BACKGROUND LEAKAGE FOR HOUSE, AND CAVITY FLOW RESISTANCE	207

LIST OF TABLES

Table	Page
5.1 Building characteristics and input parameters to Local Leaks	135
5.2 Cavity characteristics and input parameters to Wetwall	136
5.3 Root-mean-square and mean errors for all air leakages	137
5.4 Root-mean-square and mean errors for air leakages under north, south, east, and west winds	137

LIST OF FIGURES

Figure	Page
2.1 Schematic of typical mass flows through the single zone in Local Leaks	38
2.2 Variation of wall pressure coefficient with wind angle	39
2.3 Schematic of indoor/outdoor pressure difference profile across a wall of a house	40
2.4 Location of the flow assembly and reference points for flow measurements	41
2.5 Schematic of the idealized wall cavity in the model Wetwall	42
2.6 A cross section of the idealized cavity showing the vapour pressure and velocity profiles	43
2.7 Partial pressure profiles showing criteria for no condensation within the insulation	44
2.8 Region of validity for Wetwall showing the inlet relative humidity and indoor/outdoor temperature difference	45
2.9 Cross section of wall cavity showing the vapour pressure profile across the cavity and exterior sheathing	46
2.10 Plot of Cleary's function based on empirical data for temperatures above 273 K and extrapolation for temperatures below 273 K and constant humidity function for temperatures below 273 K	47
2.11 Cross section of sheathing showing the nodal network for diffusion across the sheathing	48
2.12 Schematic of exterior sheathing showing the upper and lower zone coordinates in Wetwall	49

3.1	Schematic of house 6 located at the Alberta Home Heating Research Facility (AHHRF)	67
3.2	Exterior view of house 6 with the test panel located on the north wall	68
3.3	Schematic of house 6 showing the location of the supply fan attached to the bottom of the flue and dimensions of the flue assembly	69
3.4	Schematic of the test cavity with a listing of the composition of the cavity	70
3.5	Schematic of a designated zone on the exterior sheathing showing the locations of the moisture pins and surface sensor	71
3.6	Location of the measurement zones for internal moisture content and surface deposition	72
3.7	Location of thermocouples in the cavity	73
3.8	Location of relative humidity sensors in the cavity	74
3.9	The interior of the test cavity during construction	75
3.10	Surface sensor placed on the cavity face of the exterior sheathing. The photography shows the sensor before mounting and the schematic shows the interwoven wire mesh of the sensor	76
3.11	Schematic of the calibration set up of the fan and flue attachment	77
3.12	Calibration curve of the fan and flue attachment	78
3.13	Schematic of the orifice-flow anemometer assembly	79
3.14	Photograph of the orifice-flow anemometer assembly fitted over the interior cavity opening during instrument testing	80
3.15	Schematic of the calibration set up of the orifice-flow anemometer assembly	81

3.16	Location of the orifice-flow assembly in the house and reference points for pressure flow measurements	82
4.1	Measured rates of infiltration and exfiltration through the cavity from February 7, 1994 to April 28, 1995	96
4.2a	Measured infiltration rates across wall cavity for all wind directions (fan off)	97
4.2b	Measured exfiltration rates across wall cavity for all wind directions (fan off)	97
4.3a	Measured infiltration rates across wall cavity for all wind directions (fan on)	98
4.3b	Measured exfiltration rates across wall cavity for all wind directions (fan on)	98
4.4a	Measured infiltration across wall cavity for north winds (-22.5° to 22.5°) (fan off)	99
4.4b	Measured exfiltration across wall cavity for north winds (-22.5° to 22.5°) (fan off)	99
4.5a	Measured infiltration across wall cavity for south winds (157.5° to 202.5°) (fan off)	100
4.5b	Measured exfiltration across wall cavity for north winds (157.5° to 202.5°) (fan off)	100
4.6a	Measured infiltration across wall cavity for west winds (247.5° to 292.5°) (fan off)	101
4.6b	Measured exfiltration across wall cavity for west winds (247.5° to 292.5°) (fan off)	101
4.7a	Measured infiltration across wall cavity for east winds (67.5° to 112.5°) (fan off)	102
4.7b	Measured exfiltration across wall cavity for west winds (67.5° to 112.5°) (fan off)	102
4.8a	Normalized average leakage rates for all wind speeds greater than 1 m/s (fan off)	103

4.8b	Normalized leakage rates sorted into bins of 22.5° (fan off) (experimental data)	103
4.9	Normalized leakage rates with the fan in operation (experimental data)	104
4.10a	Measured infiltration across wall cavity for all wind speeds below 1 m/s (fan off)	105
4.10b	Measured exfiltration across wall cavity for all wind speeds below 1 m/s (fan off)	105
4.11	Daily averaged moisture content in the five zones (February 1994 to April 1995)	106
4.12	Daily averaged surface sensor output in the five zones (February 1994 to April 1995)	107
4.13	Change in the moisture content with air leakage flow rate (February 1994 to May 1994)	108
4.14	Change in the moisture content with air leakage flow rate (December 1994 to April 1995)	109
4.15	Change in surface sensor output with air leakage flow rate (February 1994 to May 1994)	110
4.16	Change in surface sensor output with air leakage flow rate (December 1994 to April 1995)	111
4.17	Humidity ratio at the mid depth of the cavity for the first 600 hours of the experiment	112
4.18	Relative humidity at mid cavity depth in zone 1 (February 1994 to April 1995)	113
4.19	Typical temperature profile along the height of the cavity (hour 17 of the experiment)	114
4.20	Typical temperature profile across the depth of the cavity (hour 17 of the experiment)	115
5.1	Rates of infiltration and exfiltration predicted by Local Leaks from February 7, 1994 to April 28, 1995	138

5.2	Comparison of measured and predicted flow rates without the fan in operation	139
5.3	Comparison of measured and predicted flow rates with the fan in operation	139
5.4	Comparison of measured flow rates with Local Leaks predictions for north winds only	140
5.5	Comparison of measured flow rates with Local Leaks predictions for south winds only	140
5.6	Comparison of measured flow rates with Local Leaks predictions for east winds only	141
5.7	Comparison of measured flow rates with Local Leaks predictions for west winds only	141
5.8	Normalized average leakage rates for all wind speeds greater than 1 m/s (Local Leaks predictions)	142
5.9	Comparison of the normalized leakage rates of the experiment and Local Leaks (normalized leakage rates are sorted into bins of 22.5°)	142
5.10	Comparison of measured flow rates with Local Leaks predictions for wind speeds below 1 m/s	143
5.11	Surface deposition in Node 1 for all zones predicted by Wetwall (Daily averages)	144
5.12	Moisture content in Node 1 for all zones predicted by Wetwall (Daily averages)	145
5.13	Moisture content in Node 2 for all zones predicted by Wetwall (Daily averages)	146
5.14	Moisture content in Node 3 for all zones predicted by Wetwall (Daily averages)	147
5.15	The location of moisture pins in the experiment relative to the nodal network in Wetwall	148
5.16a	Comparison of Wetwall predictions at node 1 and surface deposition with measured surface sensor	

output in zone 1 (February 1994 to April 1994)	149
5.16b Comparison of Wetwall predictions at node 1 and surface deposition with measured surface sensor output in zone 2 (February 1994 to April 1994)	150
5.16c Comparison of Wetwall predictions at node 1 and surface deposition with measured surface sensor output in zone 3 (February 1994 to April 1994)	151
5.16d Comparison of Wetwall predictions at node 1 and surface deposition with measured surface sensor output in zone 4 (February 1994 to April 1994)	152
5.16e Comparison of Wetwall predictions at node 1 and surface deposition with measured surface sensor output in zone 5 (February 1994 to April 1994)	153
5.17a Comparison of measured moisture content with predictions for node 2 and node 3 in zone 1 (February 1994 to April 1994)	154
5.17b Comparison of measured moisture content with predictions for node 2 and node 3 in zone 2 (February 1994 to April 1994)	155
5.17c Comparison of measured moisture content with predictions for node 2 and node 3 in zone 3 (February 1994 to April 1994)	156
5.17d Comparison of measured moisture content with predictions for node 2 and node 3 in zone 4 (February 1994 to April 1994)	157
5.17e Comparison of measured moisture content with predictions for node 2 and node 3 in zone 5 (February 1994 to April 1994)	158
5.18a Comparison of Wetwall predictions at node 1 and surface deposition with measured surface sensor output in zone 1 (May 1994 to November 1994)	159
5.18b Comparison of Wetwall predictions at node 1 and surface deposition with measured surface sensor output in zone 2 (May 1994 to November 1994)	160

5.18c	Comparison of Wetwall predictions at node 1 and surface deposition with measured surface sensor output in zone 3 (May 1994 to November 1994)	161
5.18d	Comparison of Wetwall predictions at node 1 and surface deposition with measured surface sensor output in zone 4 (May 1994 to November 1994)	162
5.18e	Comparison of Wetwall predictions at node 1 and surface deposition with measured surface sensor output in zone 5 (May 1994 to November 1994)	163
5.19a	Comparison of measured moisture content with predictions for node 2 and node 3 in zone 1 (May 1994 to November 1994)	164
5.19b	Comparison of measured moisture content with predictions for node 2 and node 3 in zone 2 (May 1994 to November 1994)	165
5.19c	Comparison of measured moisture content with predictions for node 2 and node 3 in zone 3 (May 1994 to November 1994)	166
5.19d	Comparison of measured moisture content with predictions for node 2 and node 3 in zone 4 (May 1994 to November 1994)	167
5.19e	Comparison of measured moisture content with predictions for node 2 and node 3 in zone 5 (May 1994 to November 1994)	168
5.20a	Comparison of Wetwall predictions at node 1 and surface deposition with measured surface sensor output in zone 1 (December 1994 to April 1995)	169
5.20b	Comparison of Wetwall predictions at node 1 and surface deposition with measured surface sensor output in zone 2 (December 1994 to April 1995)	170
5.20c	Comparison of Wetwall predictions at node 1 and surface deposition with measured surface sensor output in zone 3 (December 1994 to April 1995)	171

5.20d	Comparison of Wetwall predictions at node 1 and surface deposition with measured surface sensor output in zone 4 (December 1994 to April 1995)	172
5.20e	Comparison of Wetwall predictions at node 1 and surface deposition with measured surface sensor output in zone 5 (December 1994 to April 1995)	173
5.21a	Comparison of measured moisture content with predictions for node 2 and node 3 in zone 1 (December 1994 to April 1995)	174
5.21b	Comparison of measured moisture content with predictions for node 2 and node 3 in zone 2 (December 1994 to April 1995)	175
5.21c	Comparison of measured moisture content with predictions for node 2 and node 3 in zone 3 (December 1994 to April 1995)	176
5.21d	Comparison of measured moisture content with predictions for node 2 and node 3 in zone 4 (December 1994 to April 1995)	177
5.21e	Comparison of measured moisture content with predictions for node 2 and node 3 in zone 5 (December 1994 to April 1995)	178
5.22a	Comparison of Wetwall predictions at node 1 and surface deposition with measured surface sensor output in zone 1. (Mass diffusivity = $3 \times 10^{-8} \text{ m}^2/\text{s}$)	179
5.22b	Comparison of Wetwall predictions at node 1 and surface deposition with measured surface sensor output in zone 2. (Mass diffusivity = $3 \times 10^{-8} \text{ m}^2/\text{s}$)	180
5.22c	Comparison of Wetwall predictions at node 1 and surface deposition with measured surface sensor output in zone 3. (Mass diffusivity = $3 \times 10^{-8} \text{ m}^2/\text{s}$)	181
5.22d	Comparison of Wetwall predictions at node 1 and surface deposition with measured surface sensor output in zone 4. (Mass diffusivity = $3 \times 10^{-8} \text{ m}^2/\text{s}$)	182

5.22e	Comparison of Wetwall predictions at node 1 and surface deposition with measured surface sensor output in zone 5. (Mass diffusivity = $3 \times 10^{-8} \text{ m}^2/\text{s}$)	183
5.23a	Comparison of Wetwall predictions at node 2 and node 3 with measured moisture content in zone 1 (Mass diffusivity = $3 \times 10^{-8} \text{ m}^2/\text{s}$)	184
5.23b	Comparison of Wetwall predictions at node 2 and node 3 with measured moisture content in zone 2 (Mass diffusivity = $3 \times 10^{-8} \text{ m}^2/\text{s}$)	185
5.23c	Comparison of Wetwall predictions at node 2 and node 3 with measured moisture content in zone 3 (Mass diffusivity = $3 \times 10^{-8} \text{ m}^2/\text{s}$)	186
5.23d	Comparison of Wetwall predictions at node 2 and node 3 with measured moisture content in zone 4 (Mass diffusivity = $3 \times 10^{-8} \text{ m}^2/\text{s}$)	187
5.23e	Comparison of Wetwall predictions at node 2 and node 3 with measured moisture content in zone 5 (Mass diffusivity = $3 \times 10^{-8} \text{ m}^2/\text{s}$)	188
5.24a	Comparison of Wetwall predictions at node 1 and surface deposition with measured surface sensor output in zone 1. (Mass diffusivity = $3 \times 10^{-10} \text{ m}^2/\text{s}$)	189
5.24b	Comparison of Wetwall predictions at node 1 and surface deposition with measured surface sensor output in zone 2. (Mass diffusivity = $3 \times 10^{-10} \text{ m}^2/\text{s}$)	190
5.24c	Comparison of Wetwall predictions at node 1 and surface deposition with measured surface sensor output in zone 3. (Mass diffusivity = $3 \times 10^{-10} \text{ m}^2/\text{s}$)	191
5.24d	Comparison of Wetwall predictions at node 1 and surface deposition with measured surface sensor output in zone 4. (Mass diffusivity = $3 \times 10^{-10} \text{ m}^2/\text{s}$)	192
5.24e	Comparison of Wetwall predictions at node 1 and surface deposition with measured surface sensor output in zone 5. (Mass diffusivity = $3 \times 10^{-10} \text{ m}^2/\text{s}$)	193

5.25a	Comparison of Wetwall predictions at node 2 and node 3 with measured moisture content in zone 1 (Mass diffusivity = $3 \times 10^{-10} \text{ m}^2/\text{s}$)	194
5.25b	Comparison of Wetwall predictions at node 2 and node 3 with measured moisture content in zone 2 (Mass diffusivity = $3 \times 10^{-10} \text{ m}^2/\text{s}$)	195
5.25c	Comparison of Wetwall predictions at node 2 and node 3 with measured moisture content in zone 3 (Mass diffusivity = $3 \times 10^{-10} \text{ m}^2/\text{s}$)	196
5.25d	Comparison of Wetwall predictions at node 2 and node 3 with measured moisture content in zone 4 (Mass diffusivity = $3 \times 10^{-10} \text{ m}^2/\text{s}$)	197
5.25e	Comparison of Wetwall predictions at node 2 and node 3 with measured moisture content in zone 5 (Mass diffusivity = $3 \times 10^{-10} \text{ m}^2/\text{s}$)	198

NOMENCLATURE

A	Area of a zone [m^2]
B₃	Constant for evaluating wood moisture content [$^{\circ}\text{C}$]
B₄	Constant for evaluating wood moisture content
B₅	Constant for evaluating wood moisture content
B₆	Constant for evaluating wood moisture content
B₇	Constant for evaluating wood moisture content
C₁	Constant for evaluating saturation pressure
C₂	Constant for evaluating saturation pressure
C₃	Constant for evaluating saturation pressure
C₄	Constant for evaluating saturation pressure
C₅	Constant for evaluating saturation pressure
C₆	Constant for evaluating saturation pressure
C₇	Constant for evaluating saturation pressure
C_p	pressure coefficient for a surface
C	Flow coefficient [$\text{m}^3/(\text{sPa}^n)$]
D₁	Mass diffusivity of water vapour through glass fiber insulation [m^2/s]
D_w	Mass diffusivity of water through wood [m^2/s]
d	Depth of wall cavity [m]
g	Gravity [m/s^2]
h	Cavity height [m]
H	Distance from grade level to leakage site [m]
H_c	Distance between the interior and exterior opening [m]
H₁	Distance of interior opening from grade level [m]
H₂	Distance of exterior opening from grade level [m]
K_D	Discharge coefficient
L	Width of wall cavity [m]
m	Mass of moisture at a node in the sheathing [kg]
m_{dwt}	wood dry weight at a node in the sheathing [kg]
M	Mass flow rate [kg/s]
M_{fan}	Mass flow rate created by a fan [Kg/s]
\dot{m}	Moisture deposition rate [kg/s]
M_w	Molecular weight of water [kg/kmol]
MC	Wood moisture content [%wt]
n	Flow exponent
n_{fan}	Flow exponent for fan mass flow equation
P_∞	Ambient pressure [Pa]
P_{in}	Indoor pressure [Pa]
P_{out}	Outdoor pressure [Pa]
P_w	Partial pressure of water vapour [Pa]
P_{w,c}	Vapour pressure at the sheathing surface [Pa]
P_{w,inlet}	Vapour pressure at the inlet opening of the cavity [Pa]
P_{w,s}	Saturation vapour pressure [Pa]

P_{w1}	Vapour pressure at node 1 [Pa]
P_{w2}	Vapour pressure at node 2 [Pa]
P_{w3}	Vapour pressure at node 3 [Pa]
P_{w4}	Vapour pressure at node 4 [Pa]
Q_{in}	Infiltration flow rate [m^3/hr]
Q_{out}	Exfiltration flow rate [m^3/hr]
Q_{rated}	flow rate at zero pressure drop across fan [m^3/s]
R_o	Universal gas constant [J/kmol K]
R_w	Gas constant for water [J/kg K]
S_w	Shelter factor
T_{in}	Indoor air temperature [$^{\circ}C$]
T_{out}	Outdoor air temperature [$^{\circ}C$]
T_{mean}	Mean temperature (average of indoor and sheathing temperature) [K]
T_1	Temperature at node 1 [K]
T_2	Temperature at node 2 [K]
T_3	Temperature at node 3 [K]
T_4	Temperature at node 4 [K]
U	Wind speed [m/s]
U_{eaves}	Wind speed at eaves height [m/s]
U_{tower}	Wind speed at the top of a 10 m high tower [m/s]
V	Voltage [V]
w	Velocity of air flow along the height of the cavity [m/s]
z_i	Lower zone height limit [m]
z_j	Upper zone height limit [m]
ΔP	Pressure difference across opening [Pa]
ΔP_{fan}	Pressure drop across fan [Pa]
ΔP_{fluc}	Pressure drop across the flue assembly [Pa]
ΔP_{rated}	Pressure drop across fan at zero flow rate [Pa]
ΔP_{ref}	Outdoor/indoor pressure difference at grade level [Pa]
ΔP_{ST}	Pressure difference due to the indoor/outdoor temperature difference [Pa]
ΔP_T	Reference stack pressure
ΔP_u	Pressure difference due to wind effects [Pa]
ΔP_w	Reference wind pressure
$\Delta x_{1,2}$	Distance between node 1 and node 2 [m]
$\Delta x_{2,3}$	Distance between node 2 and node 3 [m]
$\Delta x_{3,4}$	Distance between node 3 and node 4 [m]

GREEK SYMBOLS

ρ	Density
ρ_{in}	Indoor air density [kg/m^3]
ρ_{out}	Outdoor air density [kg/m^3]
λ_n	Separation constant
τ	Time interval

SUPERSCRIPTS

i Time index

CHAPTER 1

INTRODUCTION

According to ASTM Committee E241, Practices for Increasing Durability of Building Constructions Against Water-Induced Damages, "Except for structural error, about 90% of all building construction problems are associated with water in some way." The types of moisture damage range from nuisances such as peeling paint, staining of walls, and mildew to potential structural damage to a house due to wood decay and buckling of walls. Of the moisture problems, moisture deposition within the wall and ceiling cavities of a house is of the greatest concern. Unlike deposition on an exposed wall surface, moisture deposition inside enclosed cavities is not visible and does not provide any indications of potential damage. Consequently, the moisture content in the wall cavities may reach a level which can lead to severe problems in the building envelope.

In order for moisture deposition to occur, a moisture source, driving mechanism for moisture transfer, path of moisture flow, and condensation surface are required. The amount of moisture deposition inside a wall cavity is strongly dependent on air leakage flow through the cavity from the indoor of the house to the outside. Typically, during the heating season moist warm air from the inside of the house flows through the cavity to the outside through cracks and openings in the wall. As the moist warm air migrates through the cavity, it contacts the backside of the exterior sheathing and condenses on the cold surface. The condensation may accumulate over time to a level which results in moisture damage. If the temperature of the sheathing is below freezing the

condensation will be locked in place as ice or frost. The effects of the moisture accumulation are delayed until the spring when the ice melts.

The typical sources of moisture inside a house are human respiration, daily activities, and humidification. Human respiration and activities such as cooking, washing, showering generate between 10 to 20 kg of moisture per day (Alberta Energy and Natural Resources, 1984). Along with regular humidification, occupants and their daily activities produce moisture on a continuous basis. Another moisture source, which has a transient effect, is the moisture trapped during construction such as from pouring of concrete or the use of wet lumber for framing. In addition, moisture may penetrate the building envelope by driving rain and snow.

The moisture transfer mechanisms for condensation inside wall cavities are air convection and vapour diffusion. Air leakage flow through the cavity is driven by an indoor/outdoor pressure difference which is dependent on the weather conditions, leakage characteristic of the building envelope, and configuration of the house. Vapour diffusion, on the other hand, is driven by the difference in the vapour pressure between the interior of the house and outside. During the heating season, the vapour diffuses from the inside to the outside. Although both mechanisms contribute to the condensation process, moisture transport by air convection is dominant because it is 10 to 4000 times larger than vapour diffusion (TenWolde and Suleski, 1984).

The air leakage flow convects moisture into the cavity through cracks and openings in the wall. The typical leakage sites in the building envelope are openings around electrical outlets, windows, doors, and joints where the exterior wall meets the

floor and ceiling. In general, the path of air leakage flow consists of an interior opening in the dry wall near the floor, the cavity interior through which the flow traverses vertically, and an exit near the top of the exterior sheathing of the cavity.

As the air leakage flow convects moisture up through the cavity, water vapour diffuses across the depth of the cavity and condenses on the sheathing because the sheathing is the first cold surface which the water vapour encounters. The moisture deposition tends to occur on the sheathing surface and not within the insulation as observed by Timusk and Doshi (1985). Condensation problems occur when the wood moisture reaches a content level which leads to concerns ranging from mildew to wood rot. Wood begins to decay when the moisture content exceeds 20 %wt (by weight of wood) and the temperature is above 10°C (McRae 1995). In northern climatic regions, the summer drying season is short and the moisture is often not removed completely. Consequently, over a number of wetting and drying cycles, moisture accumulates and problems develop.

The conventional practice in preventing moisture problems is to seal up all the crevices and openings in the wall and to reduce the indoor relative humidity. Reducing the number of leakage paths is reasonable, but it is difficult to implement because there will always be accidental punctures in the vapour retarder and openings for which are not accounted for. Sealing all openings, however, may also create a "tight" house where the exchange of fresh air and indoor air is limited. Health problems may arise from the concentration of air contaminants. Furthermore, for comfort and other health reasons, the optimum indoor humidity should be kept between 40% and 50% at 20°C as

recommended by Sterling et al (1985) instead of typical values of under 30% (Kent et al, 1966). A balance between preventing moisture damage and avoiding health problems is clearly essential.

One of way of attaining this balance is to develop a numerical model which a designer can readily use to predict condensation problems before construction. Hence, the design can be evaluated for moisture deposition and modifications can be made accordingly. Despite much study, there is still no reliable method of predicting moisture damage inside wall cavities of a house. Predicting the amount of condensation is difficult because moisture deposition is driven mainly by air leakage through the cavity. Since air leakage is dependent on the weather, leakage characteristics of the building envelope, and house configuration, the amount of condensation is non-linearly dependent to a number of variables. A complete model must address the amount of air leakage through wall cavities.

1.1 HISTORICAL DEVELOPMENT AND LITERATURE REVIEW

A number of numerical models have been developed to predict moisture accumulation in a wall cavity. In general, the models can be classified into two categories in terms of moisture transfer mechanisms: vapour diffusion only or vapour diffusion and air convection. A simple model is the ASHRAE (1989) method for vapour diffusion through a multi-layer wall. Each layer of the wall possesses a specific resistance to moisture diffusion. All the resistances are connected in series and the overall moisture transfer is evaluated. This model is very limited because air convection is neglected altogether.

Another model which does not include air flow through the cavity is WALLDRY developed by Schuyler et al (1989). The model is used by Canada Mortgage and Housing Corporation (CMHC) to determine the moisture transfer through a cavity of the moisture trapped in the wood during construction with the use of wet lumber. It is a finite difference method and includes the effects of latent and sensible heat gain.

Ojanen and Kohonen (1989) developed a three-dimensional finite difference model which included convective and diffusive mass transfer. It has been used by the National Research Council of Canada (NRC) as their reference model. The model, however, requires intensive numerical computation and does not address the indoor/outdoor pressure difference which drives the air leakage flow for input in their model. Recently, Ojanen and Kumaran (1992) used the model to study the amount of moisture accumulation of a number of wall cavities exposed to Canadian and Finnish weather conditions. The moisture predictions showed the expected trends of moisture accumulation during the heating season and drying during the summer. Unfortunately, the amount of exfiltration in the model was based on a fixed value instead of a calculated value based on the weather conditions, leakage distribution, and house configuration. Although the situation they modelled corresponds to houses that are mechanically ventilated, the present study shows that fan biased air leakage flow rates through the cavity are not constant and depend on the weather conditions.

A more recently developed model by Burch and Thomas (1992), did include air convection, but again the air leakage flow rate was based on an assumed fixed value. The model developed by TenWolde and Carll (1992) used measured flow rates for

predicting the moisture deposition in a wall cavity. The measured flow rates, however, were based on an imposed 4 Pa pressure difference across the wall. Since the pressure difference is strongly dependent on the local climatic conditions, leakage distribution of the envelope and house configuration, the model is limited.

One of the better models is Wetwall developed by Nikel (1991). It is a two-dimensional, steady-state, analytical model which uses measured flow rates for predicting moisture deposition inside a wall cavity. In the model, water vapour diffuses horizontally across the cavity while being convected vertically up the cavity. With a limited data set of field measurements for sheathing moisture content, Wetwall was observed to predict the correct wetting and drying trends and to display a vertical moisture distribution along the height of the sheathing. The main advantage of Wetwall over the model developed by Ojanen and Kohonen (1989) is that Wetwall is much more straight forward in numerical computation which allows easier implementation of the model. The drawback with Wetwall, however, is that the measured flow rates used as input to the model are generally not known. This limits the use of the model. It is therefore necessary to couple a ventilation model which predicts the air leakage flows through the cavity with Wetwall to expand the scope of the moisture deposition model.

1.2 VALIDATION OF THE VENTILATION AND MOISTURE DEPOSITION MODELS

The work presented in this thesis consists of the validation of the numerical model Local Leaks developed by Walker (1993) which was adapted to predict cavity air leakage flow rates and Wetwall created by Nikel (1991). Local Leaks is a ventilation model which predicts the overall ventilation in a house. Wetwall predicts the moisture

deposition inside a wall cavity for a given air leakage flow rate through a wall cavity. A field experiment was initiated to generate data on air leakage flow through a wall cavity and moisture deposition inside a wall cavity for comparisons with model predictions.

The intent of validating Local Leaks and Wetwall individually was to provide the basis to eventually couple the two models. With some modifications to Local Leaks, the air leakage flow rates through a wall cavity can be predicted and then be used as input to Wetwall. Consequently, the scope of Wetwall was expanded such that a tool for predicting moisture deposition is available for various regions with different climatic conditions. The first half of Chapter 2 summarizes and outlines the changes to Local Leaks necessary to be able to predict flow rates. The second half of the chapter presents and shows the further development of Wetwall. Since Wetwall was limited to moisture deposition inside the cavity, the model was coupled to a numerical model for moisture diffusion across the exterior sheathing. The inclusion of moisture exchange between the cavity, exterior sheathing, and outside allows the model to capture the moisture deposition process more completely. Chapter 3 provides a description of the test facility, test cavity, and experimental procedure. The field experiment was conducted inside a house located in an exposed rural field so that the dynamics of the weather could be incorporated in the study. Chapter 4 presents the measured air flow rates and moisture deposition from the field experiment which show interesting correlations with wind speed, wind direction, and indoor/outdoor temperature difference. Chapter 5 discusses the comparisons between the experimental results and the predictions from Local Leaks

and Wetwall. It is shown that there is reasonable agreement between the predicted and measured air leakage flow rates and wood moisture content. Finally, Chapter 6 summarizes the results of the validation and provides recommendations.

CHAPTER 2

MODEL DEVELOPMENT

The amount of moisture deposition inside a wall cavity is strongly dependent on the air leakage flow rate through the cavity. Consequently, in developing a complete moisture deposition model, both the prediction of air leakage through a wall cavity leakage path and the prediction of moisture deposition in the wall cavity should be included. In this chapter, a ventilation model, Local Leaks, and moisture deposition model, Wetwall are presented. Both models are to be validated separately to provide the basis for coupling Local Leaks and Wetwall to produce a complete moisture deposition model. The first half of Chapter 2 provides a summary of Local Leaks and the modifications to the model necessary to predict air leakage flow rates. In the second half of the chapter, a summary of Wetwall is presented and the development of Wetwall to include diffusion across the exterior sheathing is discussed.

2.1 SUMMARY OF Local Leaks MODEL

In this section, a brief summary of the ventilation model, Local Leaks (Walker 1993), is presented. This model predicts the overall air leakage rate across the envelope of a house for given leakage characteristics and local climatic conditions such as wind speed, wind direction, and indoor/outdoor temperatures. It is a single zone model which accounts for the background leakage, the air leakage across intentional openings, and the air flow induced by fans. The overall ventilation rate is determined by a mass balance of the total air flow into and out of the specified leakage sites. A schematic of the typical mass flows addressed by Local Leaks is shown in Figure 2.1

Local Leaks makes use of three key assumptions:

- 1) The air in the zone is well mixed which implies that the temperature in the zone is uniform. This assumption of no thermal gradient within the living space is reasonable because the thermal boundary layer in the house is only about 5% of the wall height or less for still air as determined by Dale and Ackerman (1993).
- 2) A single average pressure coefficient is used for each exterior wall section of a house and intentional openings do not affect the average wall pressure coefficient.
- 3) The flow into and out of the building envelope is quasi-steady since the predictions are compared with hourly averages.

The mass flow rate of air through any section of a house shown in Figure 2.1 is described by the general flow equation

$$M = \rho C \Delta P^n \quad 2.1$$

where M = mass flow rate [kg/s]
 ρ = density of air [kg/m³]
 C = flow coefficient [m³/(sPaⁿ)]
 ΔP = pressure difference across opening [Pa]
 n = flow exponent

The indoor/outdoor pressure difference, ΔP , is defined as $P_{out} - P_{in}$. The flow coefficient, C , in the equation is dependent on the leakage area and the flow exponent, n , is a value between 1.0 and 0.5, where 1.0 is for laminar flow and 0.5 is for turbulent orifice flow. Typically, the flow coefficient and flow exponent for a house are approximately $5 \times 10^{-3} \text{ m}^3/(\text{sPa}^n)$ and 0.67 respectively (Wilson and Walker 1991a).

In Equation 2.1, a positive indoor/outdoor pressure difference ($P_{out} > P_{in}$)

produces a positive mass flow which by convention is denoted as inflow. Inflow or infiltration occurs if air flows from the outside into the inside of the house. Conversely, a negative indoor/outdoor pressure difference ($P_{out} < P_{in}$) produces a negative mass flow which is defined as outflow. Outflow or exfiltration occurs if air flows from the inside to the outside of a house. The air density in the equation is equal to the outdoor air density when infiltration occurs and the indoor air density when exfiltration arises.

2.1.1 Pressure Difference For Leakage Flow Across The House

The driving force for air leakage across openings of a house is the indoor/outdoor pressure difference. The pressure difference is created naturally by the wind and the indoor/outdoor temperature difference (stack effect). We consider each of these separately.

The pressure created by the wind is the stagnation effect of air flow upon a surface. It is defined as,

$$\Delta P_u = \rho_{out} C_p \frac{(S_w U)^2}{2} \quad 2.2$$

where ΔP_u = pressure difference due to wind effects [Pa]

ρ_{out} = outdoor air density [kg/m³]

C_p = pressure coefficient

S_w = shelter factor

U = wind speed [m/s]

The pressure difference, ΔP_u , is defined as the difference between the pressure on the building due to the wind and the atmospheric reference pressure, P_∞ , where the building does not influence the flow field. The wind speed in the equation, as used in Local Leaks, is the value at eaves height which is the reference point for all calculations

involving wind speed in the model. The pressure coefficient, C_p , in Equation 2.2 is highly sensitive to wind direction. For the walls of a house, the pressure coefficient is positive on the windward surface normal to the flow and negative on the leeward face. If the wind direction is shifted by 90° , the same wall would experience a negative pressure coefficient, but the value would depend on whether the house is isolated or sheltered within a row of houses. In Local Leaks, the pressure coefficient is determined with the use of a continuous harmonic trigonometric function developed by Walker (1993) which is dependent on the wind direction. A plot of the pressure coefficient as a function of the wind direction is shown in Figure 2.2.

If there are obstacles surrounding a house, the wind obstruction that they create on the house is accounted for by a wind shelter factor, S_w , which is defined as the ratio of the obstacle-reduced wind speed to the free stream wind speed. It is a multiplier between 1.0 and 0, where $S_w = 1.0$ implies that the surface of the building is entirely exposed to the air flow and $S_w = 0$ presumes that the surface of the building is completely sheltered from the air flow. The shelter factor, similar to the pressure coefficient, varies greatly with the wind direction. The wind shelter is also expressed as a function of the wind direction by Walker (1993) with the use of the wind-shadow technique (Wilson and Walker, 1991b).

The stack effect is the buoyancy effect created by a difference in the indoor and outdoor air densities due to an indoor/outdoor temperature difference. The pressure difference created by the stack effect for any height is defined as,

$$\Delta P_{ST} = -gH(\rho_{out} - \rho_{in}) \quad 2.3$$

Using the ideal gas law, the difference in the indoor and outdoor density is expressed in terms of a difference in the indoor and outdoor temperatures.

$$\Delta P_{ST} = -gH\rho_{out}\left(\frac{T_{in} - T_{out}}{T_{in}}\right) \quad 2.4$$

where ΔP_{ST} = pressure difference due to the indoor/outdoor temperature difference [Pa]
 H = distance from grade level to the leakage site [m]
 g = gravity [m/s²]
 ρ_{out} = outdoor air density [kg/m³]
 T_{in} = indoor air temperature [°C]
 T_{out} = outdoor air temperature [°C]

The driving force for air flow at any location on a wall is the indoor/outdoor pressure difference across the leakage site caused by the combined action of wind and stack effect. The pressure on the outside wall at any height is

$$P_{out} = P_{out}|_{H=0} + \rho_{out}C_pS_w^2\frac{U^2}{2} - \rho_{out}gH \quad 2.5$$

where grade level is the reference height used in Local Leaks. In the same manner, the pressure on the inside wall is,

$$P_{in} = P_{out}|_{H=0} - \Delta P_{ref} - \rho_{in}gH \quad 2.6$$

where ΔP_{ref} is the outdoor/indoor pressure difference at grade level ($\Delta P_{ref} = P_{out}|_{H=0} - P_{in}|_{H=0}$). The difference between Equation 2.5 and Equation 2.6, shown in Figure 2.3, yields the pressure difference across an opening at any height in a wall.

$$\Delta P = P_{out} - P_{in} = \Delta P_{ref} - (\rho_{out} - \rho_{in})gH + \rho_{out}C_pS_w^2\frac{U^2}{2} \quad 2.7$$

If the stack effect term is written in terms of Equation 2.4, the pressure difference becomes,

$$\Delta P = P_{out} - P_{in} = \Delta P_{ref} - \Delta P_T H + C_p S_w^2 \Delta P_w \quad 2.8$$

where the two terms ΔP_T , the reference stack effect pressure, and ΔP_w , the reference wind pressure, are defined as,

$$\Delta P_T = \rho_{out}g\left(\frac{T_{in} - T_{out}}{T_{in}}\right) ; \quad \Delta P_w = \rho_{out}\frac{U^2}{2}$$

The point at which the indoor/outdoor pressure difference is zero, shown in Figure 2.3, is the neutral height. When the indoor temperature is greater than the outdoor temperature, the flow above the neutral height is exfiltration and the flow below the neutral level is infiltration. The location of the neutral height is dependent on the distribution of the leakage sites, the stack effect and wind loading.

Equation 2.8 defines the pressure difference which drives the mass flow across any opening in the building envelope at any height. The indoor/outdoor pressure difference at grade level, ΔP_{ref} is common to all pressure differences used to describe the leakage flows shown in Figure 2.1. It is important to stress that the pressure difference induced by the stack effect and wind loading are not additive and the two interact through ΔP_{ref} .

2.1.2 Calculation Of The Ventilation Rate

The overall ventilation rate is determined from a mass balance of the total inflow and outflow across the building. The mass flow across each leakage site is determined by substituting Equation 2.8 into Equation 2.1.

$$M = \rho C (\Delta P_{ref} - H \Delta P_T + C_p S_w^2 \Delta P_w)^n \quad 2.9$$

where ρ is equal to ρ_{out} for infiltration and ρ is equal to ρ_{in} for exfiltration.

The indoor/outdoor pressure difference at grade level, ΔP_{ref} , must first be evaluated before an overall ventilation rate is determined. Since each opening has a distinct flow coefficient and flow exponent, a mass flow equation is developed for each leakage site. Consequently, a system of non-linear mass flow equations must be solved iteratively to determine ΔP_{ref} , the common unknown which balances the total inflow and outflow. The iteration process continues until convergence is reached where the difference in ΔP_{ref} from the previous iteration is less than 0.01 Pa giving a mass flow imbalance of 0.001 kg/s or less. The overall ventilation rate is then simply the sum of the total infiltration or exfiltration flow rates.

The model categorizes the leakage sites into three types: background leakage, passive vents, and fans. The leakage across each type of opening is calculated separately. For background leakage, the air flow through unintentional openings such as cracks is assumed to be distributed uniformly over the entire building envelope. This implies that the value of the flow exponent, n , for the background leakage flow is the same for all surfaces and the background leakage over a specific surface is a prescribed fraction of the overall leakage across the envelope which is determined from a fan

pressurization test. A fan pressurization test is described in Section 3.4.1.

For the flow across passive vents such as soffits and intentional openings like windows and doors, a distinct flow coefficient and exponent is used for each opening. The values for C_p and S_w are taken to be the same as that for the surface on which the opening is located. The location and size of the opening are assumed not to affect the pressure coefficient of the wall or roof surface.

The air flow induced by a fan, supply or exhaust, is addressed by incorporating a fan performance curve (pressure-flow characteristics) into the model because the operating point of the fan varies with the change in the ambient conditions. Given the pressure across the inlet and outlet of the fan, the mass flow is calculated based on the performance curve. Further details on the calculations of each type of leakage are outlined in Walker (1993).

2.1.3 Use Of The Ventilation Model In Present Study

Local Leaks originally was intended for predicting the overall ventilation rate of a house given the indoor/outdoor temperatures, ambient conditions such as wind speed and wind direction, overall house leakage behaviour, and house configuration. In the field experiment, however, the air leakage flow through a single cavity was measured instead of the overall ventilation rate. Consequently, Local Leaks was modified to include a new section for predicting the amount of air flow across a leakage path through a cavity. In addition, the calculations of the air leakage through the flue and the flow generated by a fan were modified because in the experiment a supply fan attached to the bottom of the flue was in operation for a portion of the first heating season. In the

original form of the model, supply fans were mounted on the walls and not attached to the bottom of the flue.

The prediction of the air flow through a leakage path of a wall cavity was added to Local Leaks because air leakage is the primary method of moisture transport into the wall cavity. The particular leakage path, shown in Figure 2.4, consists of an opening at the bottom of the interior wall over which a flow meter is mounted, the glass fibre insulation-filled cavity interior, and an opening at the top of the exterior wall. This type of leakage configuration is consistent with the wall cavities of a typical house where the interior leakage site may be an electrical outlet and the exterior leakage site may be small cracks at the top of the sheathing.

Unlike an opening across a wall with the inlet and outlet at the same height, the stack effect pressure at the bottom interior opening and top exterior opening is different due to the hydrostatic head. The indoor/outdoor pressure difference between point 0 and point 4, in Figure 2.4, was determined by McRae (1995).

$$\Delta P_{O,4} = \Delta P_{ref} - \Delta P_T \left(\frac{H_1 + H_2}{2} \right) + C_p S_w^2 \Delta P_w \quad 2.10$$

where $\Delta P_{O,4}$ = pressure difference across the cavity between the bottom interior and top exterior opening [Pa]

H_1 and H_2 = distance of the interior and exterior openings with respect to grade level

The pressure difference, $\Delta P_{O,4}$, is defined as $P_0 - P_4$. The mass flow equation which describes the air leakage flow through the cavity following the leakage path shown in Figure 2.4 is

$$M = \rho C(\Delta P_{0,4})^n \quad 2.11$$

where M = mass flow rate [kg/hr]

ρ = indoor density for infiltration and outdoor air density for exfiltration

ΔP = pressure difference between point 0 and point 4 [Pa]

The values of C and n are $0.084 \text{ m}^3/(\text{hrPa}^n)$ and 0.569 for infiltration and $0.058 \text{ m}^3/(\text{hrPa}^n)$ and 0.543 for exfiltration (Section 3.4.2). Equation 2.11 is the mass flow equation used in the model for predicting air leakage across the cavity.

The leakage across the single cavity is about two orders of magnitude smaller than the overall leakage rate, therefore, the cavity leakage is not included in the overall mass balance of the total inflow and outflow. Instead, the calculation of the cavity flow begins with an overall mass balance of all the specified leakages across the building to determine the reference pressure difference at grade level using the Local Leaks model. The pressure difference, ΔP_{ref} , which is calculated from the mass balance, is then substituted into Equation 2.10 to calculate the pressure across the cavity. The mass flow rate across the single cavity is finally evaluated using Equation 2.11. Typically, the predicted cavity flow rate is about 0.2 kg/hr for infiltration and 0.1 kg/hr for exfiltration compared with typical ventilation flow rates of about 50 kg/hr (Walker 1993).

In Local Leaks, the flow through a flue and across a fan are addressed separately. The flue is considered a passive vent with a prescribed flow exponent of 0.5 and a flow coefficient based on the flue diameter and a discharge coefficient, K_D , of 0.6 (Walker 1989). The pressure coefficient is taken to be -0.5 in uniform flow.

The mass flow created by a fan is determined from a fan performance curve at a particular operating point dictated by the indoor/outdoor pressure difference. The

performance curve is approximated with an equation which includes the specified rated flow rate and rated pressure.

$$M_{fan} = \rho Q_{rated} \left(\frac{\Delta P_{rated} - \Delta P_{fan}}{\Delta P_{rated}} \right)^{n_{fan}} \quad 2.12$$

where M_{fan} = mass flow rate created by a fan [kg/s]

ρ = air density [Pa]

Q_{rated} = flow rate at zero pressure drop across the fan [m³/s]

ΔP_{rated} = pressure drop across the fan at zero flow rate [Pa]

ΔP_{fan} = pressure drop across the fan [Pa]

n_{fan} = 0.3 for centrifugal fans (Walker 1993)

In Equation 2.12, the air density is equal to the outdoor air density for infiltration and indoor air density for exfiltration. The pressure drop across the fan is equal to the indoor/outdoor pressure difference evaluated at the height of the fan. The assumptions are that the pressure coefficient, C_p , is the same as the value of pressure coefficient for the wall on which the fan is mounted and the height in the stack effect pressure is the location of the fan on the wall with respect to grade level fan.

In the field study, however, a supply fan was mounted at the bottom of the flue. The air was drawn into the house through the flue instead of across an opening on the wall at a constant elevation. In this case, the stack effect pressure has an additional hydrostatic pressure component. Similar to the flow across a wall cavity with openings at the bottom and top of the wall, the effective height is the average distance between the top and bottom of the flue (McRae 1995). For the experiment, the effective distance was 2.4 m from grade.

$$\Delta P_{flue} = \Delta P_{ref} - \left(\frac{H_{Flue,Top} + H_{Flue,Bottom}}{2} \right) \Delta P_T + C_p S_w^2 \Delta P_w \quad 2.13$$

where C_p and S_w remain the same as before at - 0.5 and 1.0 respectively.

Instead of substituting ΔP_{flue} in Equation 2.13 for ΔP_{fan} in the generalized fan performance curve in Equation 2.12, ΔP_{flue} is substituted into a specific fan performance curve, calibrated with the flue pipe and flue cap in place to determine the mass flow rate. The flow generated by the fan with the flue attachment in place is described by the calibrated mass flow equation as,

$$M_{fan} = \frac{\rho_{out}}{3600} (5.357E^{-4} \Delta P_{Flue}^3 - 0.0475 \Delta P_{Flue}^2 + 1.905 \Delta P_{Flue} + 111.163) \quad 2.14$$

where M_{fan} = mass flow rate generated by the fan and flue [kg/s]

ρ_{out} = outdoor air density [kg/m³]

ΔP_{Flue} = pressure drop across the flue as described in Equation 2.13

The calibration procedure and validity of the performance curve are discussed in Section 3.3.5.

2.2 SUMMARY OF Wetwall MOISTURE DEPOSITION MODEL

In this section, a summary of a wall moisture deposition model is presented. Wetwall, developed by Nikel (1991), is an analytical model which predicts the amount of condensation formed on the exterior wood sheathing of a standard wall cavity. For given input parameters of infiltration and exfiltration rates, indoor/outdoor temperatures, and indoor/outdoor relative humidity, the model determines the mass deposition for each hour. The overall amount of accumulated moisture in the wood sheathing is expressed in terms of the moisture content, which is defined as the ratio of the mass of the moisture

in the wood to the mass of dry wood. Wetwall is based on the assumptions that air convection is the only transport mechanism of moisture from the environment to the cavity, that moisture diffuses across the wall cavity while being convected up the wall cavity by the air flow, and that the overall mass transfer process is steady state.

The model uses an idealized wall cavity for mass and heat transfer analysis. Conceptually, the idealized cavity is composed of two semi-infinite, isothermal plates with insulated sides. The assumption of insulated sides is logical because the heat transfer across the depth of the wall is much greater than that between adjacent cavity spaces. The cavity is assumed to be placed in the center of a wall in between two cavity spaces with the same level of insulation.

The physical parameters of the idealized cavity are the same as that of a typical cavity: wood sheathing on the exterior surface, gypsum board on the interior, and wooden studs form the sides of the cavity. The interior of the cavity is filled with glass fibre insulation with an overall thermal resistance of 2.2 RSI and a vapour barrier is placed on the warm side of the cavity in between the gypsum board and insulation. A schematic of the idealized wall cavity is shown in Figure 2.5.

As in a typical cavity, the leakage sites in the idealized cavity are distributed near the floor on the inside and close to the top on the outside. The idealized cavity has a single, interior opening in the gypsum board and vapour barrier which is located 0.03 m above the floor. The opening, shown in Figure 2.5, is 7 mm wide and runs across the entire width of the cavity. The exterior leakage site, which has the same dimensions, is located 2.06 m from the floor on the exterior wood sheathing.

2.2.1 Moisture Deposition In The Cavity

Wetwall is a 2-dimensional representation of a 3-dimensional phenomenon. With the leakage sites spanning the entire width of the cavity, the flow is expected to be constant along the width of the cavity in the y-direction. Thus, heat and mass transfer are assumed to only vary along the depth and height of the cavity in the x-direction and z-direction. In the model, air flow enters and exits through either the interior or exterior leakage sites only. Once inside the cavity, the flow becomes laminar plug flow and travels up or down the cavity towards the exit.

Moisture is assumed to be transported into the cavity by air convection only because the mass transfer by convection is about 10 to 4000 times larger than that of diffusion (TenWolde 1985). The diffusion of water vapour from the room to the cavity can be neglected. The mass transfer within the cavity, however, is purely diffusive and is described by the 1-dimensional form of Fick's law of diffusion. Water vapour can only diffuse across the depth of the cavity in the x-direction.

Diffusion of water vapour across the cavity (x-direction) is balanced by the convective flow of vapour up the cavity (z-direction). Using the partial pressure of vapour, P_w , as the driving force for diffusion, the governing equation is

$$w \frac{\partial P_w}{\partial z} = D_I \frac{\partial^2 P_w}{\partial x^2} \quad 2.15$$

where w = velocity of air flow along the height of the cavity [m/s]

P_w = partial pressure of vapour [Pa]

D_I = mass diffusivity of water vapour through glass fibre insulation [m²/s]

Equation 2.15 is solved by the method of separation of variables with the boundary

conditions listed below (Nikel 1991):

$$\frac{\partial P_w(0,z)}{\partial x} = 0 ; P_w(d,z) = P_{w,c} ; P_w(x,0) = P_{inlet}$$

The first condition states that there is no diffusion of moisture into the cavity through the warm side of the wall due to the vapour barrier. The second condition expresses the vapour pressure at the sheathing, P_w , as a known value, $P_{w,c}$, which is related to the moisture content of the wood and sheathing temperature. The third condition states that the vapour pressure at the inlet, $P_{w,inlet}$, is constant across the depth of the cavity and is related to the relative humidity and temperature of the air entering the cavity. The vapour pressure gradient and flow velocity profile across the cavity are shown in Figure 2.6.

The solution to Equation 2.15 is the vapour pressure profile in the form of a Fourier infinite series,

$$P_w(x,z) = P_{w,c} + (P_{w,inlet} - P_{w,c}) \sum \frac{-2\sin\lambda_n}{\lambda_n} \cos\left(\lambda_n \frac{x}{d}\right) \exp\left[-\frac{D_l \lambda_n^2 z}{w d^2}\right] \quad 2.16$$

where $P_{w,c}$ = vapour pressure at the sheathing [Pa]

$P_{w,inlet}$ = vapour pressure at the inlet [Pa]

$\lambda_n = (2n - 1)\pi/2$, $n = 1, 2, 3, \dots$ (separation constant)

d = depth of wall cavity [m]

D_l = mass diffusivity of water vapour through glass fibre [m²/s]

w = velocity of air flow along the height of the cavity [m/s]

x = distance along the depth of the cavity [m]

z = distance along the height of the cavity [m]

By substituting the derivative of the $P_w(x,z)$ with respect to x into Fick's Law of diffusion, the mass flux at any height along the sheathing is determined. The mass

deposition on the exterior sheathing is the integral of the mass flux over a given zone height. In applying Wetwall, the exterior sheathing is divided into a number of fixed-height zones; thus it is convenient to calculate the mass flux in a zone defined by $z = z_i$ and z_j , the lower and upper zone heights. Each zone spans the entire width of the cavity.

$$\dot{m} = -D_L L \frac{M_w}{R_o T_{mean}} \int_{z_i}^{z_j} \frac{\partial P_w}{\partial x} \Big|_{x=d} dz \quad 2.17$$

where \dot{m} = moisture deposition rate [kg/s]
 L = width of wall cavity [m]
 M_w = molecular weight of water [kg/kmol]
 R_o = universal gas constant [J/kmol K]
 T_{mean} = mean temperature (Average of indoor and sheathing temperature) [K]
 z_i = lower zone height [m]
 z_j = upper zone height [m]

The integrated form of Equation 2.17 is

$$\dot{m} = -D_L L \frac{M_w}{R_o T} (P_{w,inlet} - P_{w,c}) \sum \frac{-2\sin\lambda_n}{d} \sin\left(\frac{\lambda_n x}{d}\right) \left(\frac{-wd^2}{D_L \lambda_n^2} \right) \left(\exp\left[-\frac{D_L \lambda_n^2 z_j}{wd^2}\right] - \exp\left[-\frac{D_L \lambda_n^2 z_i}{wd^2}\right] \right) \quad 2.18$$

where,

$$x = d$$

$$\lambda_n = \frac{(2n - 1)\pi}{2}, \quad n = 1, 2, 3, \dots$$

Equation 2.18 is the fundamental equation used to determine the amount of moisture depositing on the exterior sheathing.

For infiltration, $P_{w,inlet}$ is equal to the indoor vapour pressure which is usually larger than $P_{w,c}$ during the heating season. Hence, the mass deposition is positive because $(P_{w,inlet} - P_{w,c})$ is positive and the summation term is negative. Conversely, when

infiltration occurs, $P_{w,inlet}$ is the outdoor partial pressure and $P_{w,inlet}$ is generally less than $P_{w,c}$. As a result, mass deposition is negative. These trends agree with the fact that exfiltration deposits moisture and infiltration dries out the cavity. Equation 2.18 also demonstrates that \dot{m}_w decreases with distance away from the interior opening along the height of the cavity. (The summation term in the equation becomes smaller with larger values of z_i and z_j .) This corresponds with accepted knowledge that condensation is localized and the deposition is largest near the opening and decreases the further away from the inlet.

2.2.2. Region Of Validity For Wetwall

According to experimental results by Timusk and Doshi (1985), condensation tends to collect at the insulation/sheathing interface and not within the cavity. Following this, one of the fundamental constraints of the condensation model is that the region of validity precludes any indoor/outdoor relative humidity and temperatures which allow the vapour pressure within the cavity to be equal to or greater than the saturation pressure. If this situation occurs, then condensation takes place inside the insulation and the vapour pressure profiles predicted by Equation 2.16 are no longer valid. The condition of model validity is shown in Figure 2.7. Nickel (1991) investigated this limitation and determined a range of indoor relative humidity versus outdoor temperature for which the model is valid. Figure 2.8 shows the valid region to be the portion below the solid line and the invalid part above the curve. The shaded area in the figure is the region of relative humidity for typically homes as measured by Kent et al (1966).

2.3 DEVELOPMENT OF THE WALL MOISTURE DEPOSITION MODEL

The moisture deposition predicted by Wetwall is limited to the interior of the cavity because the model does not include the exchange of moisture between the exterior sheathing and the outdoor air. In order to capture the actual moisture deposition process more completely, Wetwall is coupled to a model for moisture diffusion across the exterior sheathing. A schematic of the coupling of the moisture transfer across the cavity with the moisture diffusion across the exterior sheathing is shown in Figure 2.9. A function based on Walker's (1993) simplification of the empirical relation developed by Cleary (1985) is used to relate the vapour pressure to the sheathing temperature and moisture content. The following sections detail the development of the moisture deposition model using a function relating vapour pressure, temperature, and moisture content of the exterior sheathing.

2.3.1 Moisture Content\ Vapour Pressure\ Temperature Relationship For Wood

The new model uses two separate functions to relate the moisture content, vapour pressure, and temperature at the sheathing for above and below freezing: Walker's (1993) simplification of the function developed by Cleary (1985) for temperatures above 273 K and a constant relative humidity relation for temperatures below 273 K. For temperatures above 273 K, the function for vapour pressure is shown below,

$$P_w = \frac{P_\infty}{0.622} \exp\left(\frac{T}{B_3}\right) (B_4 + B_5 MC + B_6 MC^2 + B_7 MC^3) \quad 2.19$$

where P_w = vapour pressure [Pa]
 P_∞ = atmospheric pressure [Pa]
 T = sheathing temperature [$^{\circ}\text{C}$]
 MC = wood moisture content [%wt]
 $B_3 = 15.8^{\circ}\text{C}$

$$\begin{aligned}
B_4 &= -0.0015 \\
B_5 &= 0.053 \\
B_6 &= -0.184 \\
B_7 &= 0.233
\end{aligned}$$

For temperatures below 273 K, the vapour pressure is described by the function below,

$$P_w = \left(\frac{P_\infty}{0.622} \right) \left(\frac{P_{w,s}}{P_{w,s}|_{T=273K}} \right) (B_4 + B_5 MC + B_6 MC^2 + B_7 MC^3) \quad 2.20$$

where $P_{w,s}$ = saturation vapour pressure [Pa]

Equation 2.20 contains no temperature term and the vapour pressure, P_w , is only weakly coupled to the temperature through the saturation vapour pressure, $P_{w,s}$

A plot of the empirical relation developed by Clearly (1985), shown in Figure 2.10, expresses the humidity ratio as a function of sheathing temperature and wood moisture content. The lower limit of the data on which the relation was based upon was at -1°C and the portion of the function below -1°C , shown in dotted lines, was determined from an extrapolation. Instead of using extrapolated values which continually decrease to about 5 %wt at 230 K, it was decided that it would be more reasonable if the maximum wood moisture content remained constant at the 273 K value for all temperatures below 273 K. Hence, the modified constant relative humidity function shown in Equation 2.20 is used. Figure 2.10 shows the difference between the extrapolated values and the constant relative humidity function.

2.3.2 Moisture Transport Model For Exterior Sheathing

In adding diffusion across the sheathing to Wetwall, it is necessary to couple a steady state mass transfer process with a transient one. The diffusion of moisture across

the cavity is much faster than that of the sheathing. According to Crank (1955), the time it takes water vapour to diffuse across the cavity is about two orders of magnitude smaller than that for water to diffuse across the sheathing. (A mass diffusivity of $2.56 \times 10^{-5} \text{ m}^2/\text{s}$ was used for diffusion across the cavity and $3 \times 10^{-10} \text{ m}^2/\text{s}$ for diffusion across the sheathing in the calculations.) Thus, combining the steady state mass diffusion across the cavity with the transient mass diffusion across the sheathing is a valid approach.

Several procedures were used to describe the transient diffusion process. Initially, an analytical solution for diffusion in a plane sheet with the conditions of constant surface concentrations was considered (Crank, 1955). Since the solution required the integral of the concentration profile from the previous time increment, the computation of the solution was too complicated to adapt to Wetwall. Hence, the analytical solution was discarded.

Since the analytical solution could not be easily coupled to Wetwall, an numerical approach was considered instead. A nodal network with the use of a finite difference approximation, similar to the modelling of attic sheathing by Walker (1993) was used. With this approach, the analytical solution of the mass transfer across the cavity is combined with a numerical solution for diffusion across the sheathing.

In the new model, the exterior sheathing, shown in Figure 2.11, was divided into four layers with the node located at the centre of each layer. The surface layer thickness is 1 mm and the interior layer thickness is 5.35 mm. Node 1 represents the sheathing surface on the cavity side. Since the node is only 0.05 mm from the surface, it can

respond quickly to the sudden moisture deposition from exfiltration or drying from infiltration. Nodes 2 and 3, further away from the surface, respond more slowly to the moisture diffusion in the interior of the sheathing. Node 4, the exterior surface, is assumed to have the same temperature and vapour pressure as the ambient conditions.

Since the transient diffusion in the exterior sheathing is now coupled to the steady state moisture transfer across the cavity, $P_{w,c}$ (vapour pressure at the sheathing surface) varies with time depending on the moisture diffusion in the sheathing. Its value is dependent on both the moisture transfer from the cavity and the moisture transfer to the other nodes in the sheathing. An overall mass balance is required to determine the vapour pressure at each node, except for Node 4.

The transient mass balance equation states that the rate of change of moisture at a node is equal to the summation of all the mass fluxes entering or leaving the node, ie.

$$\frac{dm}{dt} = \dot{m}_{in} - \dot{m}_{out} \quad 2.21$$

The rate of change of moisture can be expressed in terms of the wood moisture content according to Walker (1993) as,

$$\frac{dm}{dt} = \frac{d(m_{dwt}MC)}{dt} = m_{dwt} \frac{d(MC)}{dt} \quad 2.22$$

where m = mass of moisture at a node [kg]
 m_{dwt} = wood dry mass at a node [kg]
 MC = wood moisture content at a node [%wt]

Since moisture content depends on the vapour pressure and temperature, the rate of change of the wood moisture content at a node is expressed as,

$$\frac{dMC}{dt} = \frac{\partial MC}{\partial P_w} \Big|_T \frac{dP_w}{dt} + \frac{\partial MC}{\partial T} \Big|_{P_w} \frac{dT}{dt} \quad 2.23$$

For $T \geq 273.15$ K,

$$\frac{\partial MC}{\partial P_w} \Big|_T = \left(\frac{P_\infty}{0.622} \exp\left(\frac{T}{B_3}\right) (B_5 + 2B_6 MC + 3B_7 MC^2) \right)^{-1} \quad 2.24$$

$$\frac{\partial MC}{\partial T} \Big|_{P_w} = \left(-\frac{B_3}{(B_4 + B_5 MC + B_6 MC^2 + B_7 MC^3)} (B_5 + 2B_6 MC + 3B_7 MC^2) \right)^{-1} \quad 2.25$$

For $T < 273.15$ K,

$$\frac{\partial MC}{\partial P_w} \Big|_T = \left(\left(\frac{P_\infty}{0.622} \right) \left(\frac{P_{w,s}}{P_{w,s}|_{T=273K}} \right) (B_5 + 2B_6 MC + 3B_7 MC^2) \right)^{-1} \quad 2.26$$

The saturation pressure is expressed in the ASHRAE Book of Fundamentals (1989) as,

$$P_{w,s} = \exp(C_1 T^{-1} + C_2 + C_3 T + C_4 T^2 + C_5 T^3 + C_6 T^4 + C_7 \ln(T)) \quad 2.27$$

where $P_{w,s}$ = saturation pressure for water [Pa]

T = sheathing temperature [K]

$$C_1 = -5674.536$$

$$C_2 = 6.392525$$

$$C_3 = -9.677843E-03$$

$$C_4 = 6.221157E-07$$

$$C_5 = 2.074783E-03$$

$$C_6 = -9.484024E-13$$

$$C_7 = 4.163502$$

Thus,

$$\frac{\partial MC}{\partial T} \Big|_{P_w} = \left(\frac{\partial T}{\partial P_{w,s}} \Big|_{P_w} \right)^{-1} \left(\frac{\partial P_{w,s}}{\partial MC} \Big|_{P_w} \right)^{-1} \quad 2.28$$

where,

$$\left. \frac{\partial T}{\partial P_{w,s}} \right|_{P_w} = \left(P_{w,s} \left(-C_1 T^{-2} + C_3 + 2C_4 T + 3C_5 T^2 + 4C_6 T^3 + \frac{C_7}{T} \right) \right)^{-1} \quad 2.29$$

$$\left. \frac{\partial P_{w,s}}{\partial MC} \right|_{P_w} = -0.622 P_{w,s}|_{T=273K} \left(\frac{P_w}{P_\infty} \right) \frac{(B_5 + 2B_6 MC + 3B_7 MC^2)}{(B_4 + B_5 MC + B_6 MC^2 + B_7 MC^3)^2} \quad 2.30$$

The vapour pressure in Equation 2.30 is defined by Equation 2.20.

A mass balance across the sheathing is performed to obtain three equations for the three unknown vapour pressures in each zone. The rate of change of moisture at j^{th} node, m_j , is equal to the difference in the mass transfer at the j^{th} node from the $(j-1)^{\text{th}}$ node, $\dot{m}_{j-1,j}$, and from $j+1^{\text{th}}$ node, $\dot{m}_{j,j+1}$. The mass balance equations at each node are

$$\text{Node 1:} \quad \frac{dm_1}{dt} = \dot{m}_{\text{cavity},1} - \dot{m}_{1,2} \quad 2.31$$

$$\text{Node 2:} \quad \frac{dm_2}{dt} = \dot{m}_{1,2} - \dot{m}_{2,3} \quad 2.32$$

$$\text{Node 3:} \quad \frac{dm_3}{dt} = \dot{m}_{2,3} - \dot{m}_{3,4} \quad 2.33$$

Using the Equations 2.23 to 2.28 and noting that the mass transfer across the sheathing is purely diffusive, the above nodal equations can be written more precisely as,

Node 1:

$$m_{dw1} \left(\frac{\partial MC_1}{\partial P_w} \frac{dP_{w1}}{dt} + \frac{\partial MC_1}{\partial T} \frac{dT_1}{dt} \right) = \frac{-D_f L}{R_w T_{\text{mean } z_1}} \int_{z_1}^{z_j} \frac{\partial P_{w1}}{\partial x} \bigg|_{x=d} \partial z \quad 2.34$$

$$- \frac{-D_w A}{\Delta x_{1,2} R_w T_2} \left(P_{w2} - \frac{T_2}{T_1} P_{w1} \right)$$

where D_1 = mass diffusivity of water vapour through glass fibre [m^2/s]
 D_w = mass diffusivity of water through wood [m^2/s]
 L = width of cavity [m]
 A = area of the zone [m]
 R_w = gas constant for water [J/kg K]
 $\Delta x_{1,2}$ = distance between node 1 and node 2 [m]
 P_{w1} = vapour pressure at node 1 [Pa]
 P_{w2} = vapour pressure at node 2 [Pa]
 T_{mean} = average temperature between the inside and sheathing surface [K]
 T_1 = temperature at node 1 [K]
 T_2 = temperature at node 2 [K]
 z_i = lower zone height [m]
 z_j = upper zone height [m]

It is important to note that with the mass balance equations, $P_{w,1} = P_{wc}$ and $P_{w,1}$ has replaced P_{wc} in the subsequent equations.

Node 2:

$$m_{dw2} \left(\frac{\partial MC_2}{\partial P_w} \frac{dP_{w2}}{dt} + \frac{\partial MC_2}{\partial T} \frac{dT_2}{dt} \right) = \frac{-D_w A}{\Delta x_{1,2} R_w T_2} \left(P_{w2} - \frac{T_2}{T_1} P_{w1} \right) - \frac{-D_w A}{\Delta x_{2,3} R_w T_3} \left(P_{w3} - \frac{T_3}{T_2} P_{w2} \right) \quad 2.35$$

where $\Delta x_{2,3}$ = distance between node 2 and node 3 [m]
 P_{w3} = vapour pressure at node 3 [Pa]
 T_3 = temperature at node 3 [K]

Node 3:

$$m_{dw3} \left(\frac{\partial MC_3}{\partial P_w} \frac{dP_{w3}}{dt} + \frac{\partial MC_3}{\partial T} \frac{dT_3}{dt} \right) = \frac{-D_w A}{\Delta x_{2,3} R_w T_3} \left(P_{w3} - \frac{T_3}{T_2} P_{w2} \right) - \frac{-D_w A}{\Delta x_{3,4} R_w T_4} \left(P_{w4} - \frac{T_4}{T_3} P_{w3} \right) \quad 2.36$$

where $\Delta x_{3,4}$ = distance between node 3 and node 4 [m]
 P_{w4} = vapour pressure at node 4 [Pa]

T_4 = temperature at node 4 [K]

The vapour pressure and temperature at node 4 are equal to the ambient conditions (P_∞ and T_∞).

The time derivatives for the i^{th} hour in the mass balance equations, Equations 2.34 to 2.36, are found by using a backward difference approximation so that

$$\frac{dP_{w,j}^i}{dt} = \frac{P_{w,j}^i - P_{w,j}^{i-1}}{\tau} \quad 2.37$$

$$\frac{dT_j^i}{dt} = \frac{T_j^i - T_j^{i-1}}{\tau} \quad 2.38$$

With the finite difference approximation, the differential equations become a system of linear first order equations with τ as a fixed interval of one hour. With the appropriate time indices, the discretized equations become:

Node 1:

$$\begin{aligned} m_{dwr1} \left(\frac{\partial MC_1^{i-1}}{\partial P_w} \frac{P_{w1}^i - P_w^{i-1}}{\tau} + \frac{\partial MC_1^{i-1}}{\partial T} \frac{T_1^i - T_1^{i-1}}{\tau} \right) &= -D_I L \frac{M_w}{R_o T_{mean}} (P_{w,inlet}^i - P_{w,1}^i) \\ &\sum \frac{-2\sin\lambda_n}{d} \sin\left(\frac{\lambda_n x}{d}\right) \left(\frac{-wd^2}{D\lambda_n^2} \right) \left(\exp\left[-\frac{D\lambda_n^2 z_j}{wd^2}\right] - \exp\left[-\frac{D\lambda_n^2 z_i}{wd^2}\right] \right) \\ &- \frac{-D_w A}{\Delta x_{1,2} R_w T_2^i} \left(P_{w2}^i - \frac{T_2^i}{T_1^i} P_{w1}^i \right) \end{aligned} \quad 2.39$$

Node 2:

$$m_{dw2} \left(\frac{\partial MC_2^{i-1}}{\partial P_w} \frac{P_{w2}^i - P_{w2}^{i-1}}{\tau} + \frac{\partial MC_2^{i-1}}{\partial T} \frac{T_2^i - T_2^{i-1}}{\tau} \right) =$$

$$\frac{-D_w A}{\Delta x_{1,2} R_w T_2^i} \left(P_{w2}^i - \frac{T_2^i}{T_1^i} P_{w1}^i \right) - \frac{-D_w A}{\Delta x_{2,3} R_w T_3^i} \left(P_{w3}^i - \frac{T_3^i}{T_2^i} P_{w2}^i \right) \quad 2.40$$

Node 3:

$$m_{dw3} \left(\frac{\partial MC_3^{i-1}}{\partial P_w} \frac{P_{w3}^i - P_{w3}^{i-1}}{\tau} + \frac{\partial MC_3^{i-1}}{\partial T} \frac{T_3^i - T_3^{i-1}}{\tau} \right) =$$

$$\frac{-D_w A}{\Delta x_{2,3} R_w T_3^i} \left(P_{w3}^i - \frac{T_3^i}{T_2^i} P_{w2}^i \right) - \frac{-D_w A}{\Delta x_{3,4} R_w T_4^i} \left(P_{w4}^i - \frac{T_4^i}{T_3^i} P_{w3}^i \right) \quad 2.41$$

The unknowns in the equations are $P_{w,1}$, $P_{w,2}$, and $P_{w,3}$. The inlet vapour pressure, $P_{w,inlet}$, is the indoor vapour pressure for exfiltration and outdoor vapour pressure for infiltration. From the equations above, the moisture content from the previous hour at each node is used to evaluate the nodal vapour pressure for the current hour. Equations 2.39 to 2.41 are the fundamental mass balance equations in the new model.

As previously mentioned, the sheathing is divided into a fixed number of distinct zones along the height of the cavity. The mass deposition in each zone is calculated, therefore, Equations 2.39 to 2.41 are solved for each zone. In addition, it is important to note that the vapour pressure for the entire sheathing surface is constant. The surface

vapour pressure, which is the vapour pressure at node 1, is based on the moisture content in the zone closest to the interior opening for exfiltration and zone closest to the exterior opening for infiltration.

2.3.3 Calculation of the Amount of Condensation

As shown in the previous section, a system of three equations with three unknowns must be solved to determine the vapour pressure at each node. The vapour pressures are then substituted back into the nodal equations to evaluate the mass transfer. The accumulated mass at each node is expressed as a ratio of mass of moisture deposition to the dry weight yielding the moisture content in the sheathing.

The evaluation of the vapour pressures requires an iterative process. A bi-sectional method was chosen over a Gaussian Elimination scheme because of the prescribed constraint that the vapour pressure cannot exceed the saturation pressure at each node. The nodal vapour pressure reaches saturation if the moisture content at the node is equal to or greater than the maximum moisture content. Hence, whenever a node is saturated, the corresponding vapour pressure is no longer an unknown, but instead, it assumes the value of the saturation pressure. This would lead to an inconsistent set of equations for Gaussian elimination with three equations and less than three unknowns. An iterative approach is used instead. In the bi-sectional scheme, the number of equations is reduced whenever a node is saturated because the mass balance equation associated with the saturated node is eliminated. The iterative process continues until convergence reaches 0.01 Pa for all three nodes.

The moisture content at each node is based on the accumulated mass deposition

over time. Each node has a minimum moisture content of 6% which is the lower limit of Equations 2.19 and 2.20. Beginning at a moisture content of 6%, the wood sheathing absorbs all mass deposition until the wood is saturated at the maximum moisture content. Once the node is saturated, subsequent mass accumulation is treated as surface deposition. At node 1, the surface deposition is considered as moisture on the surface of the sheathing and at the interior nodes, node 2 and node 3, the surface deposition is regarded as free moisture within the cells of the wood. (Moisture below saturation point is stored within the cell walls and excess moisture above saturation point is stored within the cell body of wood.) If the mass transfer for the current hour is added to the accumulated mass and the new accumulated mass exceeds the maximum moisture content, then the nodal vapour pressure is set at the saturation pressure and the mass deposition is separated into moisture content within the wood and surface accumulation. The vapour pressure for the now saturated node is then substituted back into the nodal equations to solve for new vapour pressures at the other nodes.

Since mass deposition can be negative as well as positive, the case of a negative surface accumulation also occurs. If a negative mass transfer for the current hour is greater than the surface accumulation, the amount of negative mass transfer in excess of the surface accumulation is removed from within the wood. The node would no longer be saturated and hence, a new vapour pressure can be calculated with the moisture content/vapour pressure/temperature function (Equation 2.19 for temperature above 237 K and Equation 2.20 for temperature below 273 K). The new vapour pressure and moisture content for the node are substituted back into the mass balance equations and

the vapour pressures at the other nodes are determined through iteration again.

Also, due to the variation of the maximum moisture content limit with temperature, a new limit is evaluated at the start of each hour. If the sheathing moisture content exceeds the saturation limit due to a temperature change, the free moisture is added to the surface deposition. Conversely, if the saturation limit is increased, the surface deposition is converted back to internal moisture and a new moisture content is determined. The moisture content and surface deposition are adjusted at each node before the calculation of the vapour pressures for the current hour.

In the new model, a total of five zones are designated on the surface of the sheathing. Each zone, with a height of 0.0381 m, spans the entire width of the cavity. The zones are situated along the height of the cavity corresponding to the location of the sensors in the experiment. The coordinates of the zones are shown in Figure 2.12. Figure 2.12 shows that zone 1 is closest to the interior opening, hence the vapour pressure for the sheathing which is equal to the vapour pressure at node 1, P_{w1} , is based on the moisture content in zone 1 for exfiltration. Similarly, zone 5 is closest to the exterior opening and therefore, the sheathing vapour pressure is based on the moisture content in zone 5 for infiltration. The vapour pressure at the sheathing surface, P_{w1} , is constant for the entire surface.

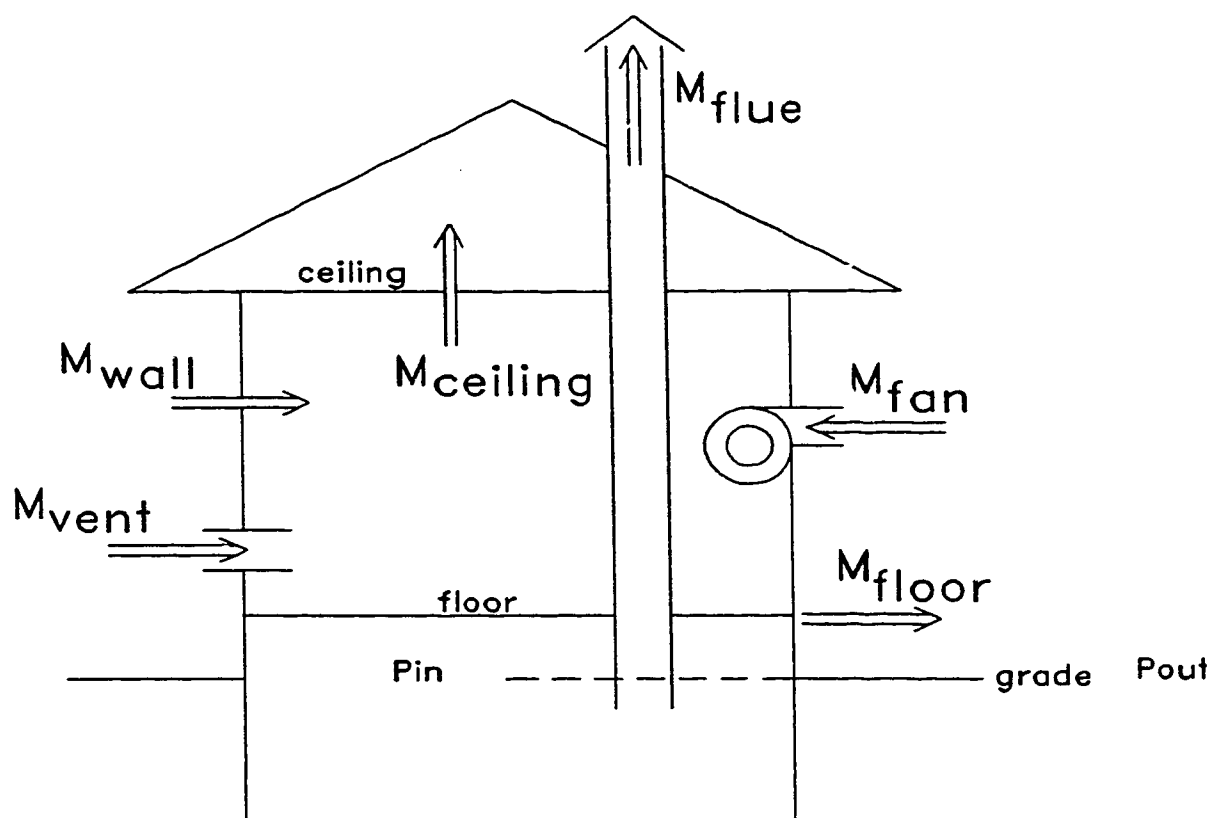


Figure 2.1: Schematic of the typical mass flows through the single zone in Local Leaks (Walker 1993)

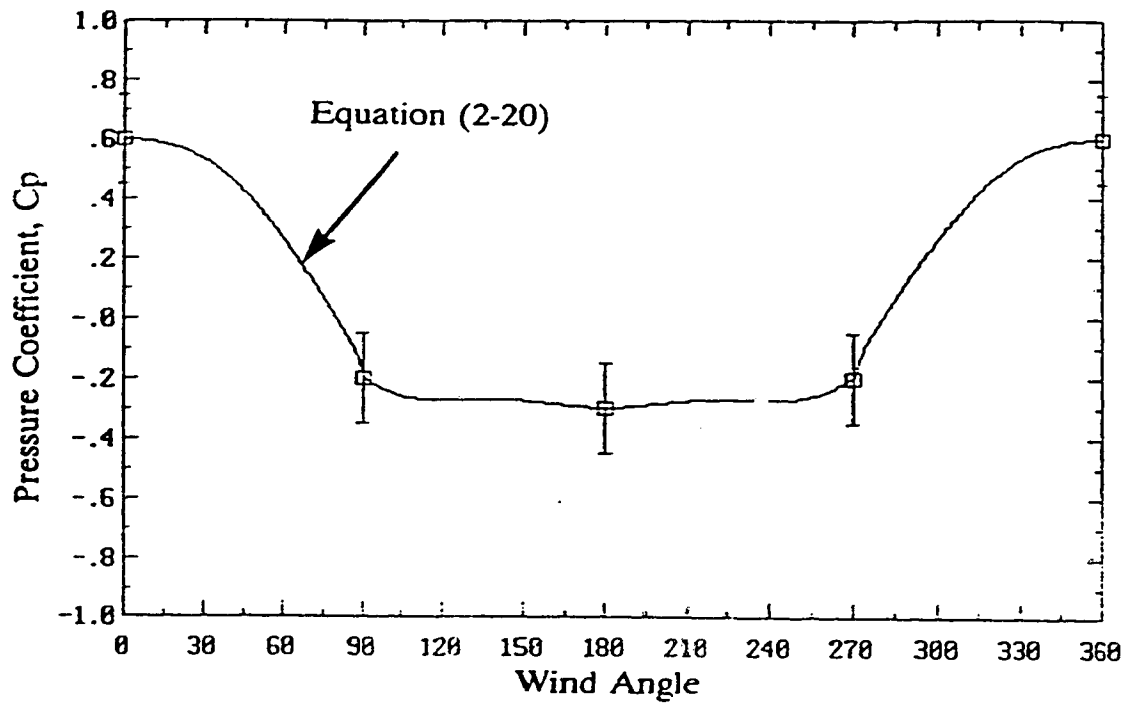


Figure 2.2: Variation of wall pressure coefficient with wind angle (graph from Walker 1993)

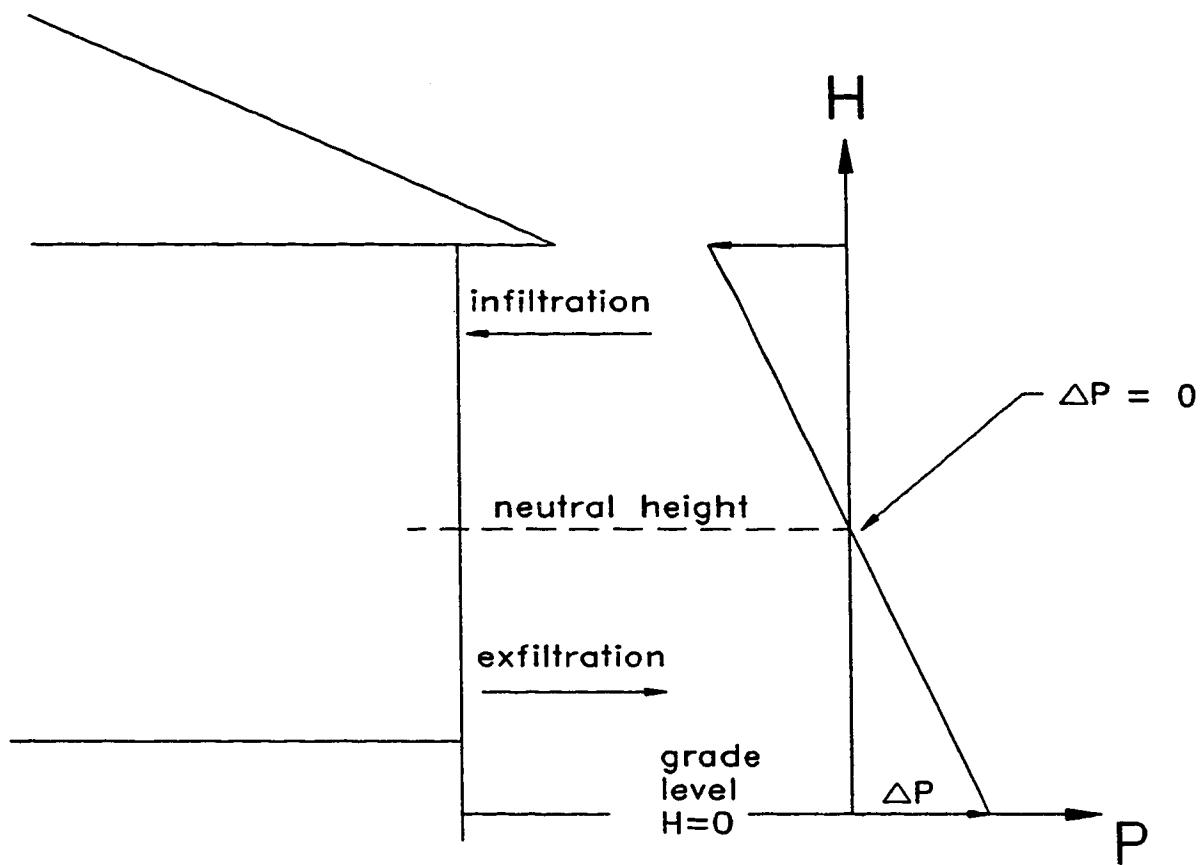


Figure 2.3: Indoor/outdoor pressure difference across wall

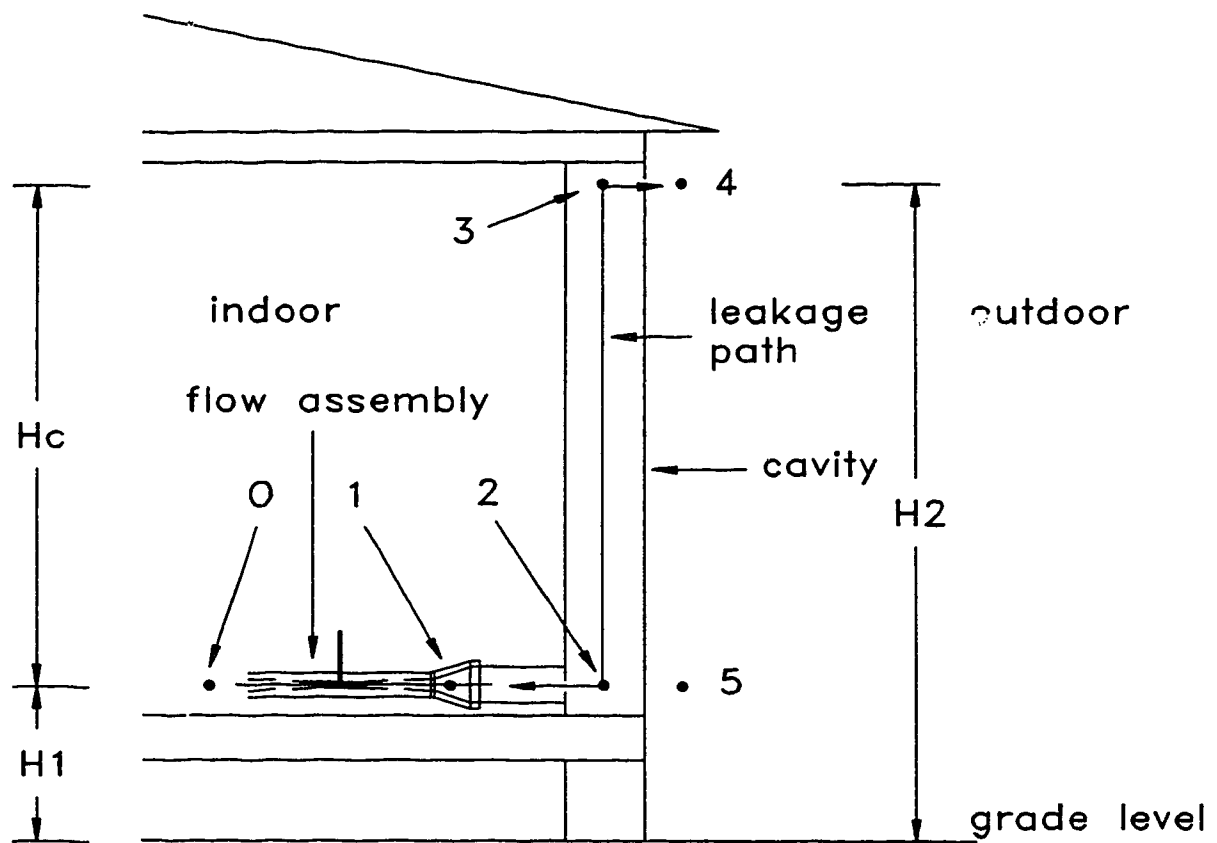


Figure 2.4: Location of the flow assembly and reference points for flow measurement

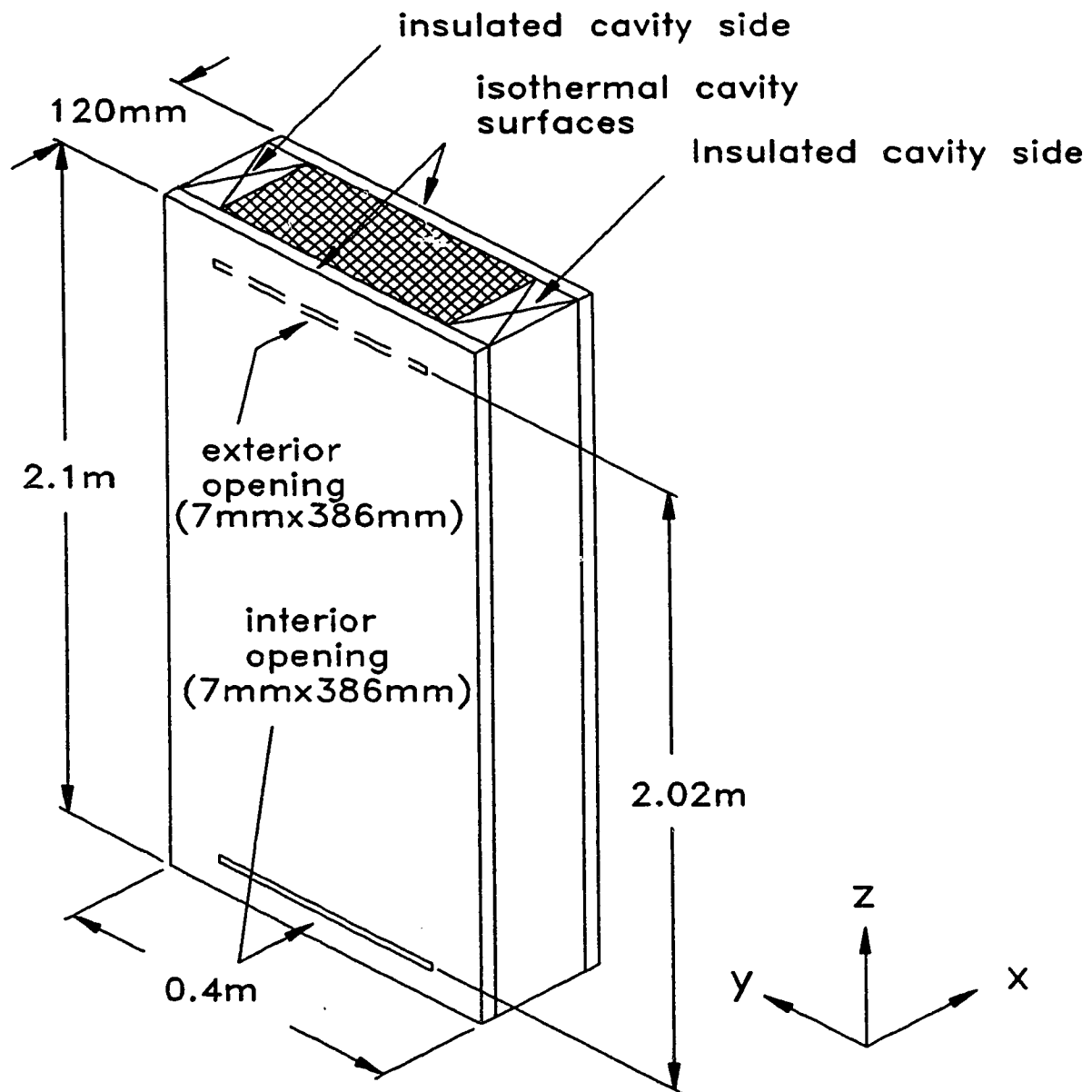


Figure 2.5: Schematic of the idealized cavity in Wetwall

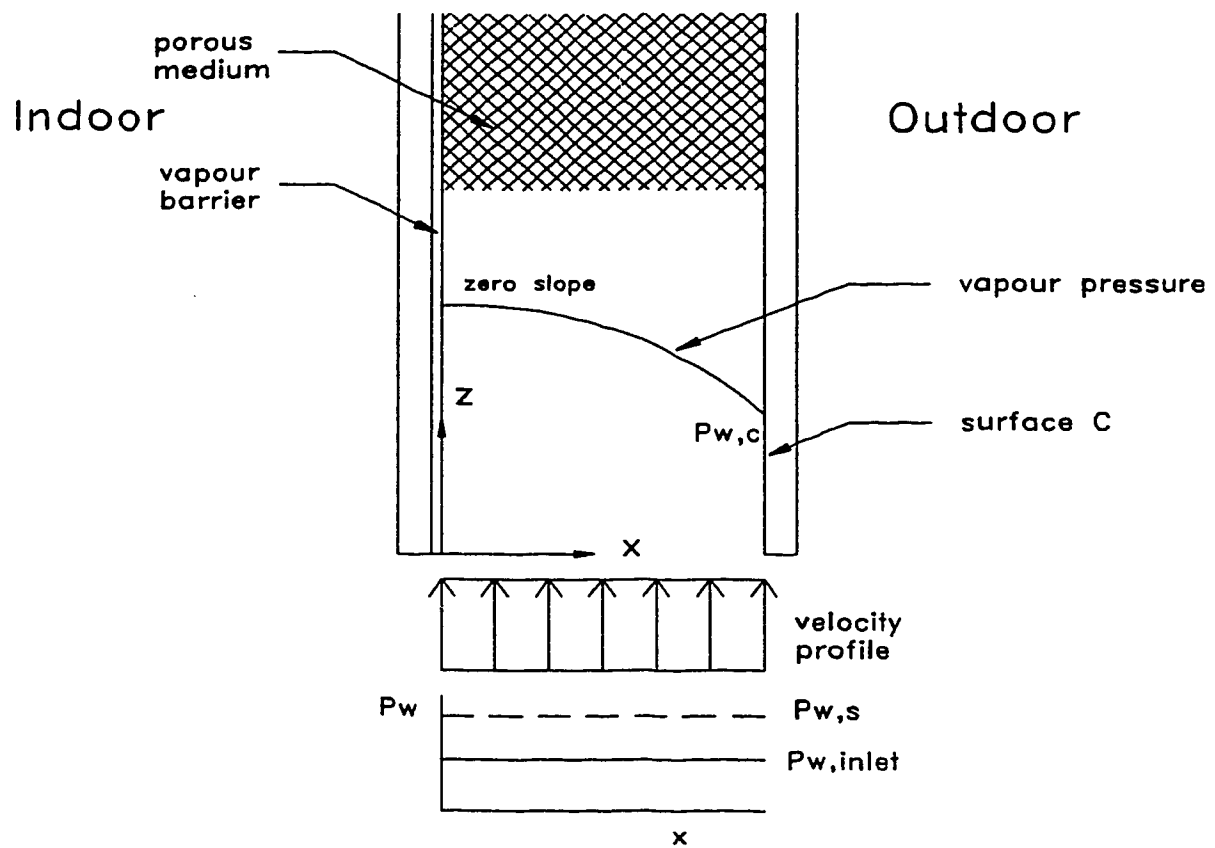


Figure 2.6: Cross section of the idealized cavity showing the vapour pressure and velocity profiles

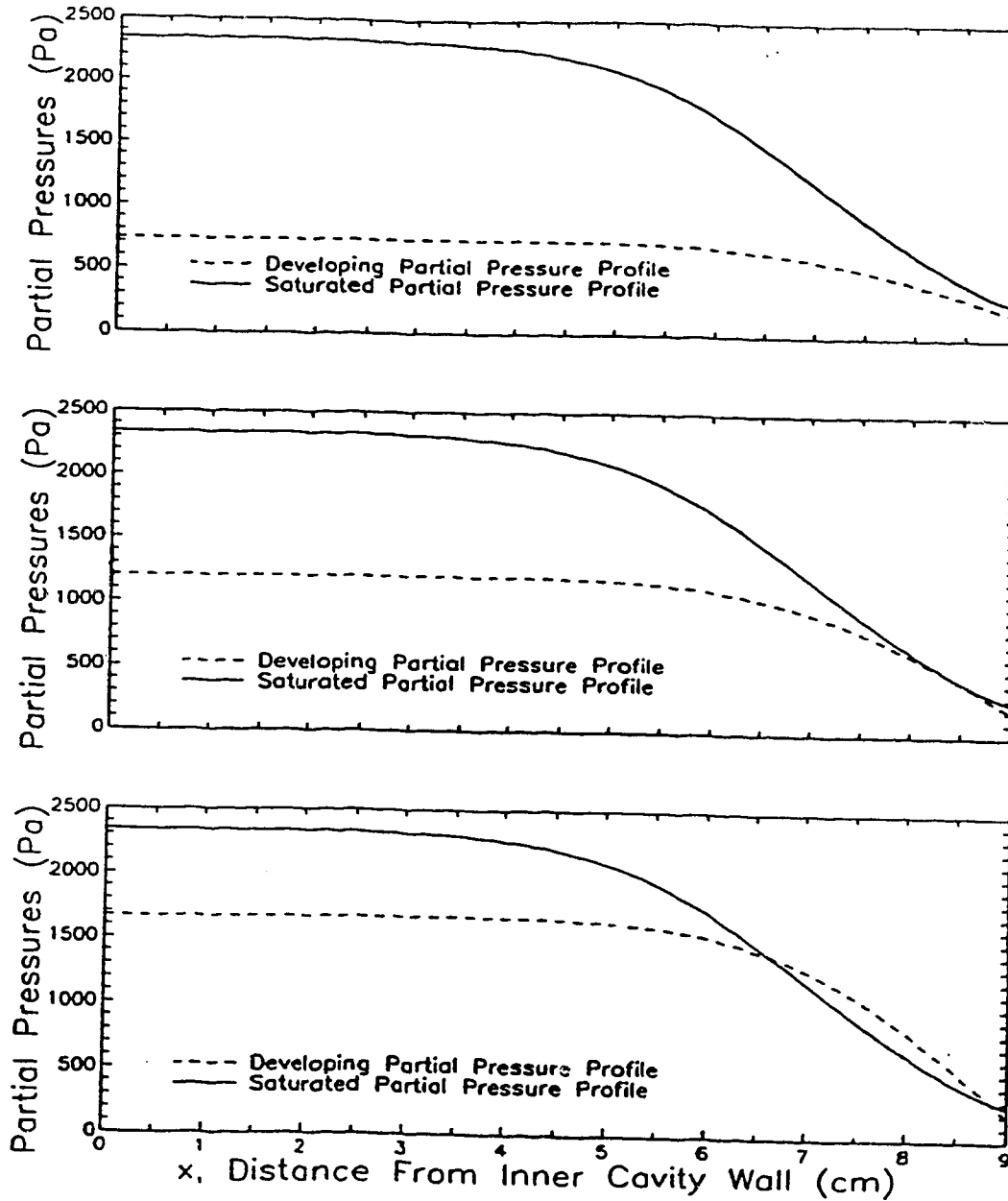


Figure 2.7: Top figure shows no condensation; middle figure shows the vapour pressure profiles just touching but condensation is considered to occur; and bottom figure indicates condensation with the insulation (Nikel 1991).

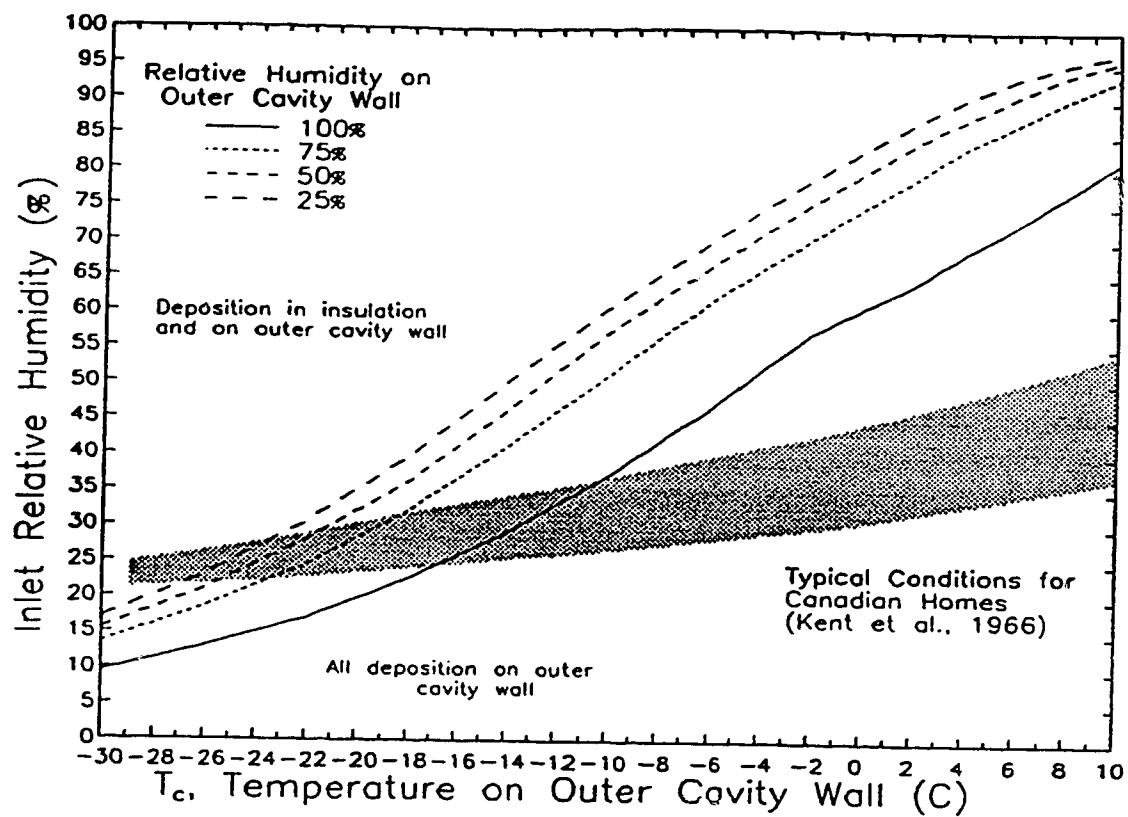


Figure 2.8: Region of validity for Wetwall showing the inlet relative humidity and indoor/outdoor temperature difference as determined by Nikel (1991). The dark region shows typical indoor conditions for Canadian homes (Kent et al. 1966).

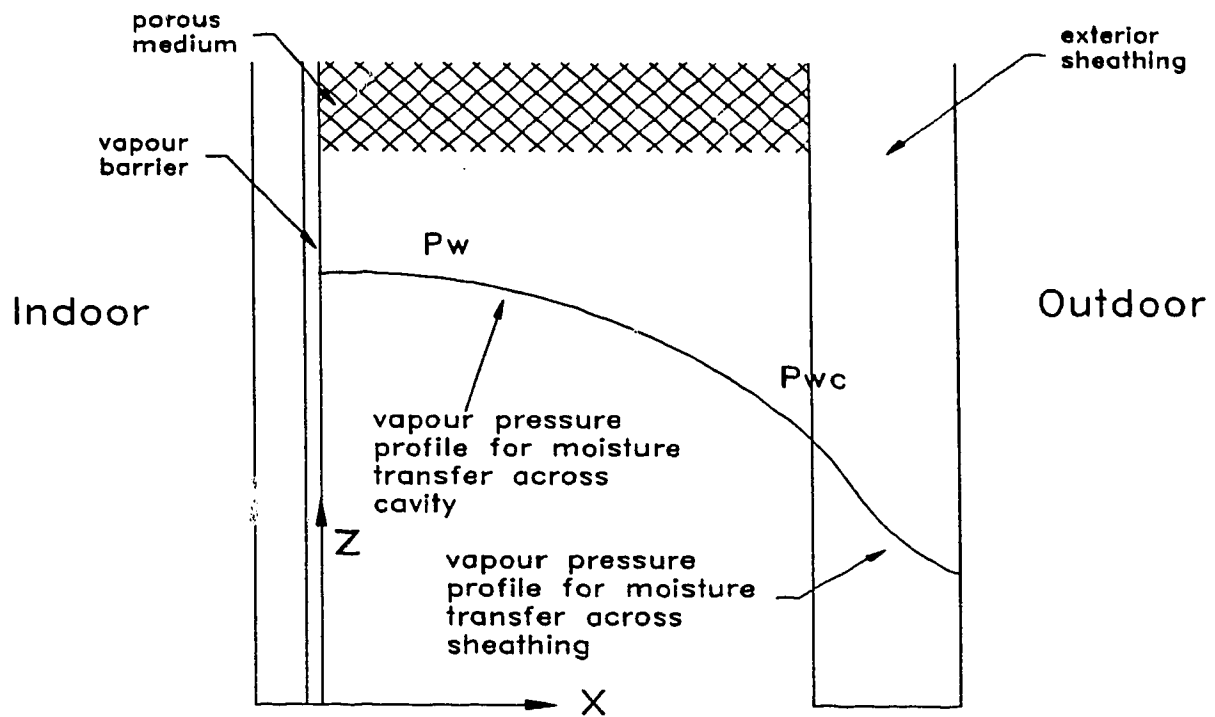


Figure 2.9: Cross section of wall cavity showing the vapour pressure profile across the cavity and exterior sheathing

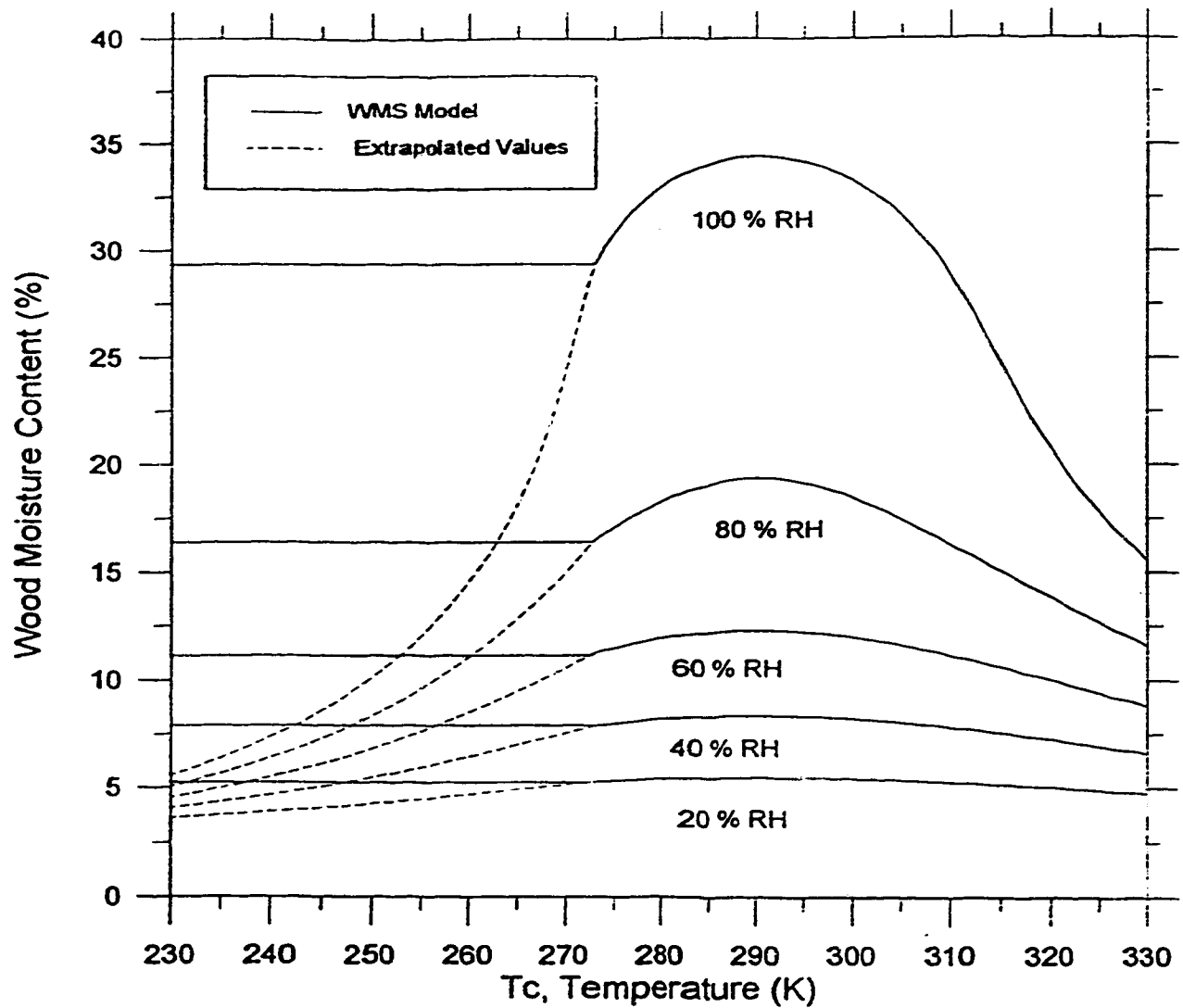


Figure 2.10: Plot of Cleary's (1985) function based on empirical data for temperatures above 272 K and extrapolation for temperatures below 273 K and constant relative humidity function for temperatures below 273 K (figure taken from McRae 1995)

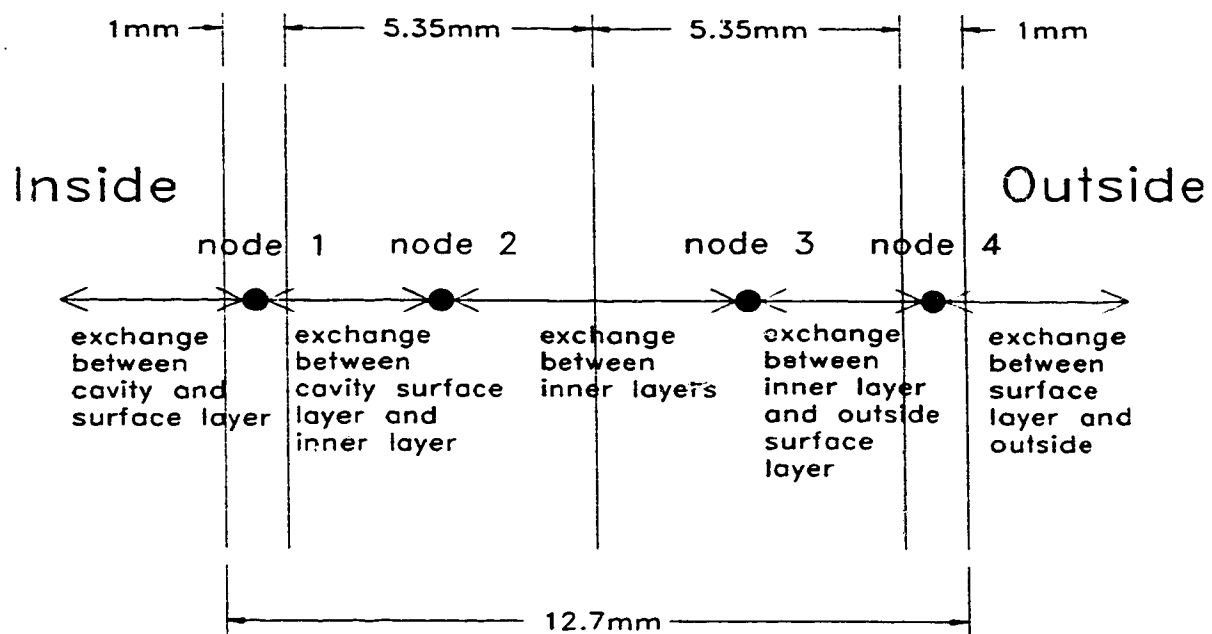


Figure 2.11: Nodal network for diffusion across the sheathing

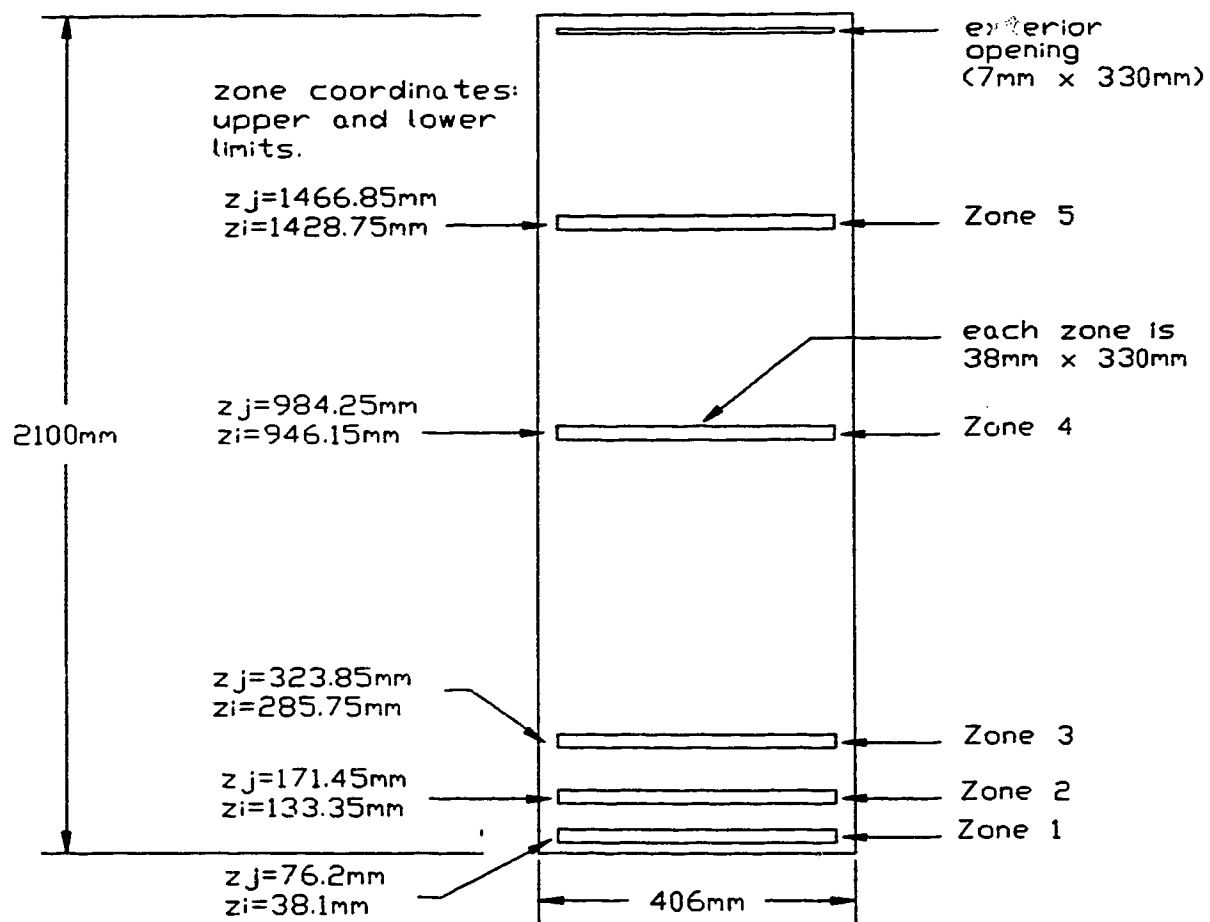


Figure 2.12: Schematic of exterior sheathing showing the upper and lower zone coordinates in Wetwall

CHAPTER 3

EXPERIMENTAL METHODS

A field experiment was initiated to collect ventilation and condensation data for the validation of the models Local Leaks and Wetwall. In order to incorporate the effects of the dynamics of the weather on air leakage and condensation, a test cavity was installed in a single story test house located on the Alberta Home Heating Research Facility (AHHRF) where the wind speed, wind direction, along with indoor/outdoor conditions such as temperature and relative humidity were monitored. The emphasis was to obtain measurements which could be used to verify air leakage flow rates predicted by Local Leaks and sheathing moisture content predicted by Wetwall. The experiment was conducted continuously over two heating seasons yielding approximately 10700 hours of data. With this large data base, the model predictions for air leakage and moisture deposition can be evaluated over a wide range of conditions. This chapter presents a description of the test facility, test cavity, instrumentation, and experimental procedure.

3.1 DESCRIPTION OF THE TEST SITE

The field experiment was conducted at the Alberta Home Heating Research Facility (AHHRF) which is located on the south side of Edmonton. The facility consists of six single storey test houses situated on a flat exposed field. The test houses are oriented in a closely spaced east-west row configuration with a separation of approximately 2.6 m between each house. False end walls, 3.7 m in height, are located next to the east and west end houses to provide wind shelter and shading similar to that created by adjacent houses in a closely spaced row. Details of the construction of the

test houses are outlined by Gilpin et. al. (1980).

The last house on the east end of the row, house 6, was used for the experiment. House 6, shown in Figure 3.1, has a floor area of 46 m² which is about 1/2 to 1/3 that of a typical house. It contains sliding windows, a fixed window unit, regular soffits, a door, a flue, a pitched roof, and a full concrete poured basement similar to a typical bungalow. The exterior walls of the house consist of stained plywood exterior siding, glass fibre insulation with a thermal resistance value of 2.2 RSI, vapour barrier on the warm side of the cavity, and painted gypsum board on the inside. A photograph of the exterior of the house is shown in Figure 3.2.

The flue in house 6 is a 6 m long, standard 152 mm ID double walled sheet metal pipe which begins about 1.45 m above the basement floor. The top of the flue was fitted with a rain cap and the bottom was blocked during the experiment except for a 600 hour period when a supply fan was attached to the flue bottom to draw air in. Figure 3.3 shows the location of the supply fan and flue assembly with respect to grade level.

The interior of the test house is not partitioned and the main floor and the basement are connected by an open stairwell. The non-partitioning helps the mixing of air which allows the living space to be treated as a single zone. The inside of the house is heated electrically and a fan is used to circulate the warm air. The fan operates continuously recirculating the air at a rate of 4.5 house interior volumes per hour (Wilson and Walker 1991a).

3.2 DESCRIPTION OF THE TEST CAVITY AND INSTRUMENTATION

The test cavity used in the field experiment was identical to the idealized wall

cavity in Wetwall and was constructed to match the characteristics of a typical wall. It is an instrumented, stand-alone portable wall cavity which fits into a 0.44 m x 2.10 m cavity opening of an exterior wall of the house.

The test cavity has a nominal width of 0.40 m, depth of 0.1 m and height of 2.1 m. The cavity, shown in Figure 3.4, was composed of a 12.7 mm gypsum board on the inside, 0.012 mm polyethylene vapour barrier on the warm side of the cavity, glass fibre batts insulation with a thermal resistance of 2.2 RSI in the cavity interior, and 12.7 mm pine sheathing on the outside. Pine sheathing was chosen instead of plywood siding because its material properties are homogeneous through its thickness (unlike plywood which consists of layers of wood glued together). The sheathing was made of two pieces of 12.7 mm pine glued together and cut inside the proper size. The sides of the cavity were constructed with 41 mm x 92 mm spruce wood studs.

The leakage sites in the cavity are similar to the ones in the model with one 7 mm x 145 mm slot located on the exterior sheathing at the top of the cavity and one on the interior surface near the floor. For exfiltration, the leakage path is from the interior opening up through the cavity interior and out across the exterior opening. For infiltration, the direction of the flow is reversed where the entrance is the exterior opening and exit is the interior opening. Any air leakage must enter and exit through the prescribed openings because the sides of the cavity, top header, base, and space between the vapour barrier and the gypsum board at the interior opening were sealed with silicon. The two slots simulate typical cracks which may exist at the base of the wall on the inside and top of the wall on the outside.

The interior of the cavity was instrumented with sensors to measure moisture deposition, temperature, and relative humidity. For moisture deposition along the height of the cavity, moisture pins and surface moisture sensors were placed in designated zones on the inside surface of the exterior sheathing. Each zone, 38 mm x 330 mm, contained three sets of moisture pins and a single surface sensor. As shown in Figure 3.5, two sets of moisture pins were located close to the outer portion of the zone and one set was placed just off of the centre. The single surface sensor was located at the centre of the zone.

The cavity contains a total of five zones. Zone 1, shown in Figure 3.6, is located directly opposite the interior leakage site; zone 2 and zone 3 are situated immediately above zone 1. Zone 4 and zone 5 are located further up along the cavity at 1/2 and 3/4 cavity height respectively. The upper and lower zone height coordinates are shown in Figure 3.6. The first three zones were designed to be situated close to the bottom opening to capture the majority of the moisture deposition because condensation typically forms near the leakage site.

The interior of the cavity was further instrumented with five rows and five columns of thermocouples, shown in Figure 3.7, to measure the temperature along the cavity height and depth. A column of thermocouples was placed along the glass fibre batt surface underneath the vapour barrier and another was installed flush with the cavity side surface of the exterior sheathing. The remaining columns of thermocouples were spaced evenly at 22 mm intervals. The rows of thermocouples, shown in Figure 3.7, span the cavity vertically at 1/4 cavity height intervals where the top and bottom rows

are at the same height as the interior and exterior openings. The thermocouples were used to measure the temperature at the mid-width of the cavity.

Five relative humidity sensors, shown in Figure 3.8, were also placed inside the cavity to monitor the vapour pressure along the height of the cavity. They were located at the same vertical positions as the rows of thermocouples and also measure the relative humidity at the mid-width of the cavity. Figure 3.9 shows the interior of the cavity during construction with the moisture pins, surface sensors, thermocouples and relative humidity sensors in place.

The air leakage across the cavity was measured with an orifice-flow anemometer assembly fitted over the interior opening of the cavity. The assembly was calibrated to measure the volumetric flow rate for infiltration and exfiltration across the cavity. Measured rates of infiltration and exfiltration were averaged separately for each hour to produce overall time weighted hourly values. Further details on the flow assembly including calibration procedures are presented later in Section 3.3.6.

3.3 MEASUREMENTS AND INSTRUMENTATION

3.3.1 Moisture Content

The moisture deposition on the exterior sheathing can be separated into moisture within the wood and surface accumulation. The internal wood moisture is typically expressed in terms of the wood moisture content which is the fraction of the mass of water in the wood to the mass of the oven dried wood, usually referred to as the dry weight. The surface deposition is the free moisture which forms on the sheathing surface when the internal wood moisture content is equal to or greater than the wood moisture

saturation limit.

The wood moisture content is inferred from the change in the electrical resistance of the wood between two stainless steel pins which are driven into the sheathing. A calibrated wood moisture meter (Lignometer) is used to measure the change in the resistance which indicates moisture content values. The pins, 3 mm in diameter and 6 mm in length, are driven into the sheathing to a depth of 9.35 mm from the interior surface and positioned laterally on the sheathing 31.8 mm apart centre to centre. The exposed ends of the pins are sealed with epoxy glue to prevent any surface moisture from affecting the measurement. Fifteen pairs of pins were placed on the sheathing with three pairs located in each of the five zones. The moisture content in each zone is the average value of the three sets of pins. The typical variation of the readings between the three sets of pins is approximately 4 %wt.

The lead wires from the stainless steel pins were extended from the cavity to the moisture meter with shielded cables which were grounded to eliminate noise on the output signal. (Even though the moisture meter is a DC device, the long cables acted as an antenna which picked up AC noise from the relay board and computer.) The output signal was also amplified which further attenuated the AC noise. Another concern was the storage of electrical charge in the wood from repeat measurements. This effect was minimized by alternating the polarity of the input signal and short circuiting the pins after each reading.

The wood moisture meter was calibrated with samples of the pine sheathing according to ASTM D4442-92 (1992) and ASTM D4444-92 (1992). The range of the

wood moisture meter is from 6 %wt to 35 %wt and the accuracy is about ± 1.5 %wt for moisture contents below 15 %wt and ± 0.5 %wt for values above 15 %wt based on calibration results discussed in Appendix A. The higher accuracy at larger moisture content values is the result of the non-linear relation between the moisture content and resistance in the wood (Siau 1984) where resistance is low for wood with high moisture content and high for dry wood. The calibration, outlined in Appendix A, was conducted with the same cable length as in the experiment and with alternating polarity of the input signal.

It is important to note that the moisture meter measurements are sensitive to temperature such that a temperature change at a given moisture content would yield a difference in the reading. To account for this, all the measurements were corrected with an empirical factor determined by Pffaf and Garrahan (1986) for the temperature of the measurement which is different from the temperature of calibration.

The presence of surface deposition in the form of water, frost, or ice is detected in a similar manner to the moisture content measurement. The surface sensor, shown in Figure 3.10, is an extremely fine interwoven wire grid mounted on a 70 mm x 120 mm, 2 mm thick substrate which is impervious to moisture. The interwoven grid is composed of 0.025 mm thick circuit traces which are spaced 0.127 mm apart. When there is no surface deposition, the grid is an open circuit and when moisture is present, the grid is a closed circuit. The variation in the resistivity between the wires of the grid is used to determine the different forms of surface deposition. The same moisture meter is used to measure the change in resistivity.

During calibration tests, it was found that the surface sensor-moisture meter system can only be used to measure deposition qualitatively. It is difficult to determine the amount of ice, frost, or water, because of the range of resistivity for which a meter must span is large. If water is present, the resistivity level is low, on the order of 10^4 ohm-cm. Conversely, if frost or ice is present, the resistivity is high, close to that of an open circuit, on the order of 10^{17} ohm-cm. The Lignometer was used because it was the only meter readily available which has a wide operational resistance range. Ideally, a meter with a large range and high resolution would define the surface deposition more quantitatively. The Lignometer produced an output voltage signal which was calibrated in terms of wood moisture content. For the surface sensor output, an open circuit produces an output of 0.2 V to 0.75 V, presence of frost or ice yields a signal of about 0.9 V to 1.0 V, and water gives an output of 2.375 V. The calibration results of the Lignometer with moisture pins and surface sensors are shown in Appendix A.

3.3.2 Relative Humidity

Polymer film capacity sensors (General Eastern RH-6) were used to measure the relative humidity inside the cavity, in the house, and on the outside. The sensors were observed to fail under prolonged contact with moisture because the polymer film was susceptible to damage. This led to rapid deterioration of the sensor accuracy. The humidity sensors, which produced a linearized output, were calibrated with constant relative humidity solutions. The accuracy of the sensors from calibration is $\pm 6\%$ relative humidity from the true value. The complete calibration results are shown in Appendix A.

3.3.3 Temperature

Type T, copper-constantan thermocouples were used for all temperature measurements. For measurements within the glass fibre insulation, the thermocouples were placed inside 3.2 mm OD, thin wall stainless steel tubes and then the tubes were inserted into the insulation. According to the manufacturer specifications, the accuracy is +/- 1°C of the true value.

3.3.4 Wind Speed and Direction

The wind speed was measured with a cup anemometer and the direction is determined with a rotating vane (Windflow 540 - Athabasca Research Corp.). Both instruments were mounted on a 10 m tower located about 30 m north of the row of houses at the mid-point of the row. The wind speed was converted to an equivalent speed at eaves height with a power law relation (Walker 1993).

$$U_{eaves} = U_{tower} \left(\frac{3.6}{10} \right)^{0.16} \quad 3.1$$

Since the wind is a vector quantity, the measurements were resolved into north and east vector components for averaging at the end of each hour. The average wind speed was the magnitude of the resultant and average wind direction was the angle of the resultant.

3.3.5 Fan Performance Test

The performance curve of the supply fan used in the experiment was determined from a pressure-flow measurement procedure according to ANSI/ASHRAE Standard 51 (1985). Since the fan was attached to the bottom of the flue inside the house, through

which air was drawn, the fan performance test was conducted with a flue cap and flue pipe attached to the fan intake. The flue assembly and fan set up inside house 6 is shown in Figure 3.3. The flue pipe was a double-walled 152 mm (ID), 6.01 m long section and the fan was a forward-curved centrifugal unit. According to the set up, shown in Figure 3.11, the flow rate was measured with a calibrated orifice and the pressure difference was determined with a Validyne pressure transducer. The signals were averaged over a period of 100 seconds to reduce the effects of fluctuation in the flow.

The flow characteristics were measured with respect to the total pressure difference across the fan and flue assembly. The rated pressure was measured from the fan performance test to be about 300 Pa and the rated flow rate was about 111 m³/hr. A polynomial fit to the data yields the mass flow rate through the fan and flue assembly.

$$M_{fan} = \frac{P_{out}}{3600} (5.3569E^{-4} \Delta P^3 - 0.04752 \Delta P^2 + 1.9049 \Delta P + 111.163) \quad 3.2$$

The performance curve for the fan-flue combination defined by Equation 3.2 appears to be reasonable because the shape of the curve, shown in Figure 3.12, is similar to the ones outlined in the ASHRAE Handbook of Equipment (1988) for forward-curved centrifugal fans.

3.3.6 Leakage Air Flow Measurements

The air leakage across the cavity was measured with an orifice-anemometer assembly which was fitted over the interior opening of the wall. The assembly, shown in Figure 3.13, consisted of a temperature compensated, heated ceramic tip anemometer (linearized Kurz prototype analog anemometer) which was placed inside a plexiglass

converging-diverging duct. The plexiglass duct was required to accelerate the air flow so that the magnitude of the air leakage velocity corresponding to typical flows fell within the range of the anemometer. Typically, the average leakage rate was about $0.2 \text{ m}^3/\text{hr}$ for infiltration and $0.15 \text{ m}^3/\text{hr}$ for exfiltration. Based on the average infiltration rate, the Reynolds number for the flow across the Kurz anemometer is about 600 which implies laminar flow. The converging-diverging duct was attached to an orifice plate with a 7 mm opening which was used to indicate the direction of the flow where a positive pressure difference across the orifice signified infiltration and a negative pressure difference indicated exfiltration. The orifice plate was necessary since the anemometer could not sense a change in flow direction. The converging-diverging duct and orifice plate were attached to a manifold which helped to distribute the air leakage flow to the slot on the interior wall. The manifold and flow assembly were sealed so that the air flow could not occur without being detected. A photograph of the flow assembly is shown in Figure 3.14.

The manifold and orifice-anemometer assembly were calibrated together to obtain a pressure-flow relation for infiltration and exfiltration. For calibration, a gas meter (Singer DTM-115) with a resolution of 0.01 l , shown in Figure 3.15, was used as the volumetric flow rate standard and a small diaphragm pump was used to drive the flow. The procedure was conducted in a laboratory with the room ventilation system shut off so that background air flow would not affect the reading.

The manifold and orifice-anemometer assembly was calibrated over a range of range of flow rates of 0 to $0.7 \text{ m}^3/\text{hr}$. The calibration equations of flow versus pressure

drop across the assembly for infiltration and exfiltration are defined as,

$$Q_{in} = 0.477(\Delta P)^{0.59} \quad 3.3$$

where Q_{in} = volumetric flow rate [m^3/hr]

ΔP = pressure difference between the flow assembly and ambient pressure [Pa]

$$Q_{out} = 0.503(\Delta P)^{0.5} \quad 3.4$$

where Q_{out} = volumetric flow rate [m^3/hr]

ΔP = pressure difference between the flow assembly and ambient pressure [Pa]

The range of the pressure difference used was 0 Pa to 3 Pa.

Since the Kurz anemometer produces a voltage output, the overall calibration equation for infiltration and exfiltration as used in the experiment are defined as,

$$Q_{in} = 1.97 \times 10^{-4} + 0.6(V)^{1.13} \quad 3.5$$

where Q_{in} = volumetric flow rate [m^3/hr]

V = voltage output from the Kurz anemometer [V]

$$Q_{out} = 3.19 \times 10^{-3} + 0.058(V)^{1.15} \quad 3.6$$

where Q_{out} = volumetric flow rate [m^3/hr]

V = voltage output from the Kurz anemometer [V]

The range of output voltage is from about 0.2 V to 9.0 V.

3.3.7 Data Acquisition and Storage

An automated data acquisition system was set up inside house 6 to conduct the measurements on the moisture content, temperature, relative humidity and air leakage through the cavity. The wind speed, wind direction, indoor/outdoor temperatures, and indoor/outdoor relative humidity were also recorded. The sensors were connected to a

series of relays which were coupled to a computer via an interface card (MetraByte PIO12). A software program was developed to open and close the relays in sequence in order to conduct the measurements automatically. The analog output signals from the sensors were converted to digital output with an analog to digital (A/D) converter card (MetraByte DAS-8). The 12 bit A/D converter card has a voltage range of ± 5 V which yields a resolution of 0.00244 V. The accuracy of the A/D card was calibrated to be ± 0.00244 V.

At the start of the experiment and the beginning of each hour, a zero reading of the pressure difference across the orifice plate in the flow measurement assembly was taken due to the low magnitude of the air leakage flow rates. This minimized the zero drift of the pressure transducer (Modus T30). A total of 59 sensors were activated in each cycle of measurements over a period of a minute. The sequence of the readings was surface sensors, moisture pins, thermocouples, relative humidity sensors, air leakage flow rate, and wind speed and direction. The measurement taken from a sensor in each cycle was an average value of 20 to 30 samples. The measurements from each cycle were temporary stored in the computer until the end of each hour when an hourly average and standard deviation were determined and recorded onto a diskette.

3.4 LEAKAGE FLOW CHARACTERISTICS

3.4.1 Background Leakage of the Test House

The background leakage of house 6 was determined from a fan pressurization/depressurization test according to CAN/CGSB-149.10-M86 (1986), "Determination of the Airtightness of Building Envelopes by the Fan Depressurization

Method". A variable speed fan was connected to a 457 mm diameter damper controlled opening over the east-wall window of house 6 to draw in or discharge air from the interior of the house. Infiltration across the envelope was induced by depressurizing the house and exfiltration was created by pressurizing the building interior. The flow rate was measured with a laminar flow element located on the intake opening of the fan where flow straighteners were placed up stream of the flow element.

The test was conducted over an indoor/outdoor pressure difference range of 1 to 100 Pa for both pressurization and depressurization. The outdoor pressure measurement was spatially averaged with a pressure tap on each side of the house and the indoor pressure was a single measured value because the interior was considered to be a single well mixed zone. Each indoor/outdoor pressure difference reading was averaged over 100 seconds with the zero-flow value subtracted. (The zero-flow value was taken before each pressure difference measurement). Also, each reading was taken only if the wind speed was below 1.5 m/s to reduce the influence of the wind on the leakage measurement. The measurement system was automated and the test was conducted over about a two week period in the summer yielding approximately 140 complete tests. A detailed description of the test procedure is outlined by Wilson and Walker (1991a).

The background leakage of house 6 based on the results from the fan pressurization tests is defined by the flow equation,

$$Q = C(\Delta P)^n \quad 3.7$$

where Q = volumetric flow rate [m^3/s]

ΔP = pressure difference across the building envelope [Pa]

C = 0.00881 [$\text{m}^3/(\text{sPa}^n)$]

$$n = 0.648$$

The flow coefficient, C , is related to the leakage area and the flow exponent, n , is a value between 0.5 and 1.0 where 0.5 is for flow through sharp edged holes and 1.0 is for laminar flow through long thin cracks. The measured flow exponent is reasonable because the value falls within the accepted range and it is also close to the typical value of 0.67 as suggested by Wilson and Walker (1991a) for the background leakage of a house. The equivalent leakage area based on a 4 Pa reference pressure difference is $7.65 \times 10^{-3} \text{ m}^2$ which is consistent with the measurement conducted by Walker (1993). The reference pressure difference of 4 Pa was used because the equivalent leakage areas of various building components listed in the ASHRAE Book of Fundamentals (1989) are based on this value.

3.4.2 Leakage Characteristic of the Cavity

The leakage characteristic of the cavity was determined from a pressure-flow measurement across the wall. Similar to the background leakage measurement, a fan was used to pressurize and depressurize the interior of the house to induce exfiltration and infiltration across the cavity. The cavity flow rate was measured with the orifice-flow anemometer assembly used in the experiment (Section 3.3.6). The pressure difference across the cavity between point 0 and point 5 in Figure 3.16 was measured with a diaphragm type transducer (Setra Model 264) which has a range of $-/+24 \text{ Pa}$. The test was conducted when the wind speed was below 1.5 m/s and the indoor/outdoor temperature difference was less than 5°C .

As discussed in Section 2.1.3, the pressure difference across the cavity used in

the model is between point 0 to point 4 in Figure 3.16. Consequently, the hydrostatic head between point 4 and point 5 was subtracted from the measured pressure difference. The hydrostatic head was determined to be 20 Pa based on a fixed height of 2.02 m and an outdoor temperature of 20°C. The resulting mass flow equation is

$$M = \rho C(\Delta P)^n \quad 3.8$$

where M = mass flow rate [kg/hr]

ρ = indoor air density for exfiltration and outdoor air density for infiltration

ΔP = pressure difference across the cavity between point 0 and point 4

C = 0.058 m³/(hrPaⁿ) for exfiltration and 0.084 m³/(hrPaⁿ) for infiltration

n = 0.543 for exfiltration and 0.569 for infiltration

3.5 TEST PROCEDURE

The objective of the study was to monitor the amount of air leakage across the cavity and the level of moisture condensation inside the cavity under typical conditions of a heating season. The indoor and outdoor conditions such as the temperature, relative humidity, wind speed, and wind direction were also monitored because they greatly influence air leakage and condensation in the cavity.

For the experiment, the test cavity was installed in the north exterior wall of house 6. The north wall was selected because it experiences the largest moisture load as determined by Forest et al (1990). The interior of the house was maintained at 20°C with the indoor relative humidity controlled at 45% ($\pm 5\%$) by a rotatory drum humidifier. This humidity level was selected because it is the mid point of the optimum range of indoor humidity for human health (Sterling et al 1985). The indoor humidity was maintained at 45% for about two months prior to the start of the experiment to

condition the interior portion of the house.

The experiment was conducted continuously over two heating seasons from February 7, 1994 to April 28, 1995. It was interrupted by a fan pressurization test, cavity flow resistance test, and system failures. (The fan pressurization test, described in Section 3.4.1, was conducted from July 5th to 26th and the cavity flow resistance test, outlined in Section 3.4.2, was carried out from October 16th to November 6th). During the first heating season, a supply fan was attached to the bottom of the flue to pressurize the interior of the house. The increase in the amount of exfiltration was designed to create a sustain period of moisture deposition. This condition is typical of houses with fresh air furnaces which usually have a slightly higher indoor pressure than outdoor pressure. The fan was in operation for 600 hours, from February 24, 1994 to March 21, 1994. After the fan was removed, the flue was blocked.

In the second heating season, the flue was kept closed and the air leakage was induced naturally by the stack effect and wind pressure. This condition was typical of houses which are heated with furnaces without an outdoor air intake duct where the background leakage is the only source of fresh air. The two conditions allowed the observation of the effect of sustain periods of exfiltration. Overall, the experiment produced about 10700 hours of data which serves as a large data base for validating Local Leaks and Wetwall.

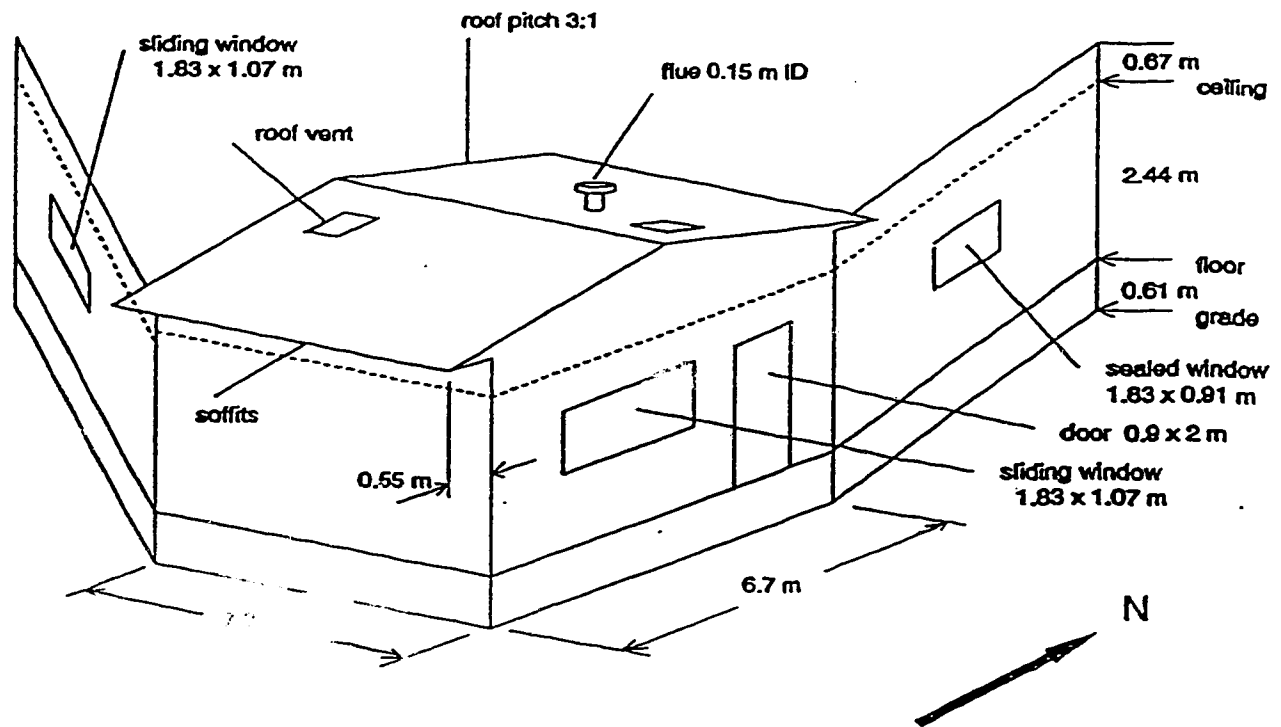


Figure 3.1: Schematic of house 6 located at the Alberta Home Heating Research Facility (AHHRF)



Figure 3.2: Exterior view of house 6 with the test panel located on the north wall. A wind shelter is situated to the east of house 6 and row of houses are located to the west.

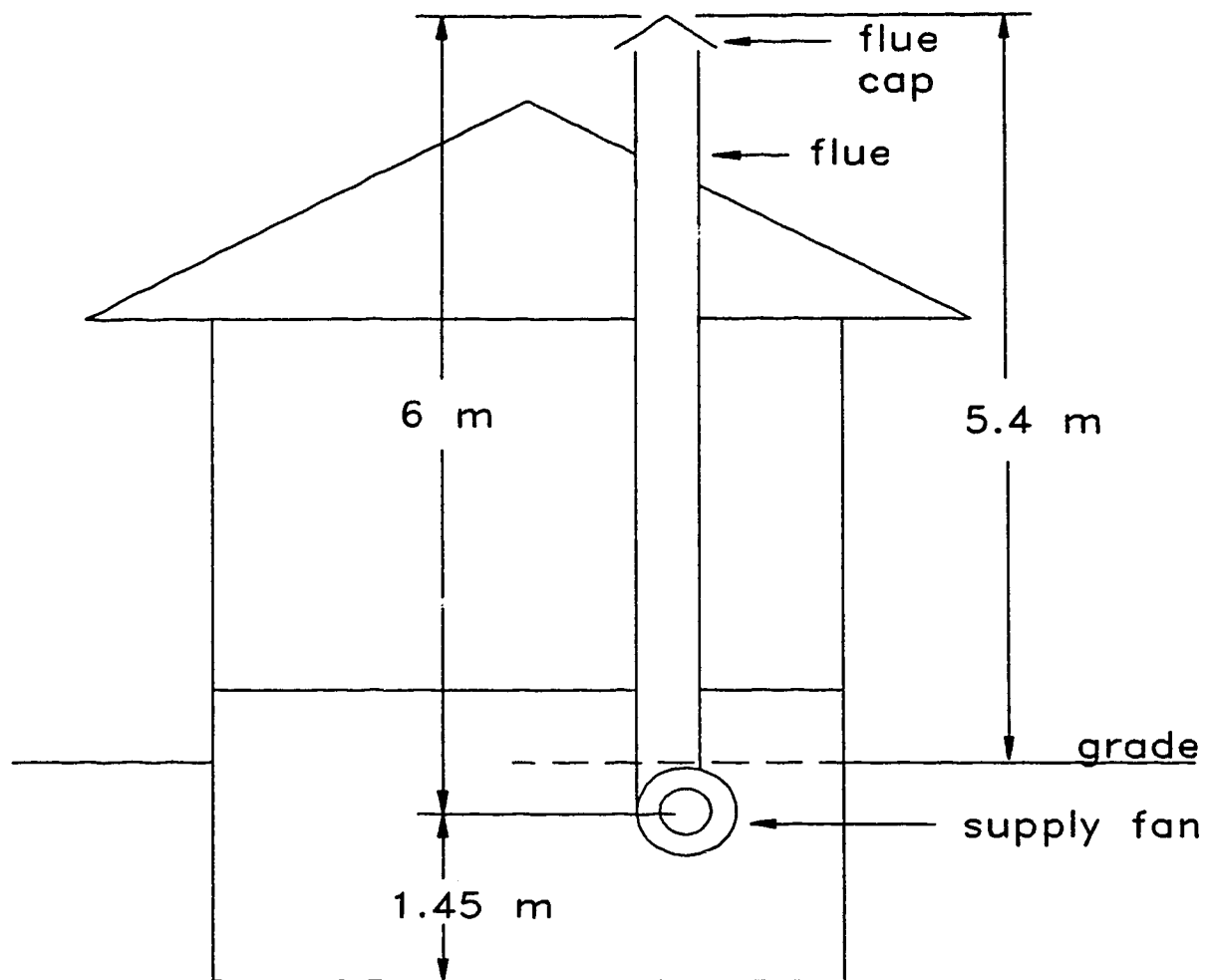


Figure 3.3: Schematic of house 6 showing the location of the supply fan attached to the bottom of the flue and the dimensions of the flue assembly.

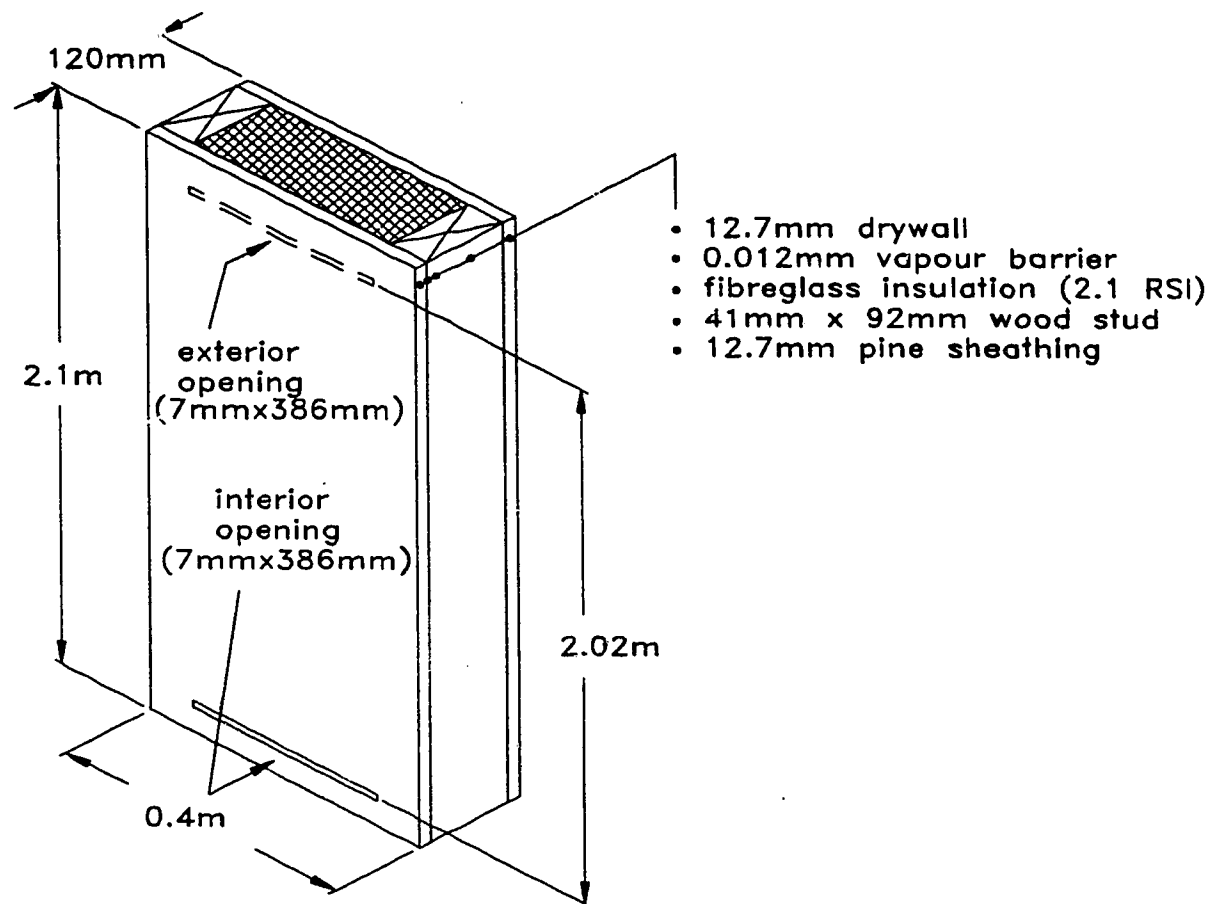


Figure 3.4: Schematic of the test cavity with a listing of the composition of the cavity

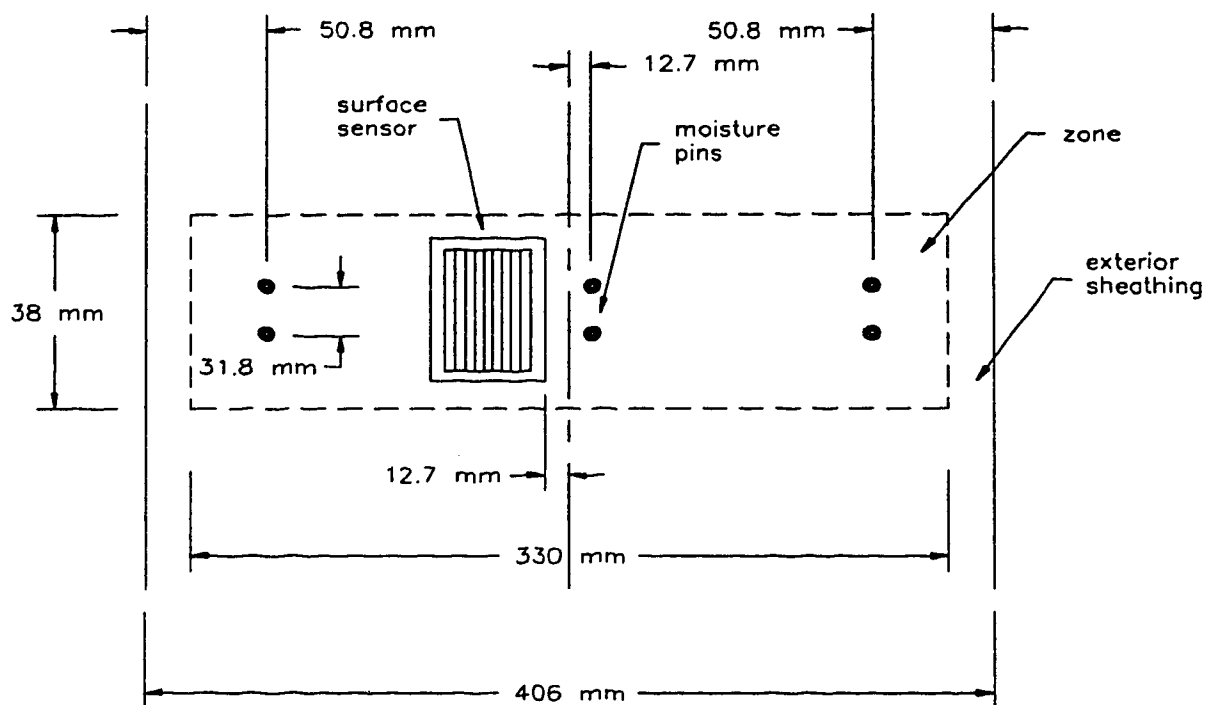


Figure 3.5: Schematic of a designated zone on the exterior sheathing showing the locations of moisture pins and surface sensor

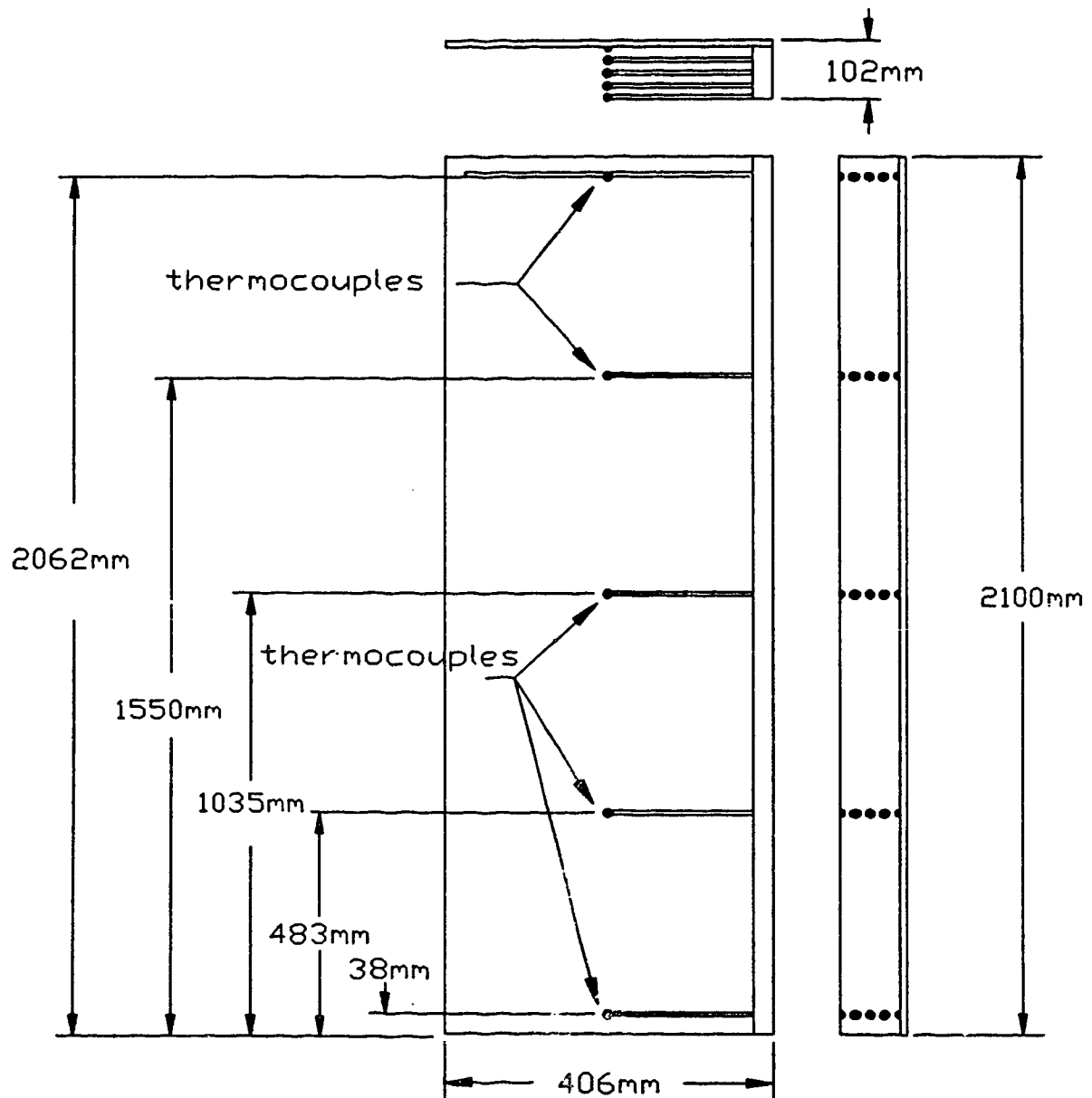


Figure 3.7: Location of the thermocouples in the cavity

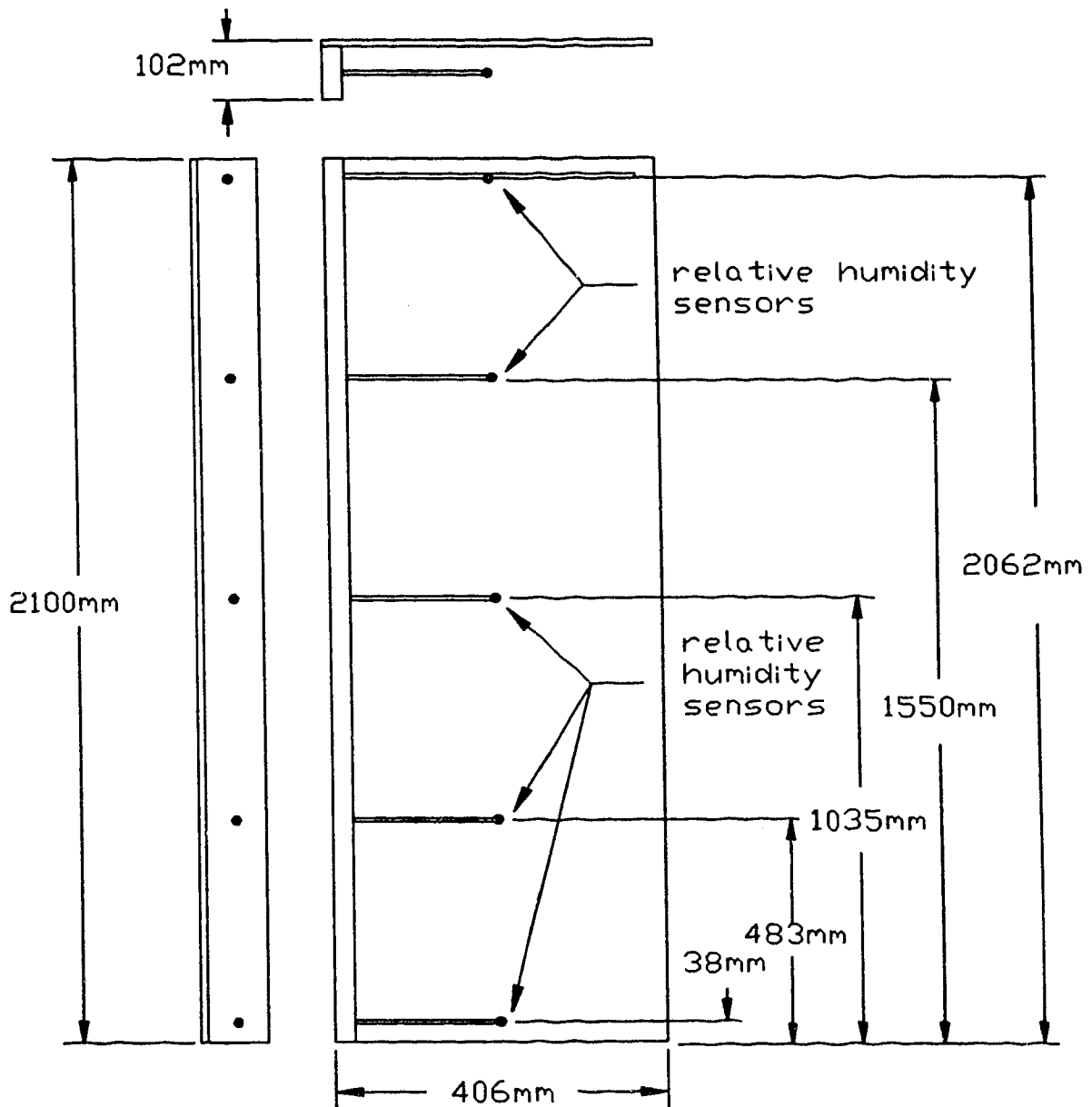


Figure 3.8: Locations of relative humidity sensors in the cavity

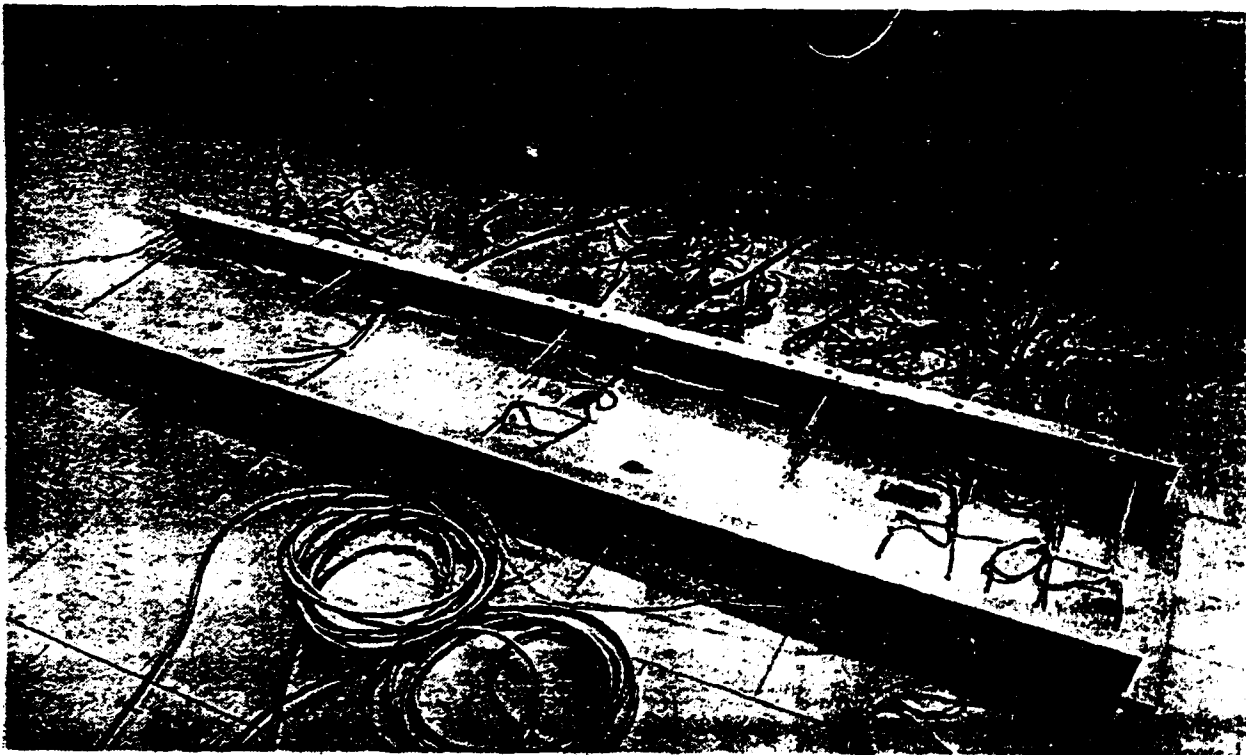


Figure 3.9: The interior of the test cavity during construction (insulation not yet in place)

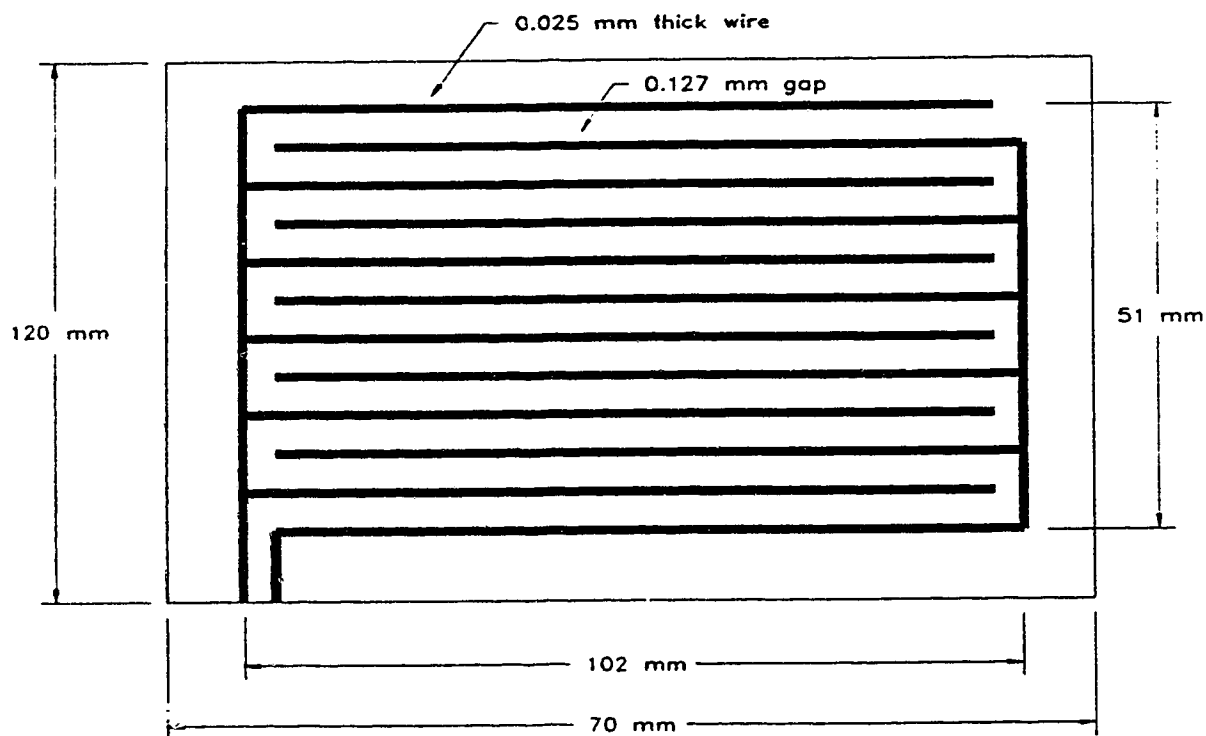
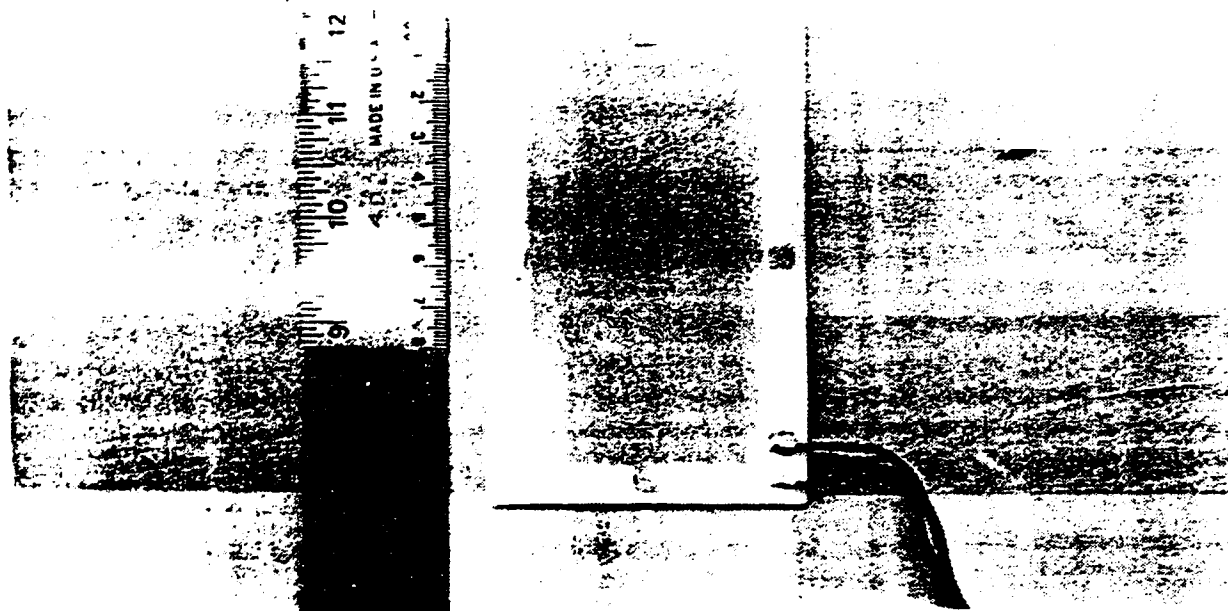


Figure 3.10: Surface sensor placed on the cavity face of the exterior sheathing. The photograph above shows the surface sensor before being mounted on the sheathing and the figure below shows a schematic of the interwoven wire mesh of the sensor.

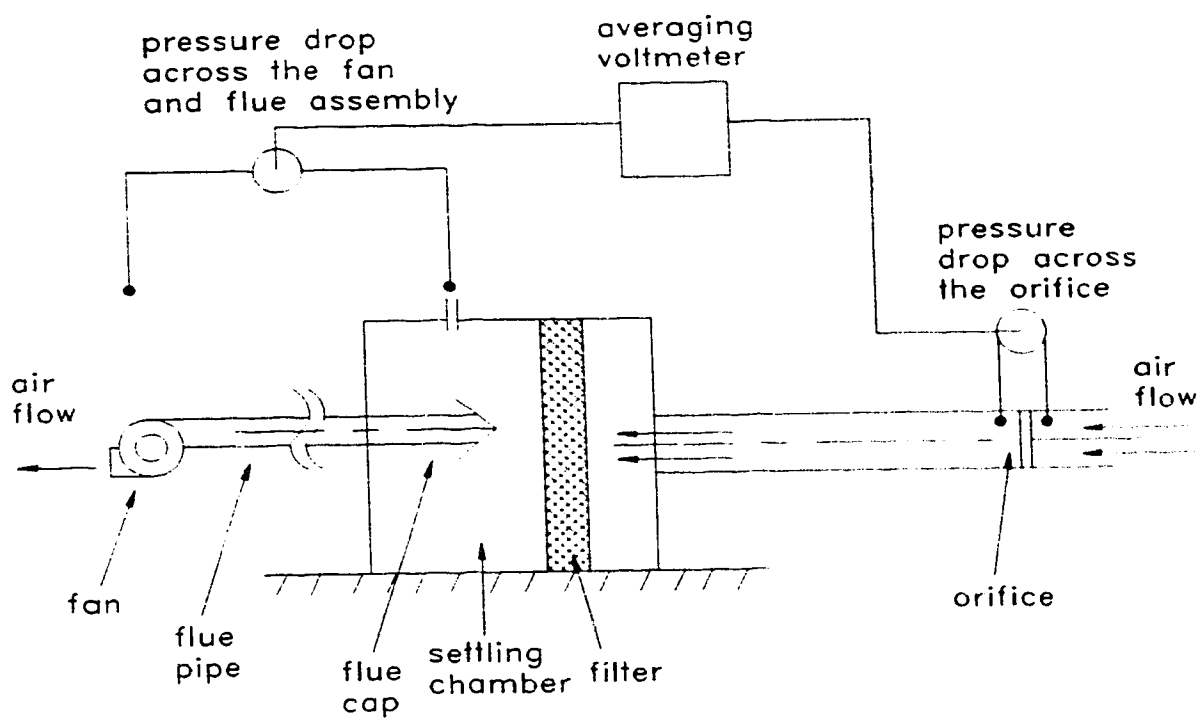


Figure 3.11: Calibration of the fan and flue attachment

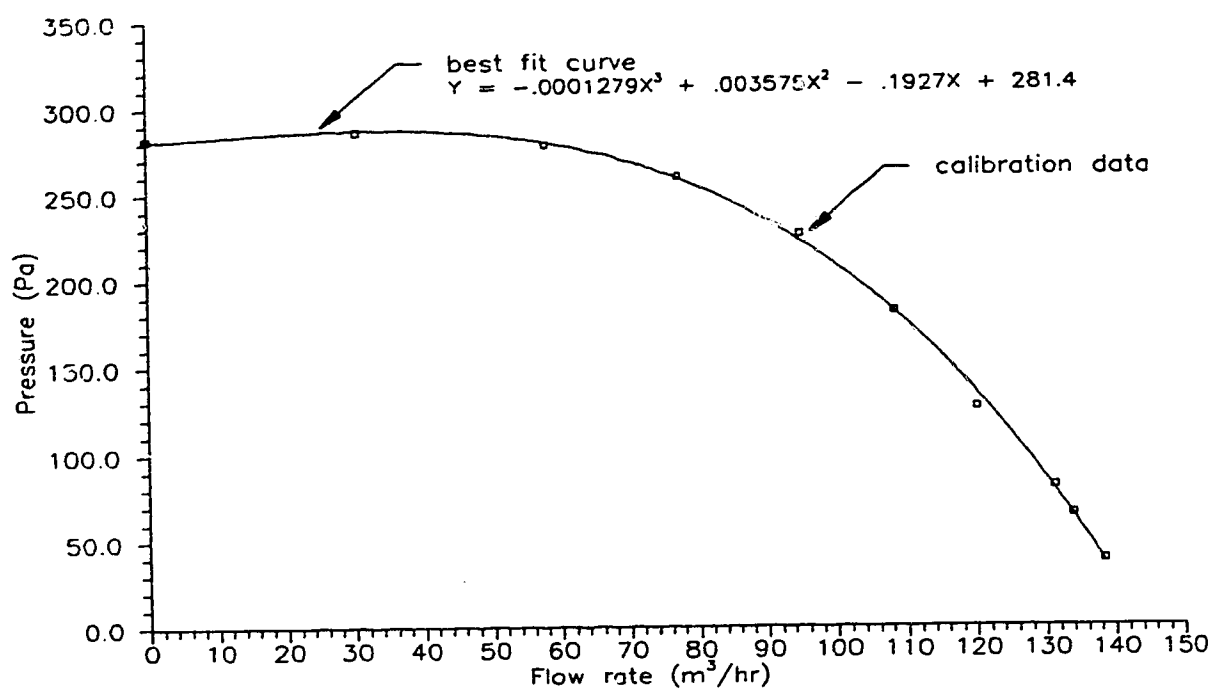


Figure 3.12: Calibration curve of the fan and flue attachment

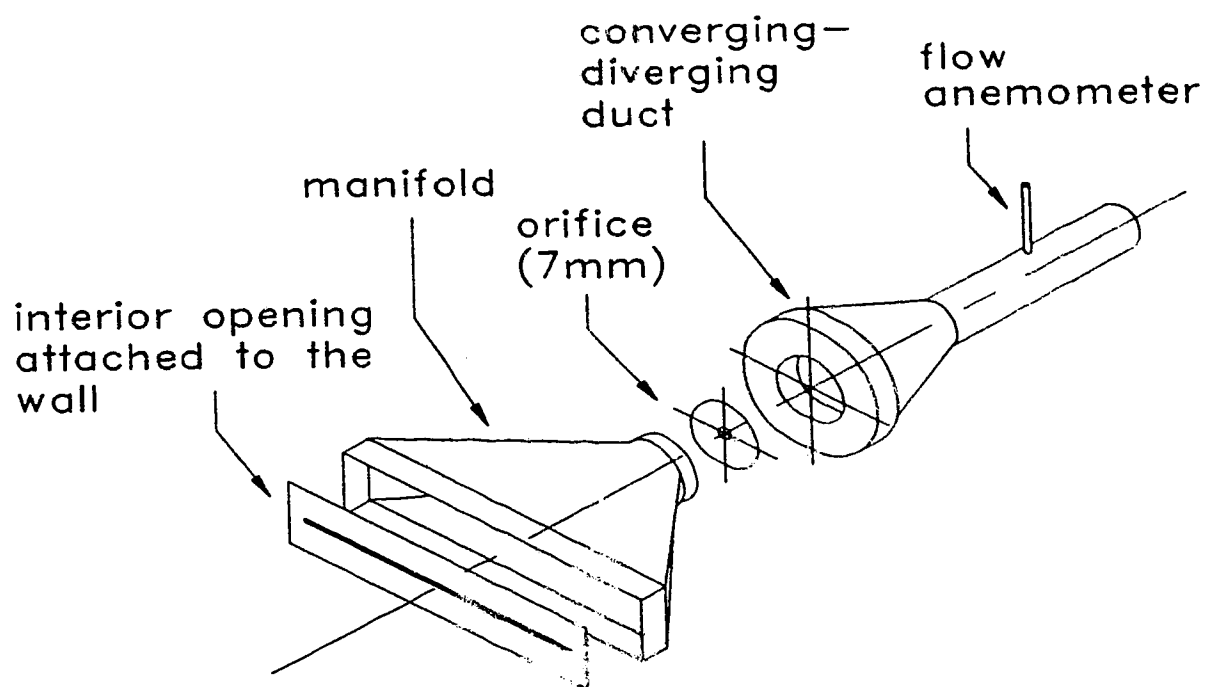


Figure 3.13: A schematic of the orifice-flow anemometer assembly

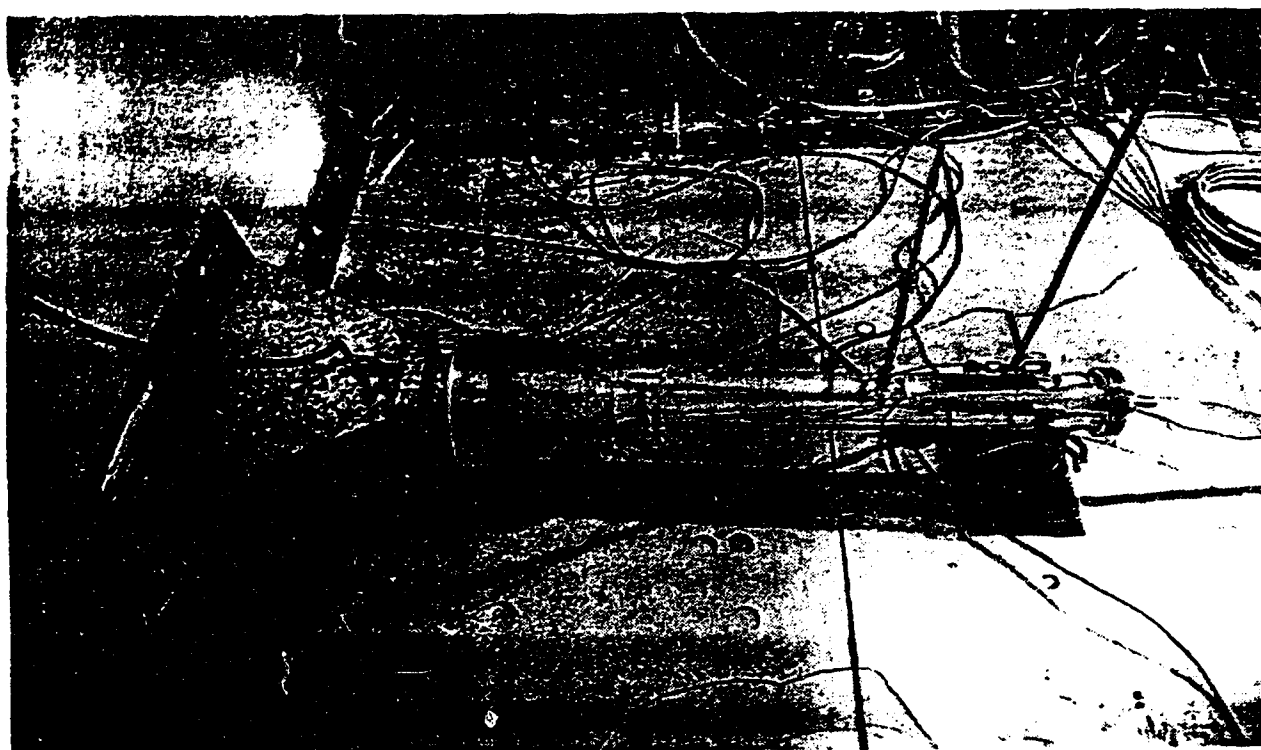


Figure 3.14: A photograph of the orifice-flow anemometer assembly fitted over the interior cavity opening during instrument testing

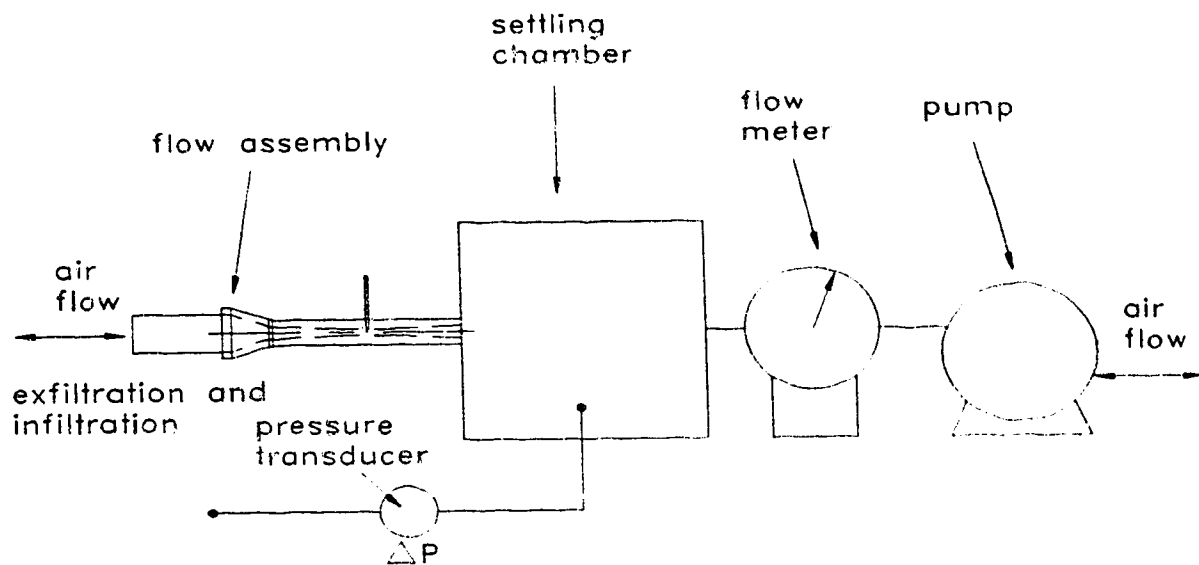


Figure 3.15: Calibration of the orifice flow anemometer assembly

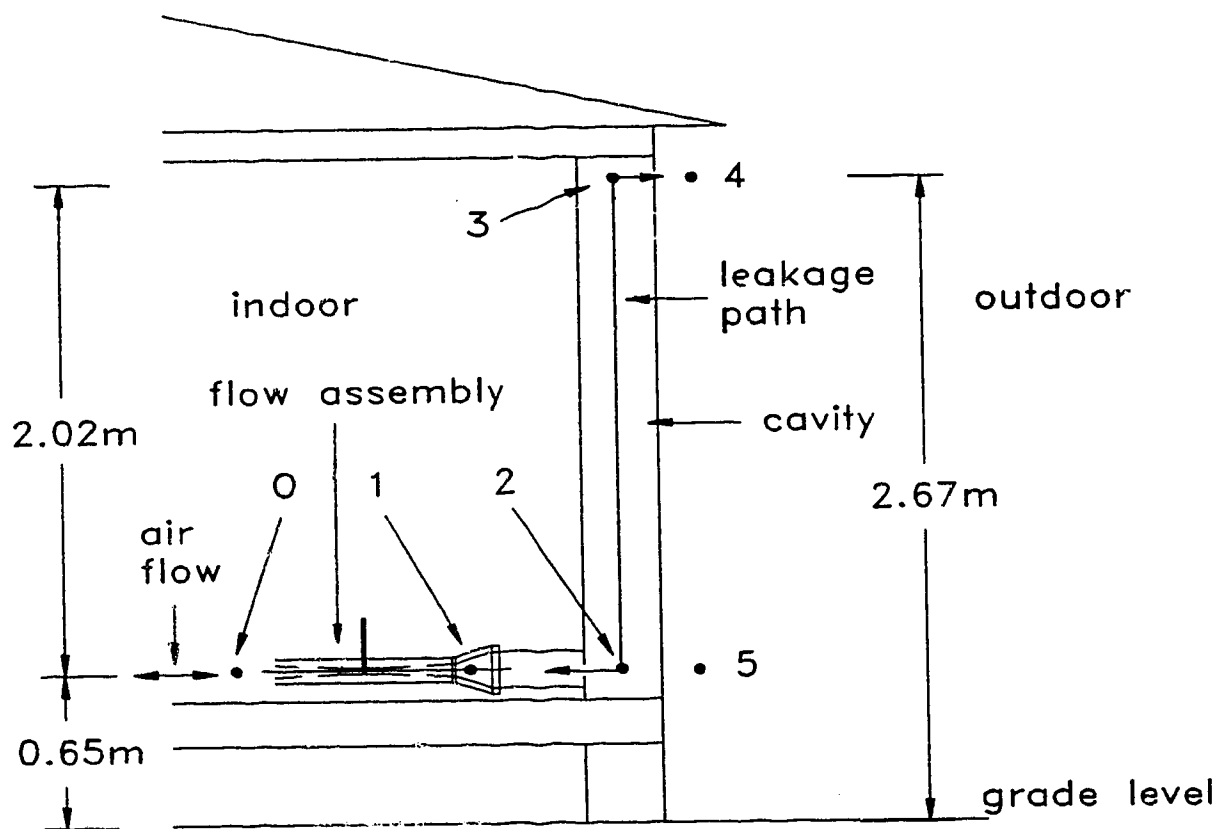


Figure 3.16: Location of the orifice-flow assembly in the house and the reference points for pressure-flow measurements

Chapter 4

EXPERIMENTAL RESULTS

The field experiment was conducted continuously from February 7, 1994 to April 28, 1995. A total of approximately 10700 hours of measurements of air leakage, wind speed, wind direction, indoor/outdoor relative humidity and temperatures, and sheathing moisture contents were collected for validating the models Local Leaks and Wetwall. The experiment was carried out under two separate conditions. In the first heating season, a supply fan was placed inside the house for a portion of the heating season to pressurize the interior and in the second heating season, no supply fan was used. The first condition simulates a house with a fresh air intake duct connected to the return air of a gas furnace where the fan tends to pressurize the house. The second condition is similar to a house with a furnace which uses the background leakage of the house for air supply. The complete range of results from the experiment is presented in this chapter.

4.1 AIR LEAKAGE MEASUREMENTS

The air flow across the leakage path in the test cavity was measured over the course of the experiment. In the experiment, the magnitude and duration of the air leakage flow were accounted separately for infiltration and exfiltration over an hour. At the end of the hour, the total volume of air leakage and the duration of the flow were recorded. Time weighted average air leakage rates over an hour were then determined by multiplying the total volume by the duration of the flow as a fraction of an hour. Hence, the total flow volume was spread over an hour giving an average air leakage flow

rate. In the case of short durations of strong air leakage flows in an hour which is dominated by the air leakage flow in the other direction, the short durations of flow will be spread over an hour. The average air leakage rate is weighted according to the duration of the flow over an hour. The time weighted average infiltration and exfiltration rates are shown in Figure 4.1. The leakage rates are time weighted averages evaluated by multiplying the average flow rate by the fraction of flow over an hour. By convention, infiltration is denoted as positive flow and exfiltration as negative flow. The flow data are continuous except for the periods of system failure, fan pressurization test, and cavity flow resistance test. The peak infiltration measurements, shown in Figure 4.1, were clipped at $0.37 \text{ m}^3/\text{hr}$ due to the upper limit of the measurement system. In the experiment, the output signal of the orifice-anemometer flow measurement assembly was processed with an Analog to Digital (A/D) converter before the measurements were recorded by the data acquisition system. Although the orifice-anemometer flow measurement assembly was calibrated over a range of 0 to $0.7 \text{ m}^3/\text{hr}$ for an output signal of 0 to 9.46 V, the measurement system was limited by the 0 to 5 V range of the A/D converter card. The signal from the flow measurement system was not reduced with an attenuator because the flow rates were typically low.

Despite the periodic gaps in the data and clipping of the peak infiltration rates, the measurements appear to be reasonable as they demonstrate expected trends. The leakage across the cavity is driven by an indoor/outdoor pressure difference and over an hour, the pressure difference is either predominately positive ($P_{\text{out}} > P_{\text{in}}$) or negative ($P_{\text{out}} < P_{\text{in}}$) yielding either infiltration or exfiltration. Consequently, when infiltration is

strong, exfiltration is small or zero. In the same manner, when exfiltration is large, infiltration is small or non-existent. For example, over the period of hour 200 to 300 in Figure 4.1, when the fan was not in operation, the infiltration rate was extremely large at $0.37 \text{ m}^3/\text{hr}$ or greater and correspondingly the exfiltration was zero. Conversely, during the operation of the fan the exfiltration was consistently large and infiltration occurred rarely.

As mentioned, the fan created a sustained period of exfiltration from hours 440 to 1038 by pressurizing the interior of the house. The exfiltration, shown in Figure 4.1, reached a peak value of about $0.35 \text{ m}^3/\text{hr}$ when the fan was operating and the average flow rate over the period was approximately $0.15 \text{ m}^3/\text{hr}$. In the second heating season (hours 7142 to 10701), when the leakage was driven naturally by the wind pressure and stack effect, the peak exfiltration rate was about $0.28 \text{ m}^3/\text{hr}$ and the average flow rate was approximately $0.038 \text{ m}^3/\text{hr}$. A prolonged period of exfiltration did not occur without the fan.

Although the fan created a bias in the air flow, it did not negate entirely the dynamics of the weather. The fluctuation in the exfiltration rate suggests that the fan operating point changed in response to the variation in the indoor/outdoor pressure difference. In addition, brief stages of infiltration occurred while the fan was in operation which corresponded to strong northerly winds at hours 839 to 846 and 975 to 994. Northerly winds tend to produce a positive outdoor/indoor pressure difference which will reverse the direction of flow through the cavity.

4.1.1 Variation of Air Leakage With Wind Speed

The air leakage rate across the cavity was observed to depend strongly on the wind speed. The infiltration and exfiltration rates, shown in Figure 4.2a and Figure 4.2b, increased with an increase in the wind speed. Although some of the measured air leakage rate corresponding to wind speeds of 5 m/s or greater probably exceeded the upper limit of the measurement system at 0.37 m³/hr, the measurements were included in Figure 4.2a. The linearity in the two figures is reasonable because wind pressure varies with the square of the wind speed and the flow exponent in the cavity leakage relation is nearly 0.5 (0.569 for infiltration and 0.543 for exfiltration). Although the indoor/outdoor pressure difference across the cavity depends on the overall indoor/outdoor pressure difference which is a function of other parameters, it can be argued that wind pressure is the dominant driving force. Consequently, the square of the wind speed and the flow exponent nearly cancel each other which tends to produce a linear relation.

The two figures also show a definite difference in the slope of the air leakage flow rate-wind speed relation for infiltration and exfiltration across the cavity. The slope of the infiltration in Figure 4.2a is distinctly larger than that of exfiltration in Figure 4.2b. Southerly winds tend to create a negative outdoor/indoor pressure which will induce exfiltration. Since the pressure coefficient on the north wall for southerly winds is smaller than that for northerly winds, which induce infiltration, the magnitudes of the exfiltration through the cavity are smaller than infiltration.

As discussed in Section 4.1, the supply fan created a prolonged period of

exfiltration, but did not negate entirely the effect of the wind. A small amount of infiltration, shown in Figure 4.3a, occurred when the wind speed was typically over 4 m/s and wind direction was from the north. The exfiltration rate, shown in Figure 4.3b, varied between 0.10 m³/hr to 0.20 m³/hr for wind speeds below 4 m/s because the fan dictated the flow over this range. At wind speeds over 4 m/s, however, the leakage rate was observed to increase with an increase in wind speed.

4.1.2 Variation of Air Leakage Flow With Wind Direction

The wind direction was observed to have a definite effect on the leakage rate across the cavity. The flow rates were sorted into bins of north, south, east, and west directed winds. The north wind (-22.5° to 22.5°) produced almost entirely infiltration and nearly no exfiltration. The infiltration rate, shown in Figure 4.4a, increased linearly with the wind speed reaching the upper limit of the measurement system at 0.37 m³/hr. Conversely, the exfiltration, shown in Figure 4.4b, was below 0.03 m³/hr at wind speeds below 1 m/s, which suggests the air leakage was driven by the stack effect. The results agree with the fact that a north wind creates a positive pressure coefficient on the windward surface which induces infiltration across the cavity.

The south wind (157.5° to 202.5°), in contrast, generated mainly exfiltration and only a small amount of infiltration. The exfiltration, shown in Figure 4.5b, increased almost linearly with the wind speed to a value of about 0.22 m³/hr. A south wind produces a negative pressure coefficient on the cavity because the north wall is the leeward surface and as expected, the flow is predominately exfiltration. The majority of the infiltration across the cavity below 0.05 m³/hr, shown in Figure 4.5a, was driven

by the stack effect where the wind speeds were under 2 m/s. The infiltration at higher wind speeds suggests that a south wind is not always the dominant factor on the indoor/outdoor pressure difference across the cavity and pressures on other surfaces of the house also have an influence. The pressure coefficient for south winds is smaller than that for north winds and therefore, the magnitude and direction of the air leakage flow rate is more sensitive to other changes which affect the overall indoor/outdoor pressure difference.

The air leakage rate across the cavity for east and west winds did not exhibit any distinct patterns with respect to the wind speed. Since house 6 is sheltered by the rest of the row houses to the west and a 3.7 m high wall to the east, the effects of the wind from the east and west were less than that created by north and south winds. The infiltration rates for west winds (247.5° to 292.5°), shown in Figure 4.6a, produced little correlation with the wind speed. The exfiltration rates, shown in Figure 4.6b, were consistently low at a flow rate below $0.03 \text{ m}^3/\text{hr}$ for all wind speeds. The west wind did not induce any significant amount of exfiltration and the majority of the outflow was driven by the stack effect.

The infiltration rates for east winds (67.5° to 112.5°), shown in Figure 4.7a, behaved similarly to that for west winds. There was little correlation for the effect of wind speed on infiltration rates. The exfiltration rates, shown in Figure 4.7b, however were noticeably larger than that for west winds. The wind speed affected the exfiltration rate more significantly with a pattern of an increase in the leakage rate with an increase in wind speed. The contrast in the exfiltration rate for east and west winds is due to the

difference in the shelter effect provided by the row houses on the west side and the 3.7 m high wall on the east side of house 6. The flow pattern along the row of houses and over the end wall are not the same.

To highlight the effect of wind direction, the normalized air leakage flow rates are shown in Figure 4.8a. In this figure, the air leakage flow rates are divided by wind speed raised to the power $2n$, where n is equal to 0.556 - the flow exponent for mass flow through the cavity. It reduced the scatter in the data associated with the wind speed. The bin-averaged normalized air leakage flow rates and standard deviations are shown in Figure 4.8b to help clarify the trends shown in the raw data of Figure 4.8a. Figure 4.8b shows that the curve of normalized air leakage flow rates is not symmetric about 180° due to the difference in the sheltering on the east and west sides of house 6. Unlike the minimum normalized flow rate predicted by Walker (1993), the minimum normalized measured flow rate is shifted from 180° to 150° . The normalized flow rate for east winds is approximately 0.02 and 0.01 for west winds. The maximum normalized flow rate occurred at 0° and 360° corresponding to north winds as expected because the wind was unobstructed.

The effect of the wind direction during the operation of the fan was not noticeable. The normalized flow rate, shown in Figure 4.9, varied randomly with the wind direction, suggesting that wind direction is of less importance when a mechanical ventilation device is in operation.

4.1.3 Variation Of Indoor/outdoor Temperature Difference on Air Leakage

The influence of the indoor/outdoor temperature difference (stack effect) on the

leakage rate was seen to be much less than that of the wind. The maximum infiltration rate, shown in Figure 4.10a, was $0.13 \text{ m}^3/\text{hr}$ and the maximum exfiltration rate, shown in Figure 4.10b, was about $0.05 \text{ m}^3/\text{hr}$. In comparison, the maximum leakage rate induced by the wind was over $0.37 \text{ m}^3/\text{hr}$ for infiltration (this was limited by the measurement system) and approximately $0.3 \text{ m}^3/\text{hr}$ for exfiltration. Since the wind induced leakage rate is about three times larger than that of the stack effect for infiltration and about six times for exfiltration, wind pressure is the main driving force for air leakage flow rates.

For a given indoor/outdoor temperature difference, the infiltration rate in Figure 4.10a is noticeably larger than the exfiltration rate in Figure 4.10b. This difference in the leakage rate is consistent with the calibration results presented in Section 3.4.2 in Chapter 3 where the flow resistance across the cavity is lower for infiltrating flow than exfiltrating flow.

It is important to note, however, that although the air leakage rates are selected for wind speeds of 1 m/s or lower, as shown in Figures 4.10a and 4.10b, the flows are susceptible to small changes in the wind direction. Consequently, the direction of the air leakage flow can easily change from infiltration to exfiltration or vice versa.

4.2 MOISTURE DISTRIBUTION IN THE EXTERIOR SHEATHING

The moisture content in each zone is the average value of three sets of moisture pin readings. (The various zones are defined in Figure 3.6). Since the typical variation in the moisture pin readings is observed to be about 4 %wt, the use of an average value for the moisture content in each zone is reasonable. The hourly averaged readings were

converted to daily averages because the change in the moisture content is much slower compared to the changes in air leakage rates. Daily averaging eliminated some of the fluctuations in the measurements, but did not affect the trends in moisture deposition.

The moisture content in each zone over the course of the experiment is shown in Figure 4.11. Zone 1 was directly opposite the interior leakage site at the cavity bottom and the other zones were located along the height of the sheathing progressively further away from zone 1. Zone 5, the furthest distance away from zone 1, was situated at 3/4 cavity height.

The moisture content in zone 1 was consistently the highest. During the first heating season with the fan in operation, the moisture content climbed steadily reaching a maximum value of about 27 %wt. Over the summer, the moisture content ranged between 13 %wt to 18 %wt which is relatively wet since wood with a moisture content of over 20 %wt is susceptible to wood rot. The limited drying of the sheathing is somewhat unexpected. In the second heating season with the leakage driven naturally, the moisture content in zone 1 fluctuated, but it still reached a peak value of about 24 %wt. The moisture deposition over time in zones 2, 3, and 4 followed a similar pattern as zone 1, but the amount of moisture content in each zone decreased with distance away from zone 1. The moisture content in zone 5 was the lowest value throughout the experiment compared to the other zones. It reached about 13 %wt in the first heating season and remained at about 8 %wt throughout the second heating season.

The variation in the moisture content between the zones shows the moisture distribution along the height of the cavity where the largest moisture content is in zone 1

and smallest is in zone 5. Zone 1 was exposed to the largest potential for moisture deposition and Zone 5 was subjected to the smallest. The results agree with field observations that condensation is largest at the leakage site and the amount of moisture deposition decreases with distance away from the opening.

The surface sensor measurements, shown in Figure 4.12, also exhibit a similar distribution for the surface deposition along the height of the sheathing. The sensor is saturated with condensation at 2.375 V and completely dry at below 0.75 V. Throughout the experiment, zone 1 was the quickest to reach saturation and it remained at saturation for the longest period of time. In contrast, zone 5 was the slowest to reach saturation and the duration at saturation was the shortest of any zone.

4.3 AIR LEAKAGE AND CONDENSATION

Changes in moisture content of the sheathing were observed to correspond with exfiltration and infiltration across the cavity. The results demonstrate that exfiltration deposits moisture and infiltration removes moisture. The sustained period of exfiltration created by the fan in the first heating season was observed to produce a rapid rise in the moisture content in zone 1 as shown in Figure 4.13. In Figure 4.13, the air leakage flow rates are net flow rates, $Q_{in} - Q_{out}$, to simplify the plot of infiltration and exfiltration rates. Since exfiltration is defined as negative by convention, the magnitude of Q_{out} is used in determining the net flow rate. Although the situation of a zero net flow rate may arise if the amounts of infiltration and exfiltration are similar, it is rare because typically, flow in one direction dominates over an hour. Before the prolonged period of exfiltration, the moisture content was approximately 13 %wt and with the strong

exfiltration, the moisture content increased rapidly to a peak value of 27 %wt. After the fan was removed, infiltration dominated and the moisture content dropped dramatically from about 23 %wt to 13 %wt. Infiltration quickly dried out the cavity.

In the second heating season, the moisture content in zone 1, shown in Figure 4.14, increased over several shorter periods instead of a single sustained period. Again, the air leakage rates are net flow rates. The short periods of exfiltration deposited moisture causing the moisture content to increase and conversely, the periods of infiltration removed moisture which lowered the moisture content in the sheathing.

The surface deposition measurements further confirm the wetting and drying effect of air leakage across the cavity. Similar to the internal moisture content, the surface sensors remained saturated over the first heating season as shown in Figure 4.15 and varied between saturation and no surface deposition over the second heating season as shown in Figure 4.16. In general, the surface sensor measurements show a much faster response than the sheathing moisture content for conditions corresponding to both deposition and removal of moisture inside the cavity. This suggests that air convection deposits and removes moisture from the cavity faster than moisture diffuses across the sheathing.

4.4 RELATIVE HUMIDITY DISTRIBUTION

The relative humidity sensors were placed inside the cavity to monitor the movement of the moisture through the leakage path in the wall. The humidity ratio along the height of the wall for the first 600 hours, shown in Figure 4.17, followed expected trends of moisture deposition during exfiltration and moisture removal during infiltration.

The amount of water vapour within the cavity increased over the first 200 hours corresponding to exfiltration. The amount of water vapour, however, decreased over the next 250 hours and the humidity ratio dropped to 0.0015 during periods of infiltration. This further shows that infiltration removes water vapour and does not deposit moisture. From hour 450 to 600, the humidity ratio increased rapidly reaching a value of about 0.0090 because of the large moisture deposition due to the sustained period of exfiltration created by the fan.

Over the course of the experiment, the relative humidity for all five zones were observed to be below 1.0. The relative humidity in zone 1, shown in Figure 4.18, reached a maximum value of about 93% suggesting that condensation did not occur at the mid depth of the cavity. It can be inferred that over the course of the experiment, the condensation front has not reach the region from the interior opening to the mid depth of the cavity.

4.5 TEMPERATURE DISTRIBUTION

The temperature distribution along the height of the cavity, shown in Figure 4.19, was seen to be non-uniform. The lower temperature at the bottom of the cavity was most likely due to the lack of insulation at the junction of the basement wall and the floor which is typical of wood frame construction. The temperature at the top of the cavity was not as low as the bottom because the insulation in the exterior wall extended past the ceiling.

The temperature at the mid height of the exterior sheathing was used as the value for the isothermal outer surface in Wetwall. The mid height temperature is typically

within two degrees of the average value and is a good representation of the temperature of the idealized surface.

The temperature profile across the depth of the cavity, shown in Figure 4.20, did not follow a straight line typical of pure conduction. The non-linearity is due to the heat sink at the bottom of the cavity. Forced convection did not affect the heat loss because velocity of the leakage for the hour was under 3.5×10^{-4} m/s. For natural convection in the cavity, the range of Rayleigh number, Ra_w (Nikel 1991), is 0.47 to 0.06 responding to a velocity range of 3.4×10^{-4} m/s to 2.53×10^{-3} m/s. The Rayleigh number was calculated using the following equation (Nikel 1991),

$$Ra_w = \frac{g \beta K \Delta T}{2 w \nu} \quad 4.1$$

where g = gravity [m/s^2]

β = coefficient of thermal expansion of air

K = permeability of glass fibre [m^2]

ΔT = temperature difference [K]

w = velocity along the height of the cavity [m/s]

ν = kinematic velocity of air [m^2/s]

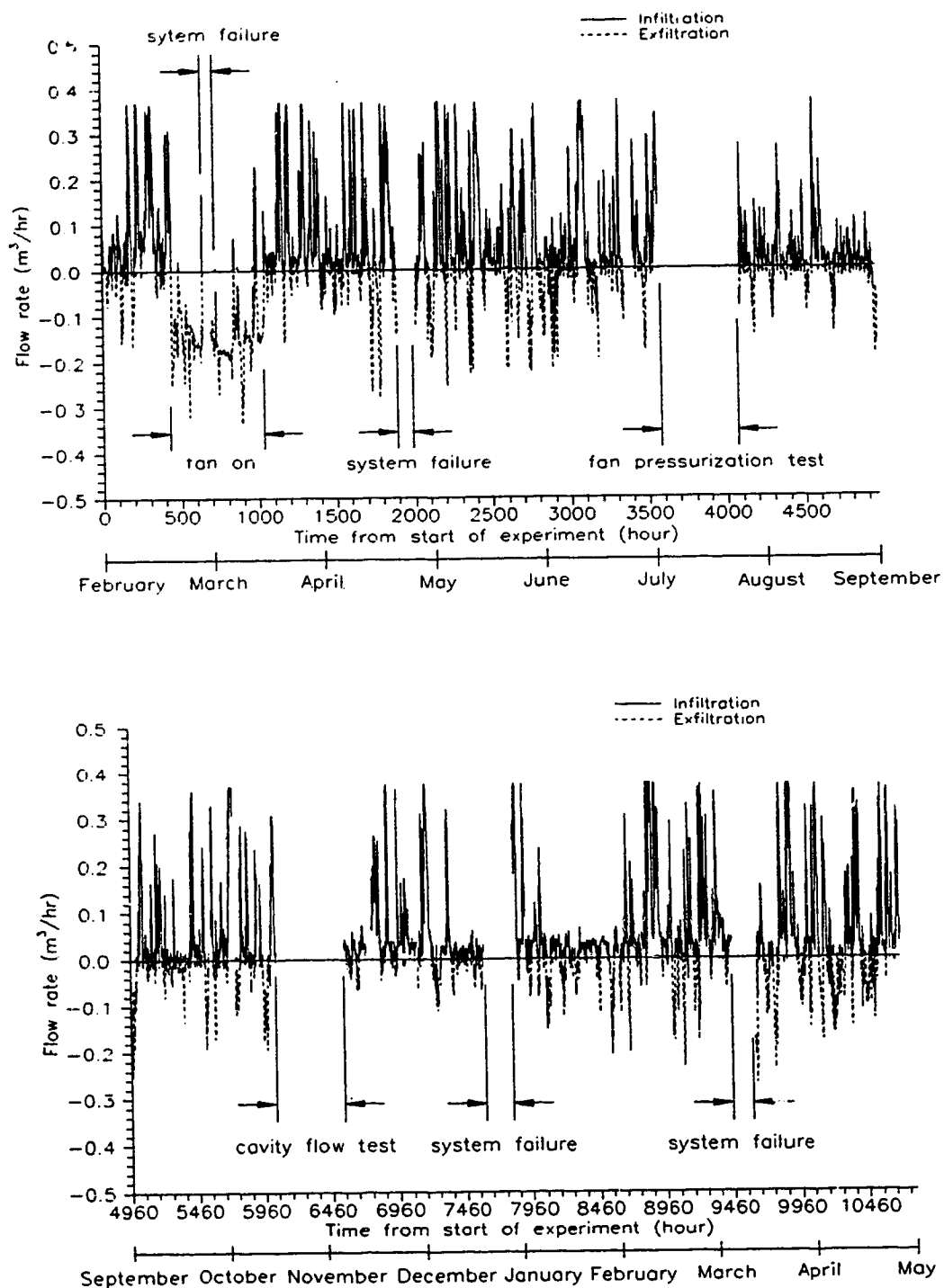


Figure 4.1: Measured rates of infiltration and exfiltration through the cavity from February 7, 1994 to April 28, 1995. The upper plot spans the first 7 months of field data and the lower plot spans the remaining 8 months of data.

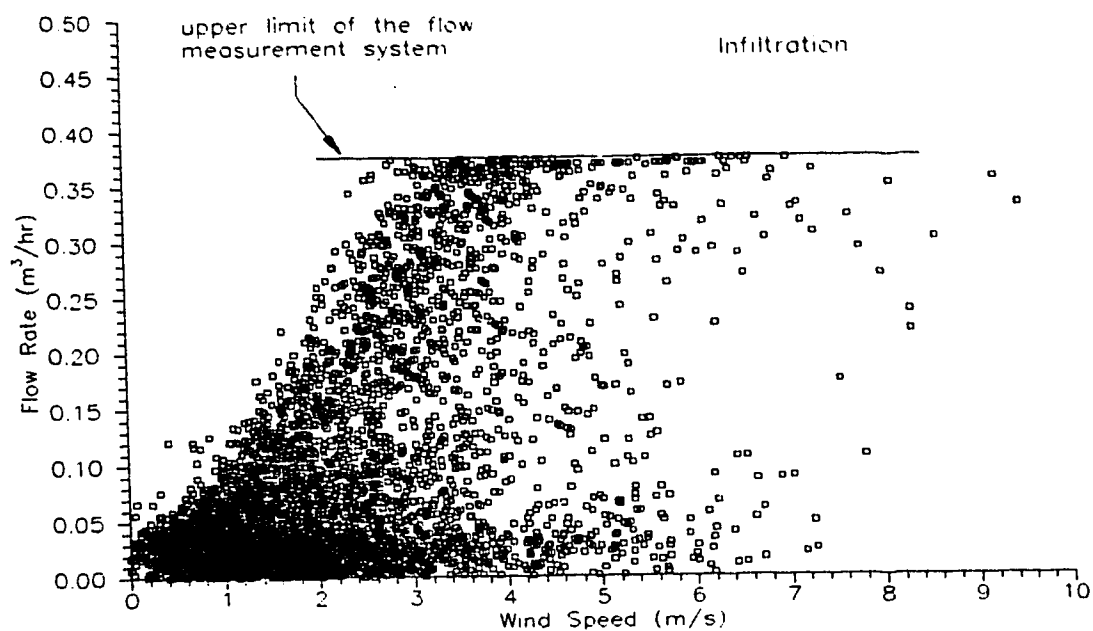


Figure 4.2a: Measured infiltration rates across wall cavity for all wind directions (fan off)

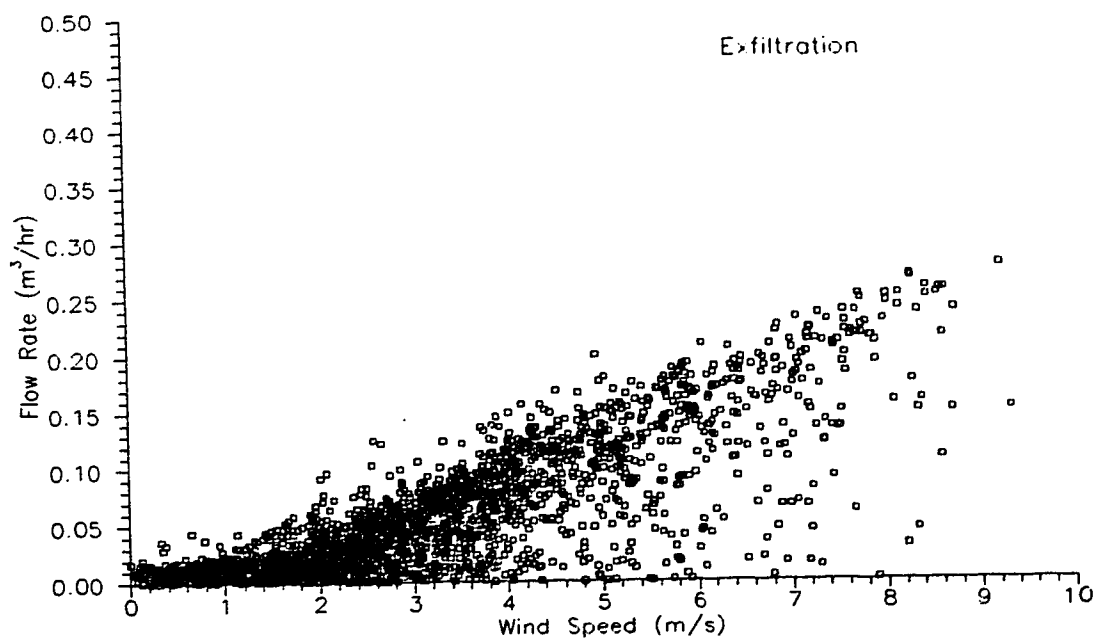


Figure 4.2b: Measured exfiltration rates across wall cavity for all wind directions (fan off)

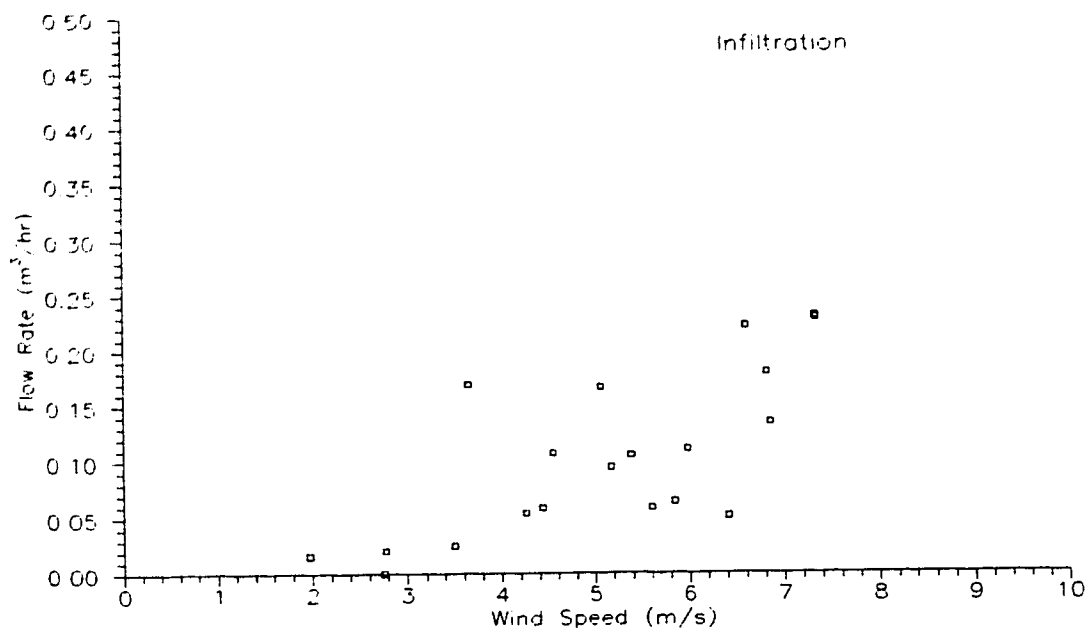


Figure 4.3a: Measured infiltration rates across wall cavity for all wind directions (fan on)

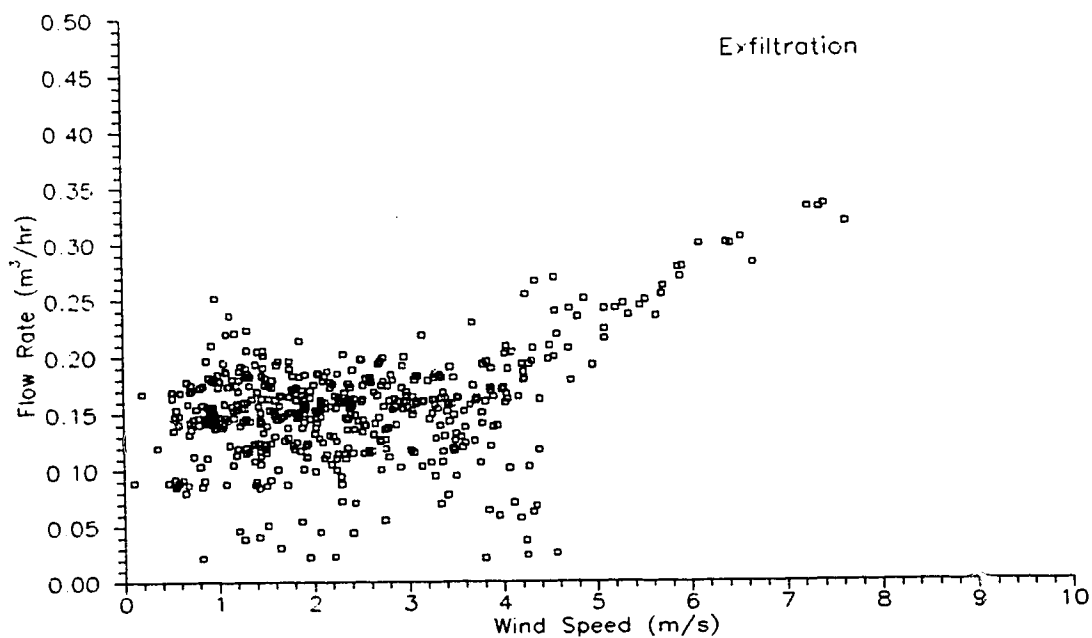


Figure 4.3b: Measured exfiltration rates across wall cavity for all wind directions (fan on)

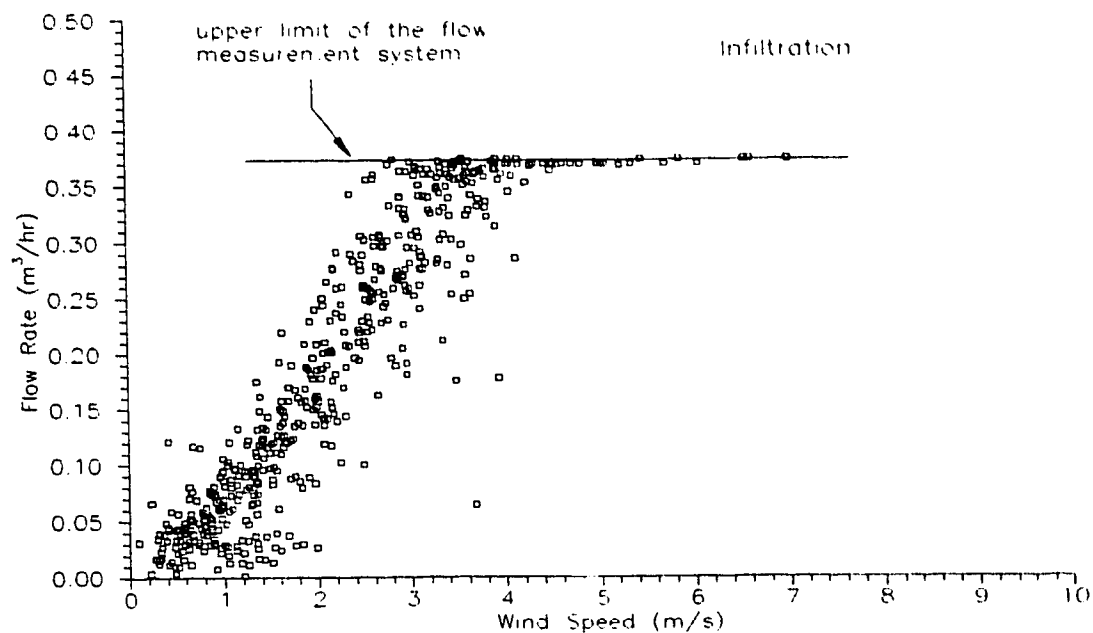


Figure 4.4a: Measured infiltration across wall cavity for north winds (-22.5° to 22.5°) (fan off)

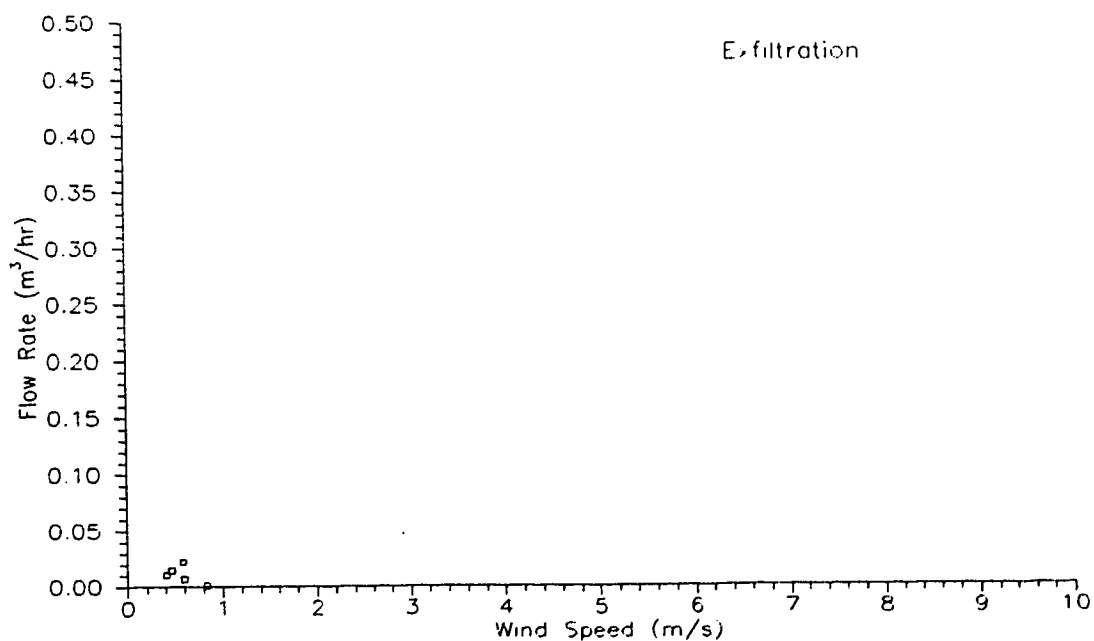


Figure 4.4b: Measured exfiltration across wall cavity for north winds (-22.5° to 22.5°) (fan off)

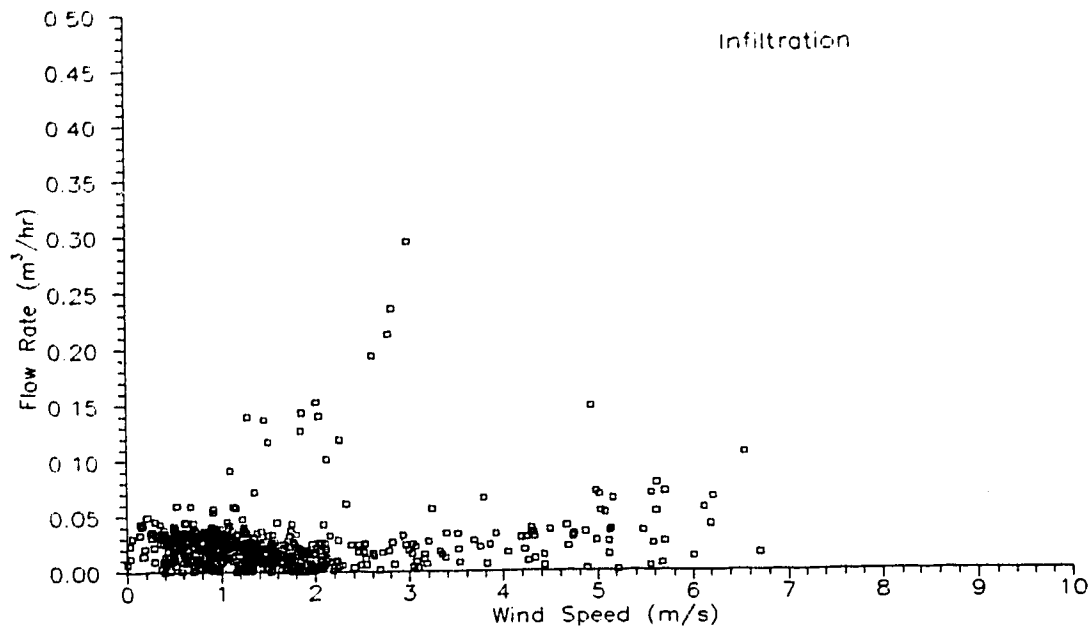


Figure 4.5a: Measured infiltration across wall cavity for south winds (157.5° to 202.5°) (fan off)

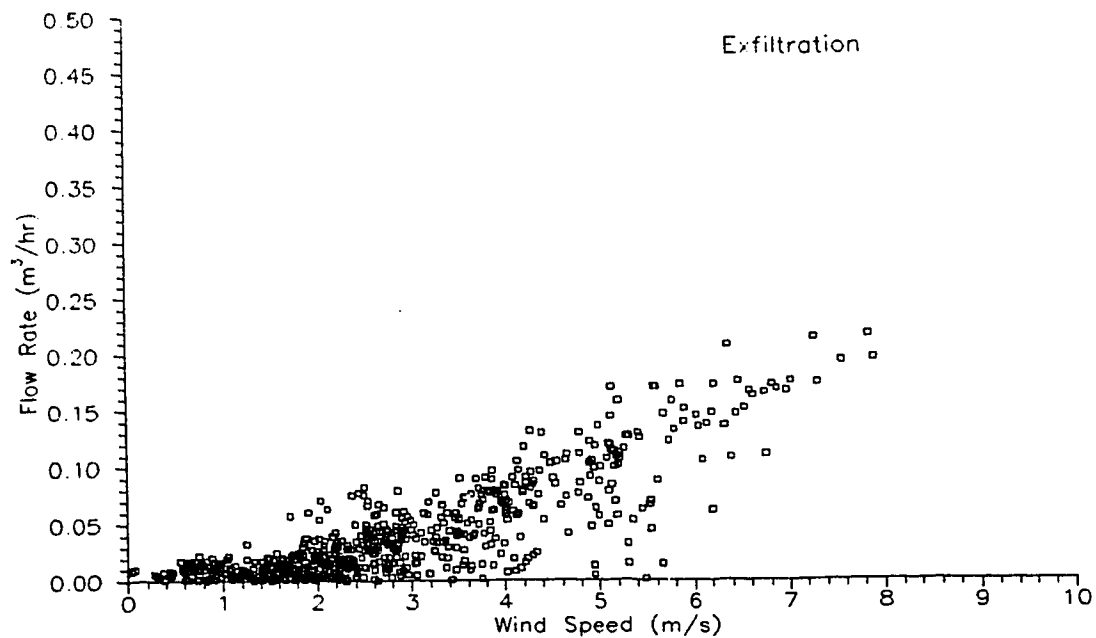


Figure 4.5b: Measured exfiltration across wall cavity for south winds (157.5° to 202.5°) (fan off)

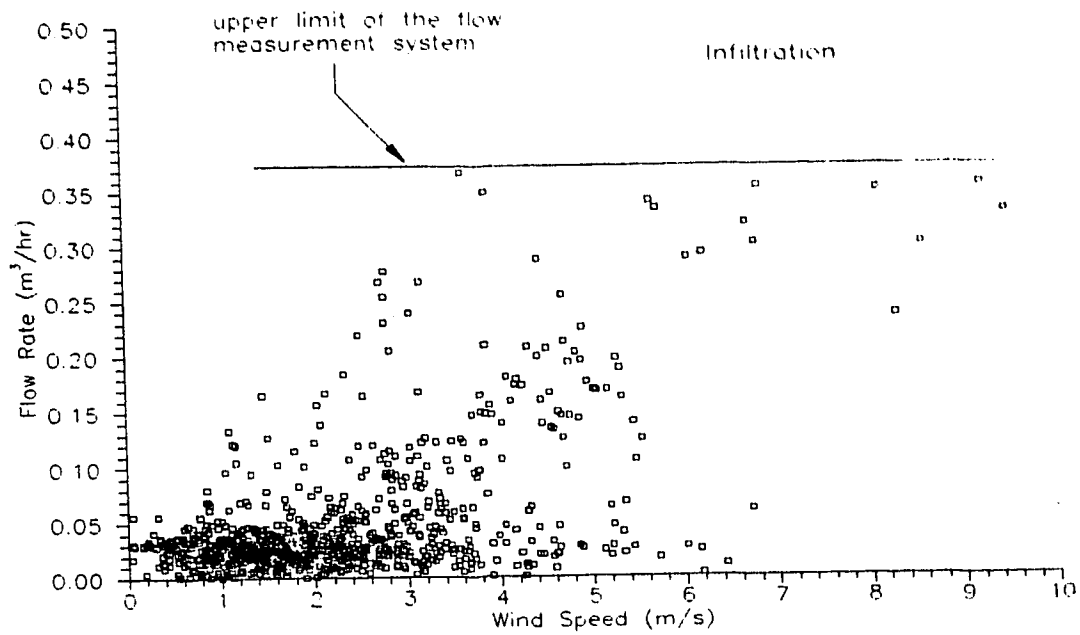


Figure 4.6a: Measured infiltration across wall cavity for west winds (247.5° to 292.5°) (fan off)

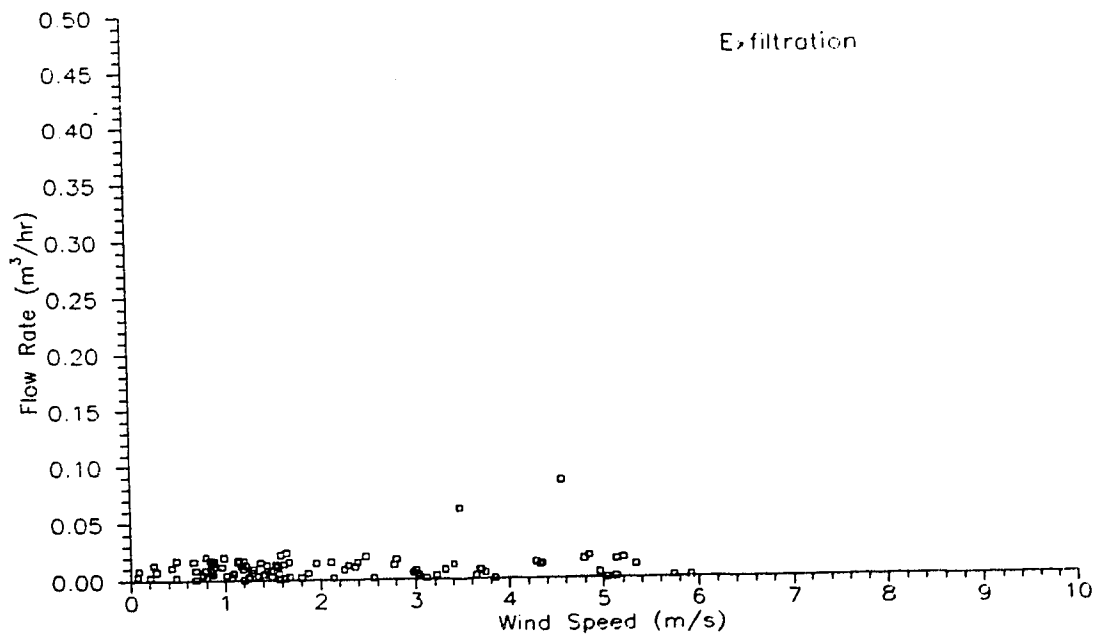


Figure 4.6b: Measured infiltration across wall cavity for west winds (247.5° to 292.5°) (fan off)

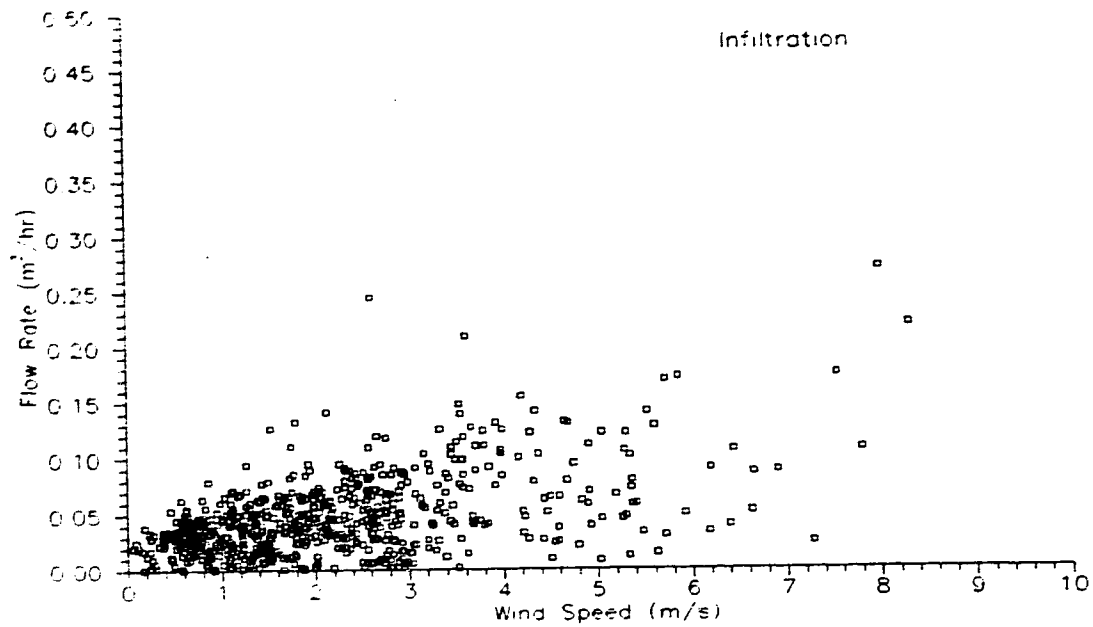


Figure 4.7a: Measured infiltration across the wall cavity for east winds (67.5° to 112.5°) (fan off)

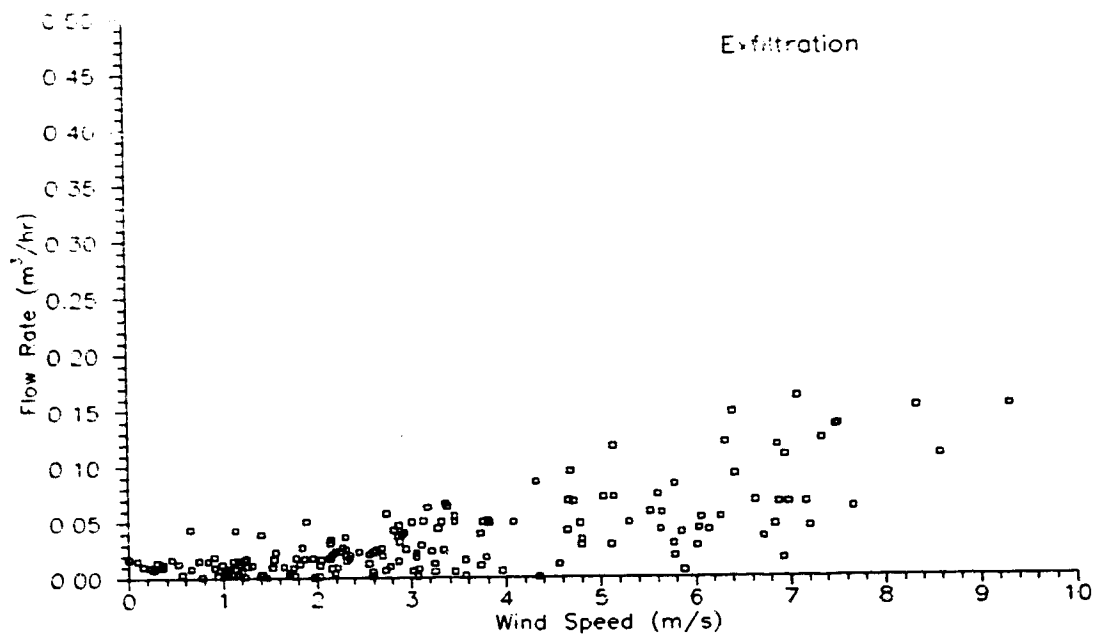


Figure 4.7b: Measured exfiltration across the wall cavity for east winds (67.5° to 112.5°) (fan off)

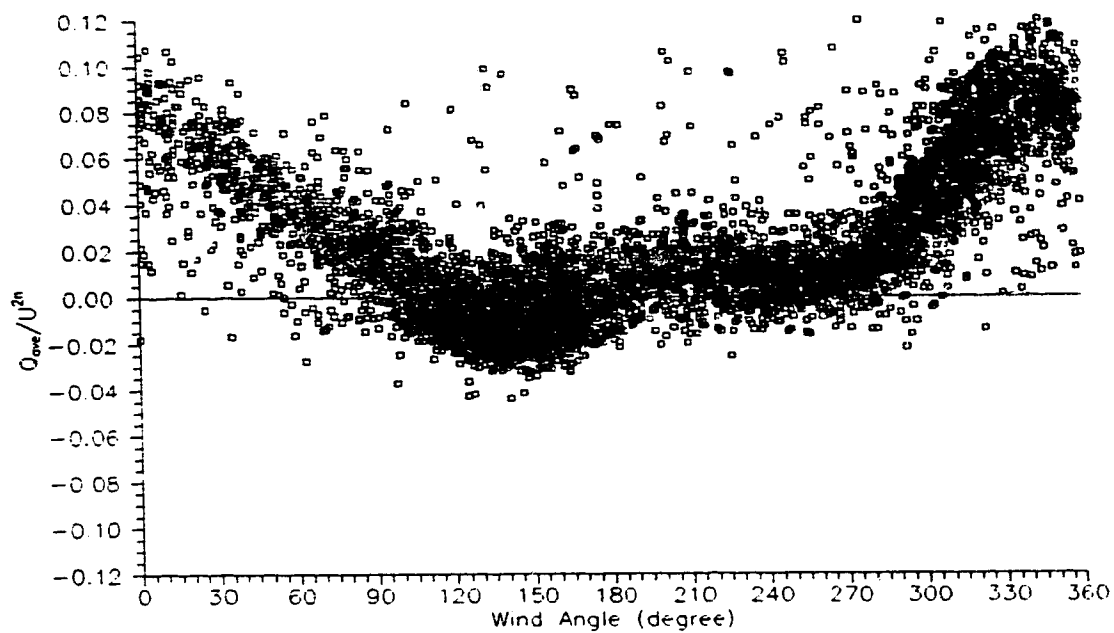


Figure 4.8a: Normalized average leakage rates for all wind speeds greater than 1 m/s (experimental data)

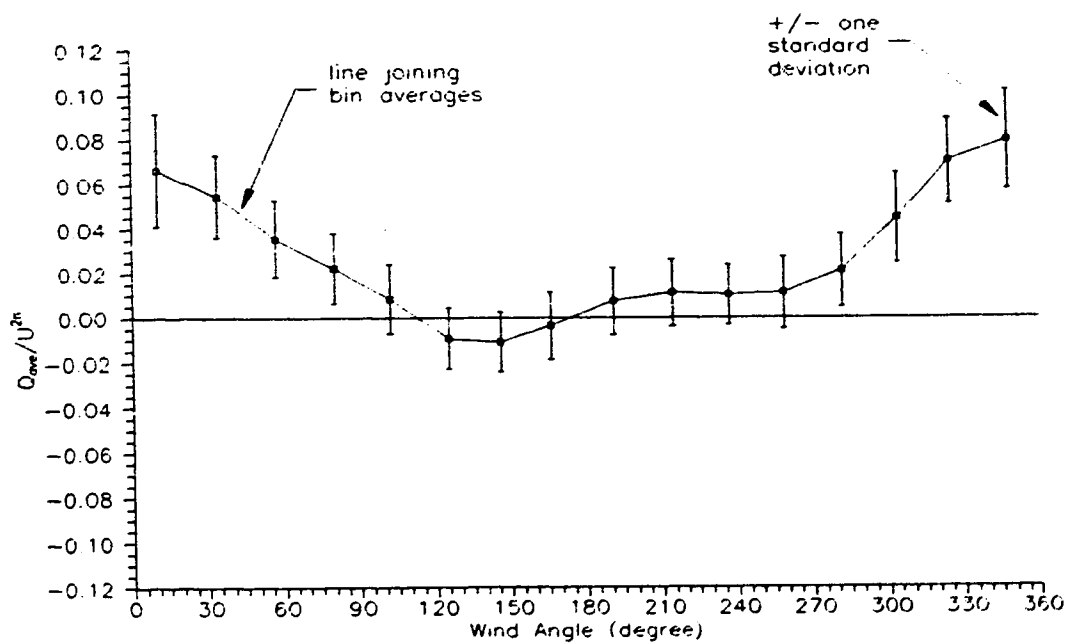


Figure 4.8b: Normalized leakage rates sorted into bins of 22.5° (experimental data)

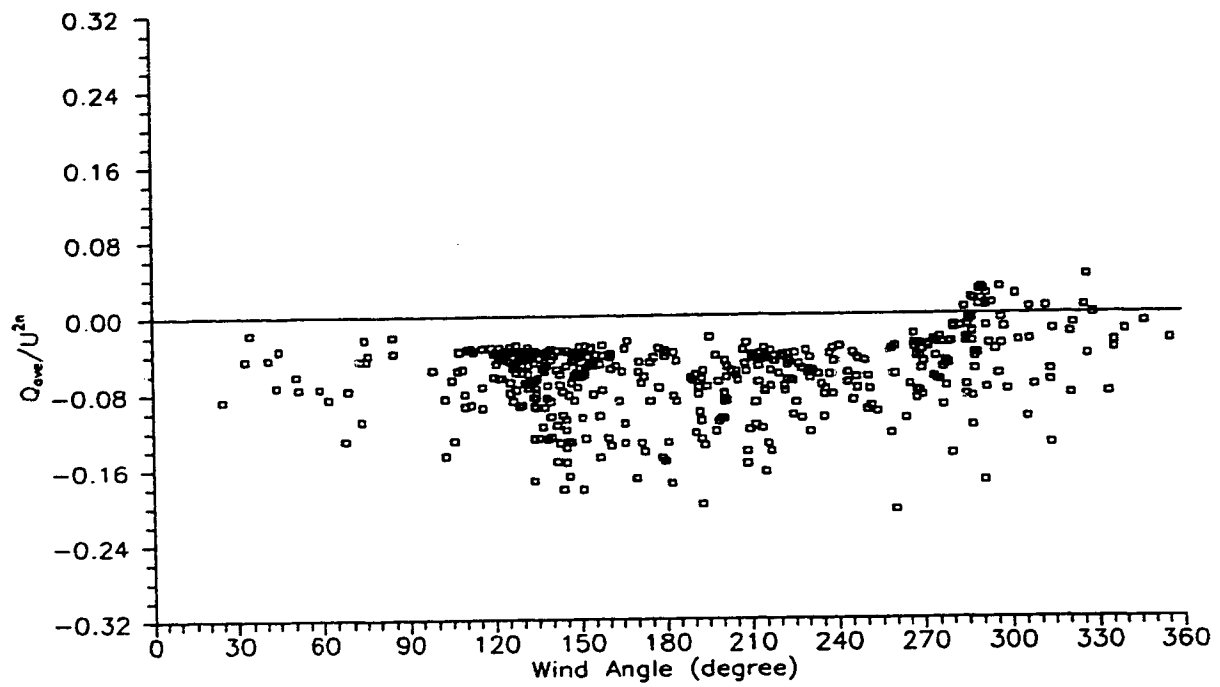


Figure 4.9: Normalized leakage rates with the fan in operation (experimental data)

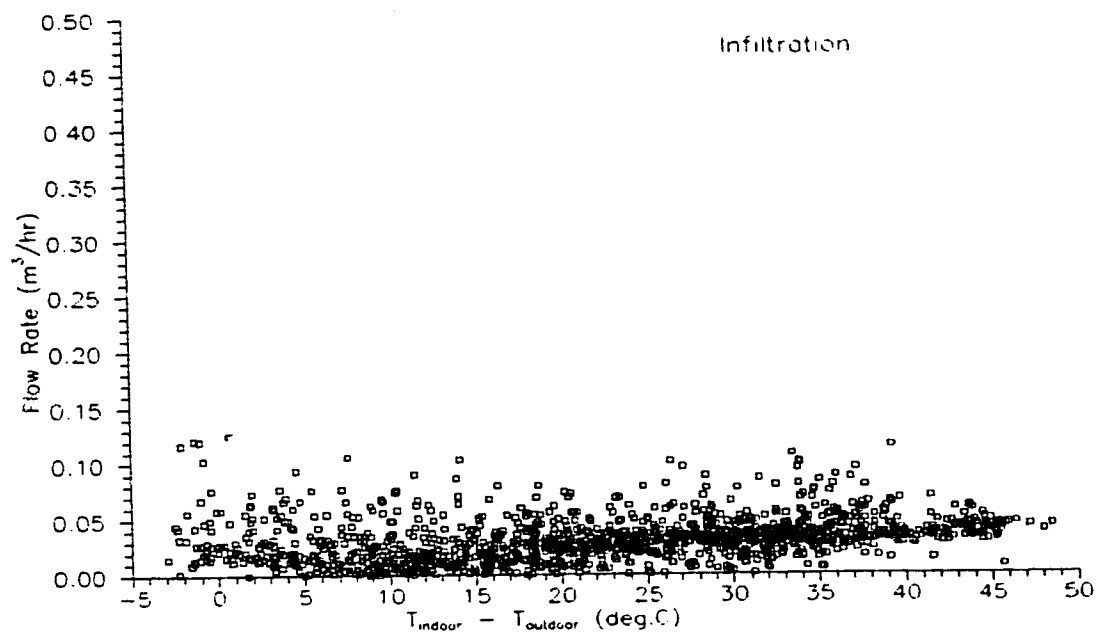


Figure 4.10a: Measured infiltration across wall cavity for all wind speeds below 1 m/s (fan off)

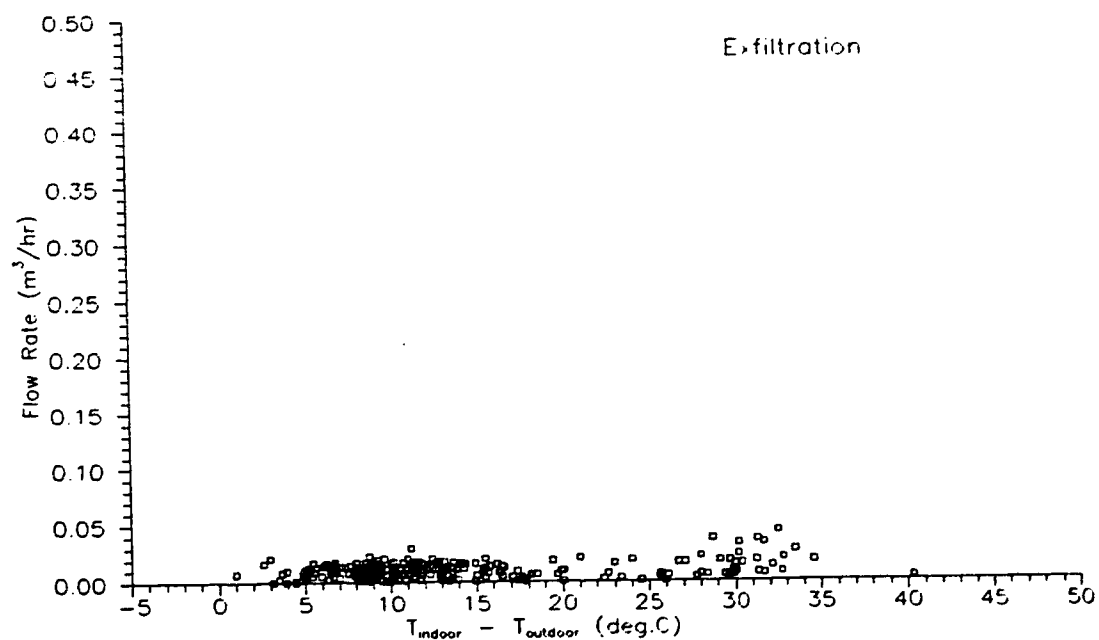


Figure 4.10b: Measured infiltration across wall cavity for all wind speeds below 1 m/s (fan off)

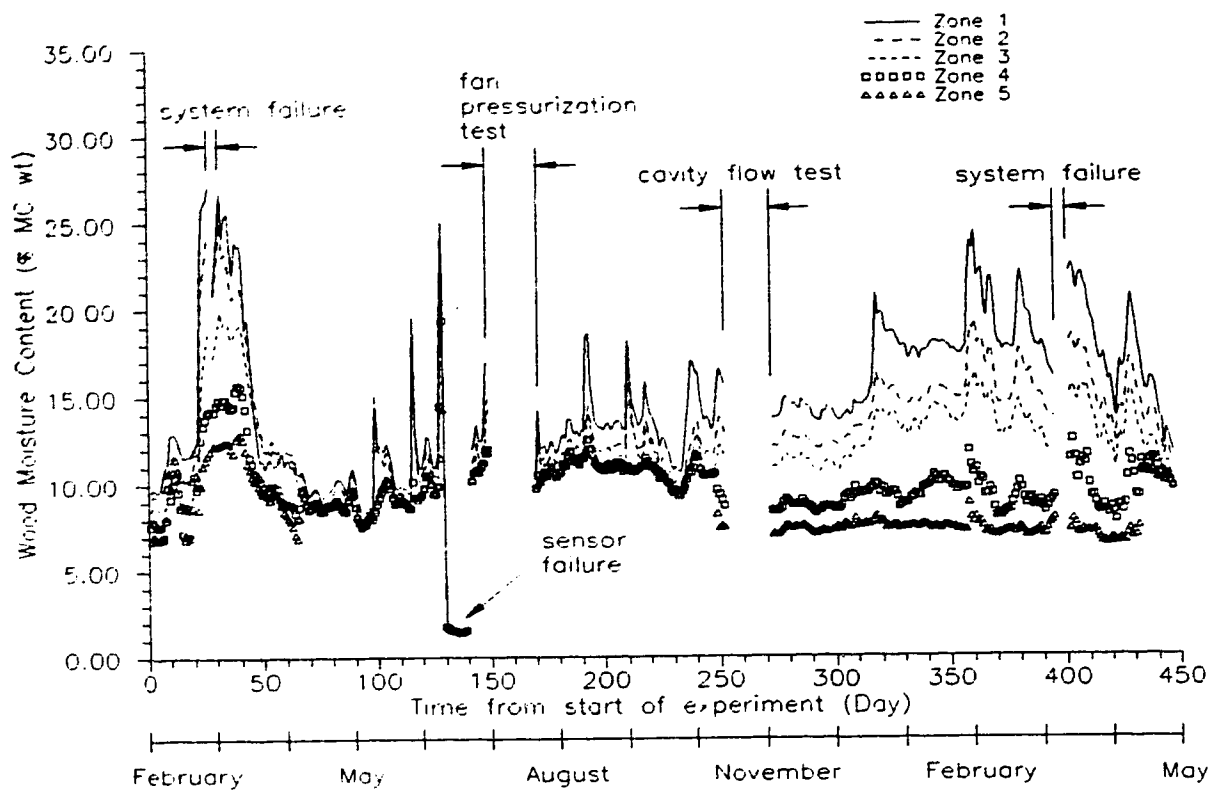


Figure 4.11: Daily averaged moisture contents in the five zones (February 1994 to April 1995)

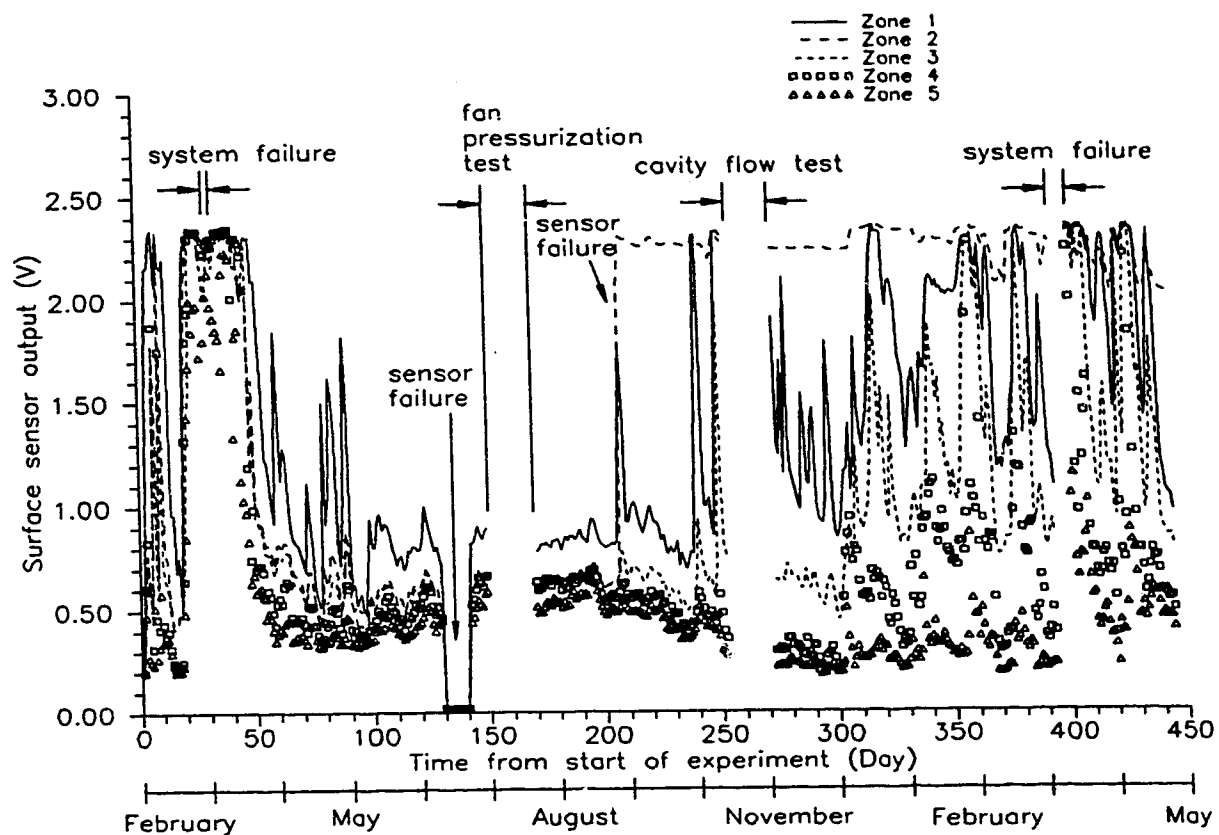


Figure 4.12: Daily average surface sensor output in the five zones (February 1994 to April 1995)

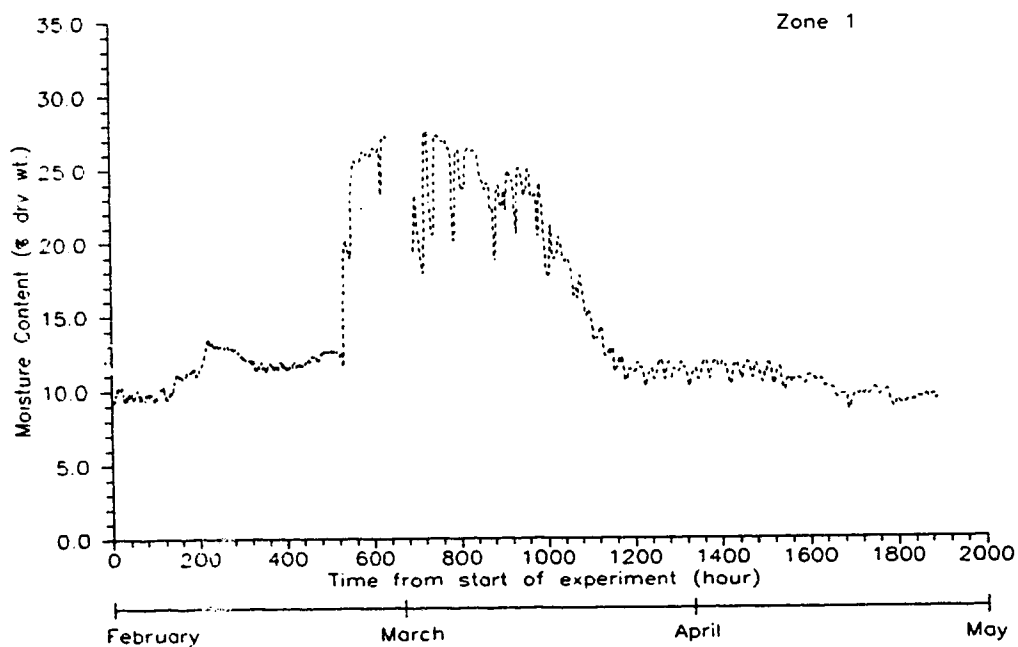
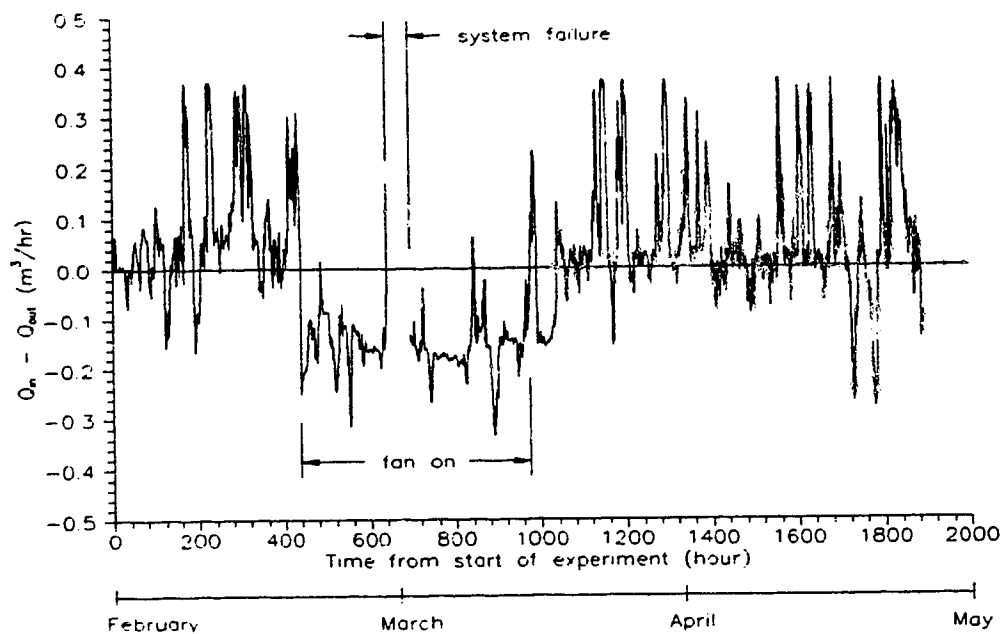


Figure 4.13: Change in the moisture content with flow rate (February 1994 to May 1994)

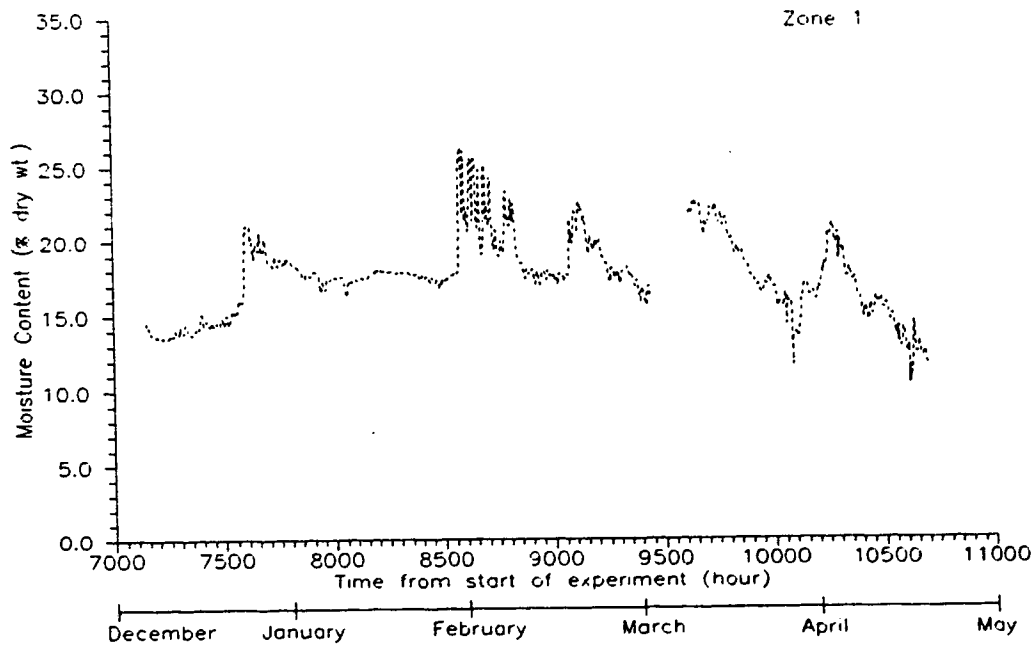
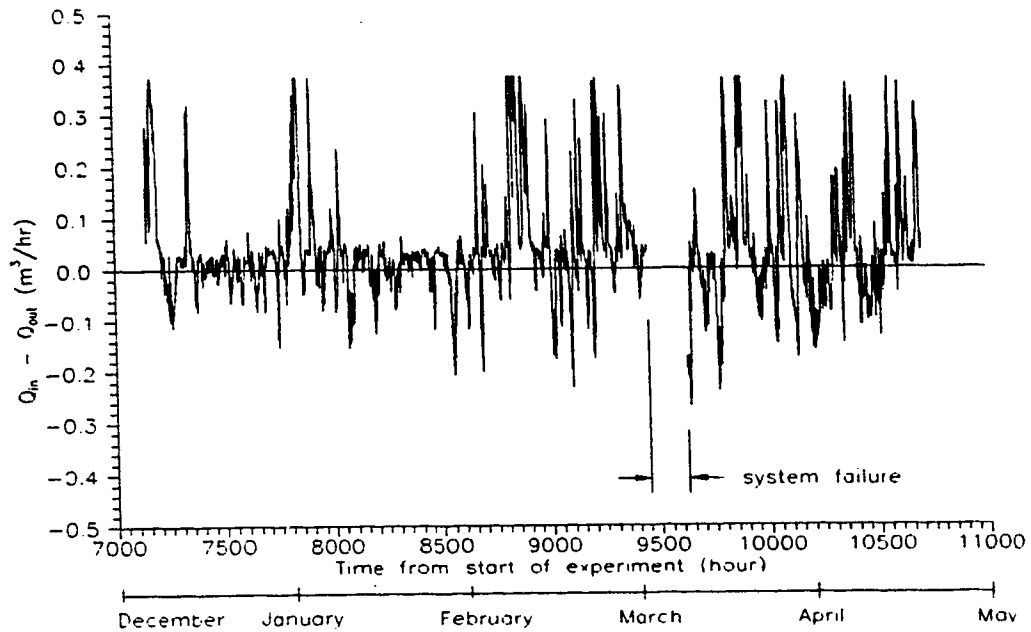


Figure 4.14: Change in moisture content with flow rate (December 1994 to April 1995)

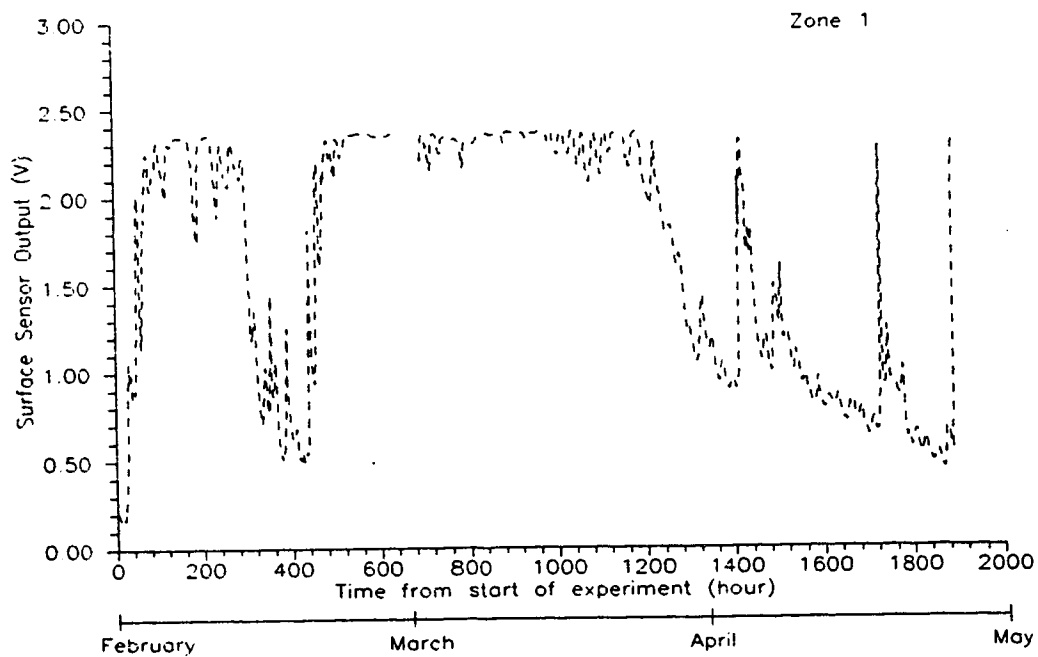
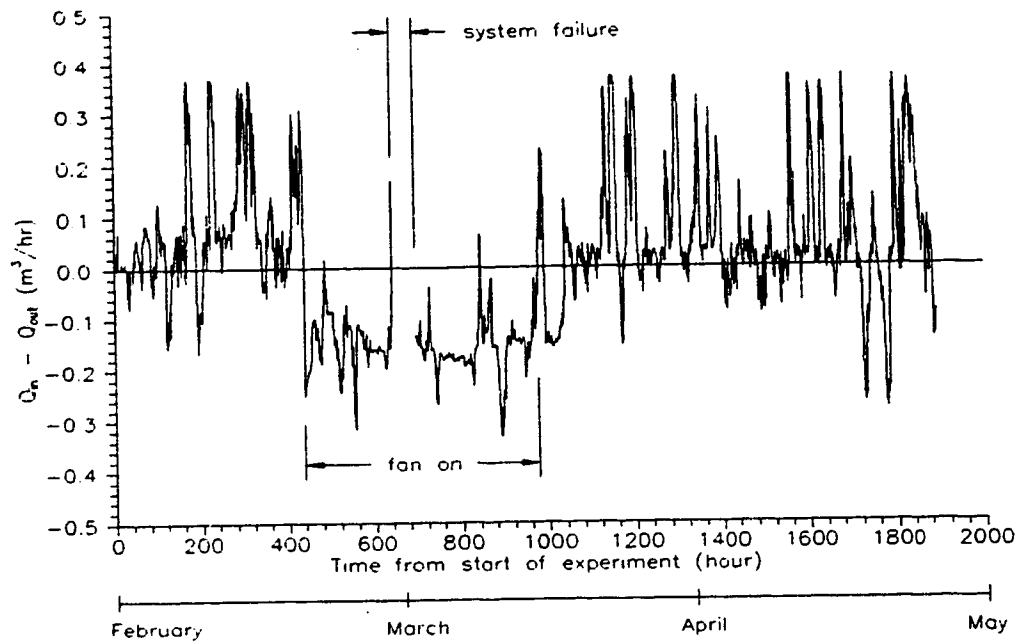


Figure 4.15: Change in surface sensor response with flow rate (February 1994 to May 1995)

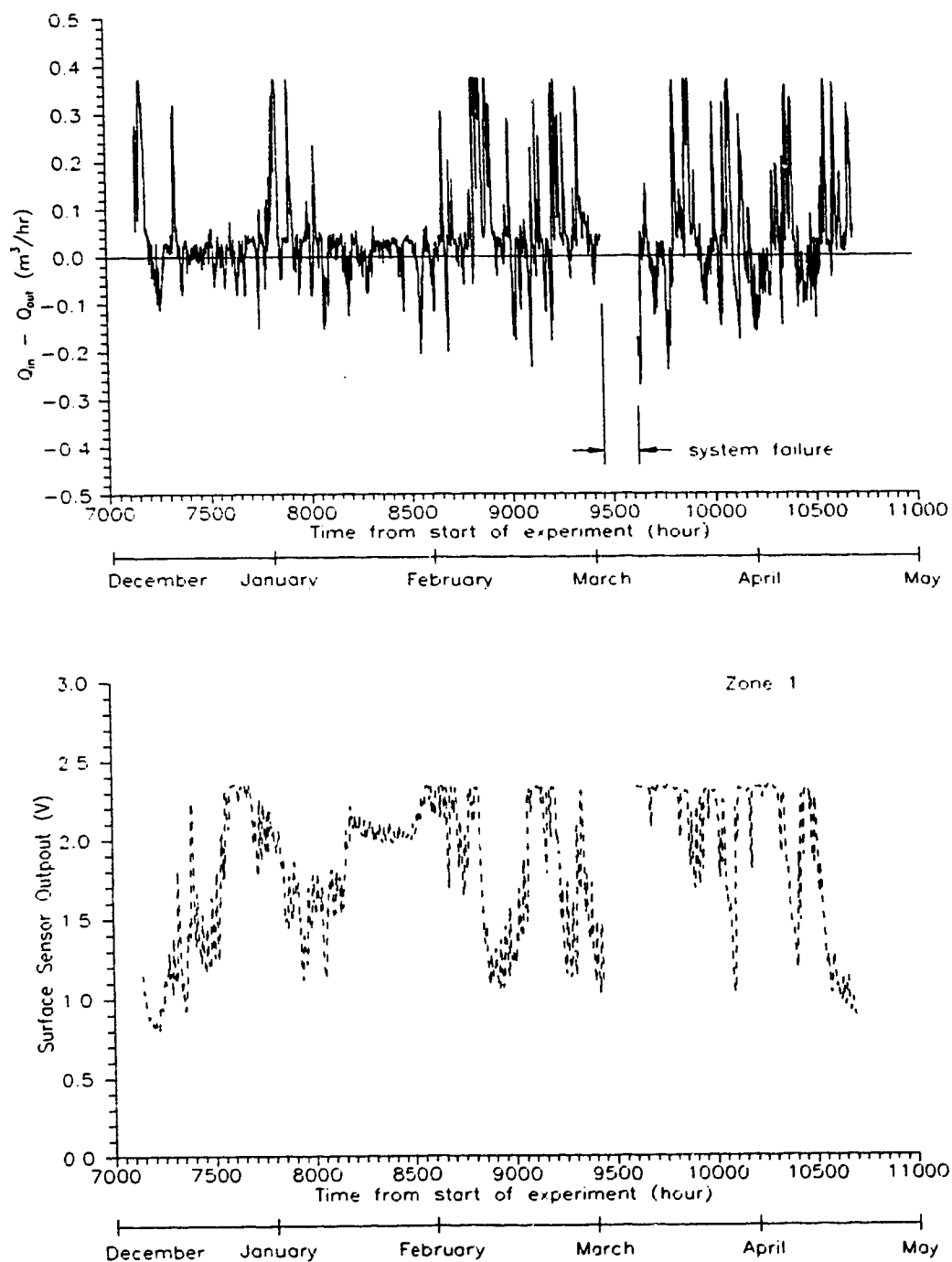


Figure 4.16: Change in surface sensor response with flow rate (December 1994 to April 1995)

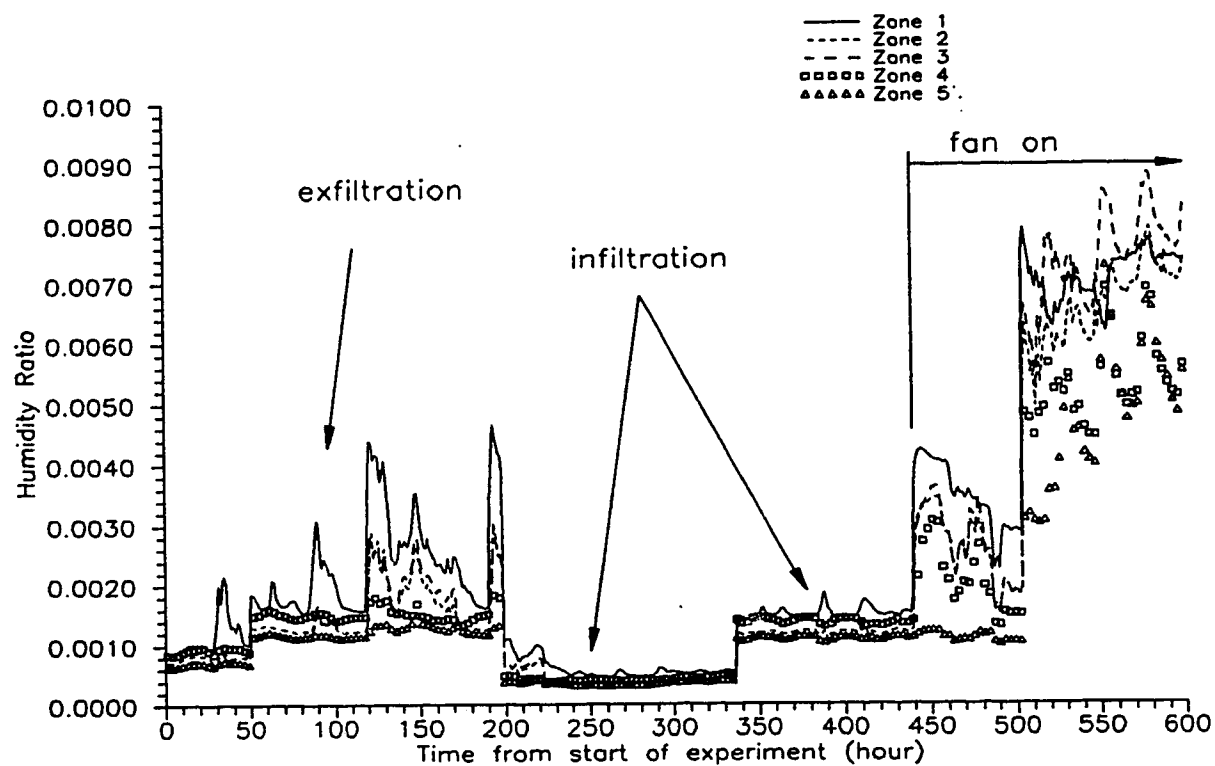


Figure 4.17: Humidity ratio at the mid depth of the cavity for the first 600 hours of the experiment

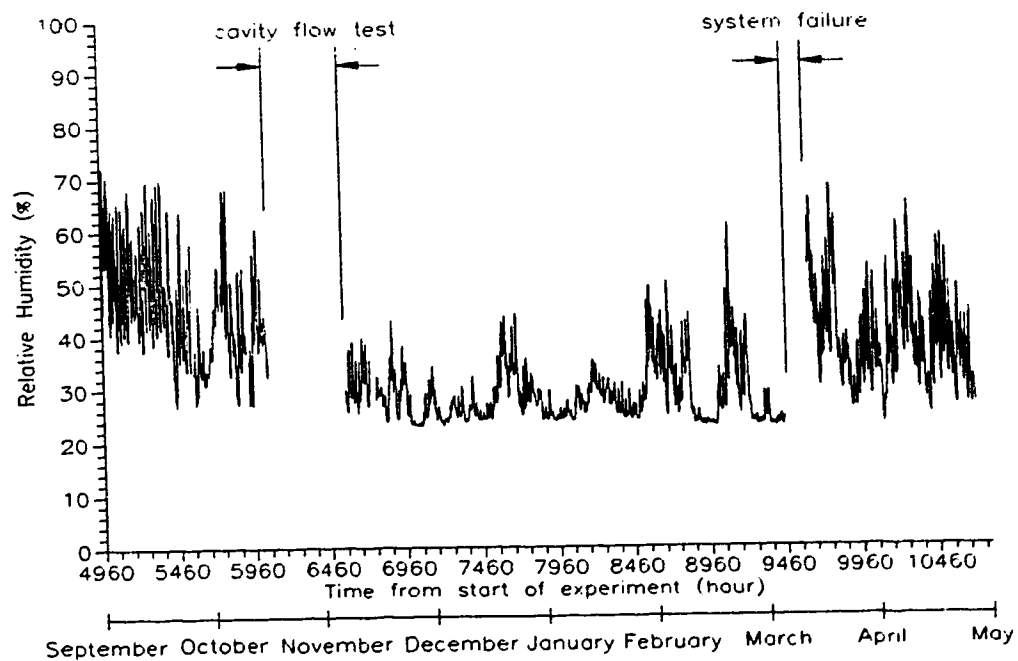
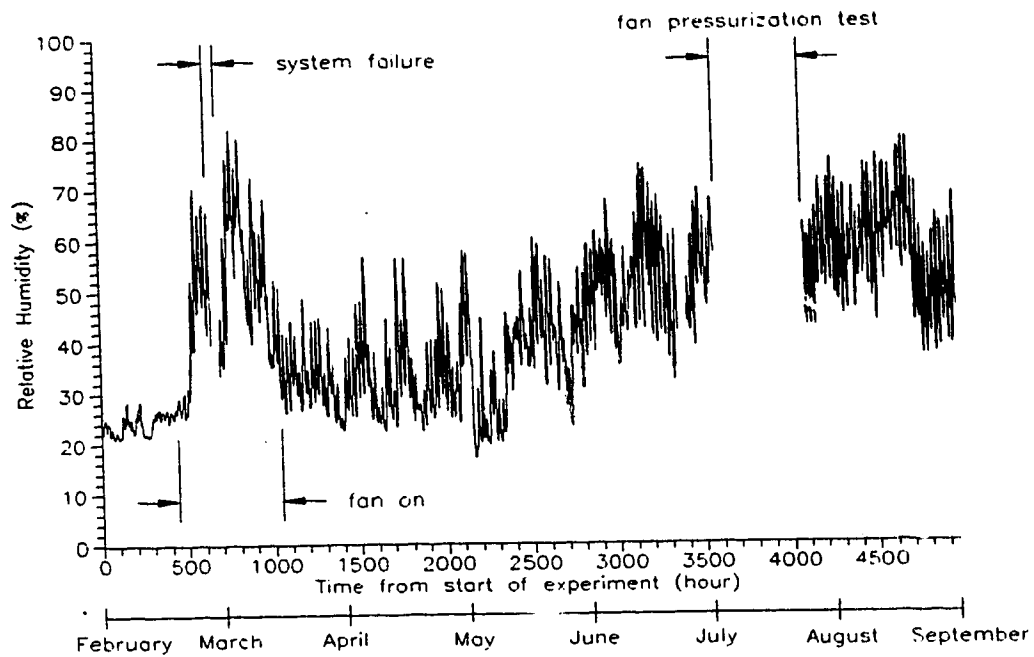


Figure 4.18: Relative humidity at mid cavity depth in zone 1 (February 1994 to April 1995)

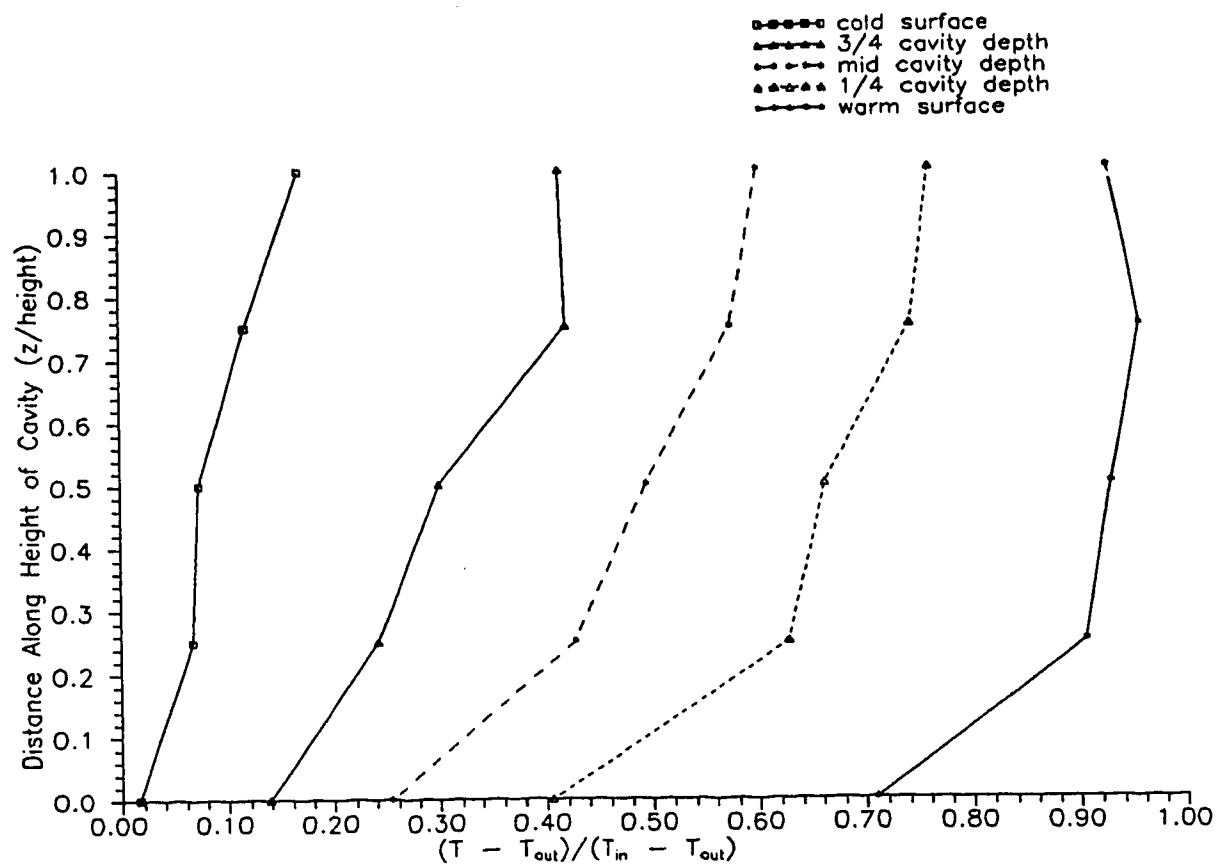


Figure 4.19: Typical temperature profile along the height of the cavity (hour 17 of the experiment)

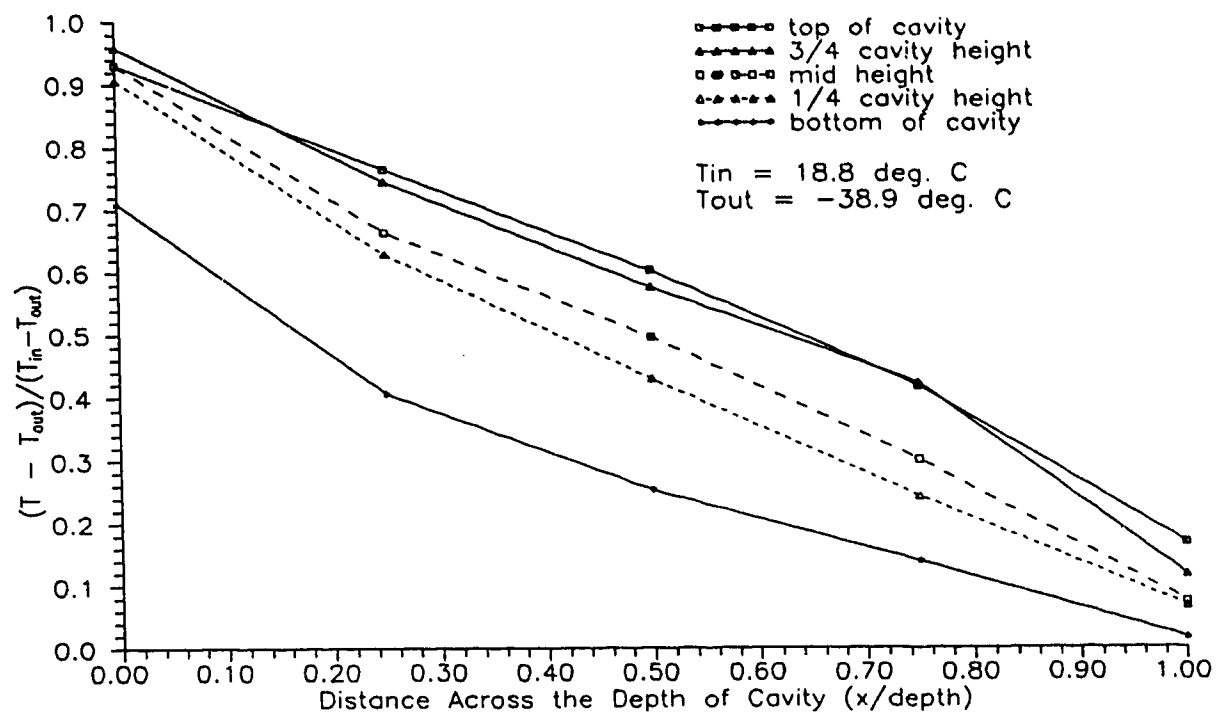


Figure 4.20: Typical temperature profile across the depth of the cavity (hour 17 of the experiment)

Chapter 5

MODEL VALIDATION

The air leakage and moisture deposition in the cavity were simulated with the models Local Leaks and Wetwall. The measured wind speed, wind direction, and indoor and outdoor temperatures collected during the experiment were used as input parameters into Local Leaks. Similarly, measured values of the air leakage flow rates through the cavity, indoor and outdoor temperatures and relative humidity, and cavity temperatures were used as input into Wetwall. The Local Leaks predictions were compared with the measured air leakage flow rates through the cavity and the Wetwall predictions were compared with the measured surface deposition and wood moisture content of the sheathing. In addition to the comparisons, the sensitivity of Wetwall to a change in the vapour diffusion coefficient in wood was examined. The mass diffusivity of water through wood is an important parameter in the model because the effect on moisture deposition predictions is significant.

5.1 COMPARISON OF MEASURED AND PREDICTED AIR LEAKAGE RATES

The air flow across the specified leakage path in the wall cavity was simulated with Local Leaks. The wind speed, wind direction, indoor and outdoor temperature measurements collected from the field experiment were used as input variables into the model. The other input parameters such as the background leakage characteristics and house configuration are summarized in Table 5.1. The air leakage flow predictions produced by Local Leaks over the duration of the simulation are presented in Figure 5.1.

The air leakage flow predictions in Figure 5.1 contain discontinuities corresponding

to the gaps in the experimental data due to the fan pressurization test, cavity flow test, and system failures. The model simulation also incorporated the conditions of a supply fan operating in part of the first heating season from hours 440 to 1038 and no fan in use in the second heating season as in the experiment. Unlike the experiment, however, the leakage predictions over an hour, shown in Figure 5.1, are either infiltration or exfiltration only instead of both. Since one type of flow usually dominates over an hour, as mentioned in Chapter 4, the hourly prediction of either infiltration or exfiltration is reasonable. The leakage predictions also differ from the experimental data in that the peak infiltration rates were not bounded by the upper limit of the measurement system at $0.37 \text{ m}^3/\text{hr}$. The peak infiltration was predicted to be about $0.45 \text{ m}^3/\text{hr}$ corresponding to a strong north wind with a speed of 7 m/s at hour 8829.

In the experiment, the air leakage rate over an hour can be both positive and negative because of the shift in the wind. The measured infiltration and exfiltration rates were accounted separately and a weighted average, as discussed in Section 4.1, was used to represent each air leakage rate. Since Local Leaks predicts either infiltration or exfiltration for each hour, the measured air leakage rates were converted to a net average flow rate, $Q_{\text{in}} - Q_{\text{out}}$, to match the form of the model predictions. Although, the situation of a zero net flow rate may arise if the amounts of infiltration and exfiltration over an hour are similar, it is rare because experimental results suggest that the air leakage flow is typically dominated by flow in one direction.

The correlation of the measured and predicted flow rates without the fan in operation is shown in Figure 5.2. The 45° line in the figure signifies an exact correlation.

For infiltration through the cavity, the data above the 45° line suggest that the model over predicts the measured air leakage rate and data below the line show that the model under predicts the air leakage rate. Conversely for exfiltration, the data above the 45° line correspond to model under prediction of air leakage flow rate and data below the line correspond to model over prediction of air leakage flow rate. As shown in Figure 5.2, the model typically under predicted both the infiltration and exfiltration with a root-mean-square error of approximately 1900% of the measured value. Local Leaks, however, was observed to predict the correct trends in the flow such that the direction of the predicted air leakage flow corresponded to that of the measured results. In general, the trends show good correlation with the experimental results except for low measured infiltration rates under $0.1 \text{ m}^3/\text{hr}$. The low measured air leakage flow rates were sensitive to small changes in the wind direction such that the direction of flow can easily change from positive to negative or vice versa. Hence, the incorrect trends in predicting the low measured air leakage flow rates is understandable.

Figure 5.3 shows the correlation of the predicted and measured air leakage flow rates with the fan in operation between hours 440 to 1038. The trends of the model predictions agree with the experimental results. The trends of the predictions were better than without the fan because the fan pressurization eliminated the low air leakage flow rates associated with the incorrect flow direction. The magnitudes of the air leakage rates, however, show poor correlation with the measured values. The root-mean-square error is approximately 975% of the measured value and the magnitude of the model predictions were seen to be lower than the measured air leakage flow rates. Overall, Local Leaks

under predicted the air leakage flow rates through the cavity for both fan biased and naturally driven flows. A summary of the root-mean-square and mean errors is shown in Table 5.3.

5.2 EFFECT OF WIND DIRECTION ON AIR LEAKAGE PREDICTIONS

The predicted and measured air leakage rates were sorted into bins of north, south, east, and west winds to observe the effectiveness of the model for different wind directions. The correlation of flow rates for north winds (-22.5° to 22.5°), shown in Figure 5.4, illustrates that Local Leaks produced nearly all the correct trends with the model predicting almost entirely infiltration. Since the air leakage rates were sorted into bins with a narrow range of wind angles, the pressure coefficient was not sensitive to the wind direction and the direction of the flow predicted by Local Leaks matched that of the field experiment.

Figure 5.4 also shows that Local Leaks under predicted the magnitude of the infiltration rate with an absolute error of approximately 244% of the measured value. The under prediction of the magnitude of the air leakage rates was due to the variation of the pressure coefficient with the height of the cavity. In the model, a single average pressure coefficient for an entire wall was used regardless of the location of the specific leakage site on the wall. From experiments conducted by Fleming (1996) however, evidence suggest that the pressure coefficient varies with the height of the wall at a range of ± 0.1 of the wall average value. Typically, the pressure coefficient at the top of the wall is larger than the average value and the pressure coefficient at the bottom is less than the wall average value. Consequently, the use of a wall average pressure coefficient in the model for the

exterior leakage site located at the top of the wall produced lower air leakage rates than the measured values.

The correlation of air leakage rates for south winds (157.5° to 202.5°), shown in Figure 5.5, displays better agreement for flows over $-0.1 \text{ m}^3/\text{hr}$ than for north winds. The root-mean-square error for the entire range of air leakage flow rates is approximately 3200% of the measured value. The better correlation was due to the fact that the variation of the pressure coefficient along the height of the wall is of less influence on the air leakage flow rates because the entire north wall is in the wake region.

Figure 5.5, also shows much scatter between measured air leakage flow rates of $0.1 \text{ m}^3/\text{hr}$ and $-0.1 \text{ m}^3/\text{hr}$. Unlike for north winds, the pressure coefficient for south winds is smaller and consequently, the magnitude and direction of the air leakage flow rates are more sensitive to the influence of the other surfaces of the house. The magnitude and sign of the pressure coefficient of the east and west walls would have a definite effect on the air leakage flow predictions for south winds.

For east winds (67.5° to 112.5°), the model under predicted both the infiltration and exfiltration rates through the cavity. As shown in Figure 5.6, the exfiltration was under estimated much worst than the infiltration. The figure also shows that Local Leaks predicted incorrectly a portion of the infiltration. The correlation of air leakage flow rates between predictions and measured values for west winds (247.5° to 292.5°), shown in Figure 5.7, displays better agreement in the direction of flow between the predictions and measurements than for east winds. The flow was predominately infiltration and the amount of exfiltration was not significant. The model, however, still under estimated the

magnitude of the infiltration. A summary of the root-mean-square and mean errors for all wind directions is outlined in Table 5.4.

The contrast in the trends between the predictions and measurements for east and west winds is due to the difference between the pressure coefficient used in the model and the actual flow behaviour of the wind observed in the field experiment. A plot of the normalized predicted air leakage flow rates, shown in Figure 5.8, displays a curve symmetrical about 180° . The pressure coefficient used in the model was developed for house 4 which has symmetrical sheltering of row houses situated to the east and west. The sheltering for house 6, however, is not symmetrical. Five houses are situated to the west of house 6 and a 3.7 m high wall is located to the east. Since the air flow along the row of houses is different from that over the wall, the pressure coefficient for the east and west walls is asymmetric which is not the same as that in Local Leaks. The difference in the sheltering between the measured data and model predictions is reflected in the plot of the normalized air leakage flow rates shown in Figure 5.9. The curve based on the experimental data is skewed such that normalized leakage rate for east winds is significantly different than that for west winds. In addition, the minimum normalized leakage rate from the experiment is at approximately 150° which partly accounts for the incorrect trends in the air leakage flow predictions for south winds. In contrast, the normalized air leakage flow rates predicted by the model is symmetric about 180° at which the minimum normalized air leakage flow rate occurs. The difference in the sheltering accounts for much of the incorrect trends in the predictions, especially for estimates under east winds. As expected, the maximum normalized leakage rate for the predicted and

measured values occurs for north winds at 0° and 360° . Figure 5.9 also shows that Local Leaks under predicted the air leakage flow rates over all wind directions.

From the correlations of Local Leaks predictions and measured air leakage flow rates, the use of a single average pressure coefficient for an entire wall produced predictions whose magnitudes were lower than the experimental results. The variation of pressure coefficient with height of the cavity probably has a significant effect of the prediction of the air leakage flow rates through a cavity.

The comparison of the predicted and measured normalized average air leakage rates, shows significant difference which is most likely due to the difference between the pressure coefficient on the east and west walls of a house situated in the middle of a row of houses as in the model and that of a house located at the end of the row as in the experiment. In addition, the incorrect trends for air leakage rates under $0.1 \text{ m}^3/\text{hr}$ were due to the flow being sensitive to small changes in the wind direction. At such low magnitudes, the measured air leakage rates can easily change from infiltration to exfiltration or vice versa due to shift in wind speed and direction.

5.3 EFFECT OF INDOOR/OUTDOOR TEMPERATURE DIFFERENCE ON AIR LEAKAGE PREDICTIONS

A comparison of the predicted and measured air leakage rates for wind speeds below 1 m/s demonstrates the ability of Local Leaks to estimate the stack effect driven flows across the cavity. As shown in Figure 5.10, the model under predicted the magnitude of both the infiltration and exfiltration. In general, Local Leaks was observed to predict incorrectly the flow direction of the measured infiltration rates which were

typically under $0.1 \text{ m}^3/\text{hr}$. Although the air leakage rates shown in Figure 5.10 corresponded with wind speeds below 1 m/s , the measured air leakage flow rates were sensitive to small changes in the wind direction such that the direction of flow could have changed easily from positive to negative or vice versa. The incorrect trends are reasonable given the small magnitudes of the air leakage rates.

5.4 WETWALL PREDICTIONS FOR EXTERIOR SHEATHING SURFACE DEPOSITION AND WOOD MOISTURE CONTENT

The moisture deposition inside the cavity was simulated using Wetwall over the same time period as the experiment. The measured values of air leakage, indoor/outdoor temperatures and relative humidity, sheathing surface temperature, and dry wall temperature from the experiment were used as inputs into the model. The sheathing and dry wall temperatures were measured values at the mid-height of the cavity because they are similar to the average temperature along the height of the wall as discussed in Section 4.8. The input parameters to Wetwall are summarized in Table 5.2. The model output consists of hourly predictions of surface deposition and wood moisture content at node 1, node 2, and node 3 in all five zones; the moisture content at node 4 is a known value corresponding to the ambient vapour pressure and temperature. The actual surface deposition in the cavity is represented by the predictions of surface accumulation and wood moisture content at node 1. The internal moisture content of the exterior sheathing is estimated by the wood moisture content at node 2 and node 3. These nodes were observed to not reach saturation and hence, no free water accumulated.

The hourly predictions of surface deposition and moisture content were averaged

over one day to observe the trends developed over the course of the experiment. The amount of surface deposition predicted by the model for each zone, shown in Figure 5.11, illustrates the expected rise and fall of the free moisture on the inside sheathing surface. The surface moisture accumulated over the first heating season from February 1994 to April 1994 and the second heating season from December 1994 to April 1995 because the cold weather created a large potential for moisture deposition. The vapour pressure at the sheathing over the heating season is reduced by the cold temperatures and typically, the vapour pressure at the inlet is much larger than the sheathing vapour pressure which induces moisture deposition. Conversely, over the summer the surface deposition was non-existent because of the small tendency for wetting during the warm months. Warmer temperatures increase the vapour pressure at the sheathing surface and often, the vapour pressure at the surface is larger than that at the inlet. Hence, a pressure gradient for drying exists where the water vapour diffuses away from the sheathing.

The wood moisture content in node 1, shown in Figure 5.12, also demonstrates the same wetting and drying trends as the surface deposition. The predicted peak moisture content in zone 1 over the first heating season was about 33 wt% due to the sustained period of exfiltration created by the pressurization of the fan. By the start of May 1994, however, the fan had been shut off and the predicted moisture content had dropped to 13 wt% due to the drying of the cavity created by the warm temperatures. At the start of the second heating season, the value in zone 1 increased promptly back to about 32 %wt even without the fan in operation.

Furthermore, the predictions of surface deposition and moisture content at node 1

shown in Figure 5.11 and Figure 5.12 both illustrate the expected moisture distribution along the height of the cavity where the amount of condensation is greatest at the interior leakage site and the amount of moisture deposition decreases with increasing distance from the opening. In the model, zone 1 is directly opposite the interior opening and zone 5 is the furthest away. The other zones are located between the top and bottom zones in an ascending order. The surface deposition in zone 1, shown in Figure 5.11, is the only zone of the five that has significant amount of moisture accumulation. Other than a small amount of moisture in zone 2, the rest of the sheathing surface is dry. Similarly, the wood moisture content in zone 1, shown in Figure 5.12, is consistently the largest value and the value in zone 5 is typically the lowest over the entire simulation. The amount of moisture in the other zones decreases respectively with the distance away from zone 1. This is clearly evident in the first heating season.

The predicted moisture contents in node 2 and node 3 follow similar trends as demonstrated in the surface deposition and node 1 predictions. The moisture contents at node 2 and node 3, shown in Figure 5.13 and Figure 5.14, are seen to rise over the two heating seasons and decrease during the summer. The moisture content in zone 1 for both nodes is always the largest and the values in the other zones decrease with the distance from zone 1 because of a progressively weaker potential for moisture deposition along the height of the cavity. In the model, the variation of moisture deposition along the height of the sheathing is influenced by the exponential term in the analytical solution for mass deposition as shown in Equation 2.18. The magnitude of the exponential term decreases with distance from the inlet of the air leakage flow. For exfiltration, the inlet is at the

bottom and consequently, zone 1 has the largest moisture deposition potential. For infiltration, the inlet is at top and as a result, zone 5 has the largest drying potential.

Unlike node 1 predictions, however, the magnitudes of the moisture content at node 2 and node 3 in Figure 5.13 and Figure 5.14, are observed to be lower than node 1 because the diffusive mass transfer at the internal nodes is much slower than the exchange at the surface. The predictions were based on a mass diffusivity for water through wood of $3 \times 10^{-6} \text{ m}^2/\text{s}$ for the exterior sheathing. The moisture deposition predictions are sensitive to the mass diffusivity of the sheathing and further discussions are presented in Section 5.6. Although no surface deposition was predicted for node 2 and node 3, node 2 is still susceptible to wood rot because the moisture content is typically over 20 %wt during the heating season. The moisture content in node 3, as expected, is less than node 2 because node 3 is closer to the outside surface which is typically drier than the interior of the cavity.

5.5 COMPARISON OF MEASURED AND PREDICTED SHEATHING SURFACE DEPOSITION AND MOISTURE CONTENT

The sheathing wood moisture content measured using the stainless steel pins in the experiment is the average value at the centre of the sheathing. According to the position of the pins relative to the internal nodes in the model, shown in Figure 5.15, the predictions at node 2 and node 3 should bracket the moisture measurements from the experiment. The predictions at the surface and to a lesser extent node 1 correspond to the surface sensor output from the experiment. Since, the surface sensor produced qualitative results, only the trends of the predictions at the surface can be compared.

For model validation, the predictions and experimental data are compared over three periods: the first heating season from hour 0 to 2000, summer from hour 2000 to 7000, and second heating season from hour 7000 to 10700. Groups of 10 figures are presented for each period. The plot of the surface sensor output along with the predicted surface accumulation and moisture content at node 1 in zone 1 is shown in Figure 5.16a. The model predictions qualitatively agree with the experiment for the moisture deposition phase, but not as well for the moisture removal period. At approximately hour 40, the jump in the predicted moisture content to saturation at node 1 coincided with the measured wetting of the surface sensor. The predicted surface deposition also closely followed the response of the surface sensor with a steady rise beginning at about hour 440 coinciding with the operation of the fan. Wetwall predictions for the wetting phase agrees qualitatively with the experimental results.

For the drying phase, whose start corresponded to the termination of the fan at approximately hour 1040, the model predicted the same trends, but not the same magnitudes of moisture deposition as the experiment. At about hour 1040 of Figure 5.16a, the surface sensor output begins to show some fluctuations unlike the steady output prior to this time. The fluctuations signify the initiation of moisture removal from the surface sensors. Since the start of the drop in the surface deposition predictions matches the measured surface sensor output, Wetwall appears to have predicted the correct trends. The drying process simulated by the model, however, responded slower than that in the experiment. At approximately hour 1900, the surface sensor indicates no moisture, but the model still predicts about 20 g of moisture deposition on the surface of the zone.

In addition, the moisture content of node 1 remained at saturation because drying a node cannot take place until all of the surface deposition has been removed. Hence, the moisture content at node 1 did not show any decrease.

As discussed previously, the model uses the moisture content at zone 1, the wettest of the five zones, to determine the sheathing vapour pressure for exfiltration. The origin for determining the coordinates of the upper and lower zone limits begins at the bottom opening. Conversely, for infiltration the sheathing vapour pressure is based on moisture content in zone 5, the driest of the five zones and the origin for the zone limits begins at the top opening. As seen in the Figure 5.16a, this arrangement works well for the wetting phase, but not for the drying phase. For infiltration, the vapour pressure gradient across the cavity is favourable for drying because the vapour pressure at the inlet is typically smaller than that of the sheathing because zone 5 is dry; water vapour diffuses away from the sheathing. Although, the pressure gradient is conducive to drying, the influence of the exponential term in the mass deposition equation, Equation 2.18, reduces the magnitude of the drying effect with the increasing distance from the zone 5 for the zone limits. By the time the air flow reaches zone 1, the wettest zone which should be the most susceptible to drying, the moisture removal potential is small. Hence, the predicted surface deposition still exists and moisture content in zone 1 remains saturated even when the experimental results indicate no moisture on the sheathing surface.

The comparisons of model prediction and experimental data on surface deposition in zone 2 and zone 3, shown in Figure 5.16b and Figure 5.16c, demonstrate similar response as in zone 1 to the moisture deposition and removal. With little predicted surface

deposition in zone 2 and none in zone 3, however, the drop in the moisture content at node 1 corresponded quite closely to the drop in the surface sensor output. The plots of the predicted responses in zone 4 and zone 5, shown in Figure 5.16d and Figure 5.16e, did not illustrate the ability of the model to track the wetting and drying trends because the actual surface deposition in these zones is small.

The ability of the model to predict the moisture content in the sheathing is observed in a plot of the predicted wood moisture content at node 2 and node 3, and the measured internal sheathing moisture content. Ideally, node 2 predictions should be the upper bound and node 3 predictions should be the lower bound to the experimental data. The comparison of the prediction and measurements in zone 1, shown in Figure 5.17a, suggests that the model at node 2 over predicted the measured sheathing moisture content without capturing the peak rise in the moisture content. As in the surface deposition and node 1 predictions, Wetwall responded to the wetting better than the drying of the cavity. Node 2 predictions in Figure 5.17a remained at about 20 %wt even though the actual moisture content had dropped to approximately 10 %wt between hours 1150 to 2000. Node 3 predictions also over estimated the moisture content in the sheathing and displayed the similar trends as in node 2, but the moisture content was lower. Since the moisture content of node 2 and node 3 is partly dependent on the amount of moisture at node 1, the slow response for the drying phase is indirectly affected by the influence of the exponential term in the mass deposition equation, Equation 2.18, for the cavity. Consequently, the drop in the moisture content at node 2 and node 3 as predicted by Wetwall also shows a lag with the experimental results.

The comparison for zone 2, shown in Figure 5.17b, displays closer agreement between predictions and measurements. Node 2 predictions typically traced the rise and fall of the change in the actual moisture content of the sheathing and was the upper bound to the measurements. The node 2 predictions in zone 2 captured the trend of the peak rise better than in zone 1 even though they still under predicted the magnitude of the moisture content. The predicted Node 3 response also closely followed the experimental data and acted as a lower limit.

The comparisons in the zone 3, zone 4, zone 5, shown in Figure 5.17c to Figure 5.17e, demonstrate that Wetwall predictions at node 2 and node 3 captured the general trends of the change in the moisture content in the sheathing. In general, the model predictions under estimated the magnitude of the moisture content and did not follow the quick rise of the moisture content observed in the first heating season.

Over the summer, the model predictions of surface deposition and node 1 moisture content for all zones, shown in Figure 5.18a to Figure 5.18e, seemed to follow the trends in the measurements. As one might expect for summer conditions, the model predicted no surface deposition and the moisture content at node 1 in all zones was consistently low without any significant periods of moisture deposition. The vapour pressure at the sheathing is typically larger than the vapour pressure at the inlet regardless of the direction of flow because of the warm temperatures. Consequently, drying of the cavity occurs for both infiltration and exfiltration during the summer.

The comparisons of predictions at node 2 and node 3 with experimental data in all zones over the same period, shown in Figure 5.19a to Figure 5.19e, also display the same

trends as the measurements. In general, the predictions bracketed the measured moisture content in the sheathing. The sudden rise and fall observed in the measurements, however, were not duplicated by the model.

In the second heating season without the fan in operation, the model matched the trends in the experimental data as in the first heating season. The comparison of the predicted surface deposition and moisture content in zone 1, shown in Figure 5.20a, suggests that the model responded well to the initial wetting process with the initial rise in the moisture content coinciding with the surface sensor response at about hour 7225. As in the first heating season, the model was slow to react to the drying effect. At hour 10700, node 1 was still at saturation when the surface sensor output indicated little moisture deposition. Again, the moisture content in node 1 could not decrease until all the surface deposition is removed and as a result, the node remained at saturation.

The comparisons in the other zones, shown in Figure 5.20b to Figure 5.20e, were incapable of showing the model's ability to predict because the actual surface deposition was too small to display any significant trends. Without the fan, a sustained period of exfiltration did not occur to generate as large of a potential for moisture deposition as in the first heating season.

The model predictions at the interior nodes in zone 1, shown in Figure 5.21a, illustrate that node 2 predictions typically over estimated the actual moisture content in the sheathing. Wetwall also was unable to match the sudden rise in the moisture content. The node 2 predictions in Figure 5.21a were seen to respond slowly to the drying of the cavity. From hour 10200 to 10700, the moisture content in the sheathing was observed to drop

significantly while the value at node 2 remained constant. The node 3 predictions underestimated the actual moisture content as expected, but matched the trends observed in the experiment.

The predictions in zone 2 and zone 3, shown in Figure 5.21b and Figure 5.21c, demonstrate closer correlation to the experimental data than in zone 1. Although the predictions at node 2 and node 3 underestimated the actual moisture content in the sheathing, the model matched all the trends in the experimental data except for the periods when the moisture content approached 20%wt.

The results in zone 4 and zone 5, shown in Figure 5.21d and Figure 5.21e, are incapable of illustrating the model's ability to follow the experimental data because the actual moisture content was too low to outline any trends. The predictions in the two zones, however, overestimated the moisture content in the sheathing consistently.

In general, the best correlation between Wetwall predictions at the interior nodes and experimental data occurred in zone 2. The model was able to match the trends in the experimental data even though the predictions in zone 2 at node 2 and node 3 were lower than the actual values.

Wetwall was also observed to produce predictions which coincided with the actual moisture deposition in the cavity. The model response to the drying of the cavity, however, was slow for both heating seasons. The lag in the drop of the moisture content predictions was due to the influence of the exponential term in the equation for mass deposition in the cavity. The interior nodes were also affected indirectly because the moisture transfer between node 2 and node 3 is strongly dependent on the amount of

surface deposition and moisture content at node 1. The model was seen to match the trends in the experimental over the summer. As expected, the moisture content predictions were consistently low and surface deposition was non-existent because the warm temperatures increase the vapour pressure at the sheathing such that it is larger than the vapour pressure the inlet. Hence, water vapour diffuses away from the sheathing regardless of the direction of flow.

In addition to the comparisons between the predictions and measured values shown in the figures, a three layer nodal network for the exterior sheathing (two surface nodes and one interior node) was also used. The trends and magnitudes of the predictions for the interior nodes, however, did not agree with the measured values as closely as that of the four layer nodal network. For a 12.7 mm thick exterior sheathing, a network with a minimum of two underlying nodes is required for adequate moisture content predictions.

5.6 MODEL SENSITIVITY TO THE MASS DIFFUSIVITY

The range of mass diffusivity across the thickness of the pine exterior sheathing used in the Wetwall is between $3 \times 10^{-6} \text{ m}^2/\text{s}$ and $3 \times 10^{-10} \text{ m}^2/\text{s}$. The upper limit was the largest value for which no surface deposition occurred at the internal nodes and the lower value, used by Walker (1993), was based on an estimate by Cunningham (1990). The value of $3 \times 10^{-6} \text{ m}^2/\text{s}$ was selected for Wetwall because it produced predictions which gave the best correlation with the experimental results. Since the mass diffusivity for pine is still not known absolutely because the value depends on the temperature and moisture content of the wood, the choice of $3 \times 10^{-6} \text{ m}^2/\text{s}$ is reasonable. More detailed

measurements of this property need to be carried out.

The effects of a smaller mass diffusivity on the moisture deposition over time is illustrated in the comparisons of Wetwall predictions for a sheathing mass diffusivity of $3 \times 10^{-8} \text{ m}^2/\text{s}$ with the experimental data. The comparisons for surface deposition and node 1 moisture content for all zones are shown in Figures 5.22a to 5.22e; node 2 and node 3 moisture content predictions for all zones are shown in Figures 5.23a to 5.23e. The figures show that the surface accumulation is greater over time and that the response of moisture content at the interior nodes is much slower. The reason is due to the fact that the mass transfer across the cavity remained the same while the mass transfer across the sheathing is smaller with the smaller sheathing mass diffusivity. As a result, the mass deposition accumulates on the surface and at node 1 more quickly and diffusion across the sheathing is much slower. The predictions for a sheathing mass diffusivity of $3 \times 10^{-10} \text{ m}^2/\text{s}$ are shown in Figures 5.24a to 5.24e and Figures 5.25a to 5.25e. For this case, the moisture contents at node 2 and node 3 did not respond at all because of the very small mass transfer across the sheathing compare to the mass transfer across the cavity.

Table 5.1: Building characteristics of house 6 for input to Local Leaks

Building Characteristics	Value
Ceiling height	3 m from grade level
Floor height	0.61 from grade level
Volume of building	200 m ³
Floor area	49 m ²
Flow coefficient (C)	0.00881 m ³ /(sPa ⁿ)
Flow exponent (n)	0.684
Flue shelter	none
Flue	blocked
Crawl space	none
Fraction of distributed leakage at floor	20%
Fraction of distributed leakage at ceiling	10%
Fraction of distributed leakage in the walls	70%
Fraction of wall leakage in Wall 1, 2, 3, and 4	25% each
Fraction of floor level leakage below Wall 1, 2, 3, and 4	25% each
Fraction of attic leakage above Wall 1, 2, 3, and 4	25% each
Roof pitch	3.0:1
Roof ridge parallel to front face	
Fraction of attic leakage in roof	100%
House configuration	Bungalow with close row shelter

Table 5.2: Cavity characteristics and input parameters to Wetwall

Cavity characteristics and model parameters	Symbol	Value
Cavity height	h	1.9304 m
Cavity depth	d	0.09 m
Cavity width	L	0.3683 m
Mass diffusivity of vapour across cavity	D_1	$2.56 \times 10^{-5} \text{ m}^2/\text{s}$
Mass diffusivity of moisture across sheathing	D_w	$3 \times 10^{-6} \text{ m}^2/\text{s}$
Density of pine	ρ_{pine}	474.53 kg/m ³
Dry weight at node 1	$m_{\text{dwt},1}$	$6.659 \times 10^{-3} \text{ kg}$
Dry weight at node 2	$m_{\text{dwt},2}$	$3.562 \times 10^{-2} \text{ kg}$
Dry weight at node 3	$m_{\text{dwt},3}$	$3.562 \times 10^{-2} \text{ kg}$
Distance between node 1 and node 2	$\Delta x_{1,2}$	0.003175 m
Distance between node 2 and node 3	$\Delta x_{2,3}$	0.00535 m
Distance between node 2 and node 3	$\Delta x_{3,4}$	0.003175 m

Table 5.3: Root-mean-square and mean error for all air leakage flow rates

	Root-mean-square Error [% of measured]	Mean Error [% of measured]
Fan Off	1900	95
Fan On	975	-35

Table 5.4: Root-mean-square and mean error for leakage flow rate under various wind directions

Wind Direction	Root-mean-square Error [% of measured]	Mean Error [% of measured]
North	244	33
South	3200	155
East	514	134
West	1016	133

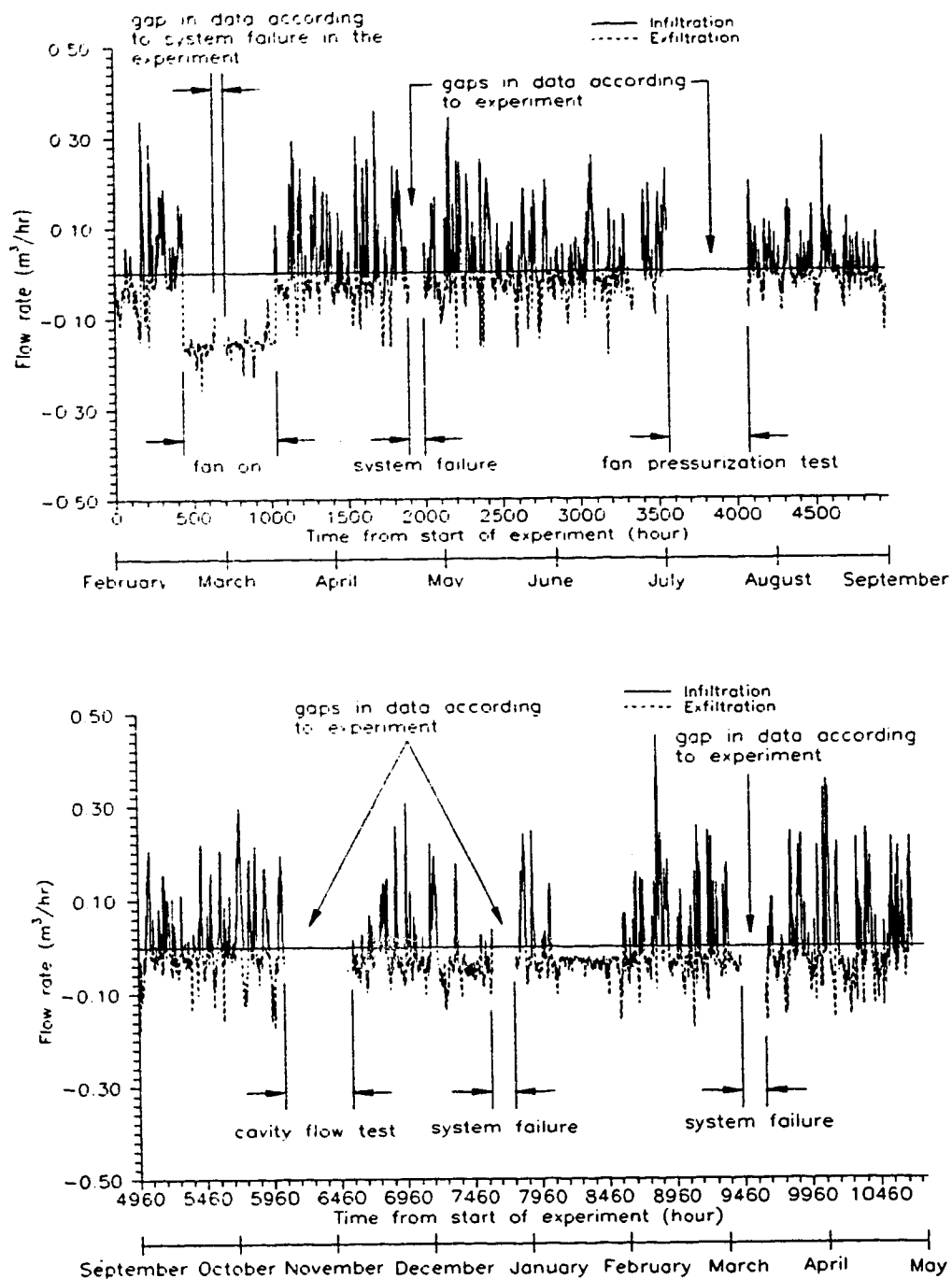


Figure 5.1 :Rates of infiltration and exfiltration predicted by Local Leaks from February 7, 1994 to April 28, 1995. Upper plot spans the first 7 months of field data and the lower plot spans the remaining 8 months of field data.

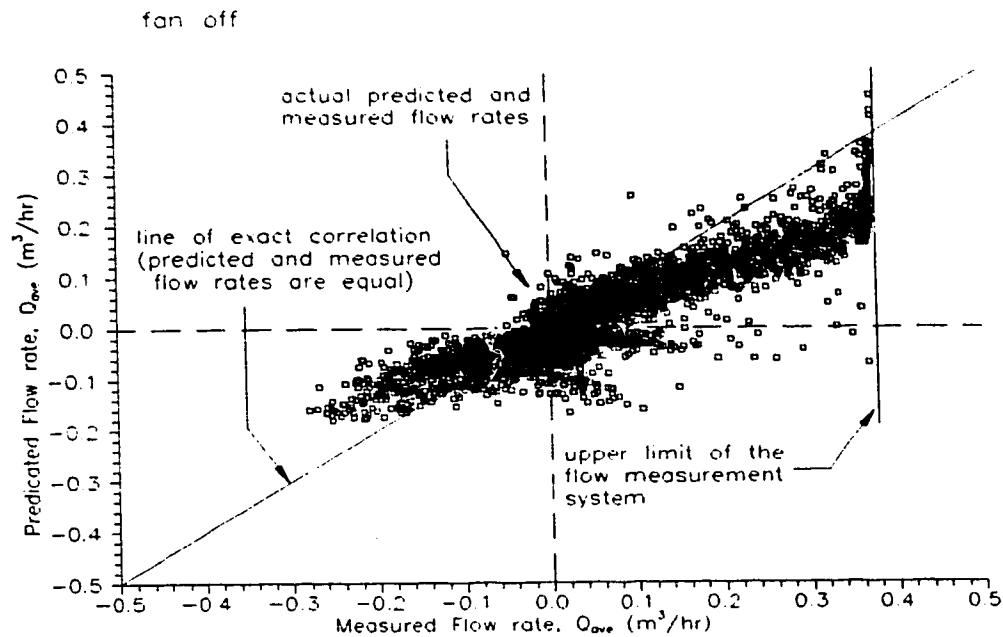


Figure 5.2: Comparison of measured flow rates with predicted flow rates without the fan in operation. Data set consists of 10102 hours of air leakage flow rates.

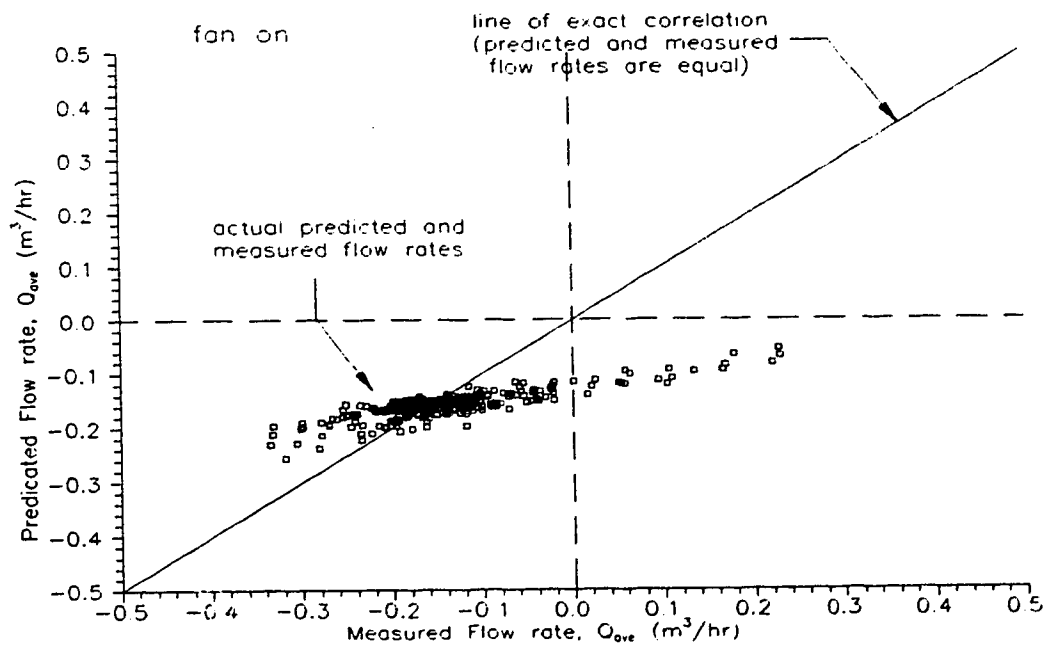


Figure 5.3: Comparison of measured flow rates with predicted flow rates with the fan in operation. Data set consists of 538 hours of air leakage flow rates.

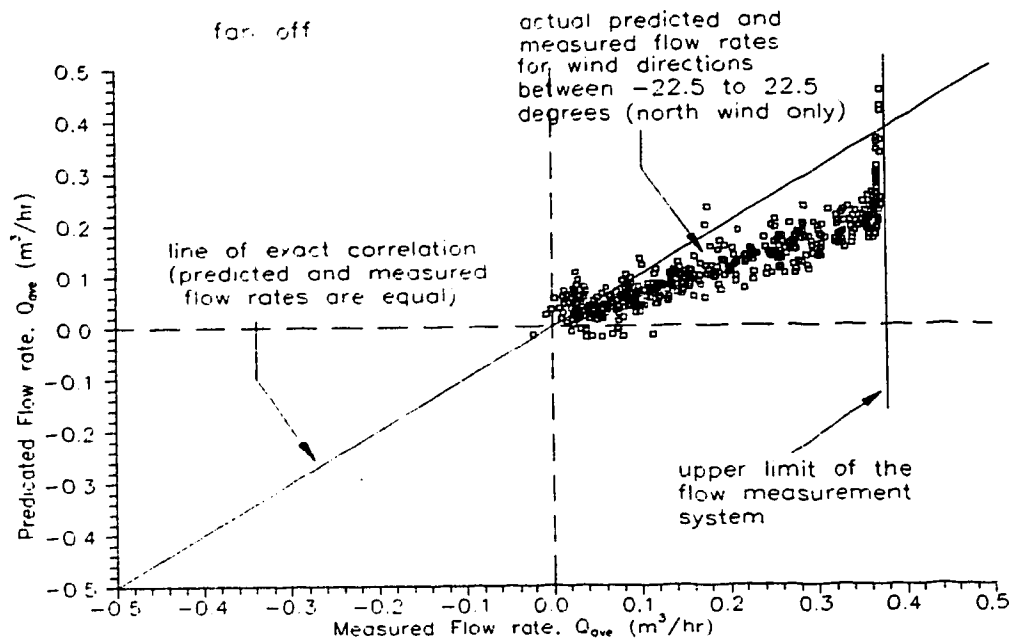


Figure 5.4: Comparison of measured flow rates with Local Leaks prediction for north winds only.

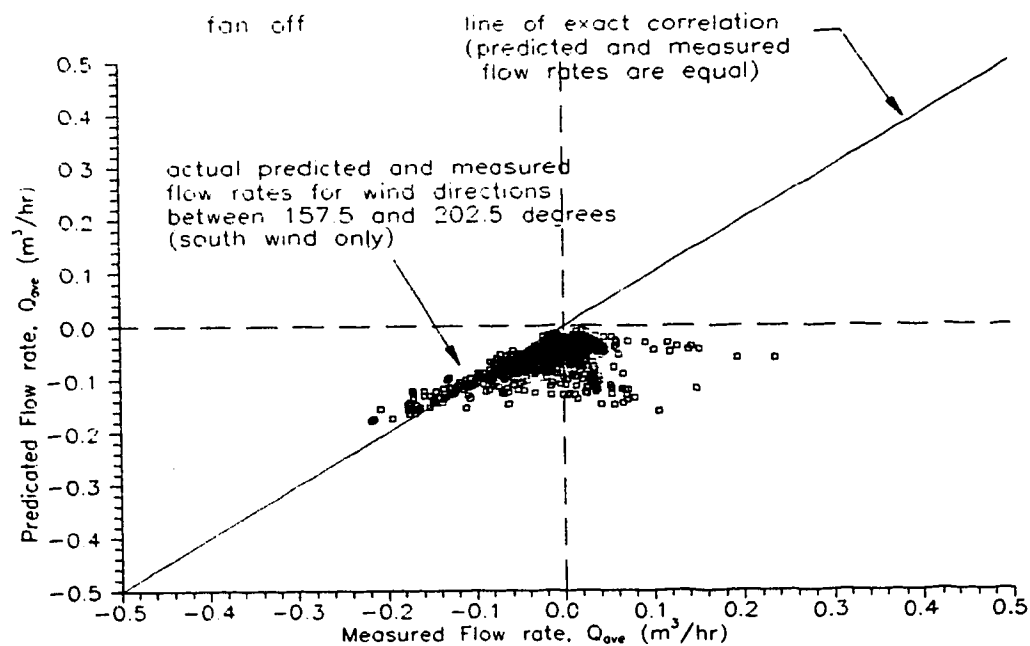


Figure 5.5: Comparison of measured flow rates with Local Leaks predictions for south winds only.

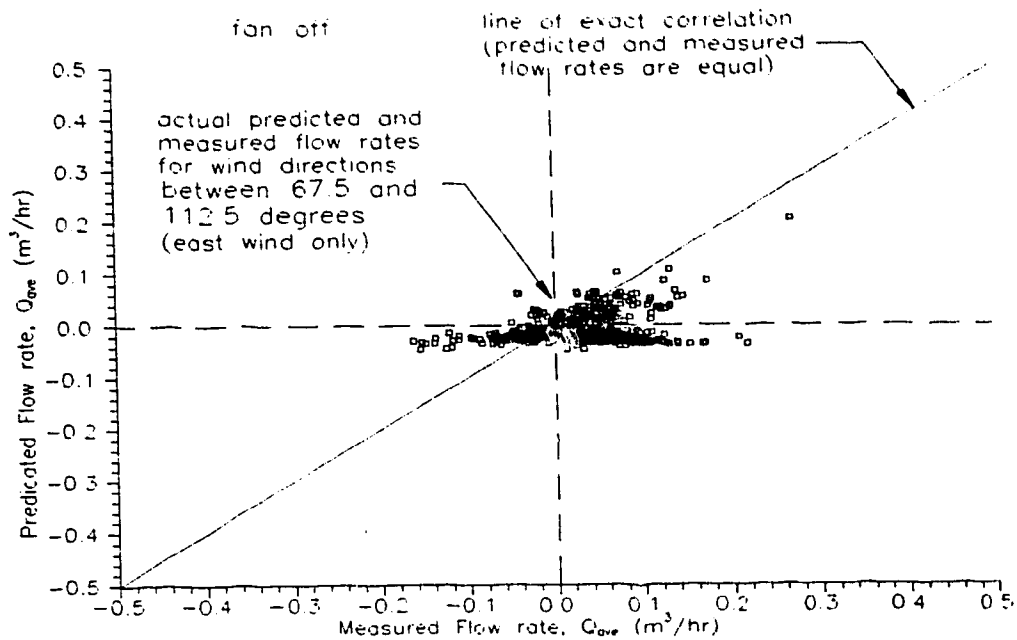


Figure 5.6: Comparison of measured flow rates with Local Leaks predictions for east winds only.

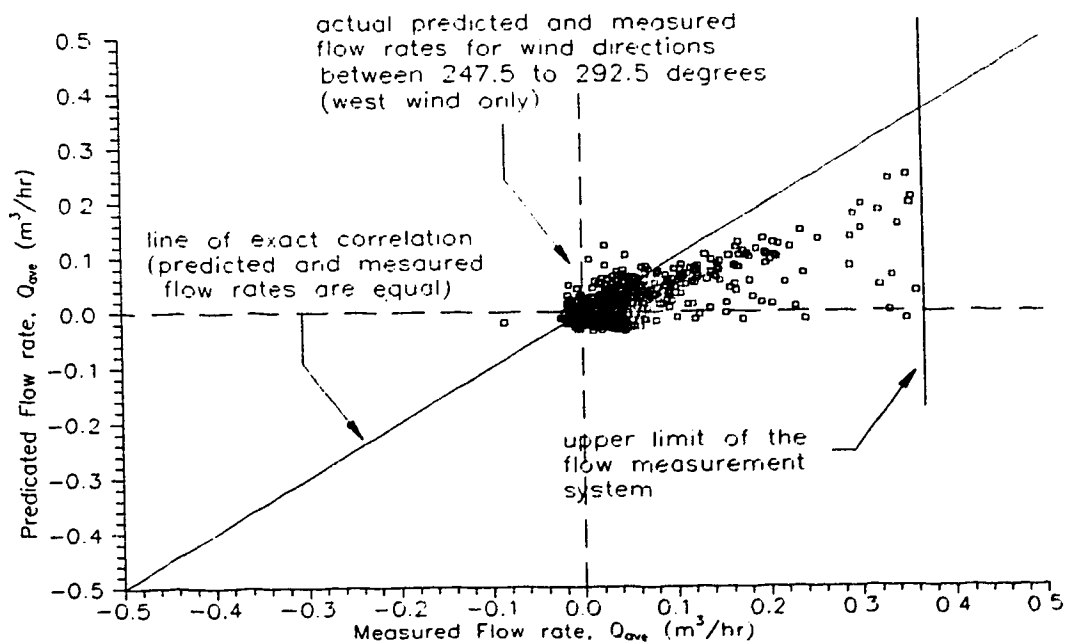


Figure 5.7: Comparison of measured flow rates with Local Leaks predictions for west winds only.

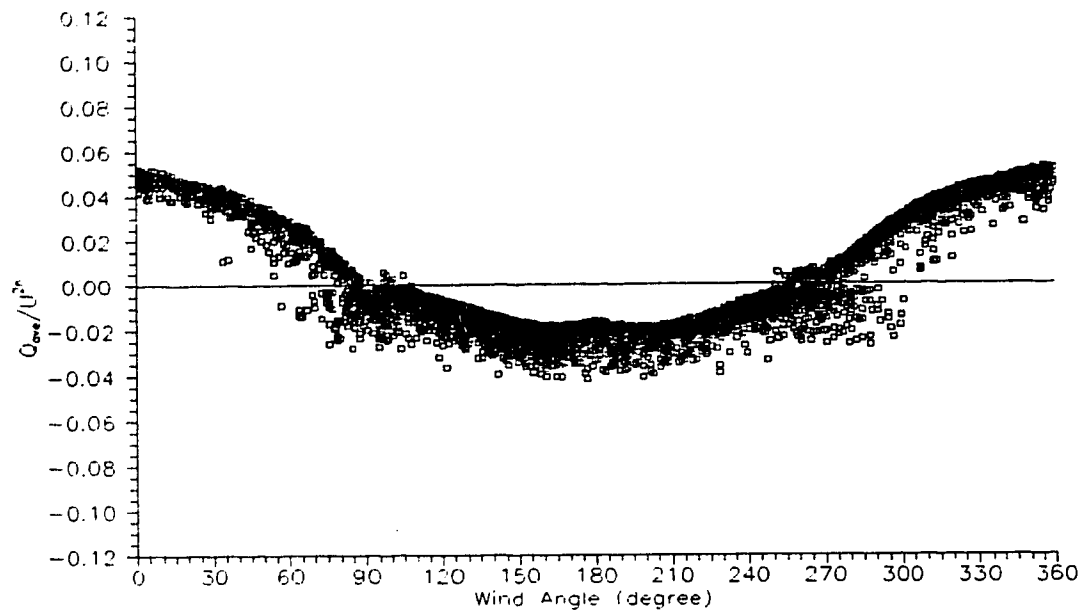


Figure 5.8 : Normalized average leakage rates for all wind speeds greater than 1 m/s (Local Leaks predictions)

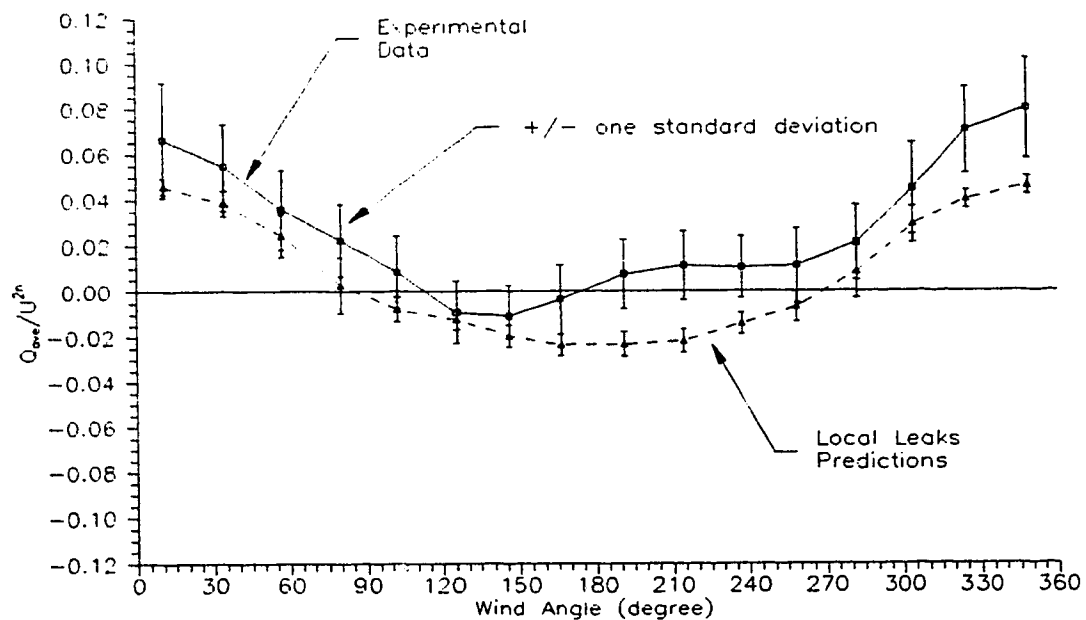


Figure 5.9: Comparison of the normalized leakage rates of the experiment and Local leaks (normalized leakage rates are sorted into bins of 22.5°).

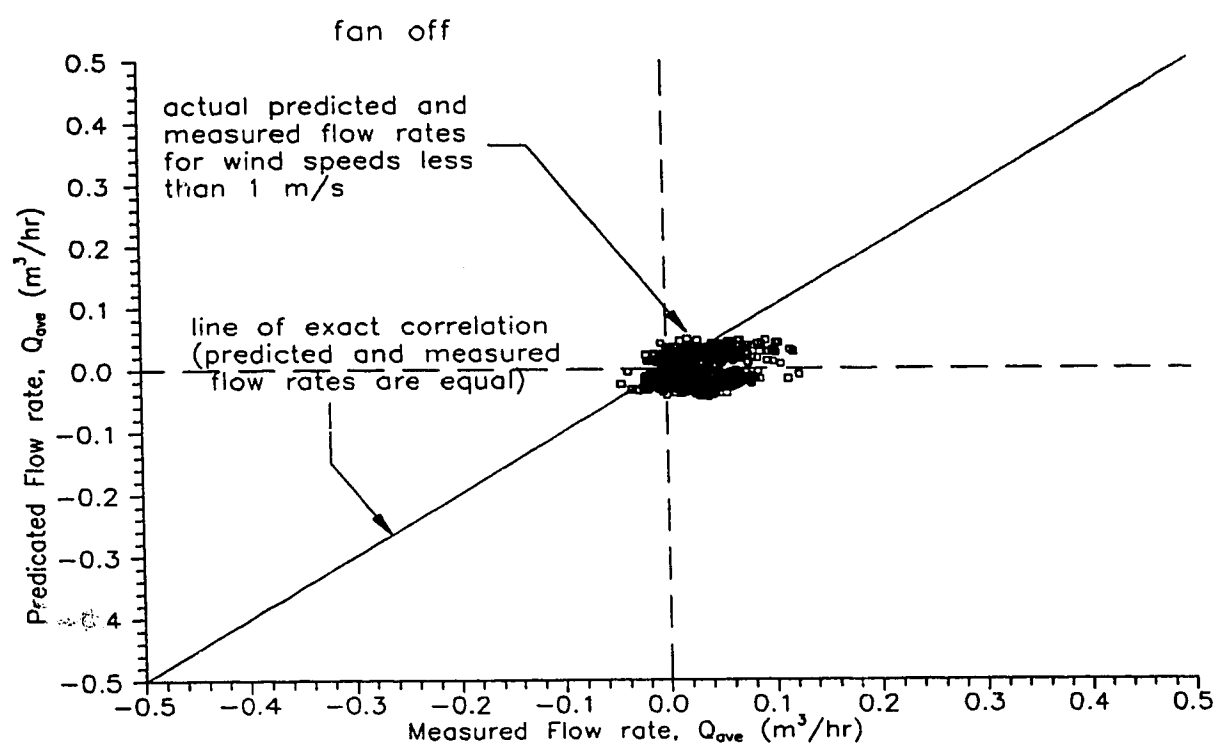


Figure 5.10: Comparison of measured flow rates with Local Leaks predictions for wind speeds below 1 m/s.

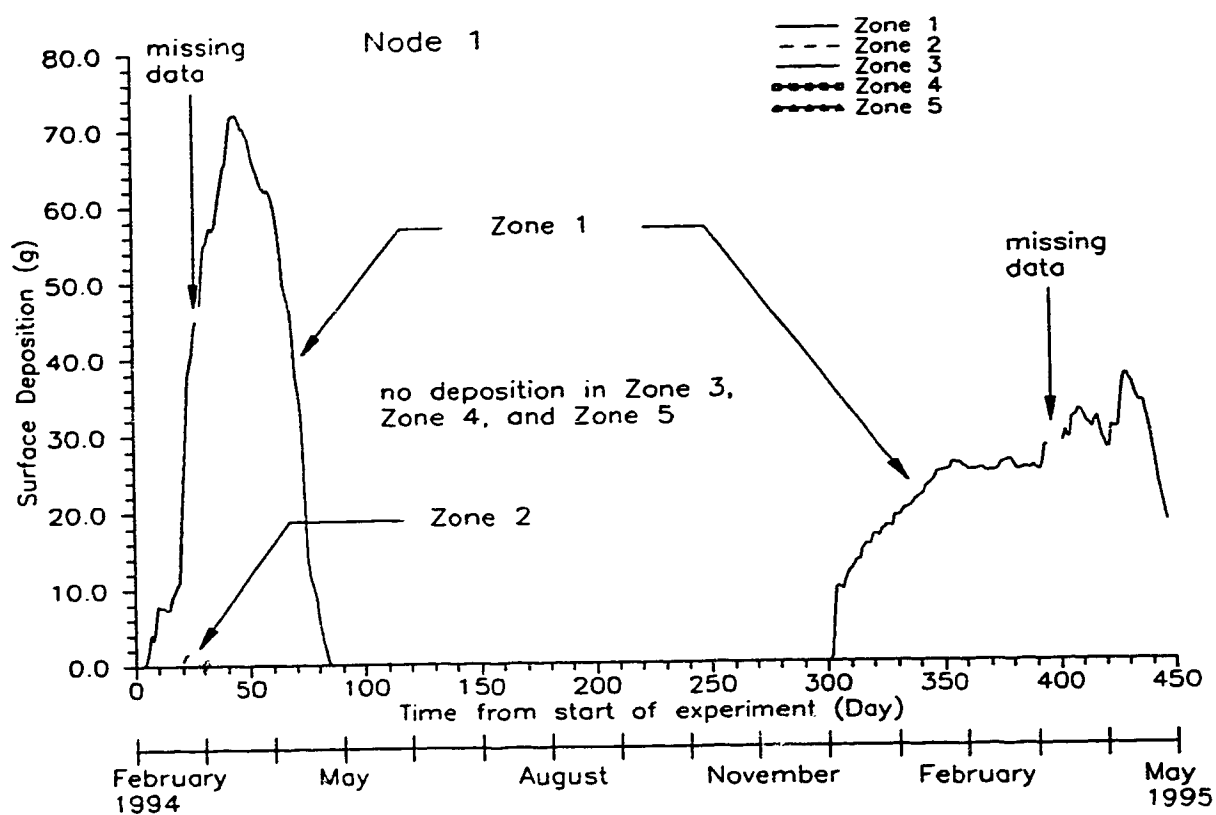


Figure 5.11: Surface deposition in Node 1 for all zones predicted by Wetwall (Daily averages). The supply fan was in operation from February 24, 1994 to March 21, 1994.

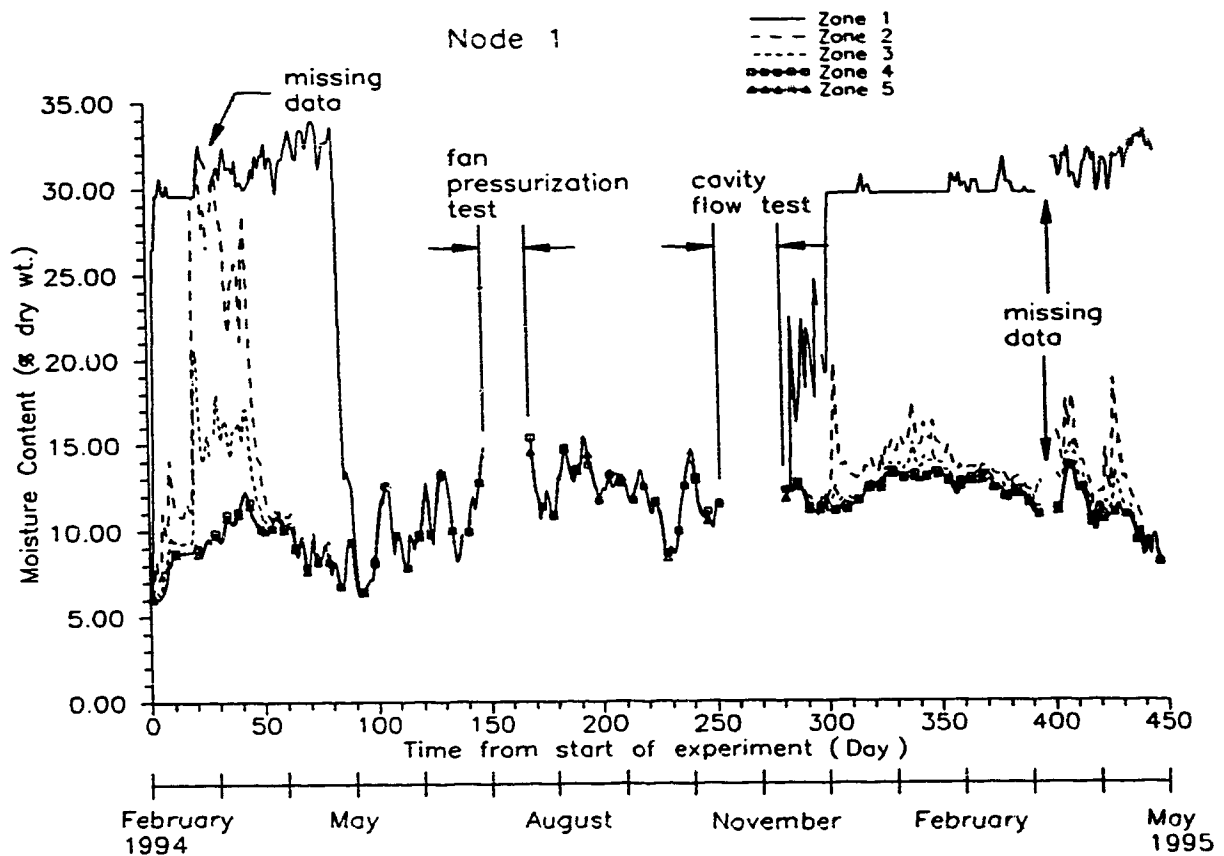


Figure 5.12: Moisture content in Node 1 for all zones predicted by Wetwall (Daily averages). The supply fan was in operation from February 24, 1994 to March 21, 1994.

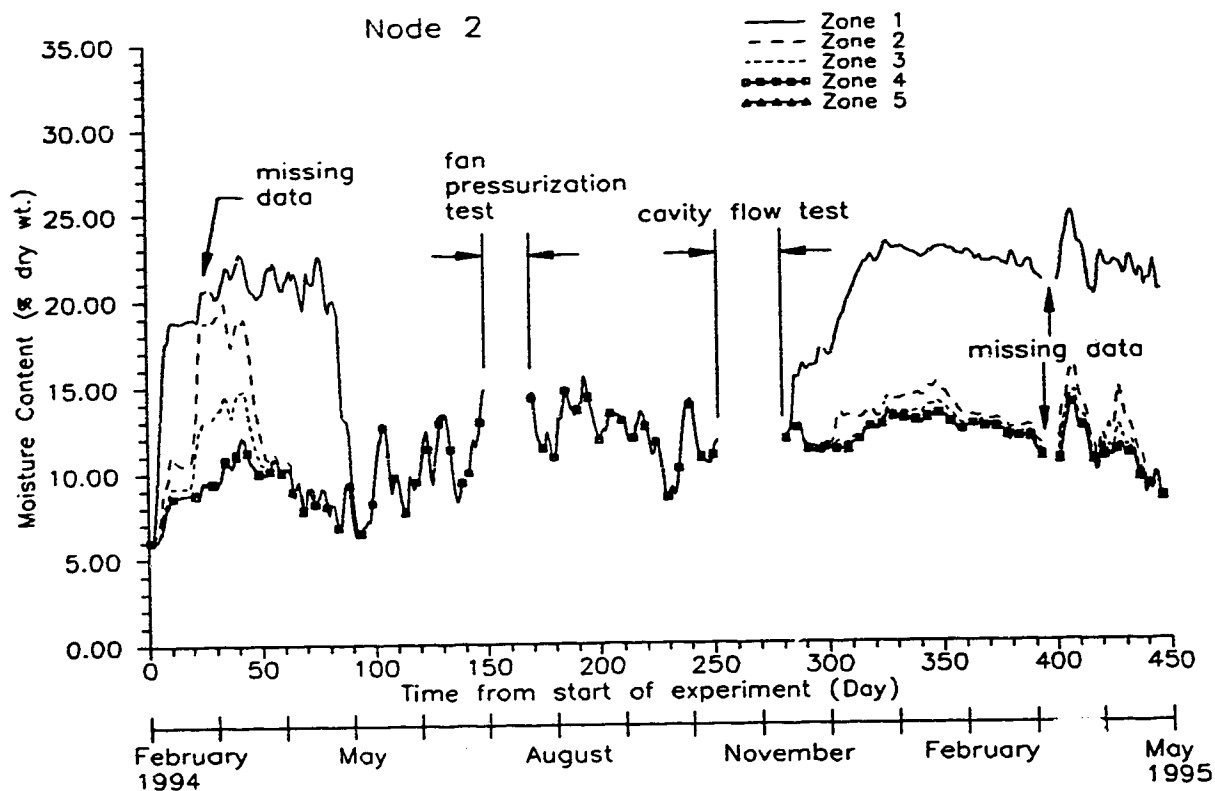


Figure 5.13: Moisture content in node2 for all zones predicted by Wetwall (Daily averages). The supply fan was in operation from February 24, 1994 to March 21, 1994.

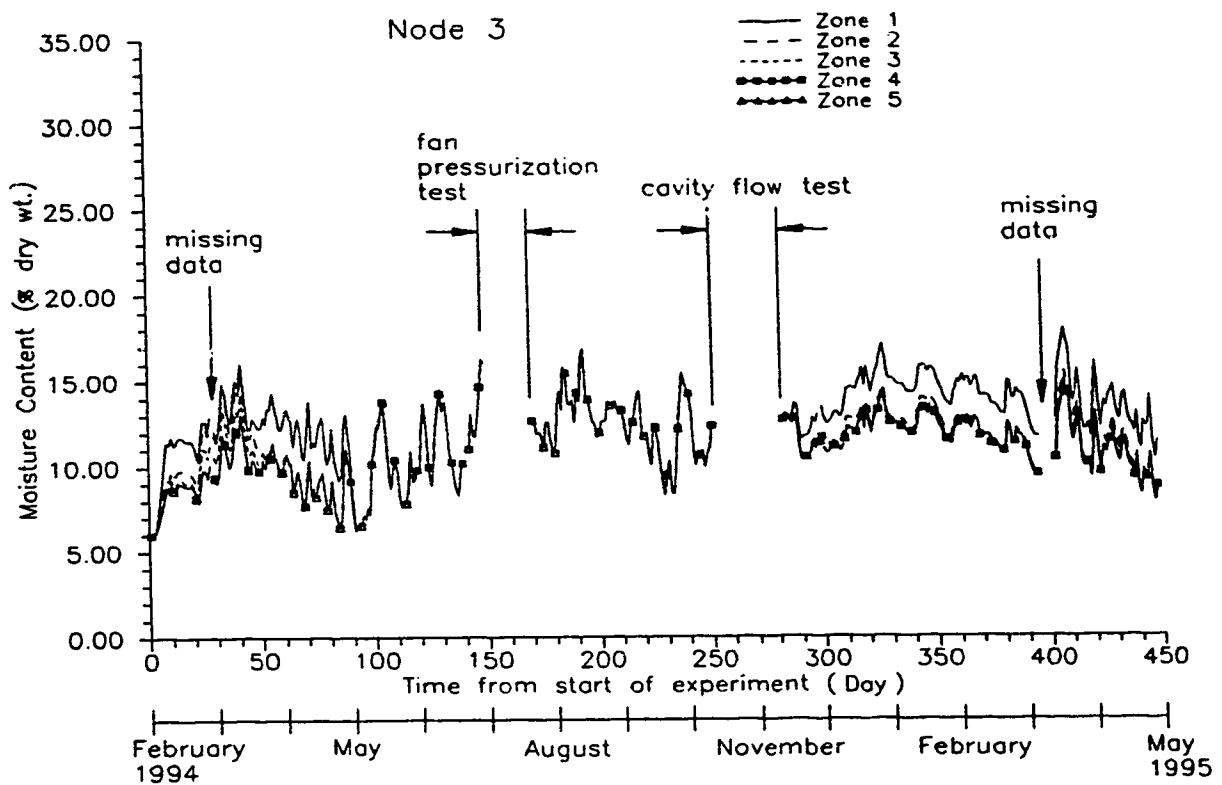


Figure 5.14: Moisture content in node 3 for all zones predicted by Wetwall (Daily averages). The supply fan was in operation from February 24, 1994 to March 21, 1994.

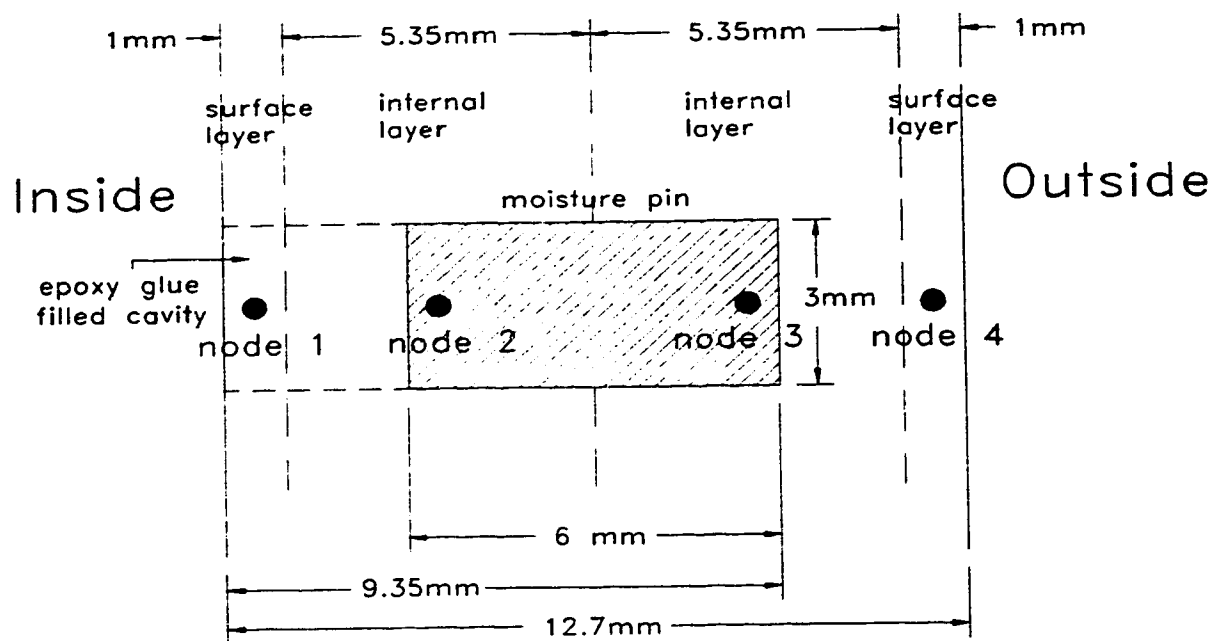


Figure 5.15: The location of moisture pins in the experiment relative to the nodal network in Wetwall. The figure is a cross section through the thickness of the exterior sheathing.

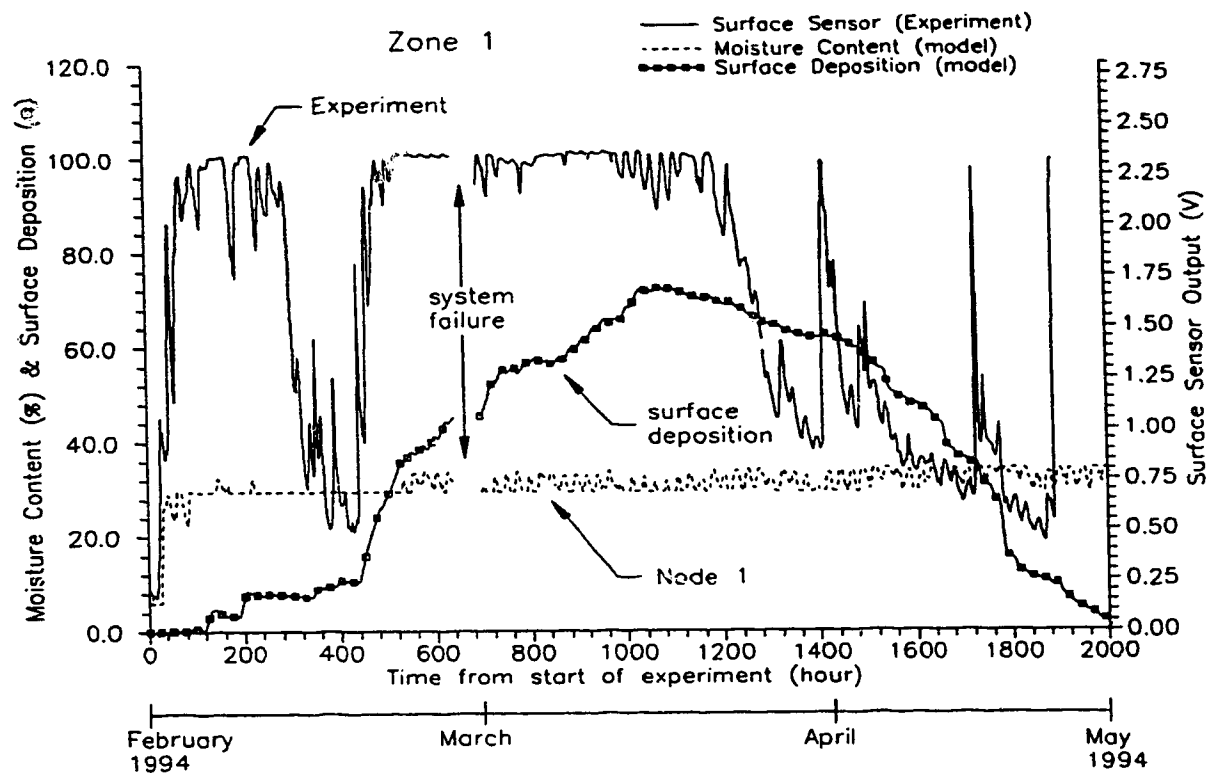


Figure 5.16a: Comparison of Wetwali predictions at node 1 and surface deposition with measured surface sensor output in zone 1 (February 1994 to April 1994). The supply fan was in operation from hours 440 to 1038.

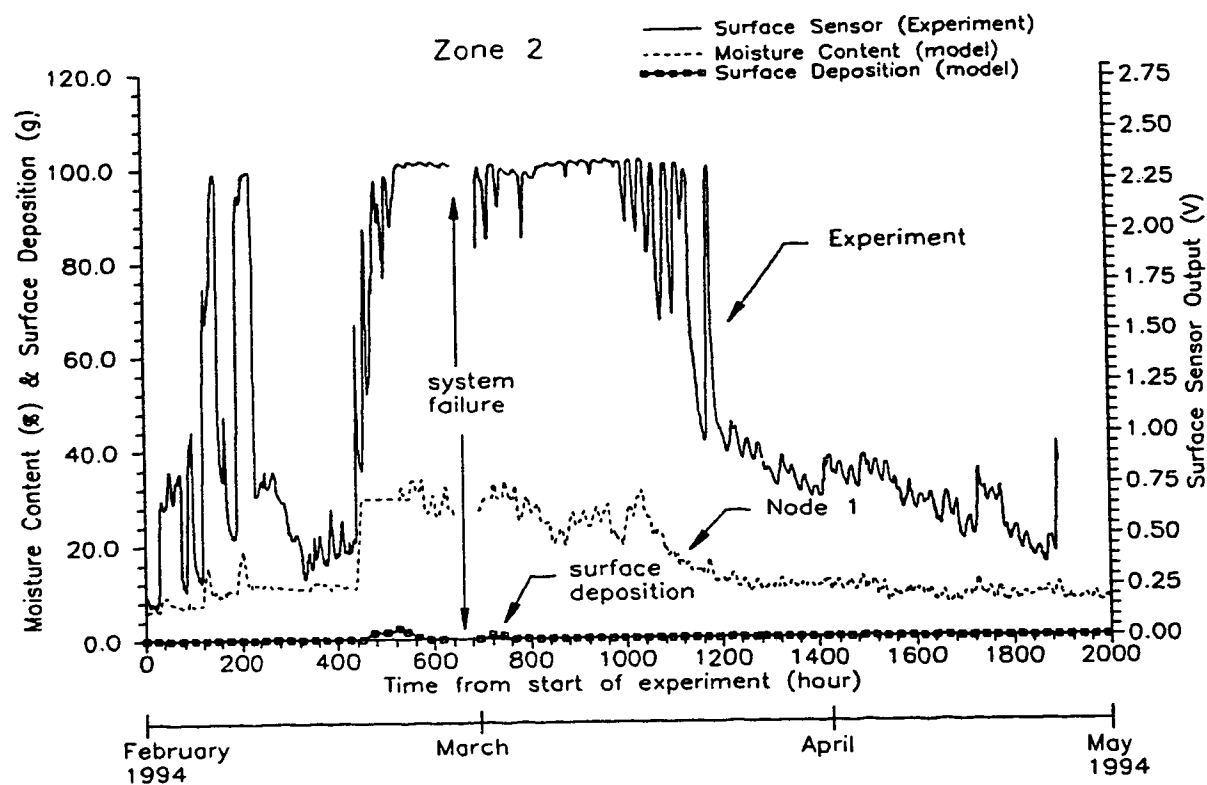


Figure 5.16b: Comparison of Wetwall predictions for node 1 and surface deposition with measured surface sensor output in zone 2 (February 1994 to April 1994). The supply fan was in operation from hours 440 to 1038.

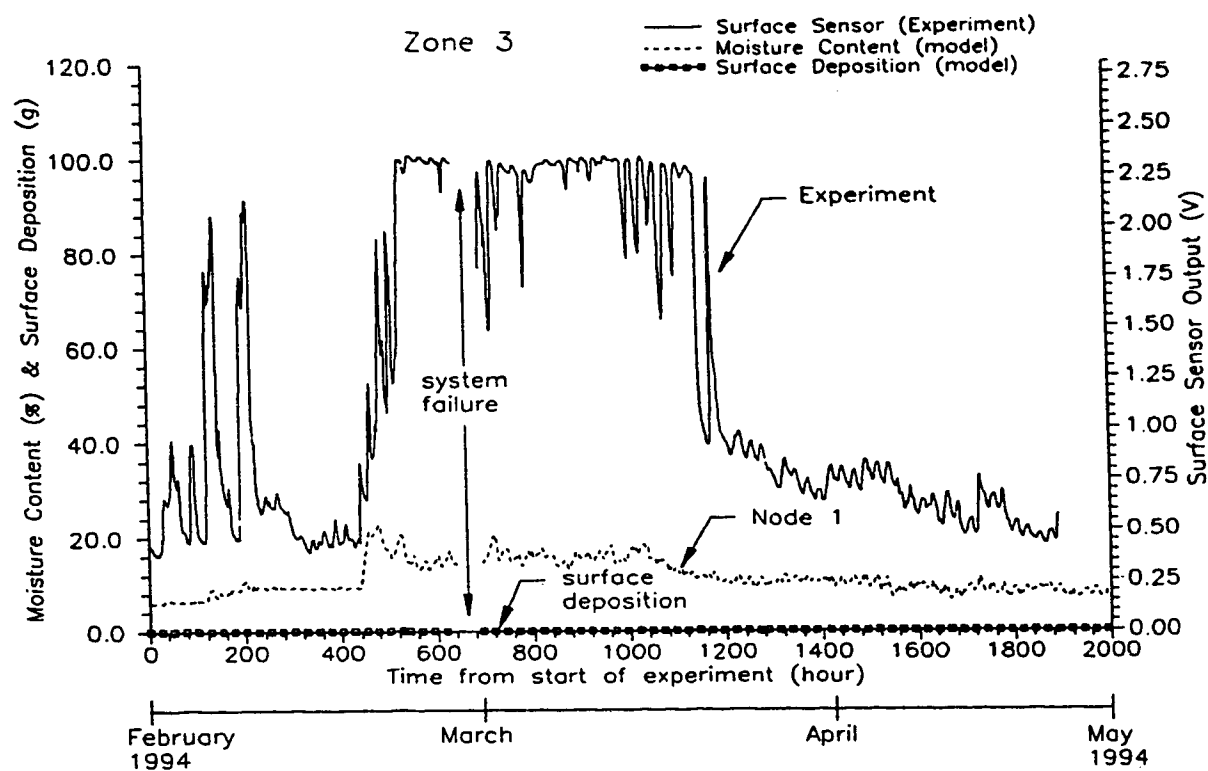


Figure 5.16c: Comparison of Wetwall predictions for node 1 and surface deposition with measured surface sensor output in zone 3 (February 1994 to April 1994). The supply fan was in operation from hours 440 to 1038.

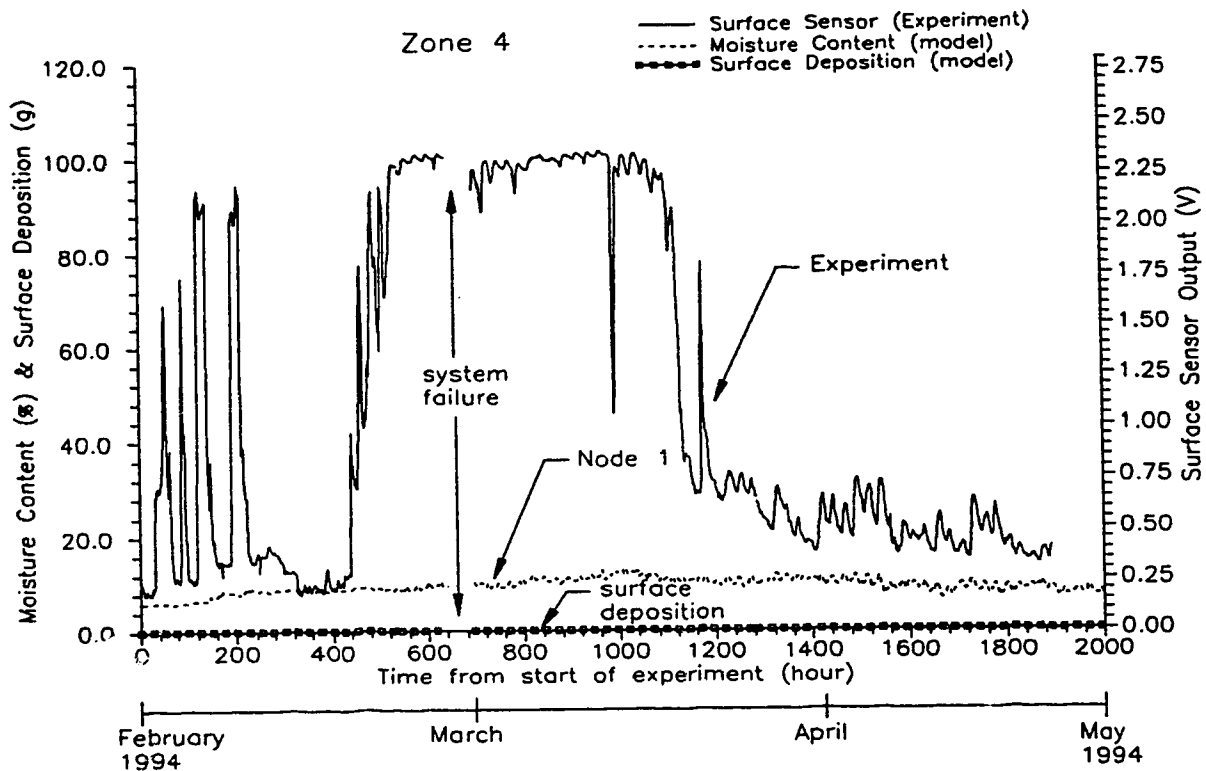


Figure 5.16d: Comparison of Wetwall predictions for node 1 and surface deposition with measured surface sensor output in zone 4 (February 1994 to April 1994). The supply fan was in operation from hours 440 to 1038.

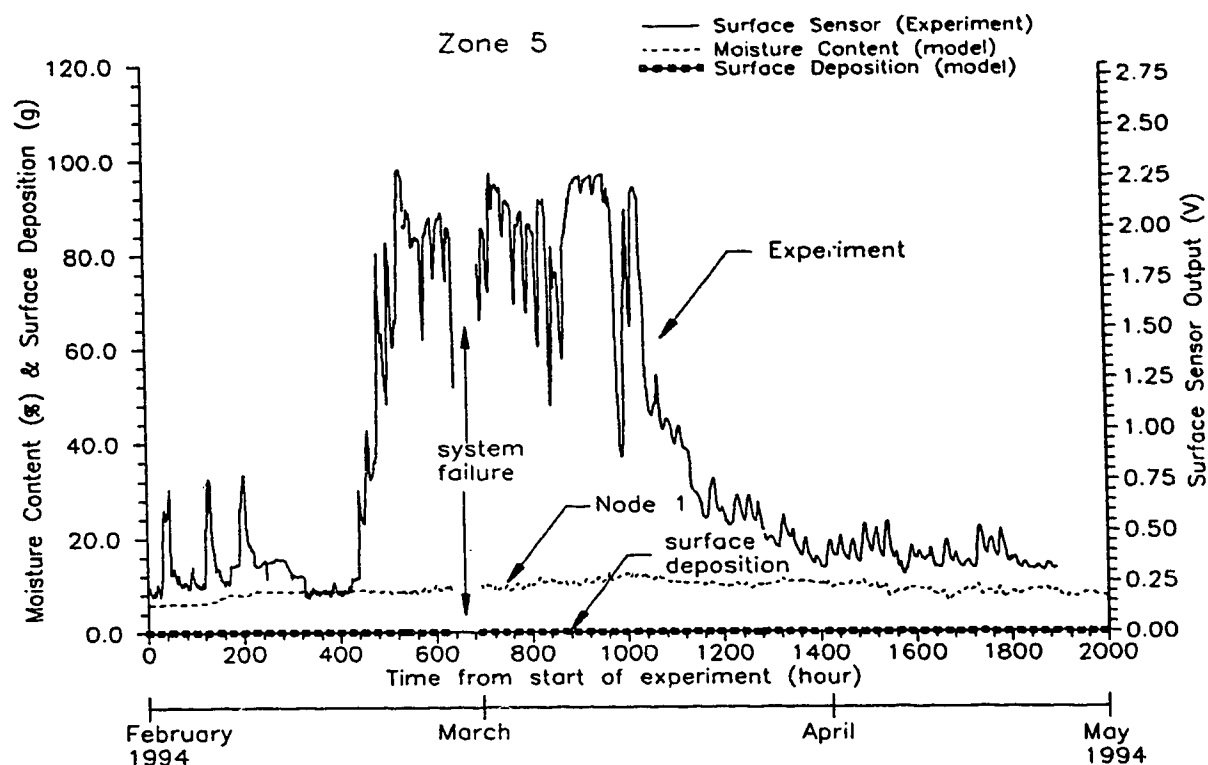


Figure 5.16e: Comparison of Wetwall predictions for node 1 and surface deposition with measured surface sensor output in zone 5 (February 1994 to April 1994). The supply fan was in operation from hours 440 to 1038.

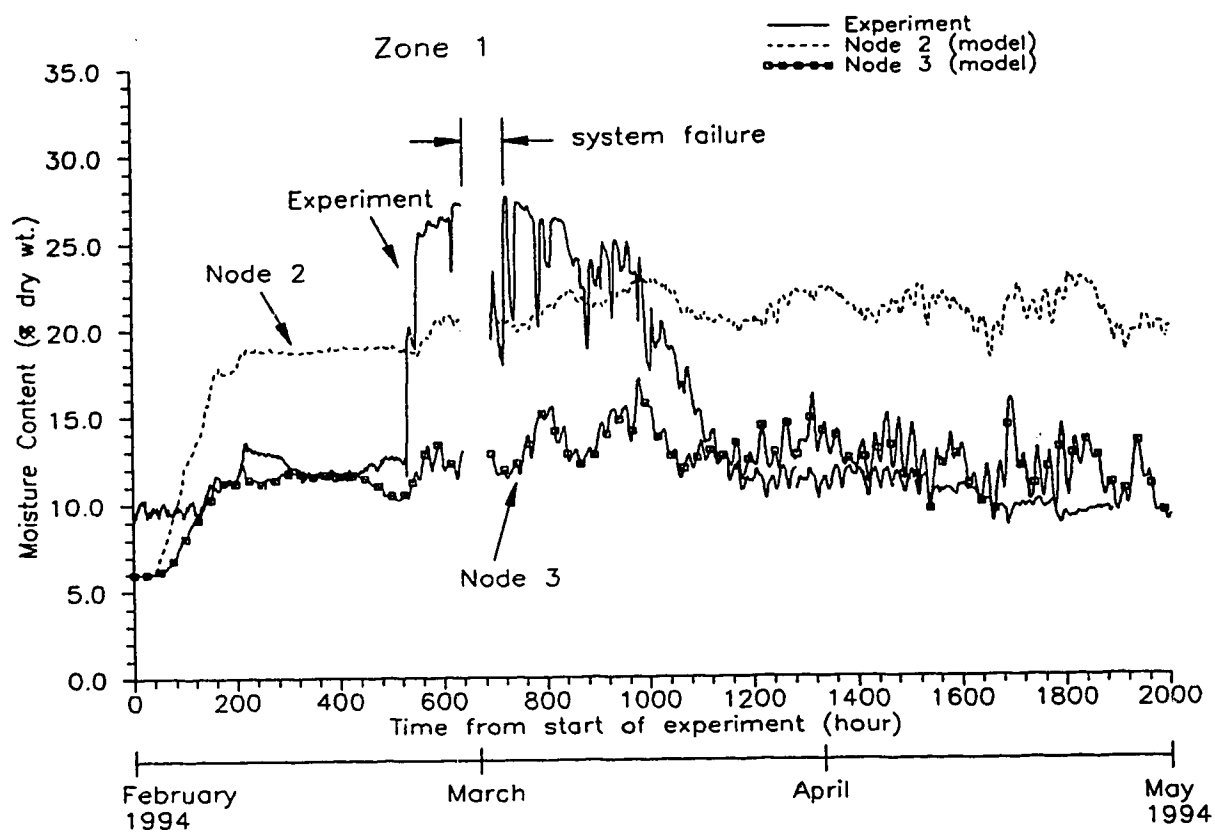


Figure 5.17a: Comparison of measured moisture content with predictions for node 2 and node 3 in zone 1 (February 1994 to April 1994). The supply fan was in operation from hours 440 to 1038.

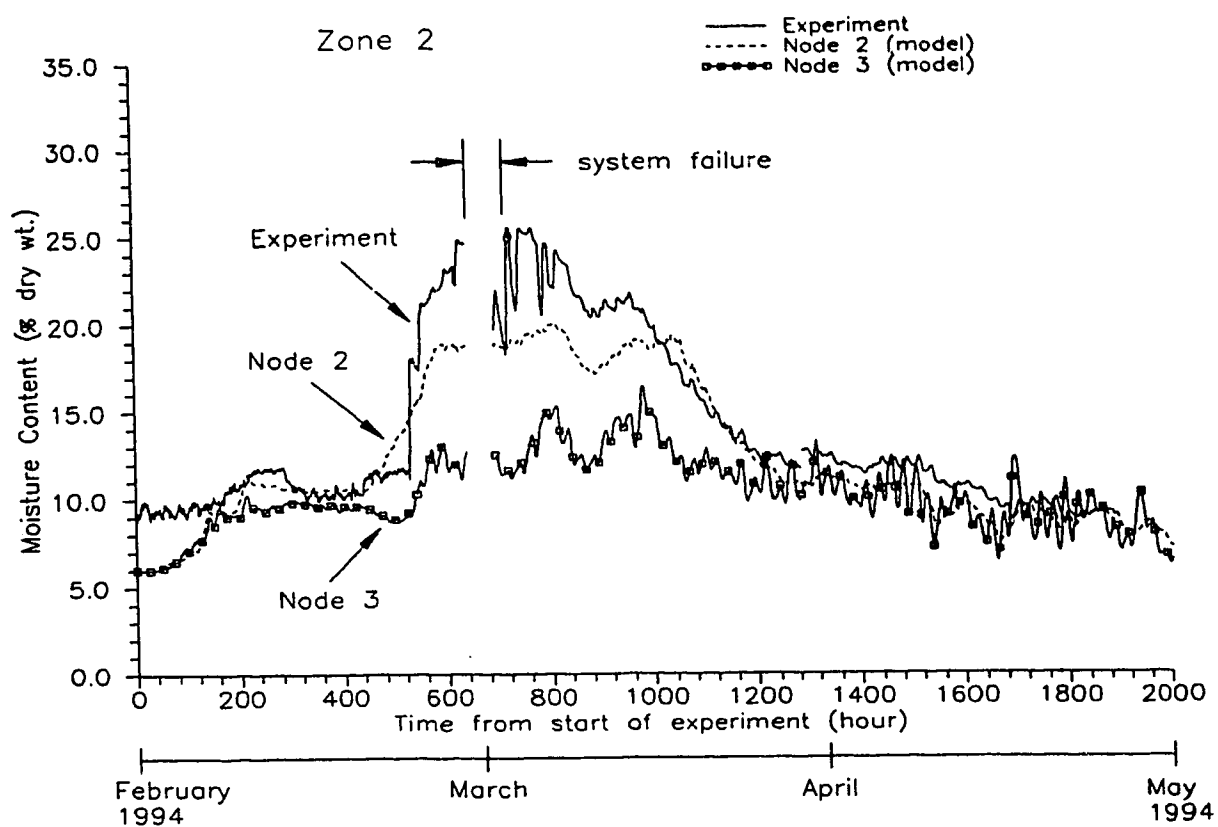


Figure 5.17b: Comparison of measured moisture content with predictions for node 2 and node 3 in zone 2 (February 1994 to April 1994). The supply fan was in operation from hours 440 to 1038.

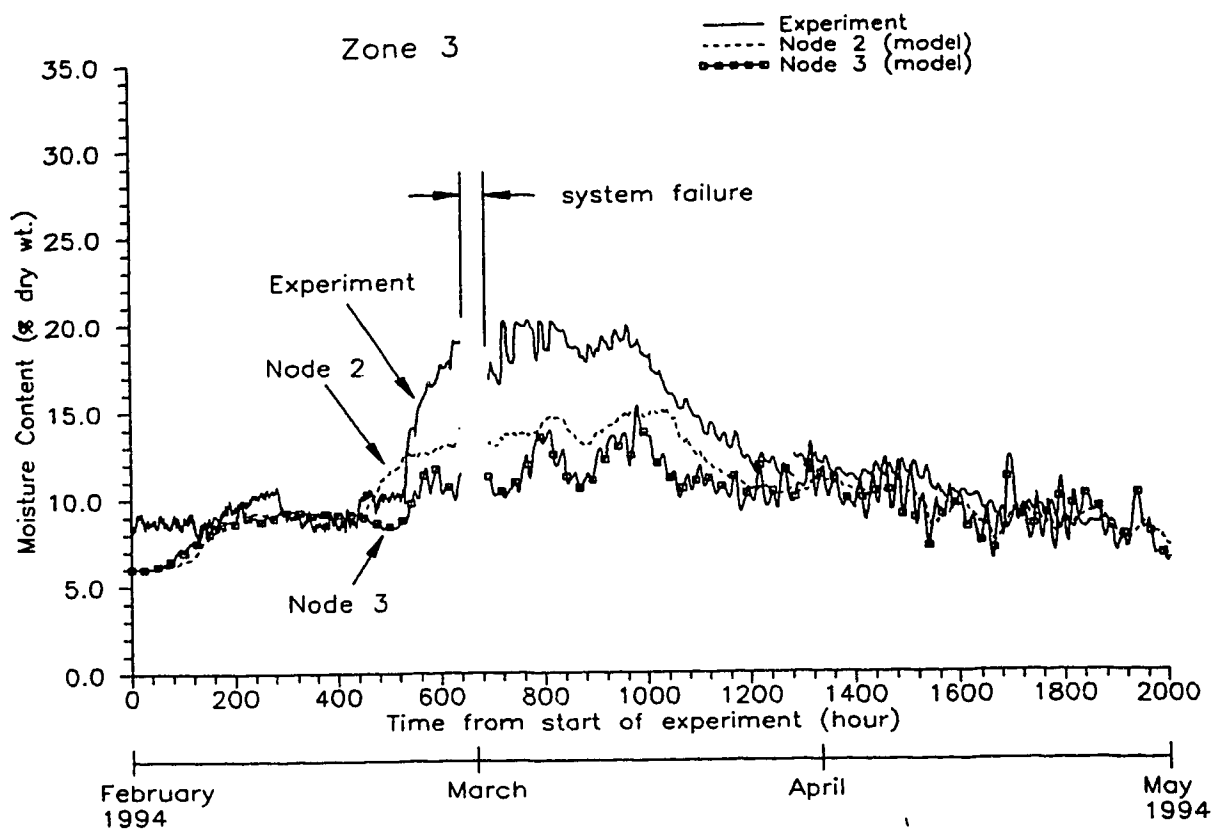


Figure 5.17c: Comparison of measured moisture content with predictions for node 2 and node 3 in zone 3 (February 1994 to April 1994). The supply fan was in operation from hours 440 to 1038.

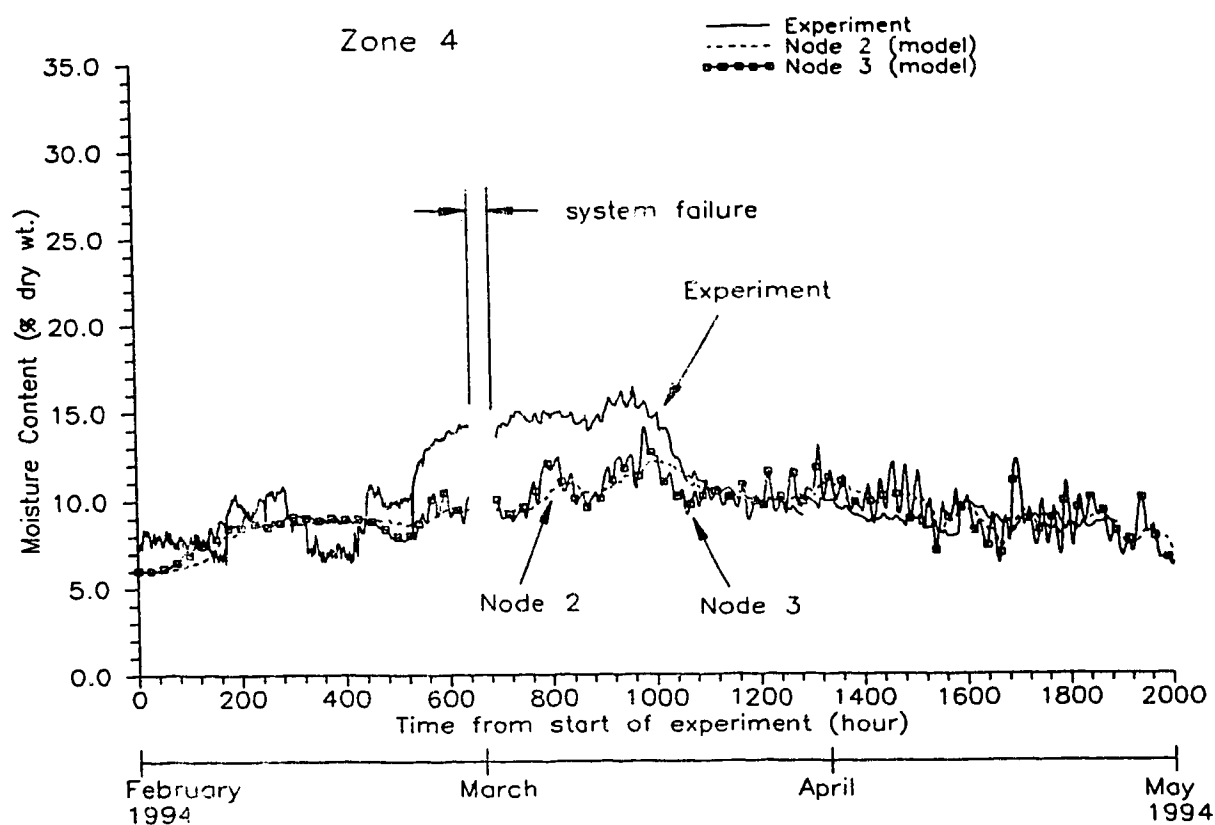


Figure 5.17d: Comparison of measured moisture content with predictions for node 2 and node 3 in zone 4 (February 1994 to April 1994). The supply fan was in operation from hours 440 to 1038.

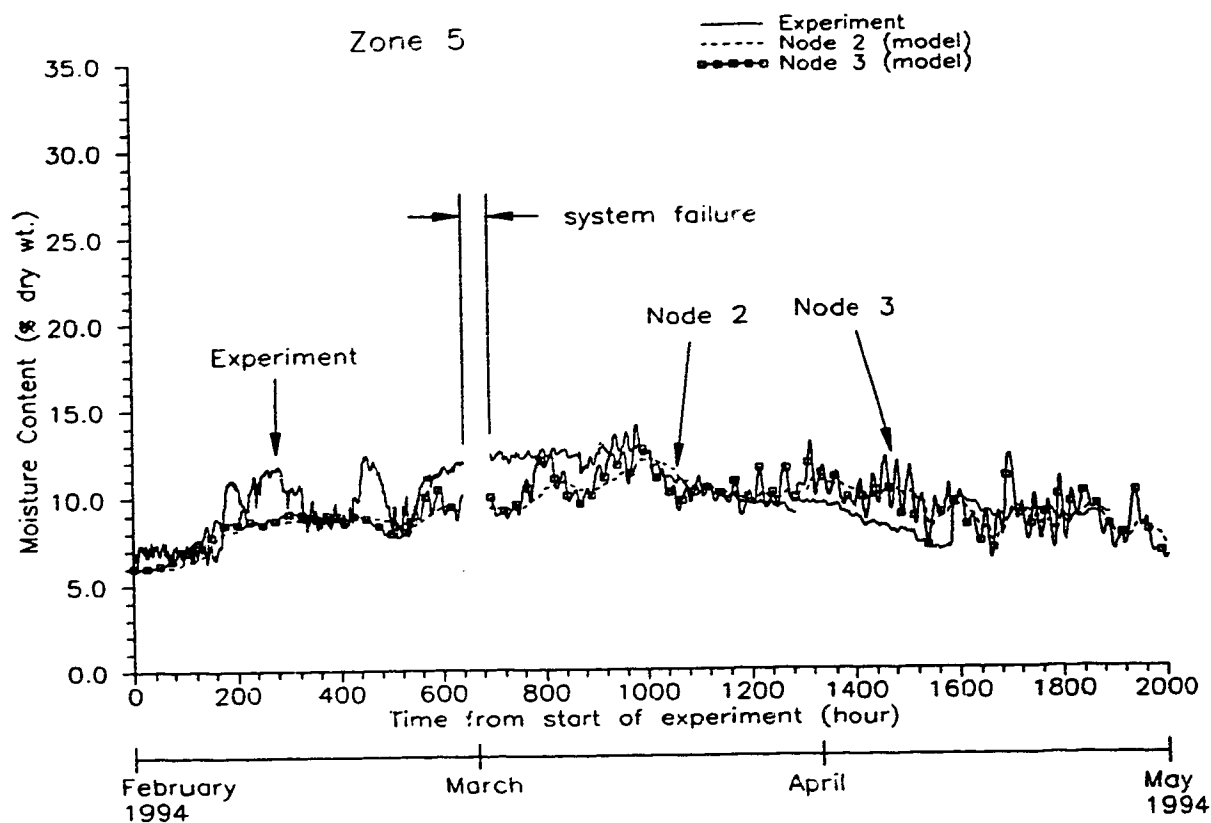


Figure 5.17d: Comparison of measured moisture content with predictions for node 2 and node 3 in zone 5 (February 1994 to April 1994). The supply fan was in operation from hours 440 to 1038.

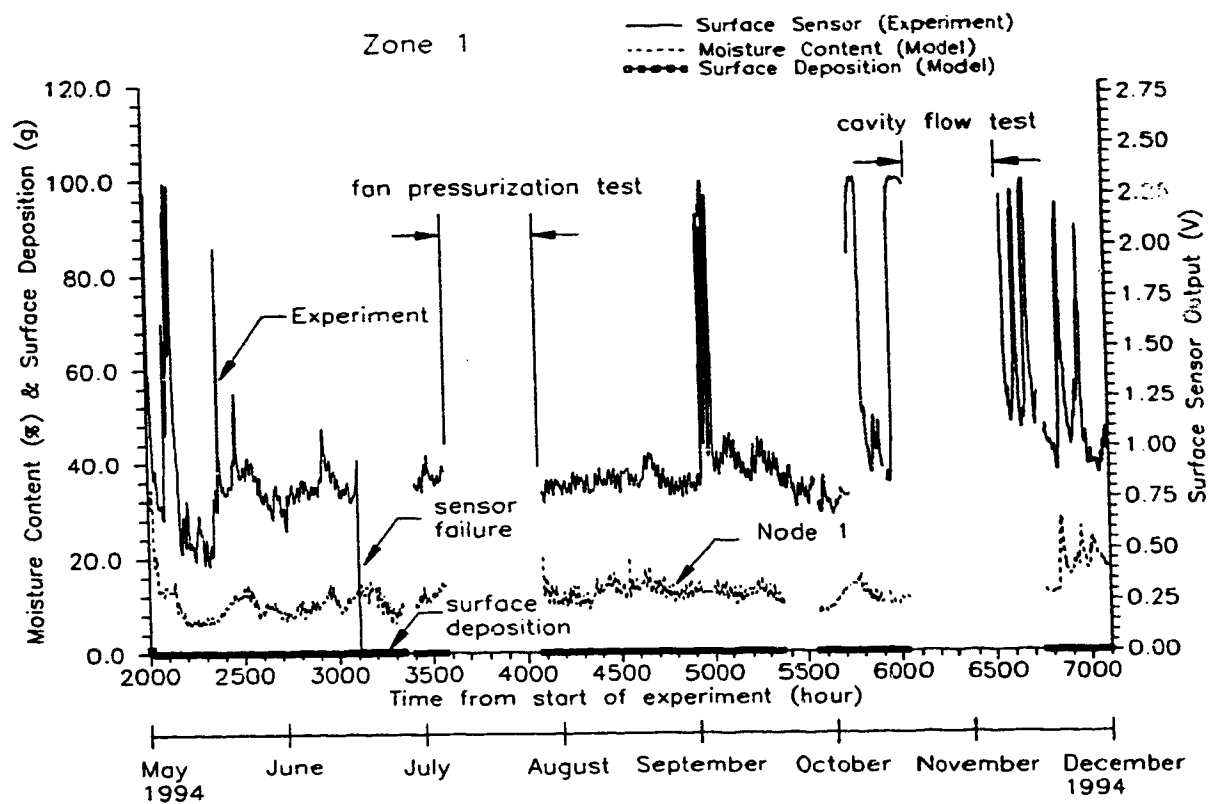


Figure 5.18a: Comparison of Wetwall predictions at node 1 and surface deposition with measured surface sensor output in zone 1 (May 1994 to November 1994).

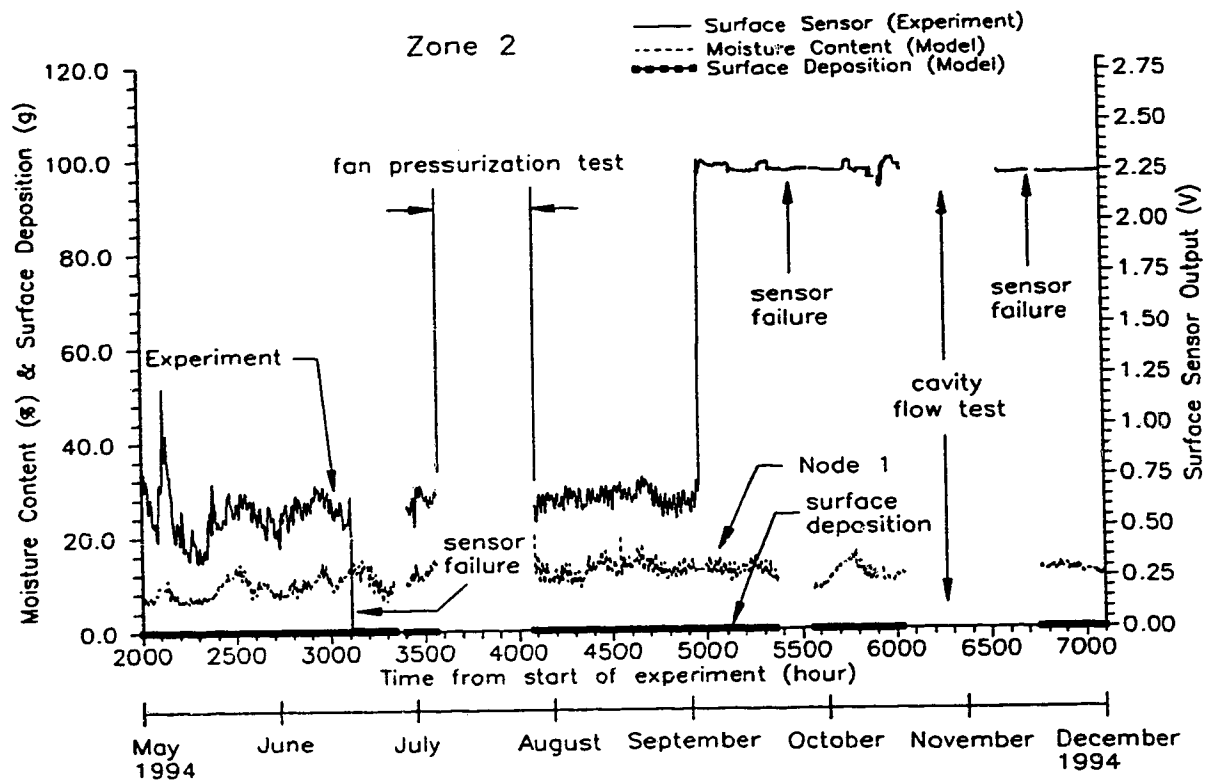


Figure 5.18b: Comparison of Wetwall predictions for node 1 and surface deposition with measured surface sensor output in zone 2 (May 1994 to November 1994).

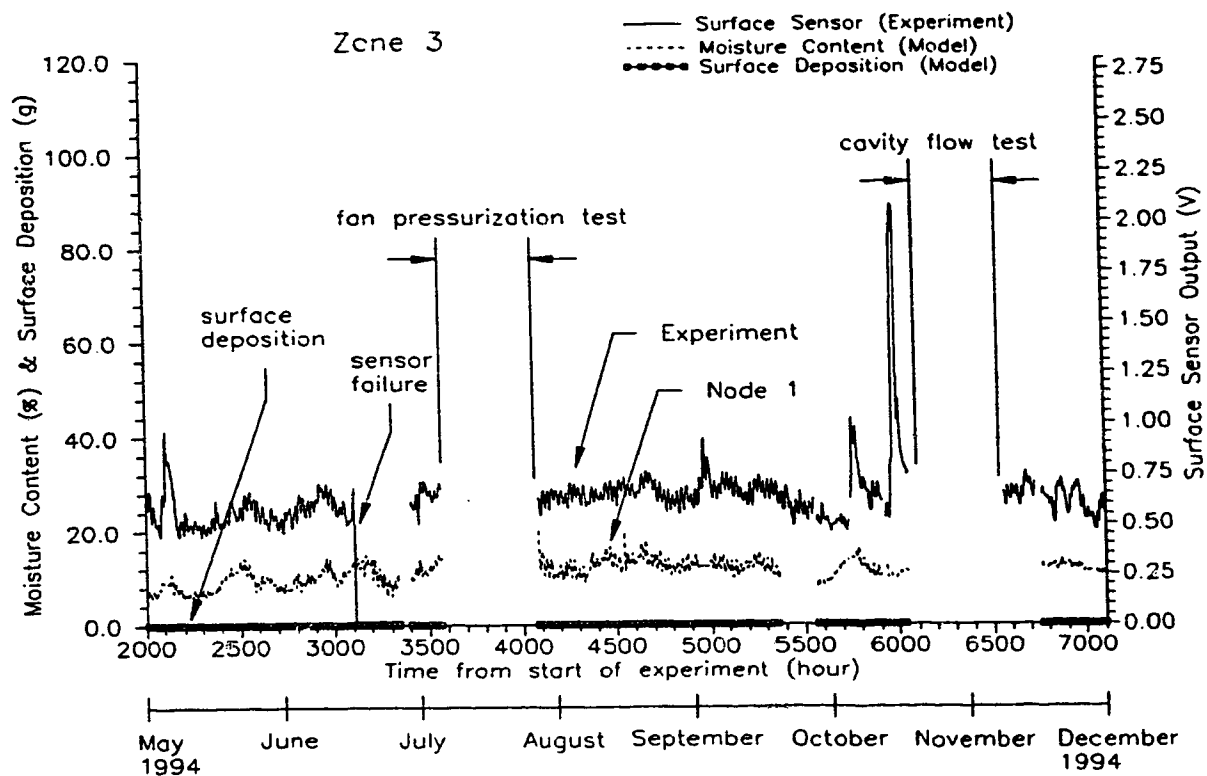


Figure 5.18c: Comparison of Wetwall predictions for node 1 and surface deposition with measured surface sensor output in zone 3 (May 1994 to November 1994).

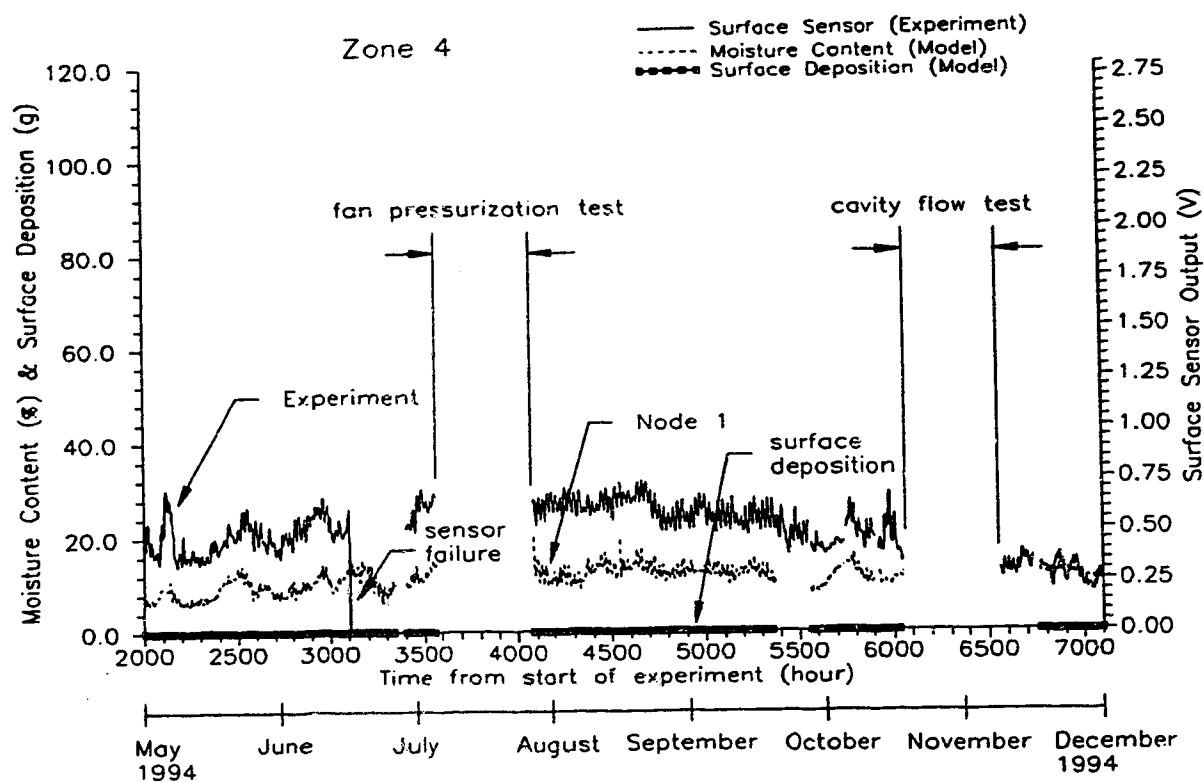


Figure 5.18d: Comparison of Wetwall predictions for node 1 and surface deposition with measured surface sensor output in zone 4 (May 1994 to November 1994).

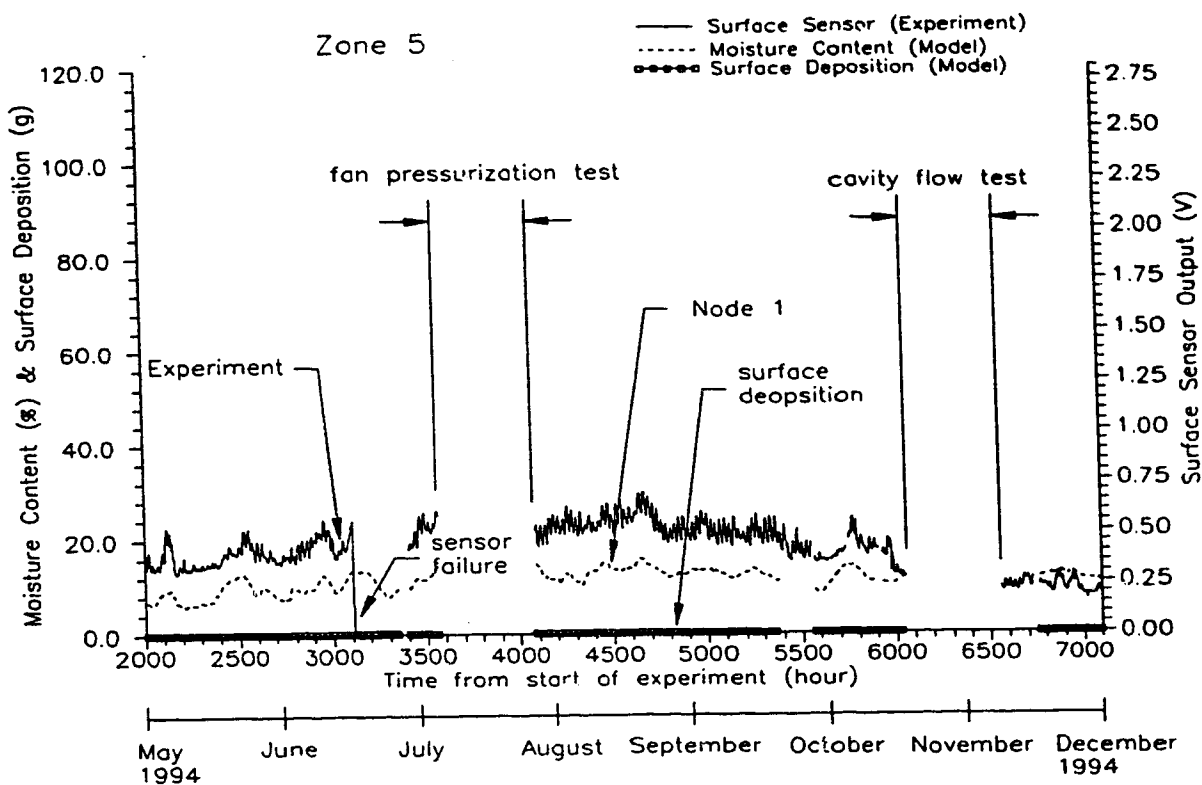


Figure 5.18e: Comparison of Wetwall predictions for node 1 and surface deposition with measured surface sensor output in zone 5 (May 1994 to November 1994).

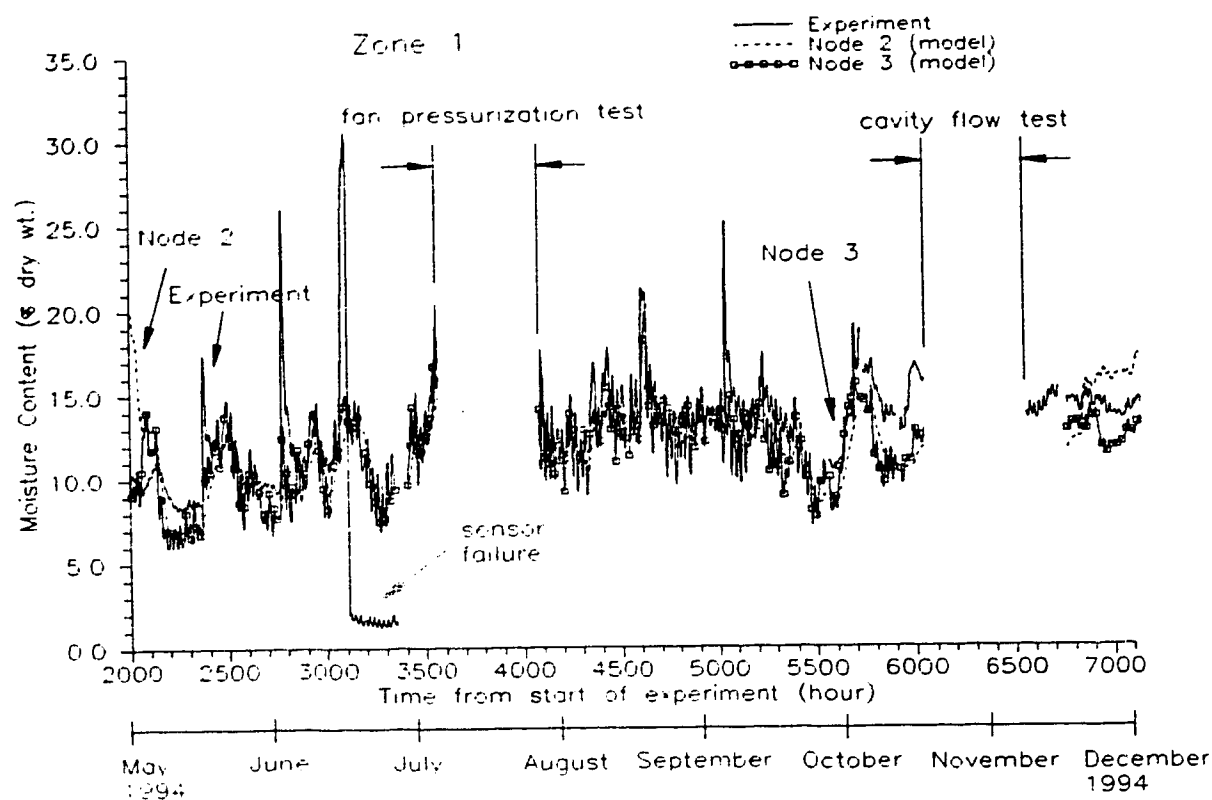


Fig. 19a: Comparison of measured moisture content with predictions for node 2 and node 3 in zone 1 (May 1994 to November 1994).

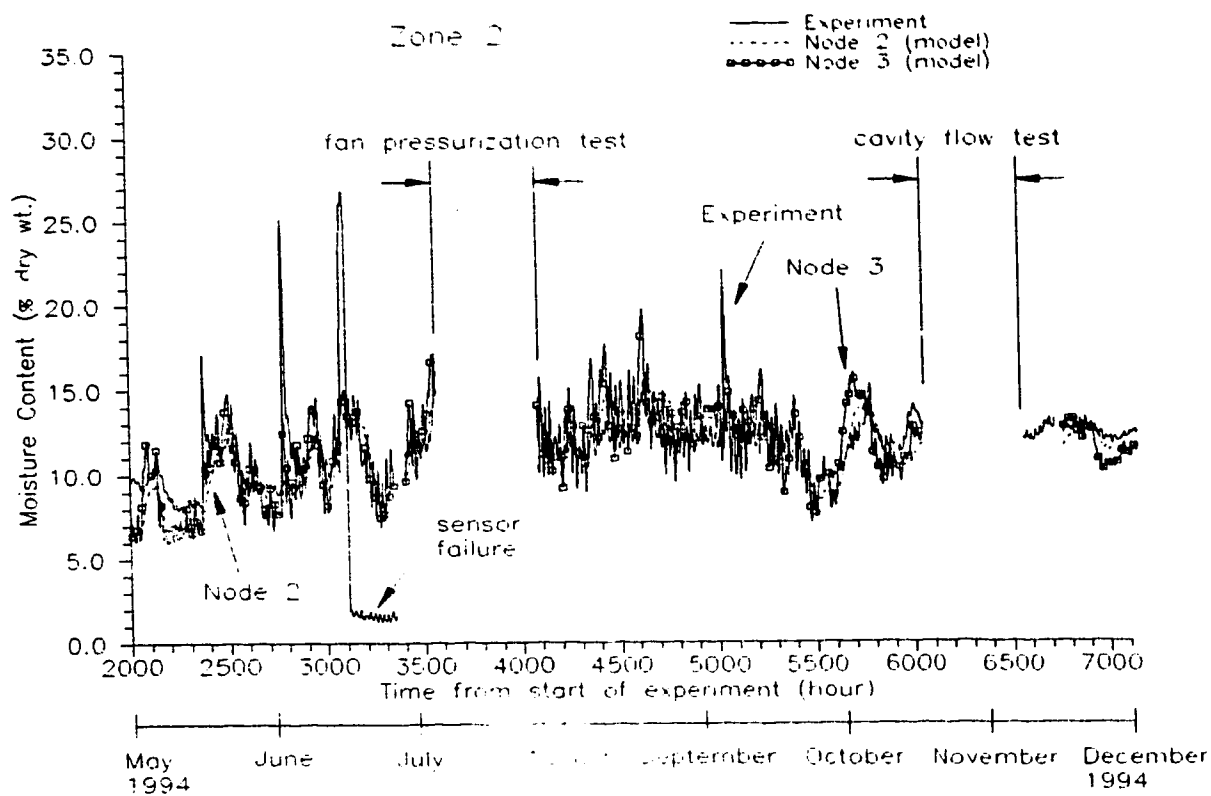


Figure 5.19b: Comparison of measured moisture content with predictions for node 2 and node 3 in zone 2 (May 1994 to November 1994).

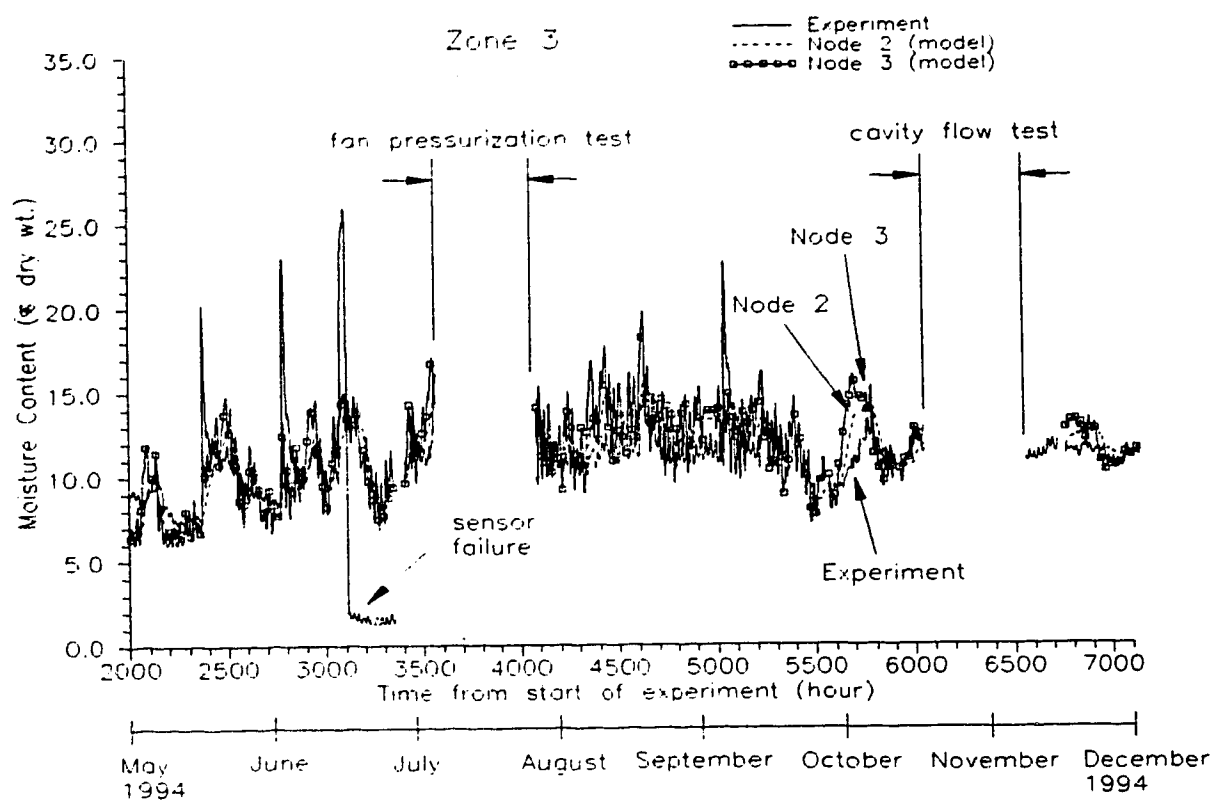


Figure 5.19c: Comparison of measured moisture content with predictions for node 2 and node 3 in zone 3 (May 1994 to November 1994).

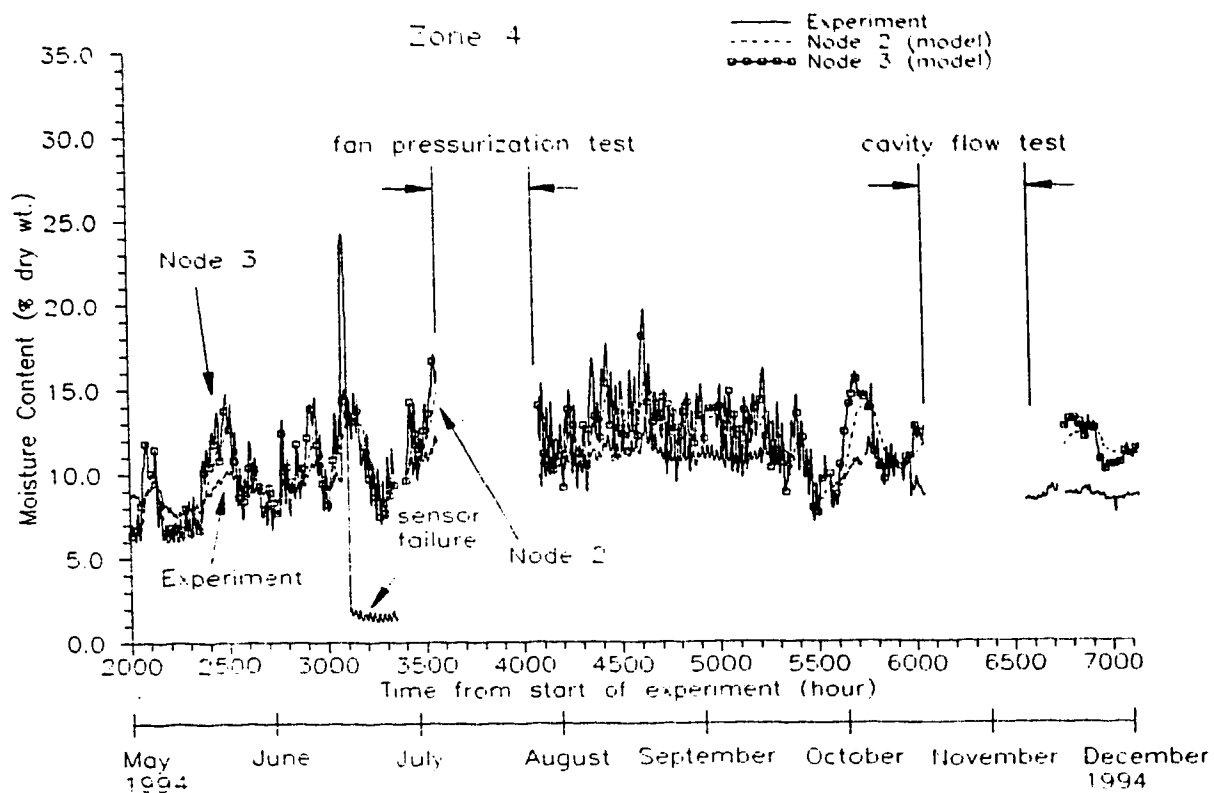


Figure 5.19d: Comparison of measured moisture content with predictions for node 2 and node 3 in zone 4 (May 1994 to November 1994).

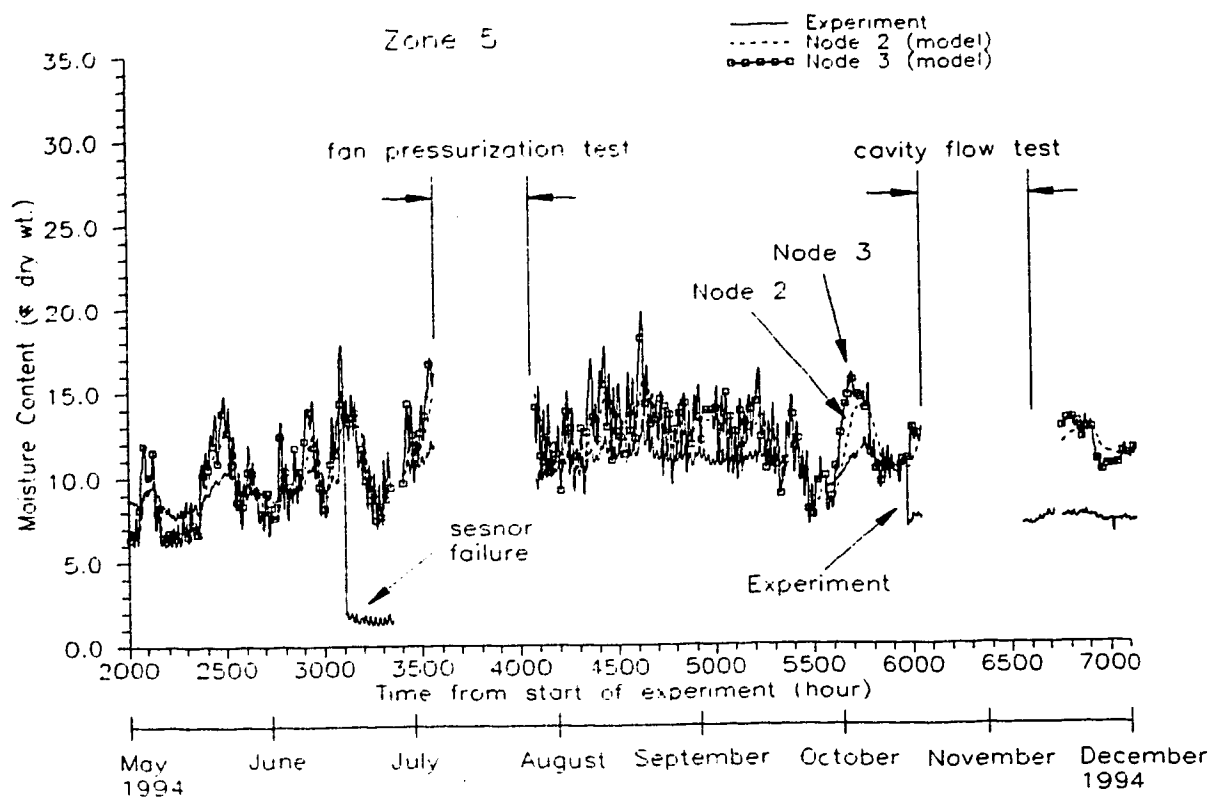


Figure 5.19e: Comparison of measured moisture content with predictions for node 2 and node 3 in zone 5 (May 1994 to November 1994).

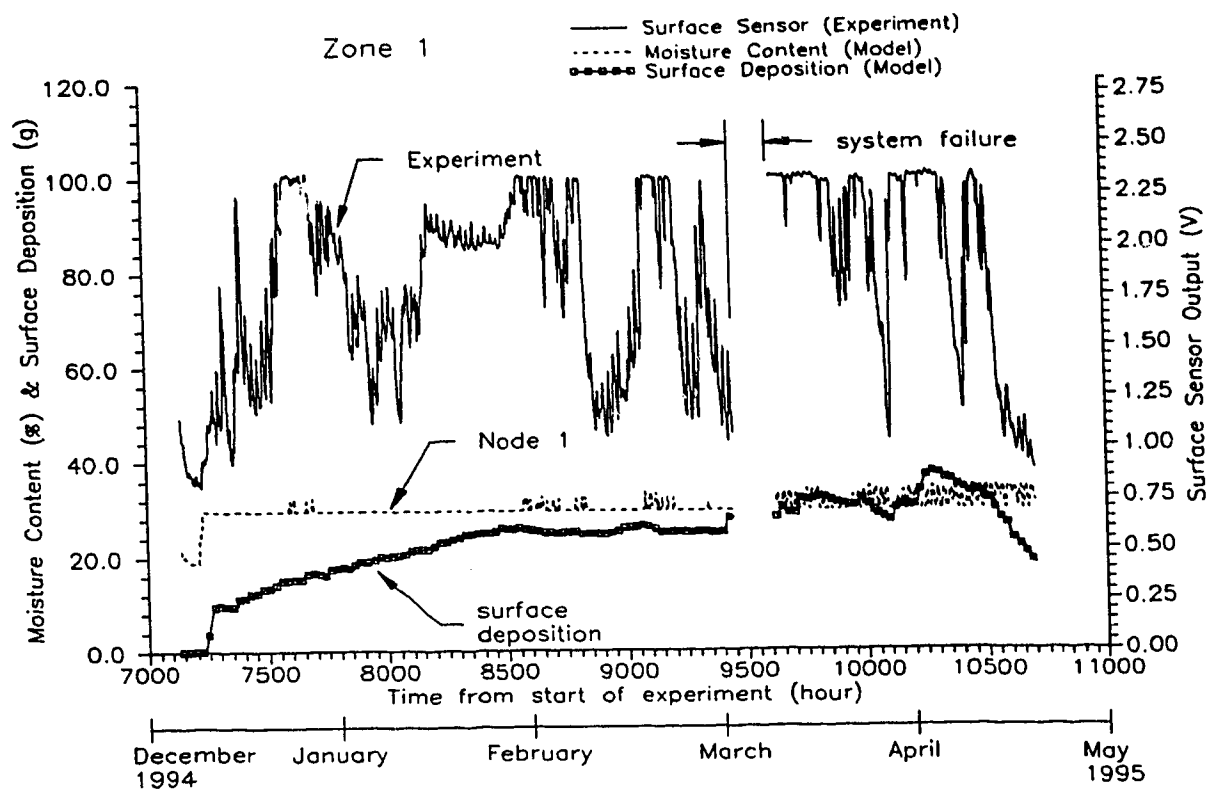


Figure 5.20a: Comparison of Wetwall predictions at node 1 and surface deposition with measured surface sensor output in zone 1 (December 1994 to April 1995).

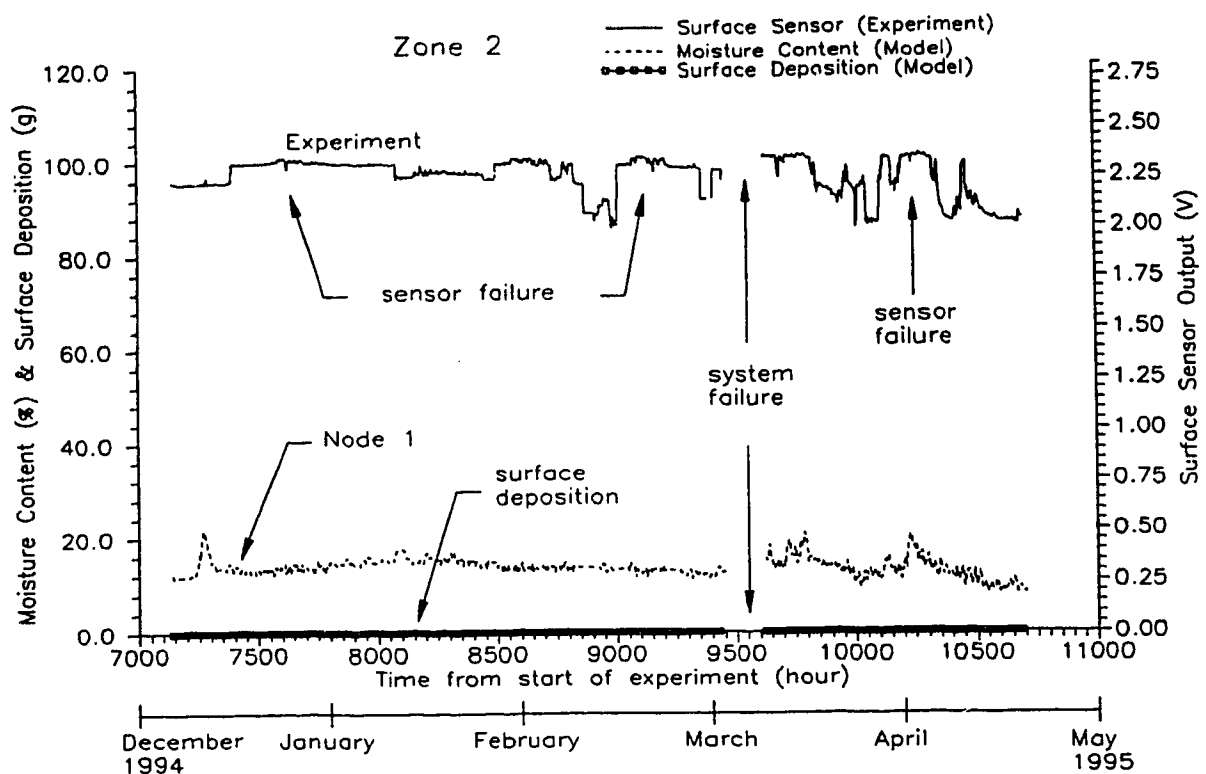


Figure 5.20b: Comparison of Wetwall predictions for node 1 and surface deposition with measured surface sensor output in zone 2 (December 1994 to April 1995).

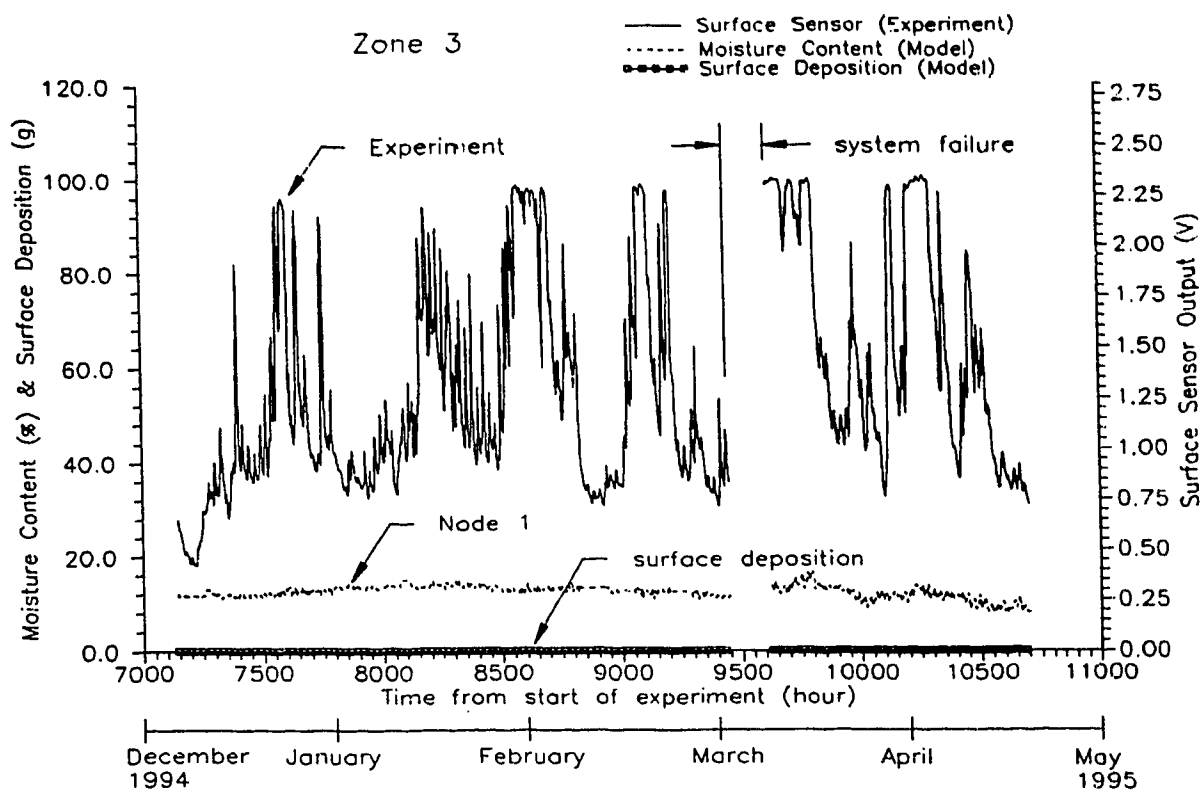


Figure 5.20c: Comparison of Wetwall predictions for node 1 and surface deposition with measured surface sensor output in zone 3 (December 1994 to April 1995).

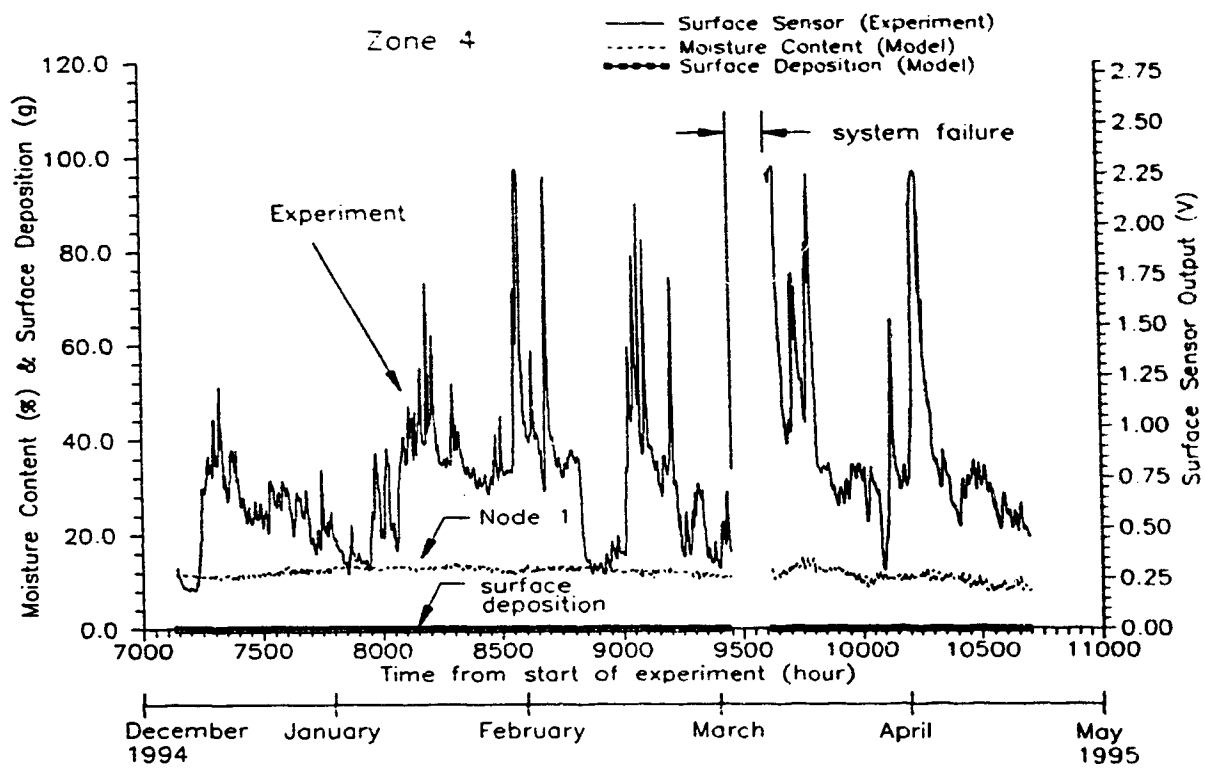


Figure 5.20d: Comparison of Wetwall predictions for node 1 and surface deposition with measured surface sensor output in zone 4 (December 1994 to April 1995).

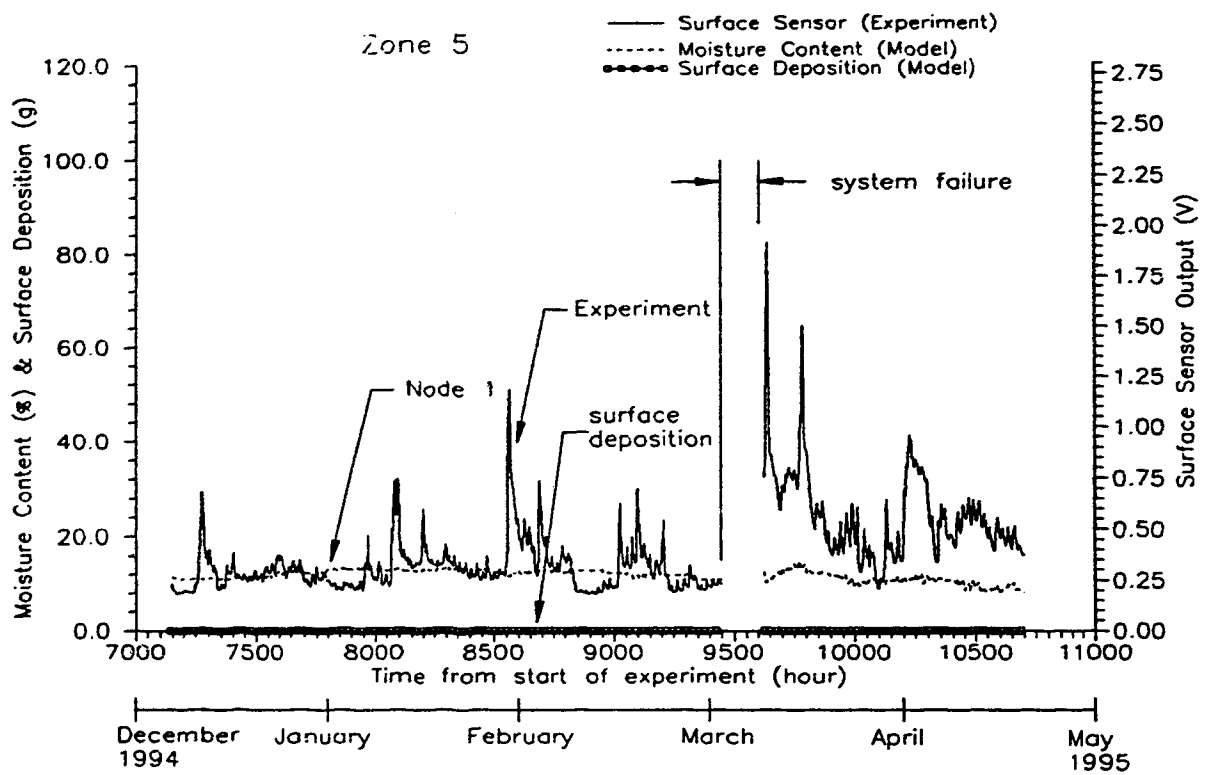


Figure 5.20e: Comparison of Wetwall predictions for node 1 and surface deposition with measured surface sensor output in zone 5 (December 1994 to April 1995).

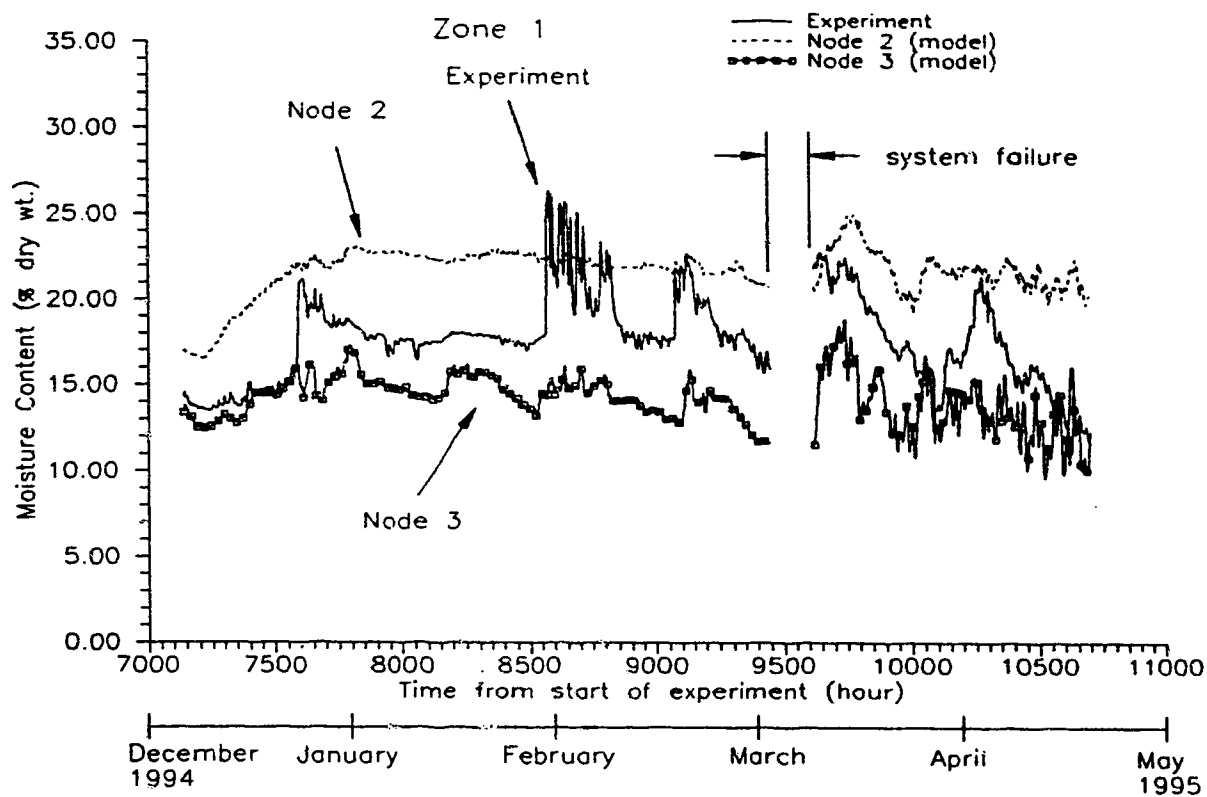


Figure 5.21a: Comparison of measured moisture content with predictions for node 2 and node 3 in zone 1 (December 1994 to April 1995).

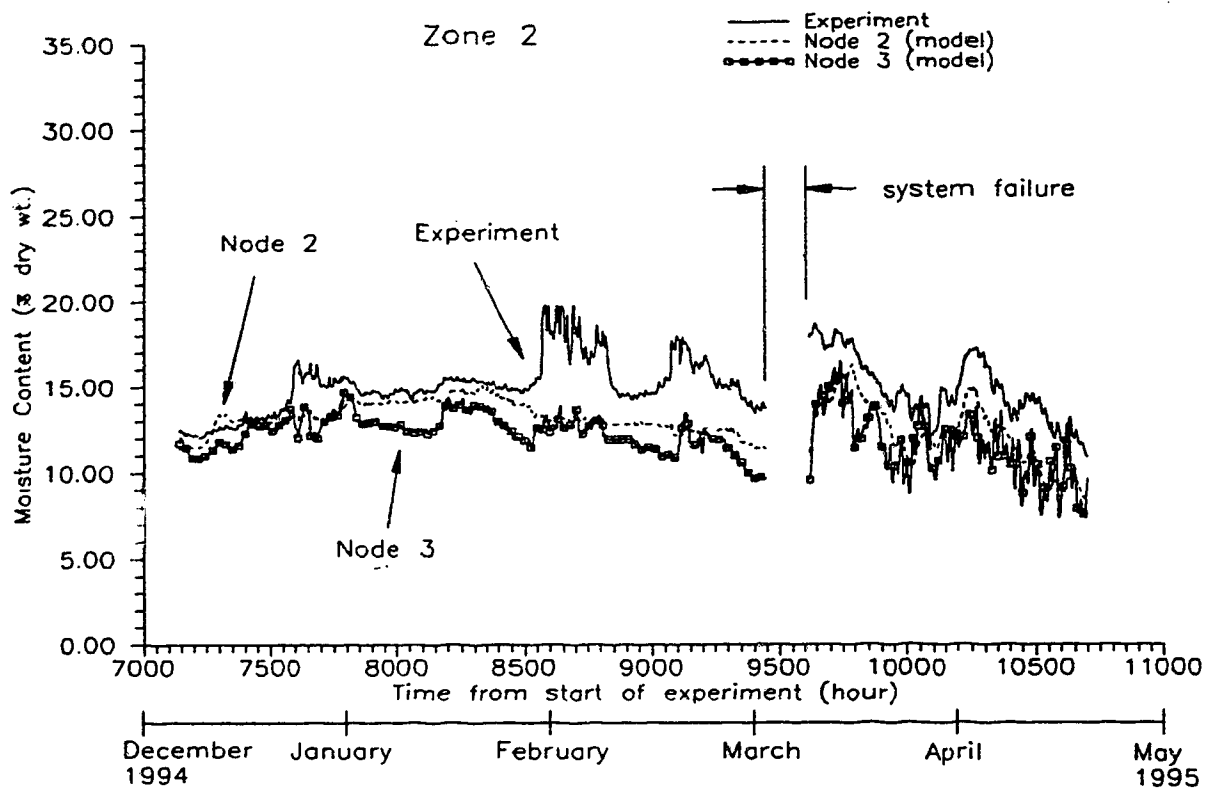


Figure 5.21b: Comparison of measured moisture content with predictions for node 2 and node 3 in zone 2 (December 1994 to May 1995).

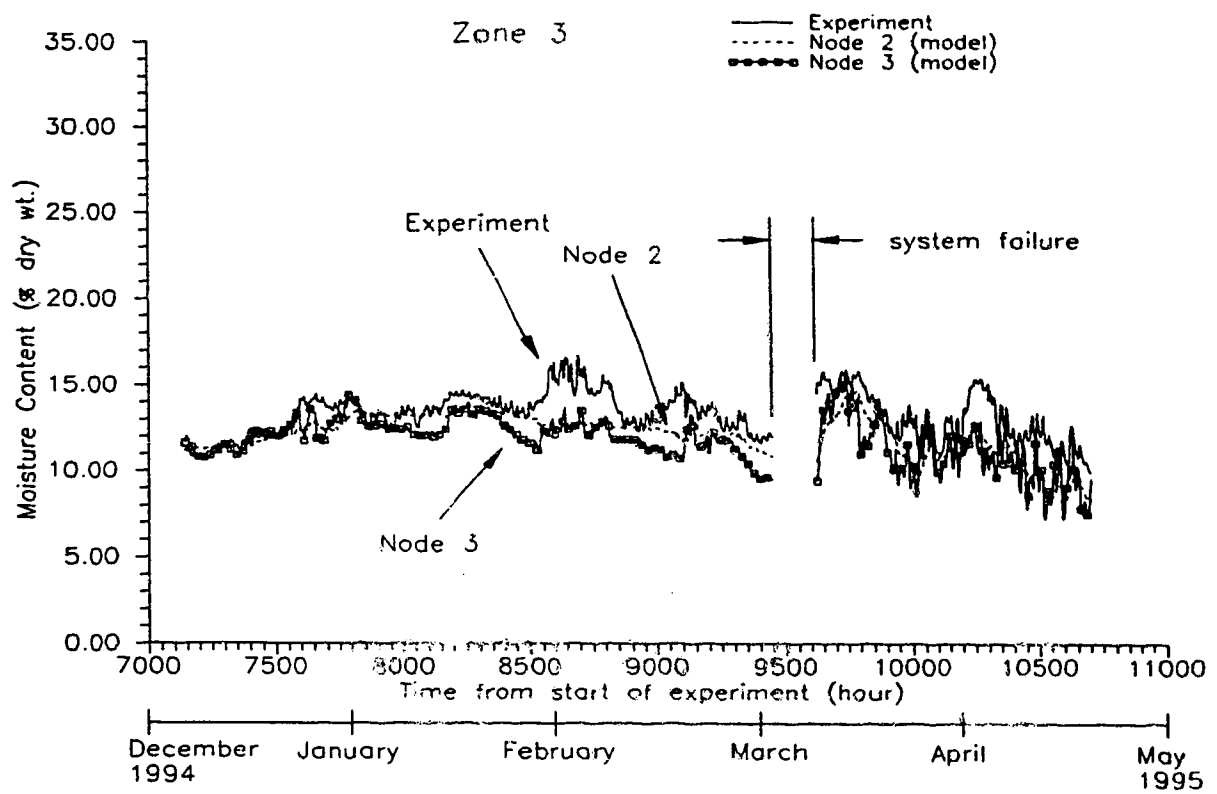


Figure 5.21c: Comparison of measured moisture content with predictions for node 2 and node 3 in zone 3 (December 1994 to May 1995).

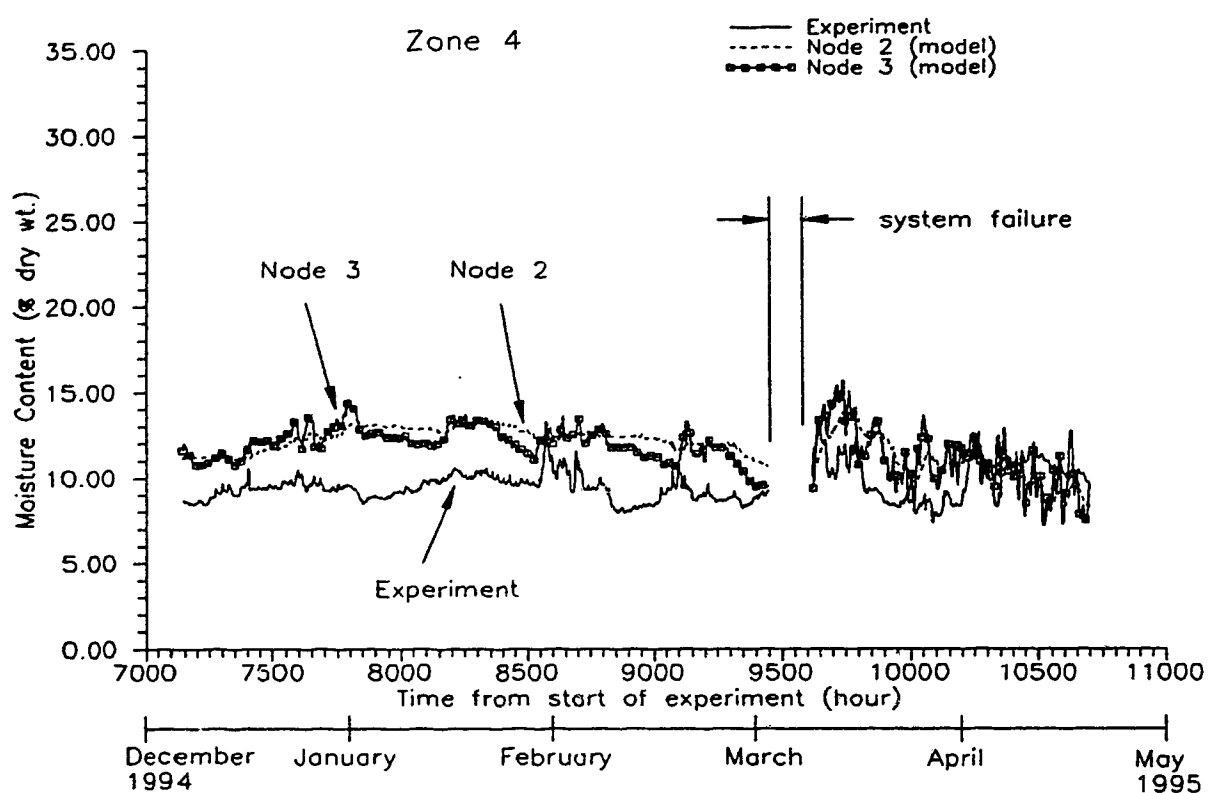


Figure 5.21d: Comparison of measured moisture content with predictions for node 2 and node 3 in zone 4 (December 1994 to April 1995).

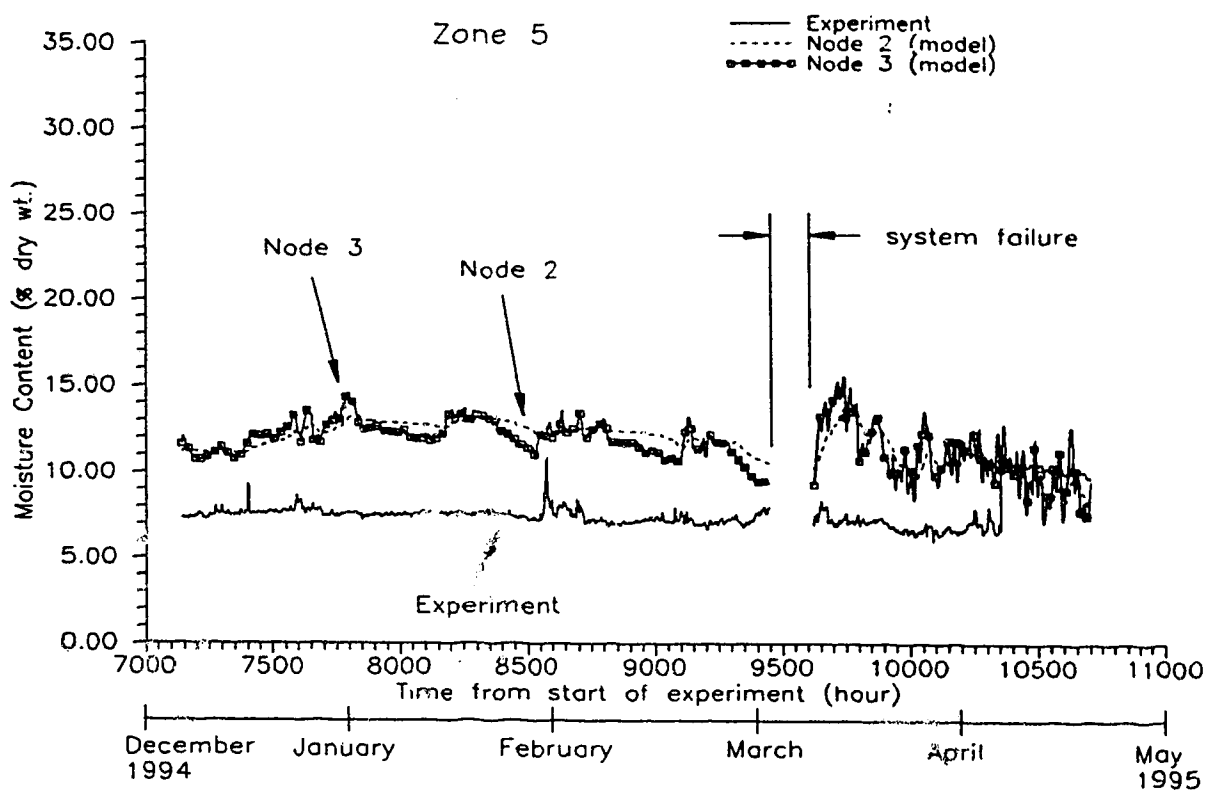


Figure 5.21e: Comparison of measured moisture content with predictions for node 2 and node 3 in zone 5 (December 1994 to April 1995).

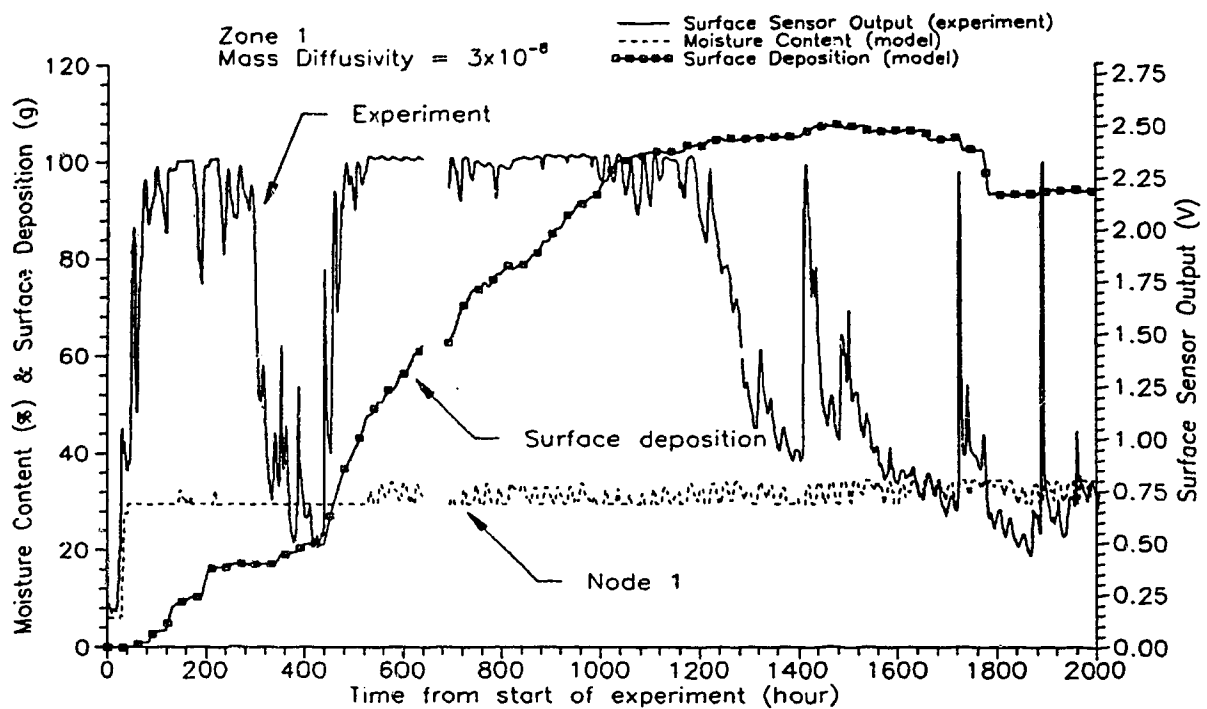


Figure 5.22a: Comparison of Wetwall predictions at node 1 and surface deposition with measured surface sensor output in zone 1. The mass diffusivity for the sheathing is equal to $3 \times 10^{-8} \text{ m}^2/\text{s}$.

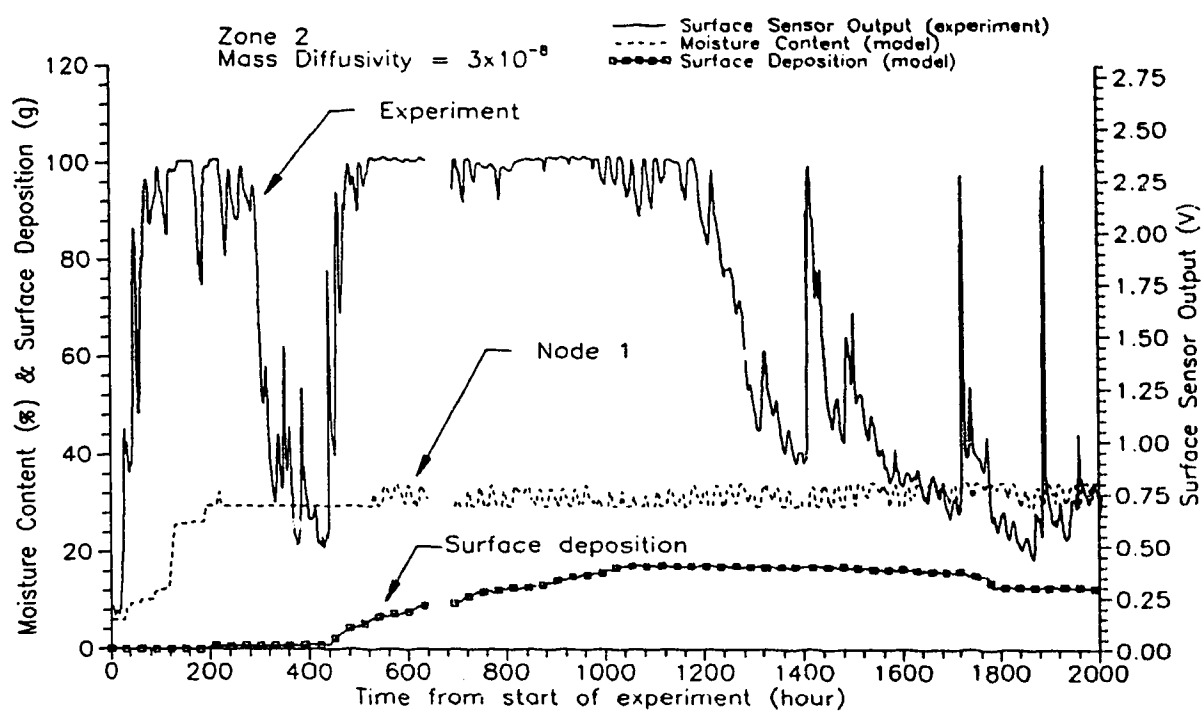


Figure 5.22b: Comparison of Wetwall predictions at node 1 and surface deposition with measured surface sensor output in zone 2. The mass diffusivity for the sheathing is equal to $3 \times 10^{-8} \text{ m}^2/\text{s}$.

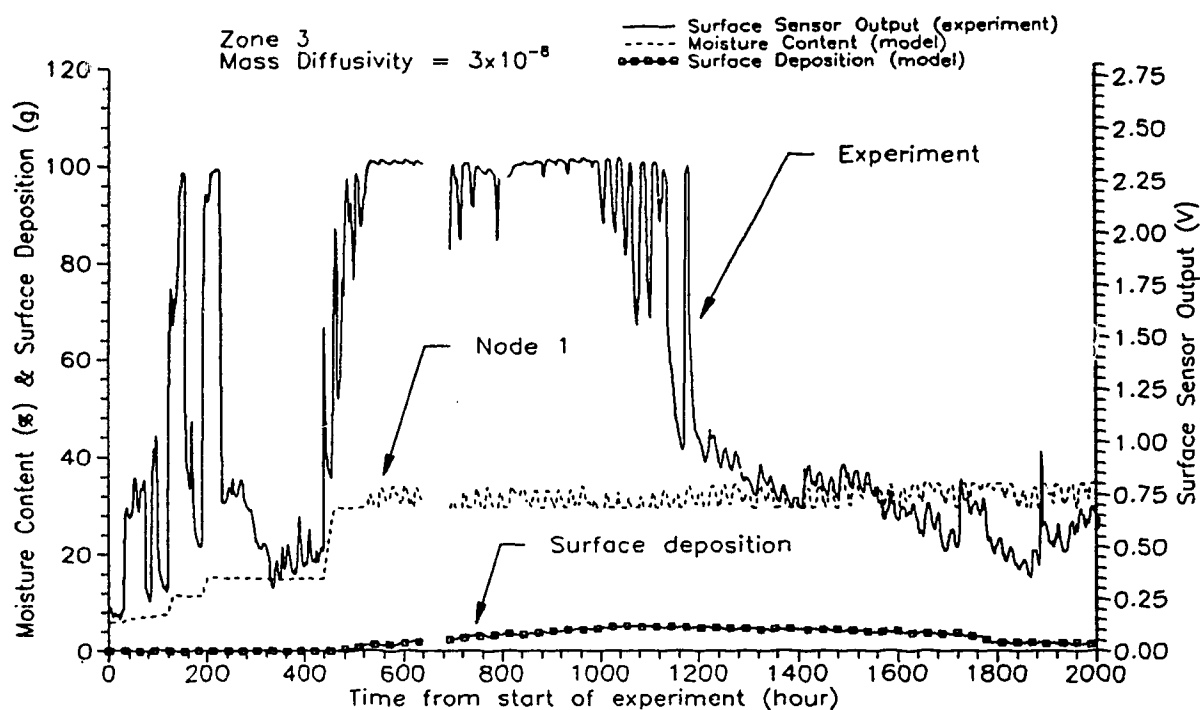


Figure 5.22c: Comparison of Wetwall predictions at node 1 and surface deposition with measured surface sensor output in zone 3. The mass diffusivity for the sheathing is equal to $3 \times 10^{-8} \text{ m}^2/\text{s}$.

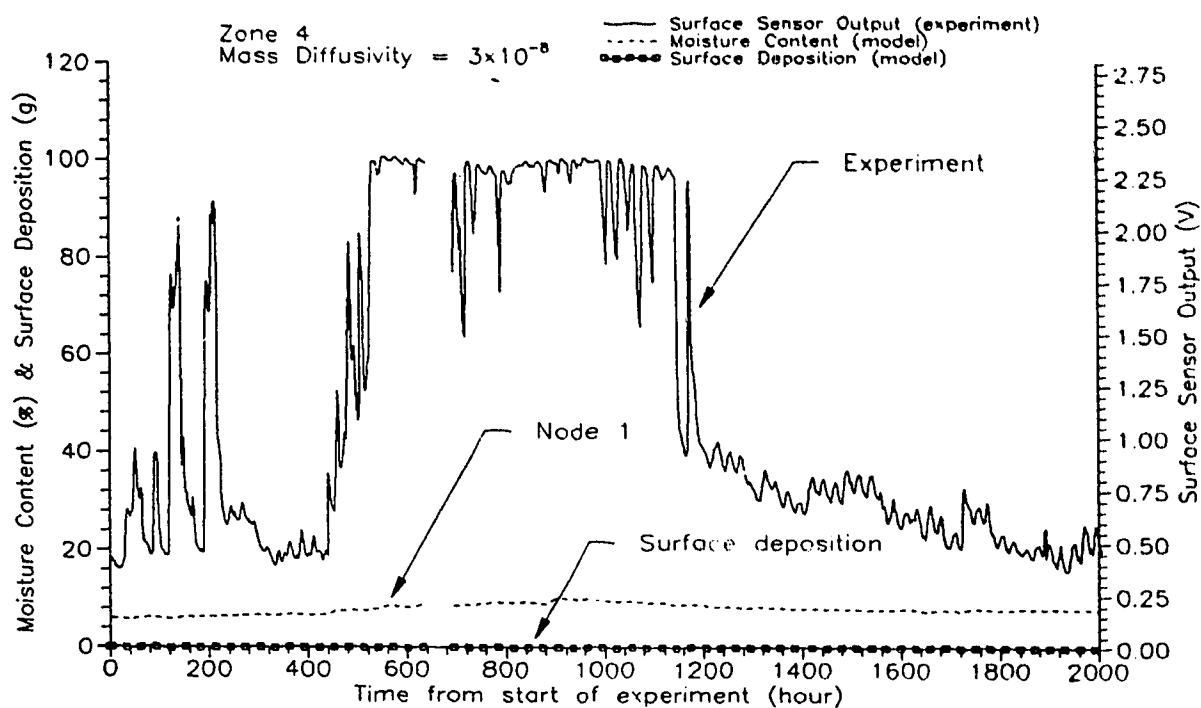


Figure 5.22d: Comparison of Wetwall predictions at node 1 and surface deposition with measured surface sensor output in zone 4. The mass diffusivity for the sheathing is equal to $3 \times 10^{-8} \text{ m}^2/\text{s}$.

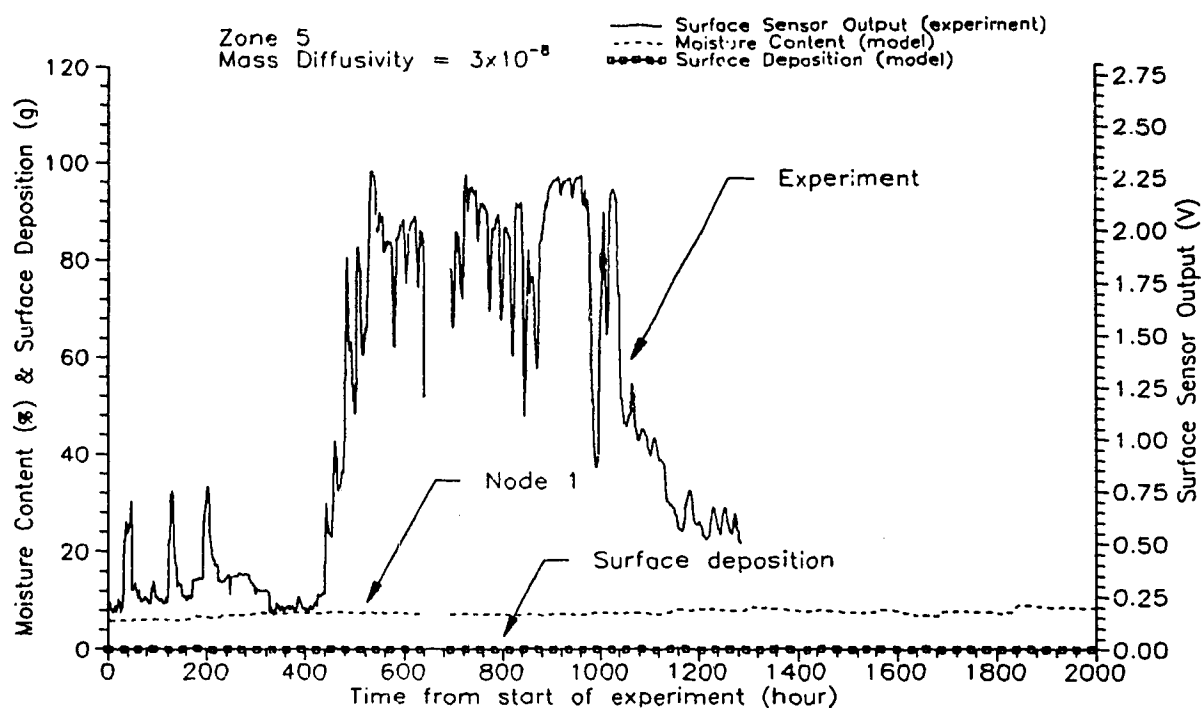


Figure 5.22e: Comparison of Wetwall predictions at node 1 and surface deposition with measured surface sensor output in zone 5. The mass diffusivity for the sheathing is equal to $3 \times 10^{-8} \text{ m}^2/\text{s}$.

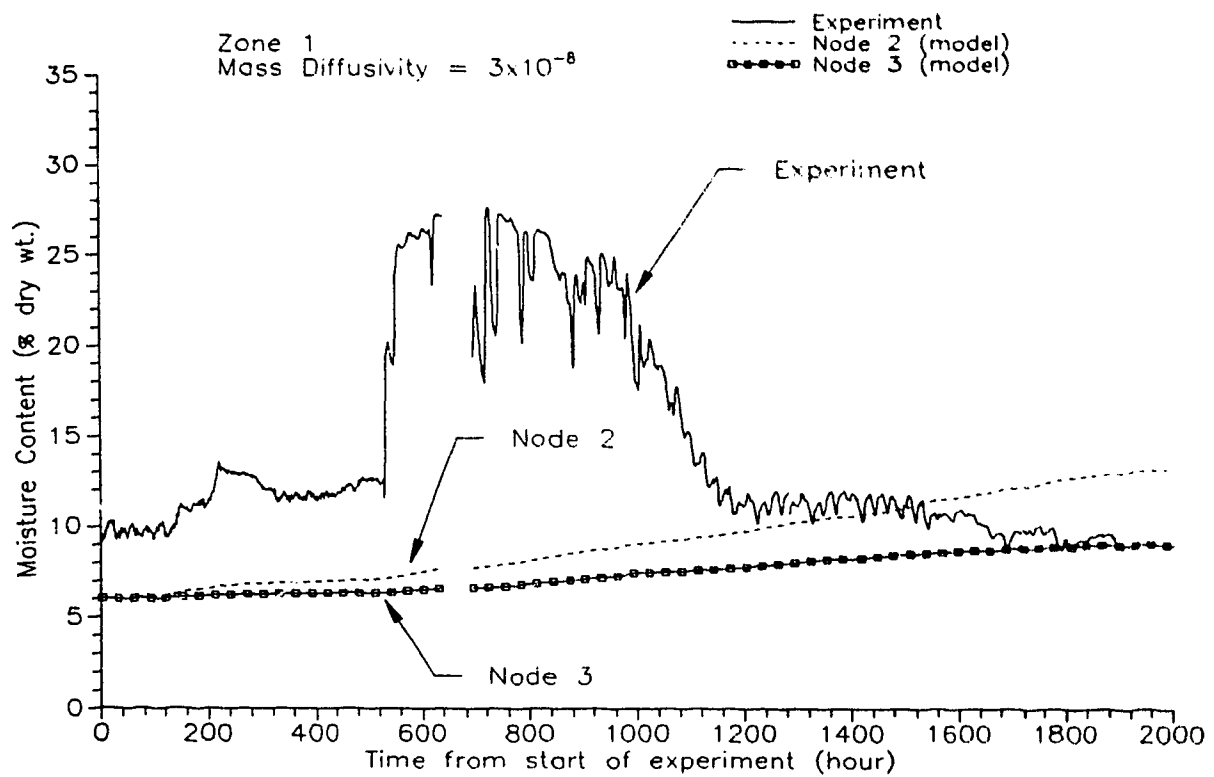


Figure 5.23a: Comparison of Wetwall predictions at node 2 and node 3 with measured moisture content in zone 1. The mass diffusivity for the sheathing is equal to $3 \times 10^{-8} \text{ m}^2/\text{s}$.

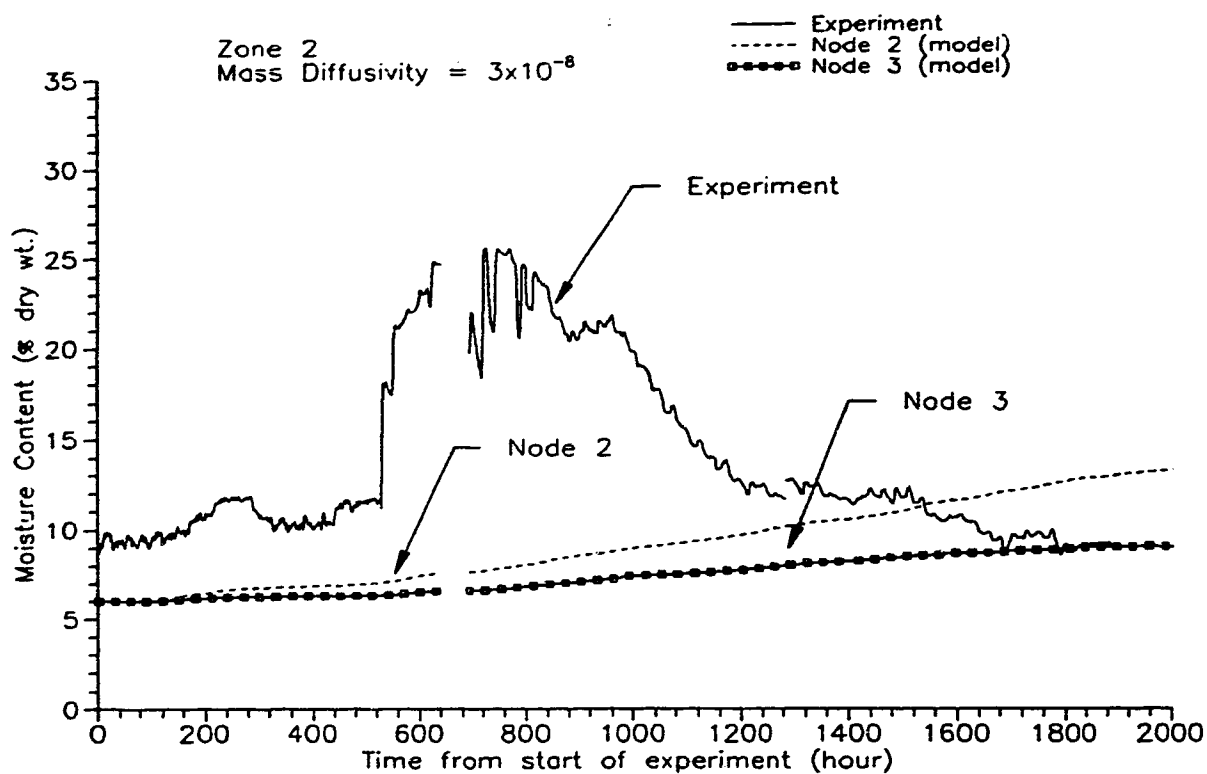


Figure 5.23b: Comparison of Wetwall predictions at node 2 and node 3 with measured moisture content in zone 2. The mass diffusivity for the sheathing is equal to $3 \times 10^{-8} \text{ m}^2/\text{s}$.

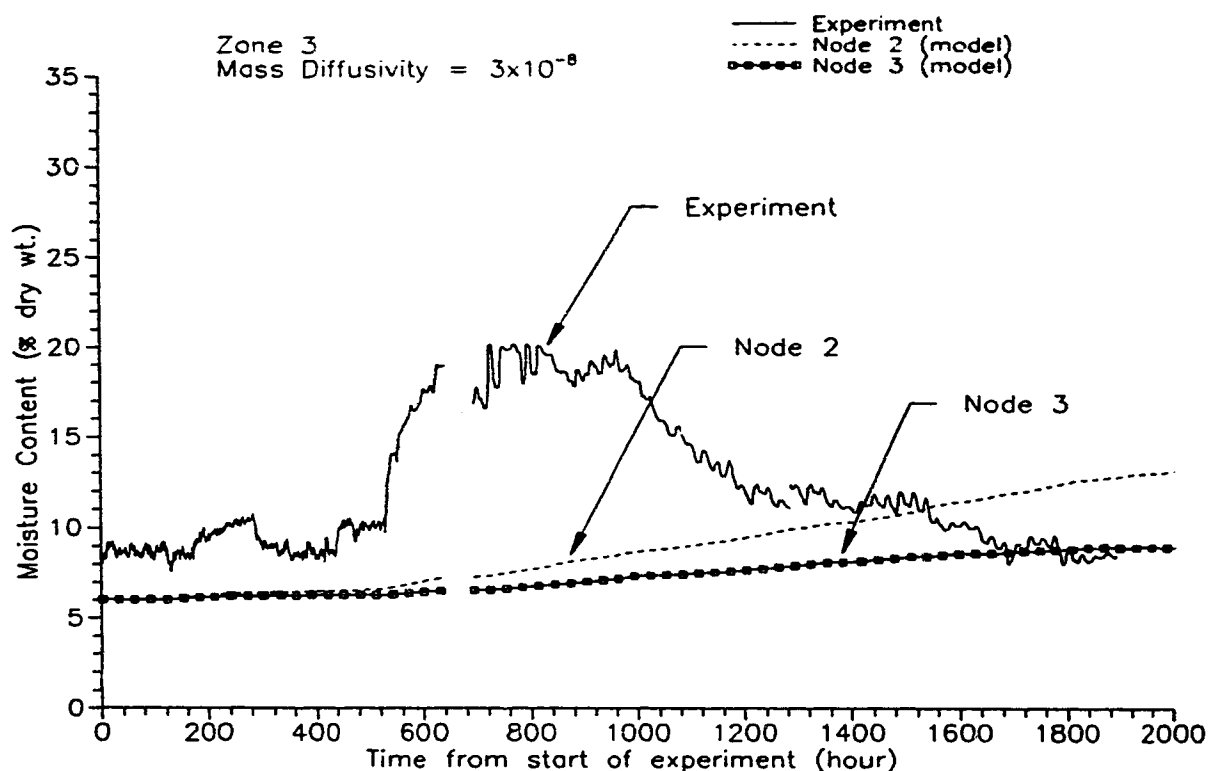


Figure 5.23c: Comparison of Wetwall predictions at node 2 and node 3 with measured moisture content in zone 3. The mass diffusivity for the sheathing is equal to $3 \times 10^{-8} \text{ m}^2/\text{s}$.

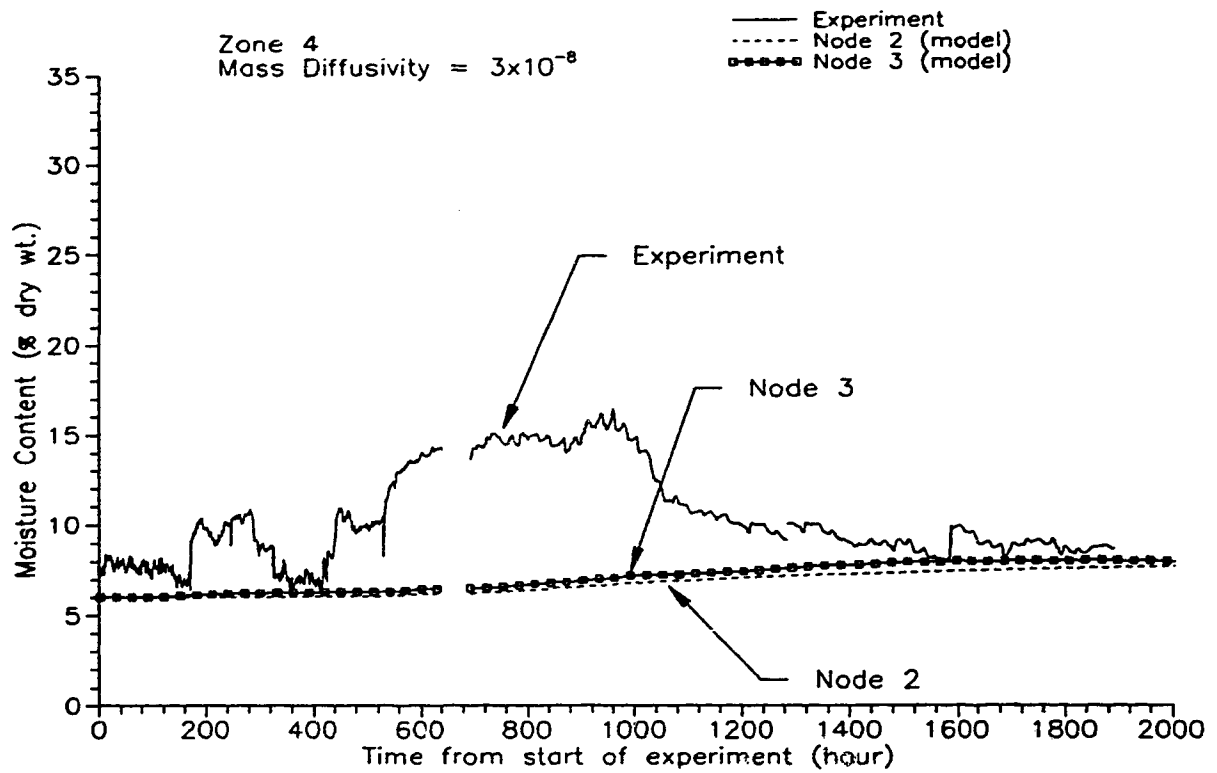


Figure 5.23d: Comparison of Wetwall predictions at node 2 and node 3 with measured moisture content in zone 4. The mass diffusivity for the sheathing is equal to $3 \times 10^{-8} \text{ m}^2/\text{s}$.

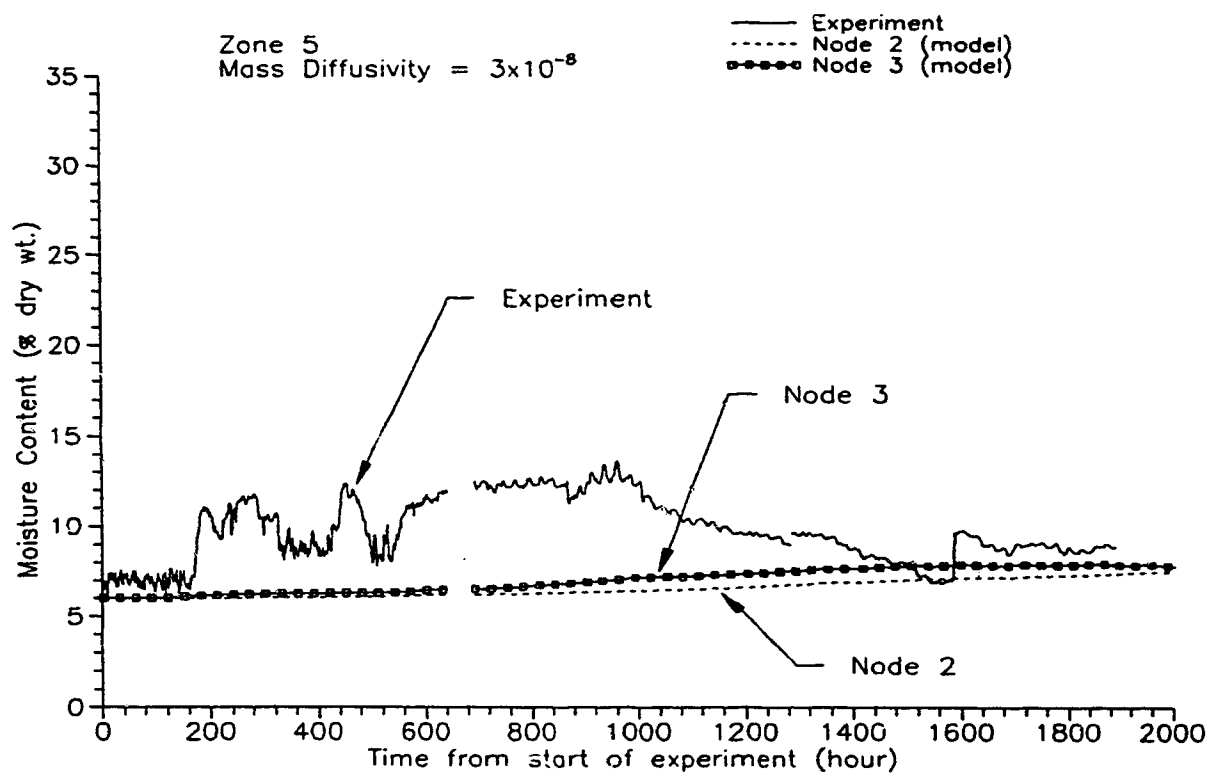


Figure 5.23e: Comparison of Wetwall predictions at node 2 and node 3 with measured moisture content in zone 5. The mass diffusivity for the sheathing is equal to $3 \times 10^{-8} \text{ m}^2/\text{s}$.

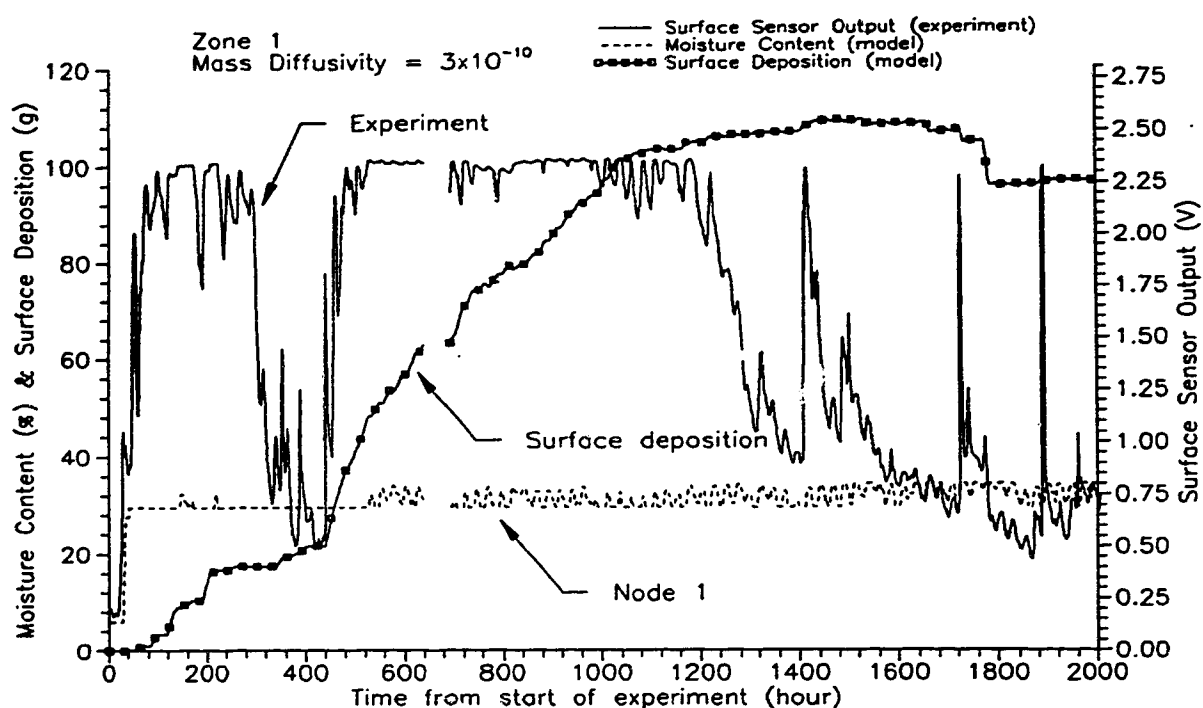


Figure 5.24a: Comparison of Wetwall predictions at node 1 and surface deposition with measured surface sensor output in zone 1. The mass diffusivity for the sheathing is to $3 \times 10^{-10} \text{ m}^2/\text{s}$.

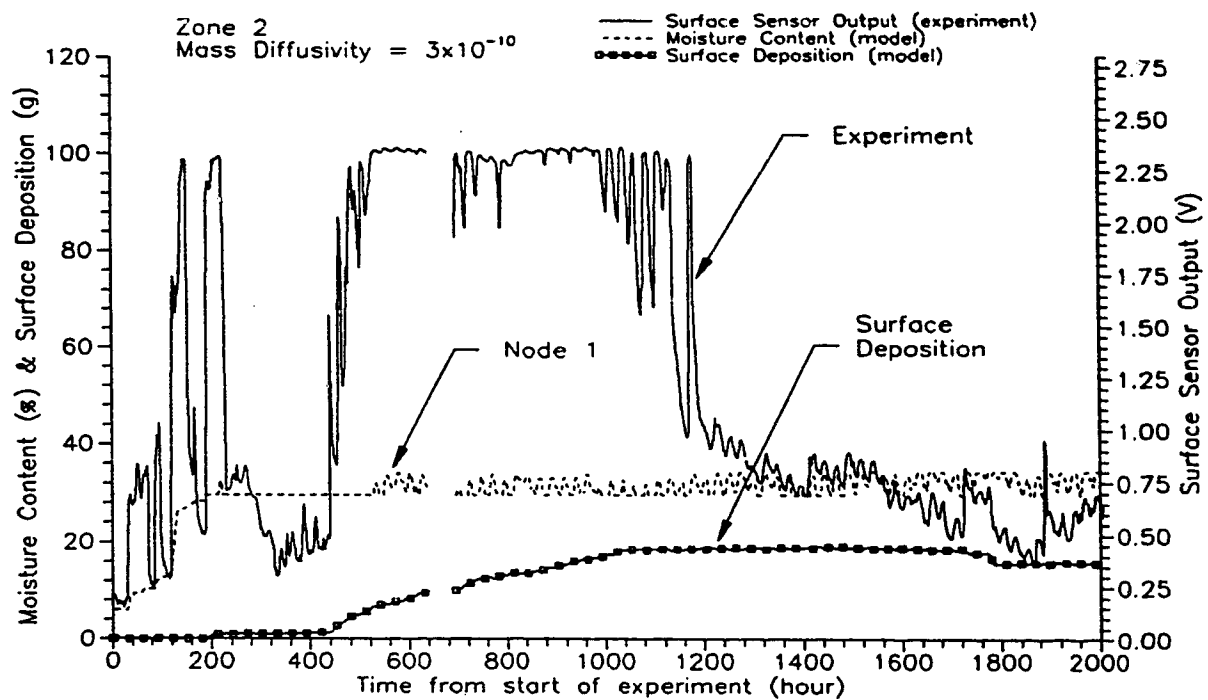


Figure 5.24b: Comparison of Wetwall predictions at node 1 and surface deposition with measured surface sensor output in zone 2. The mass diffusivity for the sheathing is equal to $3 \times 10^{-10} \text{ m}^2/\text{s}$.

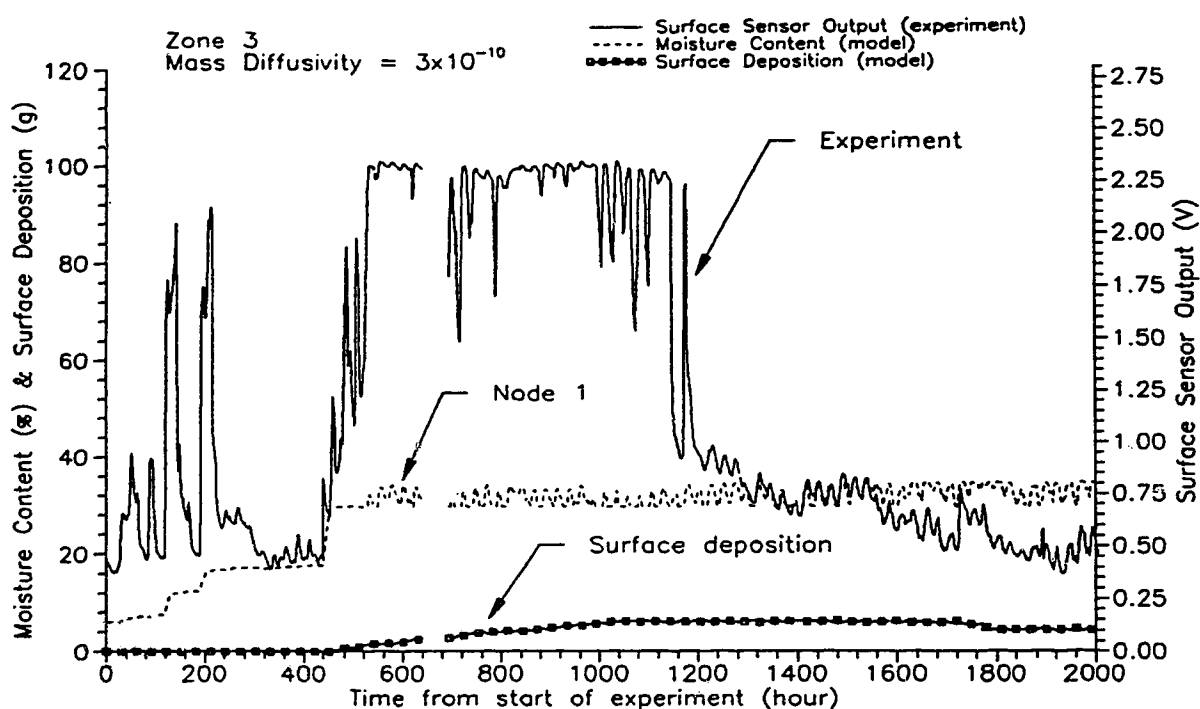


Figure 5.24c: Comparison of Wetwall predictions at node 1 and surface deposition with measured surface sensor output in zone 3. The mass diffusivity for the sheathing is equal to $3 \times 10^{-10} \text{ m}^2/\text{s}$.

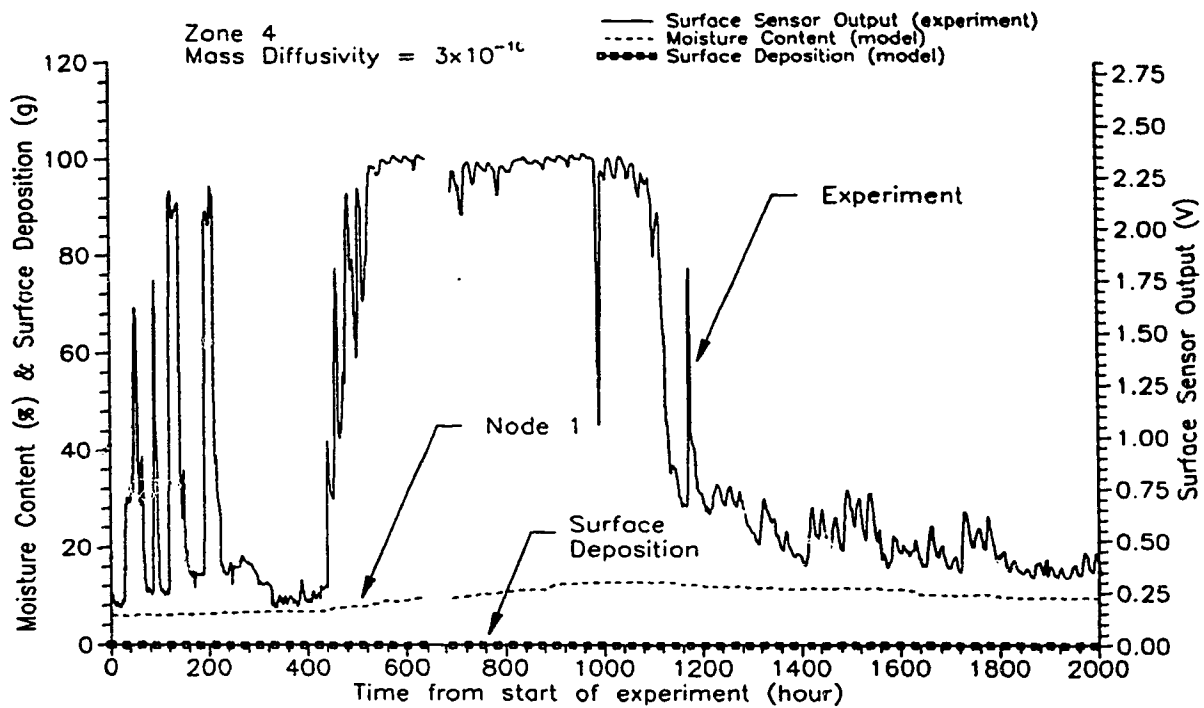


Figure 5.24d: Comparison of Wetwall predictions at node 1 and surface deposition with measured surface sensor output in zone 4. The mass diffusivity for the sheathing is equal to $3 \times 10^{-10} \text{ m}^2/\text{s}$.

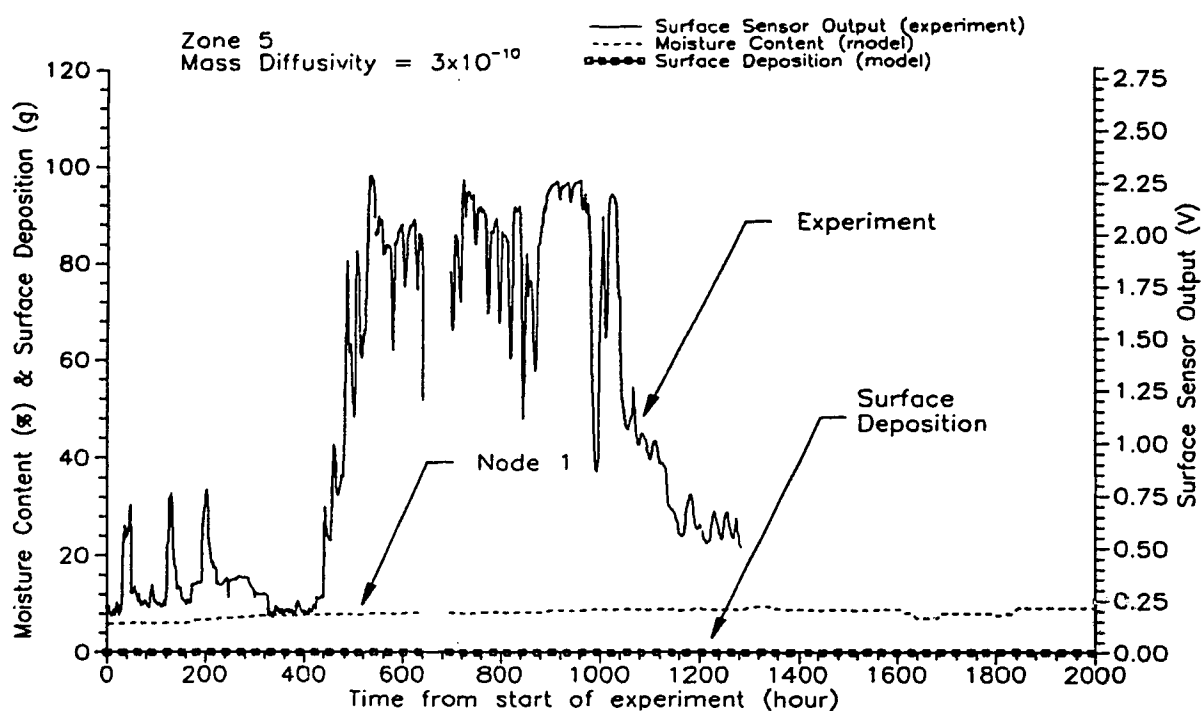


Figure 5.24e: Comparison of Wetwall predictions at node 1 and surface deposition with measured surface sensor output in zone 5. The mass diffusivity for the sheathing is equal to $3 \times 10^{-10} \text{ m}^2/\text{s}$.

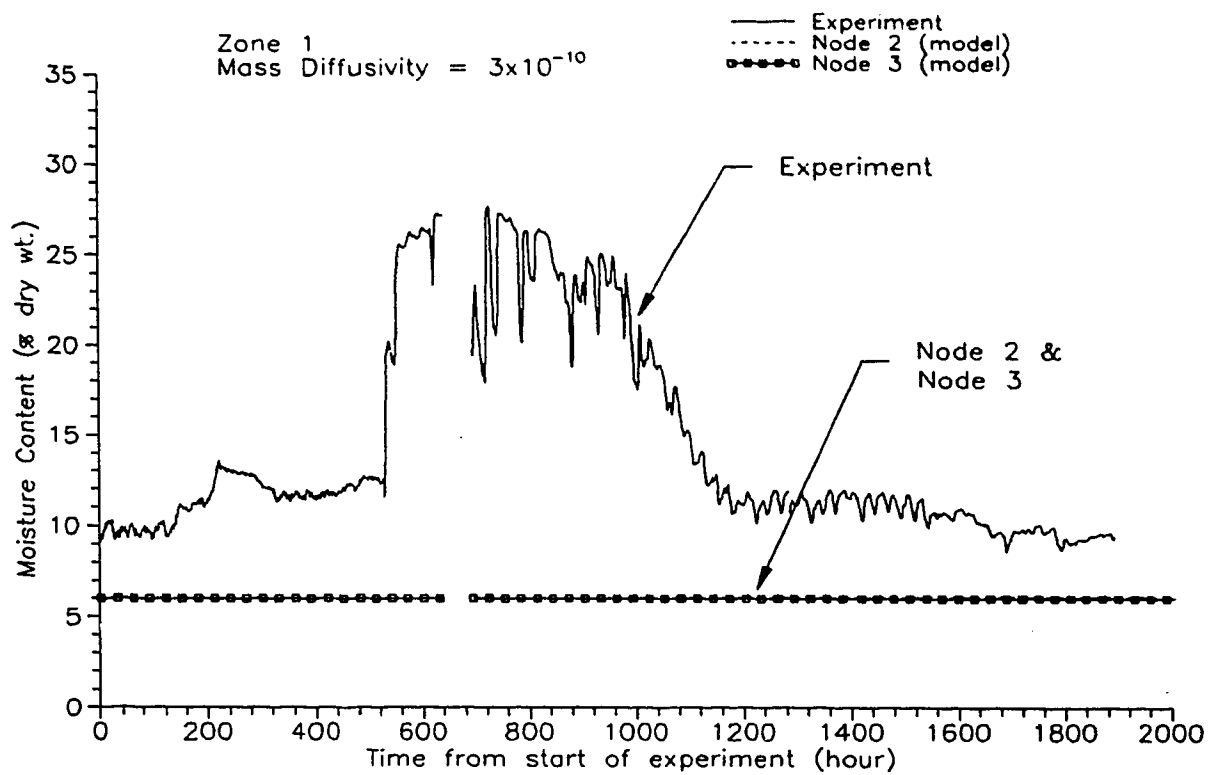


Figure 5.25a: Comparison of Wetwall predictions at node 2 and node 3 with measured moisture content in zone 1. The mass diffusivity for the sheathing is equal to $3 \times 10^{-10} \text{ m}^2/\text{s}$.

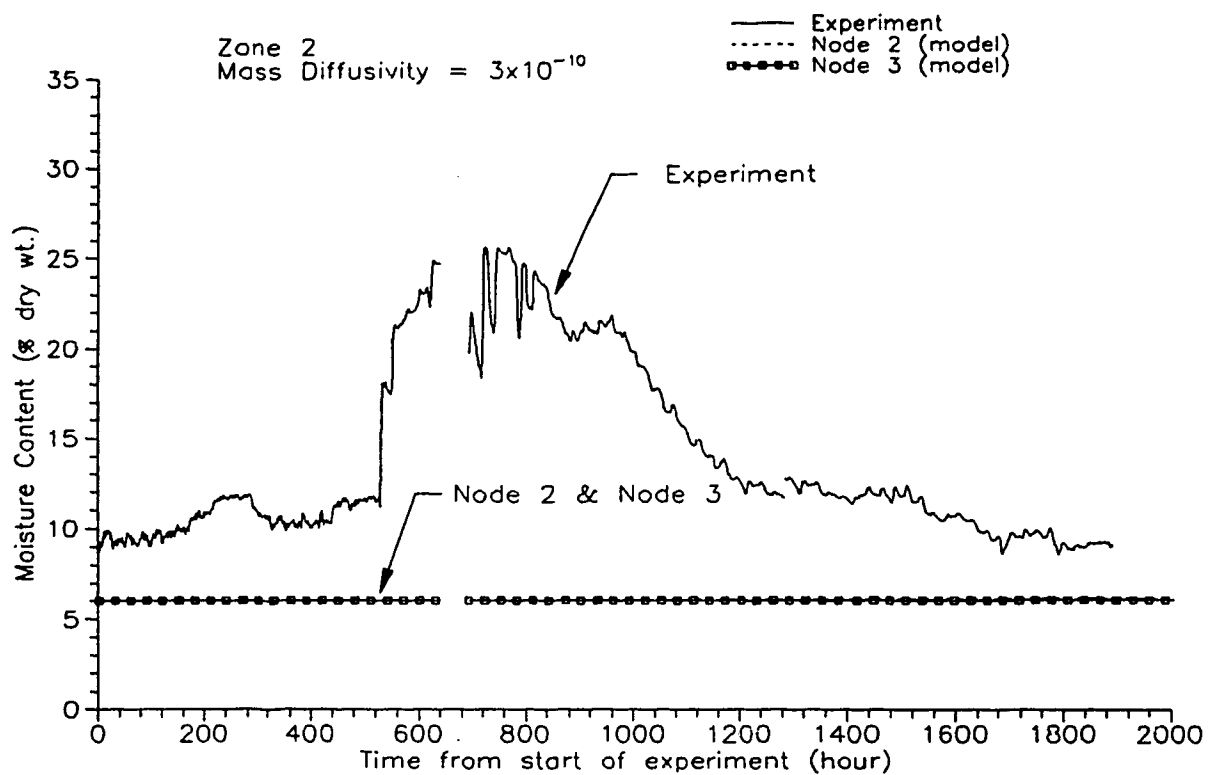


Figure 5.25b: Comparison of Wetwall predictions at node 2 and node 3 with measured moisture content in zone 2. The mass diffusivity for the sheathing is equal to $3 \times 10^{-10} \text{ m}^2/\text{s}$.

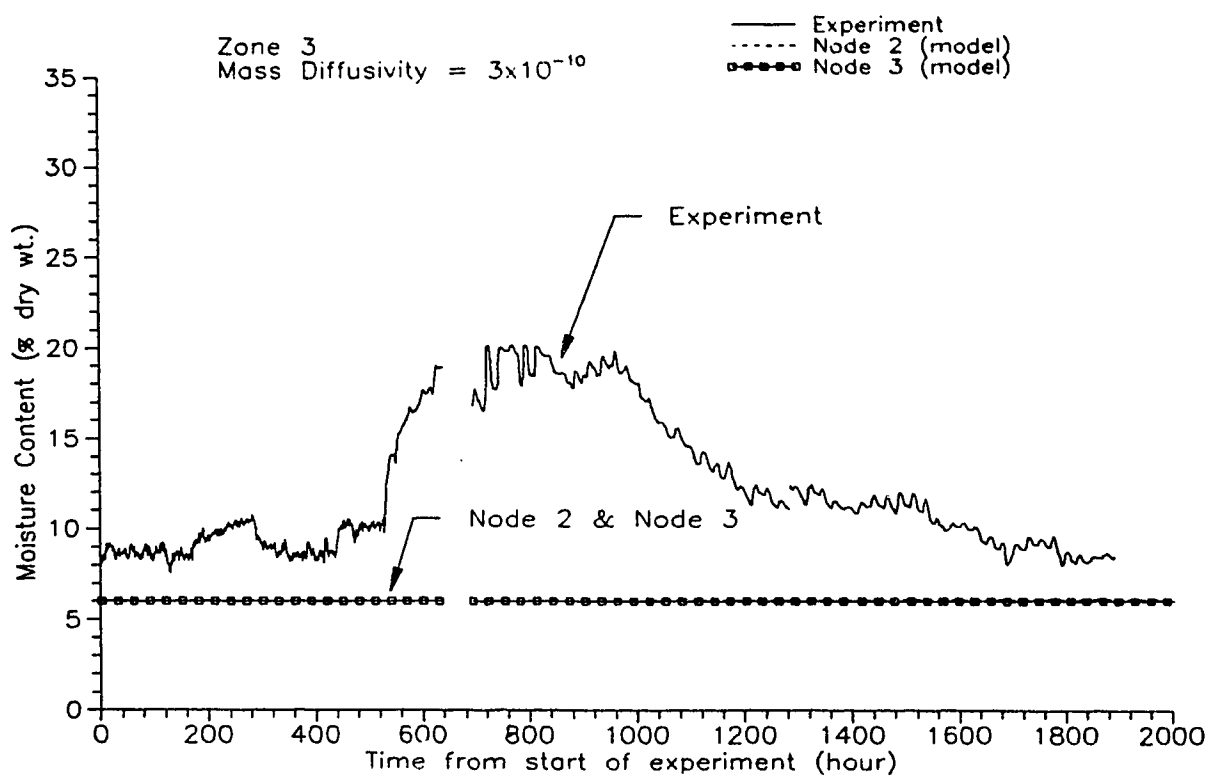


Figure 5.25c: Comparison of Wetwall predictions at node 2 and node 3 with measured moisture content in zone 4. The mass diffusivity for the sheathing is equal to $3 \times 10^{-10} \text{ m}^2/\text{s}$.

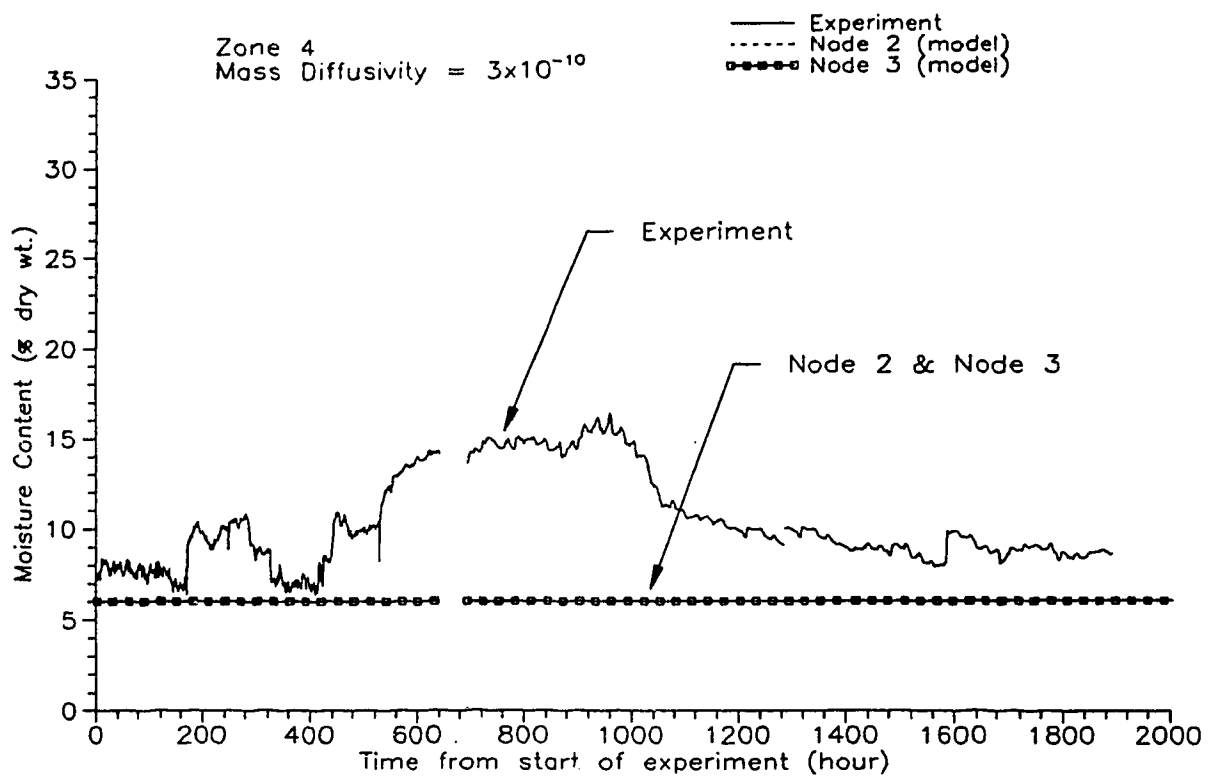


Figure 5.25d: Comparison of Wetwall predictions at node 2 and node 3 with measured moisture content in zone 4. The mass diffusivity for the sheathing is equal to $3 \times 10^{-10} \text{ m}^2/\text{s}$.

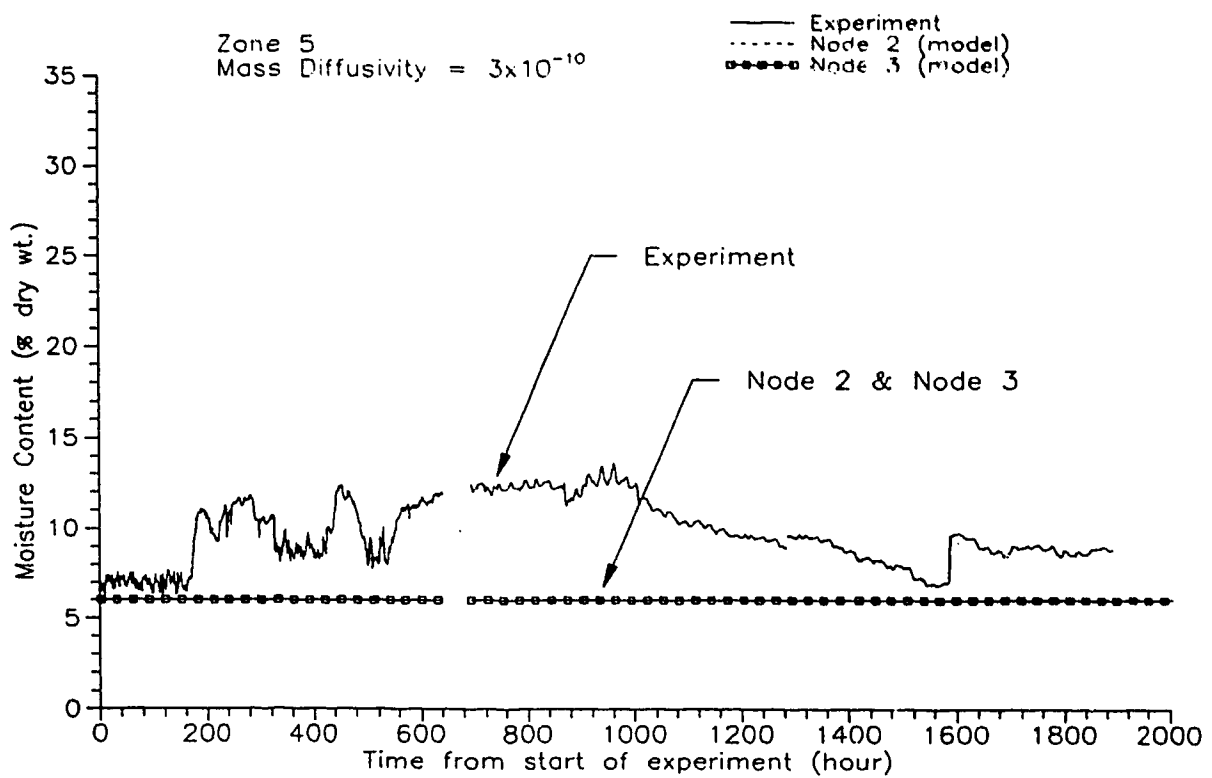


Figure 5.25e: Comparison of Wetwall predictions at node 2 and node 3 with measured moisture content in zone 5. The mass diffusivity for the sheathing is equal to $3 \times 10^{-10} \text{ m}^2/\text{s}$.

CHAPTER 6

CONCLUSIONS AND RECOMMENDATIONS

A field experiment was conducted to validate the ventilation model Local Leaks (Walker 1993) and moisture deposition model Wetwall (Nikel 1991). The field experiment was carried out at the Alberta Home Heating Research Facility (AHHRF) from February 7, 1994 to April 28, 1995. Approximately 10700 hours of data on the air leakage flow through the cavity and moisture deposition on the exterior cavity sheathing were collected. The field experiment was conducted under two conditions: a supply fan was placed inside the house for a portion of the first heating season to pressurize the interior and no supply fan was used in the second heating season.

In addition, the ventilation model Local Leaks and moisture deposition model Wetwall were modified to match the conditions of the experiment. Local Leaks was modified to predict the air flow leakage through the wall cavity with an interior opening near the bottom of the cavity and exterior opening at the top of the sheathing. The model was also altered to incorporate the supply fan mounted at the bottom of the flue in the field experiment.

Wetwall was further developed to incorporate moisture diffusion across the exterior wood sheathing. Since Wetwall is limited to moisture deposition within the cavity, it was coupled to a model for moisture diffusion across the exterior sheathing. A new function relating the vapour pressure, sheathing temperature, and sheathing moisture content was used in the sheathing moisture diffusion model. A nodal network with two surface layers and two internal layers was used to predict the moisture content

in the wood sheathing. This was necessary in order to obtain adequate spatial resolution for the variation in the moisture content across the thickness of the sheathing. The moisture content at the underlying nodes displayed similar trends to the wood moisture content measurements and the surface deposition and surface node predictions showed reasonable agreement with the surface sensor output from the field experiment.

6.1 CONCLUSIONS

A number of conclusions were reached based on the field measurements and comparisons with model predictions. The conclusions are presented in four sections: results based on the measured air leakage flow rates from the experiment; results from the comparison of the predicted and measured air leakage flow rates; results observed from the measured surface sensor output and moisture content from the experiment; and results based on the comparison of the predicted and measured surface deposition and moisture contents.

Measured air leakage flow rates from the field experiment:

- 1) The air leakage was dominated by the wind. The peak measured infiltration flow rate was at $0.37 \text{ m}^3/\text{hr}$ or greater because of the upper limit of the measurement system at $0.37 \text{ m}^3/\text{hr}$. The peak exfiltration flow rate was about $0.35 \text{ m}^3/\text{hr}$.

The peak air leakage rate created by stack effect was about $0.13 \text{ m}^3/\text{hr}$ for infiltration and $0.05 \text{ m}^3/\text{hr}$ for exfiltration.
- 2) A north wind produces a positive pressure coefficient on the north wall which generates nearly all infiltration across the north wall cavity.
- 3) A south wind produced a negative pressure coefficient on the north wall, but generated both infiltration and exfiltration. The direction of flow across the north cavity under south winds is more susceptible to other factors than north winds because the magnitude of the pressure coefficient of the north wall for south winds is smaller than that for north winds. (The pressure coefficient correlation used in Local Leaks shows that the C_p is 0.6 for north winds and -0.3 for south

winds

- 4) East and west winds produced infiltration and exfiltration across the north cavity without any significant pattern with the wind speed or wind direction.

The pressure coefficient correlation used in Local Leaks shows that the pressure coefficients for east and west winds are very sensitive to the wind direction. The pressure coefficient can change from a positive to a negative value or vice versa due to a small change in the wind direction.

- 5) The amount of the air leakage flows through the cavity under east and west winds was different because of the asymmetric sheltering about house 6. Five row houses are located to the west of house 6 and a 3.7 m high wall is located to the east of house 6. The air flow along the row of five houses is different from the air flow over the 3.7 m wall.
- 6) Air leakage with magnitudes of under $0.1 \text{ m}^3/\text{hr}$ are typically driven by the stack effect. Although these low flow rates were sorted for wind velocities under 1 m/s , they are sensitive to the change in the wind direction such that the direction of flow can easily change from infiltration to exfiltration or vice versa.

Comparison of predicted and measured air leakage flow rates:

- 1) In general, Local Leaks predicted correctly the trends of the air leakage flow rate across the cavity except for low leakage rates under $0.1 \text{ m}^3/\text{hr}$ and flow rates under east and west winds.

The incorrect trends of the low flow rates is expected because of the sensitivity of the measured air leakage flow rates to wind direction. The direction of the measured low flow rates may easily change from infiltration to exfiltration or vice versa.

The inaccurate trends for flows under east and west winds was due to the difference in the pressure coefficient correlation used in the model and that in the experiment. The pressure coefficient used in the model was developed for a house in the middle of a row of houses. The sheltering is symmetrical with houses to the east and west. In the experiment, however, the house was at the end of the row of houses where five houses were located to the west and a 3.7 m wall was located to the east. Hence, the pressure coefficient for the end house was not symmetric.

A plot of the measured normalized air leakage flow rates as a function of wind direction showed that curve is skewed and the minimum normalized leakage flow occurred at 150° . The normalized leakage rate was at 0.02 for east winds and

0.01 for west winds. The curve based on Local Leaks predictions is symmetrical about 180° at which the minimum normalized leakage flow rate occurred. The normalized leakage flows for east and west winds were at approximately zero. The maximum normalized flow rate for both predictions and experimental results occurred from the north, but the magnitude of the predictions was less than that of the measurements.

- 2) Local Leaks consistently under predicted the magnitude of the air leakage across the cavity for both infiltration and exfiltration. The under prediction was mainly due to the variation of the pressure coefficient along the height of the wall. From experiments conducted by Fleming (1996), the pressure coefficient can vary +/- 0.1 from the average value for a wall with a larger value at the top of the wall and a lower value at the bottom. Since the exterior opening is at the top of the wall, the use of a wall average pressure coefficient produced air flow rate predictions which were lower than the experimental results.

Measured surface sensor output and sheathing moisture content from field experiment:

- 1) The amount of moisture deposition is largest at the interior opening and decreases with distance along the height of the sheathing away from the opening.
- 2) Based on the response of the surface sensors, the moisture deposition inside the cavity increased during the heating season and there was none in the summer.
- 3) The moisture pin measurements show similar wetting and drying trends as the surface sensors. The peak sheathing moisture content reached 27 %wt in the first heating season and 24 %wt in the second heating season. The sheathing moisture content remained relatively high between 13 %wt and 18 %wt over the summer.

The results show that the sheathing is susceptible to wood rot because wood rot can occur if the moisture content of wood exceeds 20 %wt at a temperature over 10°C.

- 4) The surface sensor output responded much quicker than the moisture pins in the interior of the sheathing for both wetting and drying. This suggests that air movement deposits and removes moisture from the cavity faster than moisture diffusion across the sheathing.

Comparison of predicted and measured surface deposition and sheathing moisture content:

- 1) The model Wetwall responded well to the wetting phase, but not the drying phase. The model predictions coincided with initiation of moisture deposition and the magnitudes of the predictions bracketed the measured values. For the drying

phase, the model predicted the correct trends because the initial drop of the predicted surface deposition matched the decline of the surface sensors output. The magnitude of the predictions, however, did not agree with the measured values because the model response was slower than the actual drying process.

- 2) A nodal network with at least two underlying layers for a 12.7 mm thick exterior sheathing is required to give reasonable moisture content predictions.
- 3) The rise and fall of the moisture content of the internal nodes are sensitive to the mass diffusivity of water through wood. The range of values for mass diffusivity considered was $3 \times 10^{-6} \text{ m}^2/\text{s}$, the upper limit for non saturation of the interior nodes and $3 \times 10^{-10} \text{ m}^2/\text{s}$, the lower limit used by Walker (1993). A mass diffusivity of $3 \times 10^{-6} \text{ m}^2/\text{s}$ was used in the model because it produced the closest agreement with experimental measurements.

6.2 RECOMMENDATIONS

- 1) Modify the pressure coefficient to account for the variation along the height of the wall and the asymmetric sheltering. Field or laboratory measurements are required to determine the pressure coefficient with asymmetrical sheltering.
- 2) Use Local Leaks predictions as input for air leakage flow rates into Wetwall and compare model predictions with measured moisture content in the cavity. This would be required in order to conduct simulation of seasonal moisture build-up.
- 3) More testing is required to determine the mass diffusivity of wood under various moisture content and temperature. The diffusion of moisture through wood is dependent on a moisture gradient as well as a thermal gradient.
- 4) To improve the performance of Wetwall for drying, the influence of the exponential term in the analytical solution for mass deposition needs to be reduced. For infiltration, the model uses the exterior opening as the origin of the coordinates for the zone limits in the exponential term. If the origin is shifted further down at a point where the vapour profile has retained its constant uniform profile after some moisture exchange with sheathing, the moisture removal potential would remain relatively large even further down the cavity. Hence more moisture can be removed from the exterior sheathing.

REFERENCES

- ANSI/ASHRAE Standard 51 (1985): Laboratory Methods Of Testing Fans For Rating, Air Movement and Control Association, Inc. and American Society of Heating, Refrigeration, and Air Conditioning Engineers, Inc.
- ASHRAE (1988): 1988 Equipment Handbook, American Society of Heating, Refrigeration, and Air Conditioning Engineers, Inc. Atlanta, U.S.A.
- ASHRAE (1989): 1989 Fundamentals Handbook, S.I. edition., American Society of Heating, Refrigeration, and Air Conditioning Engineers, Inc. Atlanta, U.S.A.
- ASTM Designation: D 4442-92 (1992): "Standard Test Methods for Direct Moisture Content Measurement of Wood and Wood-Base Materials", Annual Book of ASTM Standards, pp. 516-520.
- ASTM Designation: D 4444-92 (1992): "Standard Test Methods for Use and Calibration of Hand-Held Moisture Meters", Annual Book of ASTM Standards, pp. 521-526.
- Alberta Energy and Natural Resources, Energy Conservation Branch (1984): Condensation Concerns, Booklet #9
- Burch, D.M. and Thomas, W.C. (1992): "An Analysis of Moisture Accumulation in a Wood-Frame Wall Subject to Winter Climate." In: Proceedings, ASHRAE/DOE/BTECC Conference on the Thermal Performance of the Exterior Envelopes of Buildings V, December 7-10, 1992, Clearwater Beach, Florida. pp. 467-479.
- CAN/CGSB-149.10-M86 (1986): "Determination of the Airtightness of Building Envelopes by the Fan Depressurization Method.", Canadian General Standards Board, Ottawa, Canada.
- Cleary, P.G. (1985): "Moisture Control by Attic Ventilation and an in-situ Study.", ASHRAE Transactions, Vol. 91, part 1.
- Crank, J. (1956): The Mathematics Of Diffusion, Oxford At The Clarendon Press, pp. 44-45.
- Cunningham, M.J. (1990): "Modeling of Moisture Transfer in Structures-II. A Comparison of a Numerical Model, an Analytical Model and some Experimental Results", Building and Environment, Vol. 25, No. 2, pp. 85-94.
- Dale, J.D. and Ackerman, M.Y. (1993), "The Thermal Performance of A Radiant Panel

Floor-Heating System", ASHRAE Transaction 1993, Vol.99, Part 1.

- Fleming, P.N. (1996): "Passive Ventilation For Combustion Air Supply", M.Sc. Thesis, Department of Mechanical Engineering, University of Alberta, Edmonton, Alberta, Canada.
- Forest, T.W., Walker, I.S. and Checkwitch, K. (1990). "Moisture Accumulation in a Building Envelope, Final Report, Alberta Home Heating Research Facility, 1989-90 Heating Season", Department of Mechanical Engineering, University of Alberta, Edmonton, Alberta, Canada.
- Gilpin, R.R.; Dale, J.D.; Forest, T.W.; Ackerman, M.Y. (1980): "Construction of The Alberta Home Heating Research Facility and Results for the 1979-80 Heating Season", Department of Mechanical Engineering, Report No. 23, University of Alberta, Edmonton, Alberta, Canada.
- Kent, A.D.; Handegord, G.O. and Robson, D.R. (1966): "A Study of Humidity Variations in Canadian Houses." ASHRAE Transactions, Vol. 72, Part II, pp. 1.1-1.8.
- McRae, K.F. (1995): "Wall Moisture Simulation Model", M.Sc. Thesis, Department of Mechanical Engineering, University of Alberta, Edmonton, Alberta, Canada.
- Nikel, K.G. (1991): "Moisture Deposition From Air Flow Through Wall Cavities", M.Sc. Thesis, Department of Mechanical Engineering, University of Alberta, Edmonton, Alberta, Canada.
- Ojanen, T. and Kohomen, R. (1989): "Hygrothermal (sic) Influence of Air Convection in Wall Structures." In: Proceedings, ASHRAE/DOE/BTECC/CIBSE Conference on the Thermal Performance of the Exterior Envelopes of Buildings IV, December 1989, Orlando, Florida. pp. 234-249.
- Ojanen, T. and Kumaran, M.K. (1992): "Air Exfiltration and Moisture Accumulation in Residential Wall Cavities." In: Proceedings, ASHRAE/DOE/BTECC Conference on the Thermal Performance of the Exterior Envelopes of Buildings V, December 7-10, 1992, Clearwater Beach, Florida. pp 491-500.
- Pfaff, F. and Garrahan, P. (1986): "New Temperature Correction Factors for the Portable Resistance-type moisture meter", Forest Products Journal, Vol. 36, pp. 28-30.
- Schuyler, G.D.; Swinton, M. and Lankin, J. (1989): "WALLDRY-A Computer model that Simulates Moisture Migration through Wood Frame Walls-Comparison to Field Data." In: Proceedings, ASHRAE/DOE/BTECC/CIBSE Conference on the

Thermal Performance of the Exterior Envelopes of Buildings IV, December 1989, Orlando, Florida. pp. 492-505.

Siau, J.F. (1984): Transport Processes in Wood, Springer Verlag.

Sterling, E.M.; Arundel, A; and Sterling, T.D. (1985): "Criteria for Human Exposure to Humidity in Occupied Buildings." ASHRAE Transactions 91, Pt. 1, pp 611.

TenWolde, A. and Suleski, J.C. (1984): "Controlling Moisture in Houses," Solar Age 9, No. 1, pp. 34-37

TenWolde, A. and Carll, C. (1992): "Effect of Cavity Ventilation on Moisture in Walls and Roofs." In: Proceedings, ASHRAE/DOE/BTECC Conference on the Thermal Performance of the Exterior Envelopes of Buildings V, December 7-10, 1992, Clearwater Beach, Florida. pp. 555-562.

Timusk, J. and Doshi, H. (1985): "Effect of Insulating Sheathing on Heat and Moisture Flow." Proceedings of the 3rd CSCE Conference on Building Science and Technology, Toronto, Nov. 1985

Walker, I.S. (1989): "Single Zone Air Infiltration Modelling", M.Sc. Thesis, Department of Mechanical Engineering, University of Alberta, Edmonton, Alberta, Canada.

Walker, I.S. (1993): "Prediction of Ventilation, Heat and Moisture Transport In Attics", Ph.D. Thesis, Department of Mechanical Engineering, University of Alberta, Edmonton, Alberta, Canada.

Wilson, D.J. and Walker, I.S. (1991a): "Passive Ventilation to Maintain Indoor Air Quality", Department of Mechanical Engineering Report #81, University of Alberta, Edmonton, Alberta, Canada.

Wilson, D.J. and Walker, I.S. (1991b): "Wind Shelter Effects on a Row of Houses", Proc. 12th AIVC Conf., Ottawa, Canada.

APPENDIX A

CALIBRATION OF INSTRUMENTS

Wood Moisture Content:

The wood moisture meter (Lignometer) was calibrated with wood samples following the guidelines in ASTM D4442-92 and ASTM D4444-92 (1992). The 12.7 mm thick pine sheathing was cut into 57.2 mm x 38.1 mm samples. Two holes, with a depth of 9.35 mm from the surface, were drilled into each sample with a size 32 bit to accommodate two stainless steel pins. The stainless steel pins, 3 mm in diameter and 6 mm in length, were spaced 31.8 mm centre to centre in the wood. The exposed ends of the pins were sealed with epoxy glue to prevent surface moisture from affecting the calibration.

The samples were oven dried to determine the dry weight. The samples were dried until the change in the weight of the samples was less than 2.5% from the previous reading. Typically, the drying process took about four days. After the dry weight of the samples was determined, the samples were soaked in water over night and then dried to the desired moisture content. The samples then were stored in sealed plastic bags at room temperature where the moisture content of the samples was allowed to reach an equilibrium level. Again, a change in the moisture content of less than 2.5% was the criteria for uniform moisture content. Typically, the samples were stored in bags for 5 to 10 days before a calibration measurement was taken.

The calibration measurements were taken with the wood moisture meter connected to long cables that were attached to the lead wires of the moisture pins used in the experiment. (It was observed that the long cables acted as an antenna which picked up

AC noise from the relay board and computer, even though the wood moisture meter is a DC device.) The moisture content of the wood samples was determined gravimetrically with a scale which has a resolution of 0.001 g and an accuracy of ± 0.001 g. The voltage output from the wood moisture meter was measured with a voltmeter with an accuracy of $\pm 0.05\%$ of the reading at a range of 2 to 1000 V. The calibration range was from 35 %wt to 6 %wt with samples at approximately 5 %wt increments.

A number samples were taken at each wood moisture content and the calibration measurements at each moisture content level were averaged. The averaged data are shown in Table A1. The repeatability of the wood moisture meter was observed to be about ± 1.5 %wt for moisture contents below 15 %wt and ± 0.5 %wt for values above. All the wood moisture meter readings within the range of the calibration were interpolated linearly to give a corresponding wood moisture content.

Table A1: Calibration results of average wood moisture content and average meter output

Wood Moisture Content [%wt]	Lignometer Output [V]
6.3	0.258
8.1	0.346
10.4	0.492
15.0	0.733
20.3	0.907
25.2	1.042
29.7	1.241
34.8	1.327

Surface Sensor Output:

The same wood moisture meter (Lignometer) used for moisture content measurements was also used with the surface sensor. The calibration of the surface sensor/lignometer was conducted inside a refrigerated room. The surface sensor was mounted onto a 6.35 mm thick plywood with thermal conducting compound (Wakefield Thermal Joint Compound Type 120). The piece of plywood was mounted vertically over an opening in an adjoining wall of two chambers in the "cold room". The side of the plywood with the surface sensor attached was exposed to 5°C temperatures set in the chamber and the other side was exposed to -30°C temperatures set in the other chamber. This allowed moisture to gradually condense on the surface sensor. The output of the Lignometer was recorded with a strip chart recorder.

The calibration procedure began with both chambers at room temperature. The temperature of the chamber which the back of the plywood was exposed to was dropped to about -30°C. The output of the Lignometer was recorded over time as the condensation process began. A number of freeze/thaw cycles were conducted continuously. It was observed that the surface sensor could only provide qualitative results. The ranges of voltage output for formation of ice, frost, and condensation are listed in Table A2.

Table A2: Surface sensor output ranges for open circuit, frost and ice formation and condensation

Surface Deposition	Lignometer/surface sensor output [V]
Open circuit	0.2 - 0.75
Frost and ice	0.9 -1.0
Water	2.375

Relative Humidity:

Table A3: Calibration results of relative humidity sensors with constant relative humidity solutions

Sensor	Sensor Output for K ₂ SO ₄ 97% RH [V]	Sensor Output for NaCl 75.5% RH [V]	Sensor Output for MgCl ₂ 33% RH [V]	Sensor Output for LiCl 11.5% RH [V]
A	1.02	0.83	0.3	0.12
B	0.92	0.65	0.24	0.12
C	0.99	0.74	0.25	0.12
D	1.01	0.83	0.32	0.11
E	0.96	0.65	0.23	0.13
F	1.01	0.78	0.28	0.12
G	1.06	0.87	0.30	0.13
H	1.04	0.76	0.24	0.14

Table A4: Linear regression of the relative humidity sensor calibration results

Sensor	Calibration Equation [% RH] = B[Volt] + A	R ² Error [% RH]
A	$Y = 87.46 X + 5.74$	3
B	$Y = 100.13 X + 6.77$	5
C	$Y = 91.44 X + 6.91$	4
D	$Y = 82.78 X + 5.24$	5
E	$Y = 96.28 X + 9.38$	6
F	$Y = 89.61 X + 5.67$	3
G	$Y = 95.99 X + 1.28$	2
H	$Y = 94.37 X + 2.62$	5

Table A5: The location of relative humidity sensors in the experiment

Sensor	Sensor Location
A	indoor
B	zone 5
C	zone 4
D	zone 3
E	zone 2
F	zone 1
G	manifold
H	outdoor

Fan Performance Curve:**Table A6: Calibration results from the fan performance test with the flue attachment included**

Flow rate across fan [m ³ /hr]	Pressure difference between fan and ambient [Pa]
0	281.9
30.56	285.9
57.94	278.7
77.33	259.6
95.15	226.1
108.52	181.3
120.21	126.0
131.32	81.0
133.92	65.0
138.40	38.4

Calibrated with flue pipe and flue cap
test conditions:

Room temperature: 24°C

Atmospheric pressure: 697 mm Hg

Sampling time for averaging voltmeter: 10 s

Calibration equation:

$$M_{fan} = \frac{\rho_{out}}{3600} (5.3569E^{-4} \Delta P^3 - 0.04752 \Delta P^2 + 1.9049 \Delta P + 111.163) \quad A1$$

where M_{fan} = mass flow rate generated by fan and flue [kg/s]

ρ_{out} = outdoor air density [kg/m³]

ΔP = pressure drop across the fan and flue assembly [Pa]

Air Leakage Flow Measurements

Kurz anemometer:

Infiltration:

Table A7: Calibration results of the Kurz anemometer for infiltration

Air Leakage Rate [m ³ /hr]	Kurz Anemometer Output [V]	Pressure Difference between flow assembly and ambient [Pa]
0	0.208	0
0.15	2.051	0.187
0.25	3.515	0.249
0.36	5.068	0.654
0.48	6.360	1.028
0.64	7.856	1.557
0.80	9.145	2.492

Calibration equation:

$$Q_{in} = 1.97E^{-4} + 0.060(V)^{1.13} \quad A2$$

where Q_{in} = volumetric flow rate [m³/hr] V = output from Kurz anemometer [V]

$$Q_{in} = 0.477(\Delta P)^{0.595} \quad A3$$

where Q_{in} = volumetric flow rate [m³/hr] ΔP = pressure difference between flow assembly and ambient pressure [Pa]

Exfiltration:**Table A8: Calibration results of Kurz anemometer for exfiltration flows**

Air Leakage Rate [m ³ /hr]	Kurz Anemometer Output [V]	Pressure Difference between flow assembly and ambient [Pa]
0	0.208	0
0.13	1.800	0.062
0.34	4.846	0.529
0.45	6.125	0.841
0.56	7.322	1.277
0.73	8.825	1.962

Calibration Equation:

$$Q_{out} = 3.19E^{-3} + 0.058(V)^{1.15} \quad A4$$

where Q_{out} = volumetric flow rate [m³/hr]
 V = voltage output [V]

$$Q_{out} = 0.503(\Delta P)^{0.5} \quad A5$$

where Q_{out} = volumetric flow rate [m³/hr]
 ΔP = pressure difference between flow assembly and ambient pressure [Pa]

LEAKAGE FLOW CHARACTERISTICS

Background Leakage Of The Test House

Equation resulting from the fan pressurization test,

$$Q = 0.00881(\Delta P)^{0.648}$$

A6

where Q = volumetric flow rate [m^3/s]

ΔP = pressure difference across the building envelope [Pa]

Results from the pressurization tests:

Tests in Module 6

- flue blocked
- 3 inch diameter hole in ceiling panel blocked

Test	U	Tin	Touts	Al4	Al10	Q50	n	C
14291 U	1.5	21.3	16.0	82.0	95.2	0.113	0.663	0.00845
14292 U	3.7	21.8	21.9	84.4	100.6	0.125	0.692	0.00835
14293 U	5.5	22.5	22.5	111.3	118.1	0.120	0.565	0.01313
14294 U	4.2	23.4	21.2	84.1	98.1	0.117	0.668	0.00861
14295 U	4.6	23.7	21.0	91.6	105.8	0.125	0.658	0.00950
14296 U	1.2	23.7	19.6	86.0	101.5	0.124	0.681	0.00864
14297 U	1.0	23.5	16.5	85.7	101.1	0.123	0.680	0.00862
14298 U	1.5	22.7	14.3	86.0	102.0	0.126	0.686	0.00858
14299 U	2.0	22.1	14.3	86.3	101.4	0.123	0.676	0.00873
14300 U	1.9	21.5	13.2	86.6	102.0	0.124	0.679	0.00872
14301 U	2.2	21.6	11.5	85.1	101.4	0.126	0.691	0.00842
14302 U	2.8	21.7	11.5	87.5	103.3	0.126	0.681	0.00879
14303 U	2.9	21.7	12.7	79.8	95.3	0.119	0.694	0.00787
14304 U	3.4	21.7	17.1	85.0	99.5	0.120	0.673	0.00864
14305 U	5.2	21.8	20.8	88.6	105.5	0.131	0.690	0.00880
14306 U	5.4	23.8	23.4	90.7	104.2	0.121	0.651	0.00949
14307 U	4.3	24.4	23.8	92.2	104.4	0.119	0.636	0.00985

Tests in Module 6

- flue blocked

- 3 inch diameter hole in ceiling panel blocked

Test	U	Tin	Touts	A14	A110	Q50	n	C
14211 U	1.7	21.4	18.3	79.0	93.5	0.115	0.683	0.00791
14212 U	1.8	22.5	28.1	82.4	97.6	0.120	0.686	0.00822
14213 U	1.8	23.9	30.0	80.6	96.7	0.121	0.699	0.00790
14214 U	2.1	24.6	24.4	78.5	93.7	0.117	0.693	0.00775
14215 U	2.3	25.3	24.5	77.8	92.2	0.113	0.686	0.00776
14216 U	2.2	25.9	23.3	75.8	91.2	0.115	0.701	0.00740
14217 U	2.8	25.8	22.7	81.5	98.1	0.124	0.703	0.00794
14218 U	2.3	25.3	21.0	77.8	94.5	0.121	0.712	0.00749
14219 U	1.8	24.6	19.7	80.9	95.8	0.118	0.685	0.00807
14220 U	2.0	23.9	18.1	81.2	98.4	0.126	0.709	0.00785
14221 U	3.3	23.0	16.6	78.3	94.9	0.122	0.710	0.00755
14222 U	3.2	22.4	16.4	80.3	96.6	0.122	0.702	0.00784
14223 U	5.2	21.8	16.6	91.3	104.7	0.121	0.649	0.00959
14224 U	3.7	21.1	15.6	76.5	93.6	0.122	0.720	0.00728
14225 U	3.3	21.5	14.5	80.5	95.6	0.118	0.688	0.00801
14226 U	4.3	21.1	16.8	79.3	92.7	0.111	0.670	0.00809
14227 U	1.6	21.6	20.3	75.8	90.7	0.114	0.696	0.00745
14228 U	1.1	23.0	25.7	78.8	95.3	0.121	0.707	0.00763
14229 U	1.2	24.2	26.0	77.1	94.5	0.123	0.721	0.00733
14230 U	1.9	25.0	23.8	76.6	92.7	0.118	0.708	0.00741
14231 U	1.5	25.9	25.2	76.7	92.9	0.119	0.709	0.00742
14232 U	1.1	26.6	25.4	77.2	93.8	0.120	0.712	0.00744
14233 U	1.0	26.6	24.4	80.0	97.1	0.125	0.712	0.00769
14234 U	5.1	26.0	21.6	73.1	91.1	0.122	0.740	0.00676
14235 U	3.2	24.8	18.5	84.7	99.7	0.121	0.677	0.00855
14236 U	2.1	23.7	17.1	81.4	98.8	0.127	0.712	0.00784
14237 U	2.4	22.8	16.1	82.7	96.8	0.116	0.671	0.00843
14238 U	2.7	22.1	15.5	82.2	96.5	0.117	0.675	0.00833
14239 U	2.6	21.5	15.0	84.9	101.1	0.125	0.690	0.00841
14240 U	1.8	21.2	14.0	80.6	97.1	0.123	0.703	0.00785
14241 U	1.6	21.5	13.5	78.5	93.0	0.114	0.684	0.00785
14242 U	3.7	21.2	13.4	81.7	94.9	0.113	0.664	0.00841
14243 U	3.4	21.4	16.3	83.3	99.0	0.122	0.688	0.00829
14244 U	3.8	21.6	18.2	88.0	102.7	0.123	0.668	0.00899
14245 U	3.3	22.1	18.8	83.0	97.7	0.119	0.678	0.00838
14246 U	2.8	22.7	19.0	73.9	90.7	0.119	0.723	0.00700
14247 U	1.8	23.1	19.4	78.7	94.6	0.119	0.701	0.00769
14248 U	1.7	23.3	19.7	76.6	94.6	0.125	0.731	0.00718
14249 U	1.1	23.1	18.5	78.9	94.8	0.120	0.701	0.00771
14250 U	1.4	22.6	15.8	77.8	93.0	0.116	0.694	0.00768

Tests in Module 6

- flue blocked

- 3 inch diameter hole in ceiling panel blocked

Test	U	Tin	Touts	A14	A110	Q50	n	C
14251 U	1.1	22.5	26.5	87.3	102.2	0.123	0.672	0.00888
14252 U	1.3	24.0	27.5	85.7	101.2	0.124	0.681	0.00861
14253 U	1.1	24.7	23.6	84.7	100.3	0.123	0.685	0.00846
14254 U	1.3	25.5	24.4	84.5	101.3	0.127	0.698	0.00830
14255 U	1.6	26.1	23.7	83.1	98.4	0.121	0.685	0.00830
14256 U	1.7	26.0	23.4	87.8	103.9	0.128	0.684	0.00879
14257 U	1.7	25.9	21.7	85.3	101.1	0.124	0.686	0.00851
14258 U	1.9	25.3	18.5	85.5	100.5	0.122	0.677	0.00863
14259 U	2.5	24.3	15.1	89.8	106.4	0.131	0.685	0.00896
14260 U	2.0	23.2	13.0	87.5	101.9	0.122	0.666	0.00896
14261 U	1.5	22.2	12.5	86.5	102.1	0.125	0.682	0.00867
14262 U	2.1	21.5	12.0	88.6	105.8	0.132	0.693	0.00876
14263 U	2.7	21.6	11.8	89.3	104.2	0.125	0.668	0.00913
14264 U	1.9	21.6	12.6	84.0	98.7	0.119	0.676	0.00850
14265 U	2.8	21.7	16.0	84.9	101.4	0.126	0.693	0.00838
14266 U	2.4	22.0	20.5	86.0	102.3	0.127	0.690	0.00853
14267 U	2.9	23.1	25.7	85.0	99.1	0.119	0.668	0.00869
14268 U	2.6	24.3	28.4	84.3	98.2	0.117	0.667	0.00863
14269 U	2.8	25.0	26.5	97.0	108.8	0.122	0.625	0.01053
14270 U	2.9	25.6	26.4	87.3	102.2	0.123	0.671	0.00889
14271 U	3.0	26.2	26.1	91.8	104.9	0.121	0.646	0.00968
14272 U	2.1	26.3	25.3	87.6	104.0	0.128	0.688	0.00872
14273 U	1.4	26.2	23.7	89.4	103.7	0.123	0.662	0.00923
14274 U	1.7	25.9	21.3	84.3	100.8	0.126	0.696	0.00829
14275 U	2.6	25.0	17.4	89.8	105.8	0.129	0.679	0.00906
14276 U	2.6	24.0	15.2	87.2	101.9	0.122	0.670	0.00890
14277 U	2.9	23.1	14.4	89.9	106.3	0.130	0.684	0.00899
14278 U	3.4	22.2	16.7	88.6	104.2	0.127	0.677	0.00895
14279 U	2.8	21.7	16.3	89.9	102.5	0.118	0.644	0.00951
14280 U	4.3	21.6	15.9	86.1	101.9	0.125	0.683	0.00862
14281 U	4.1	21.5	16.8	87.7	103.6	0.127	0.682	0.00880
14282 U	2.5	21.6	18.4	83.9	97.6	0.116	0.665	0.00862
14283 U	1.1	22.3	22.7	84.2	98.5	0.119	0.672	0.00857
14284 U	1.3	23.3	25.8	83.7	99.4	0.123	0.688	0.00833
14285 U	2.0	24.3	24.7	84.7	101.1	0.126	0.692	0.00838
14286 U	1.2	24.9	24.0	82.2	96.8	0.118	0.678	0.00829
14287 U	1.6	25.1	23.6	82.6	97.2	0.118	0.677	0.00834
14288 U	1.7	25.2	22.9	83.2	100.7	0.128	0.708	0.00805
14289 U	1.1	25.1	21.6	78.7	95.1	0.121	0.707	0.00763
14290 U	1.0	24.7	19.9	83.4	100.5	0.127	0.703	0.00812

Leakage Characteristic Of The Test Cavity
Infiltration:

Table A9: Calibration results from cavity flow resistance test for infiltration

Air Leakage Rate [m ³ /hr]	Indoor/outdoor Pressure Difference [Pa]
0.143	2.78
0.181	3.86
0.226	5.12
0.291	8.36
0.336	11.86
0.416	17.57
0.466	20.86
0.520	24.19
0.577	29.38

Calibration conditions:

T_{out}: 15°C

T_{in}: 20°C

Wind speed: under 1.5 m/s

Calibration equation:

$$Q_{in} = 0.084 \Delta P^{0.569}$$

A7

where Q_{in} = infiltration rate [m³/hr]

C = flow coefficient [m³/(hrPaⁿ)]

ΔP = indoor/outdoor pressure difference [Pa]

Exfiltration:**Table A10: Calibration results from the test flow resistance test for exfiltration**

Air Leakage Rate [m ³ /hr]	Indoor/outdoor Pressure Difference [Pa]
0.080	1.86
0.111	3.30
0.147	4.99
0.170	6.78
0.181	8.27
0.220	11.89
0.260	16.27
0.302	24.26
0.402	29.72

Calibration conditions:

Tout: 16°C

Tin: 21°C

Wind speed: under 1.5 m/s

Calibration equation:

$$Q_{out} = 0.058 \Delta P^{0.543}$$

A8where Q_{out} = exfiltration rate [m³/hr] C = flow coefficient [m³/(hrPaⁿ)] ΔP = indoor/outdoor pressure difference [Pa]